2001

Electromechanical characterization of ultrasonic NDE systems

Changjiu Dang
Iowa State University

INFORMATION TO USERS

This manuscript has been reproduced from the microfilm master. UMI films the text directly from the original or copy submitted. Thus, some thesis and dissertation copies are in typewriter face, while others may be from any type of computer printer.

The quality of this reproduction is dependent upon the quality of the copy submitted. Broken or indistinct print, colored or poor quality illustrations and photographs, print bleedthrough, substandard margins, and improper alignment can adversely affect reproduction.

In the unlikely event that the author did not send UMI a complete manuscript and there are missing pages, these will be noted. Also, if unauthorized copyright material had to be removed, a note will indicate the deletion.

Oversize materials (e.g., maps, drawings, charts) are reproduced by sectioning the original, beginning at the upper left-hand corner and continuing from left to right in equal sections with small overlaps.

Photographs included in the original manuscript have been reproduced xerographically in this copy. Higher quality 6" x 9" black and white photographic prints are available for any photographs or illustrations appearing in this copy for an additional charge. Contact UMI directly to order.

Bell & Howell Information and Learning
300 North Zeeb Road, Ann Arbor, MI 48106-1346 USA
800-521-0600

Electromechanical characterization of ultrasonic NDE systems

by

Changjiu Dang

A dissertation submitted to the graduate faculty

in partial fulfillment of the requirements for the degree of

DOCTOR OF PHILOSOPHY

Major: Engineering Mechanics

Major Professor: Lester W. Schmerr Jr.

Iowa State University

Ames, Iowa

2001

UMI Number: 3003235

UMI Microform 3003235

Bell & Howell Information and Learning Company
300 North Zeeb Road
P.O. Box 1346
Ann Arbor, MI 48106-1346

Graduate College
Iowa State University

This is to certify that the Doctoral dissertation of
Changjiu Dang
has met the dissertation requirements of Iowa State University

Signature was redacted for privacy.

Committee Member

Signature was redacted for privacy.

Committee Member

Signature was redacted for privacy.

Committee Member

Signature was redacted for privacy.

Committee Member

Signature was redacted for privacy.

Major Professor

Signature was redacted for privacy.

For the Major Program

Signature was redacted for privacy.

For the Graduate College

I dedicate this dissertation to my wife and my son who have supported me on the way of my Ph.D. career.

I dedicate this dissertation to my parents in China who have devoted their love to me without expecting anything in return.

I dedicate this dissertation to all my teachers in my life from my elementary school to current graduate education, who have shared their knowledge and wisdom with me.

TABLE OF CONTENTS

LIST OF FIGURES

LIST OF TABLES

LIST OF SYMBOLS

A Surface area (m^2)

A_{max} Voltage amplitude of the first half cycle (V)

a Transducer radius (m), Superscript to denote an acoustic quantity

b Transducer radius (m)

C Capacitance (F)

C_0 Clamped capacitance (F)

C_p Capacitance of a capacitor in parallel in a tuning circuit (F)

c Sound velocity (m/s), Elastic constant (Pa)

c_1 Sound velocity in fluid (m/s)

c_2 Sound velocity in solid (m/s)

c_L Sound velocity in semi-infinite solid (m/s)

c^D Stiffness constant with constant D (Pa)

c^E Stiffness constant with constant E (Pa)

c_{hk}^D Components of elastic constant matrix (h, k = 1..6) with constant D (Pa)

$\mathbf{D}$ Electric flux density vector (C/m^2)

D Electric flux density scalar (C/m^2), Distance (m)

D_i Components of electric flux density (i=1..3)

d Distance between two transducers (m)

$\mathbf{E}$ Electric field intensity (V/m)

$\mathbf{E}^a$ Electric field intensity for solution a (V/m)

$\mathbf{E}^b$ Electric field intensity for solution b (V/m)

$\mathbf{e}$ Unit vector

$\mathbf{e}_x$ Unit vector in x direction

$\mathbf{e}_y$ Unit vector in y direction

e Superscript to denote an electrical quantity, Piezoelectric voltage constant (C/m^2)

F Force (N), Configuration factor, Frequency

$\tilde{F}$ Lumped force (N)

$\hat{F}$ Lumped force (N)

F^a Force for solution a (N)

F^b Force for solution b (N)

F^p Configuration factor in terms of pressure

F_1 Force at mechanical port 1 (N)

F_2 Force at mechanical port 2 (N)

F_B Blocked force (N)

F_c Center frequency (Hz)

F_m Nominal center frequency (Hz)

F_{inc} Incident force (N)

F_r Radiation force (N)

F_{reflt} Reflected force (N)

F_{scatt} Scattering force (N)

F_t Transmitted force (N)

F_{th} Force source strength of a Thevenin equivalent circuit (N)

f Function, Frequency (Hz)

$f(\mathbf{x})$ Distribution function at point **x**.

f_c Center frequency (Hz)

f_M Frequency at the highest power point (Hz)

$f_{\max}$ Frequency at the higher half power point (Hz)

$f_{\min}$ Frequency at the lower half power point (Hz)

f_0 Antiresonant frequency (Hz)

f_1' Solution with transmitting transducer firing and flaw present

f_2' Solution with receiving transducer firing and flaw absent

f_3' Solution with transmitting transducer firing and flaw absent

$\mathbf{H}$ Magnetic field intensity (A/m)

$\mathbf{H}^a$ Magnetic field intensity for solution a (A/m)

$\mathbf{H}^b$ Magnetic field intensity for solution b (A/m)

H Struve function, Transfer function

H_0 Zeroth order Struve function

H_1 First order Struve function

H_r Transfer function (V/N)

H_r' Transfer function (V/N)

h Piezoelectric stiffness constant (V/m)

h_{jh} Piezoelectric stiffness constants (j=1..3, h=1..6) (V/m)

$\mathbf{I}$ Current column vector

$\mathbf{I}^a$ Current column vector for solution a

$\mathbf{I}^b$ Current column vector for solution b

I current (A)

I^a Current for solution a (A)

I^b Current for solution b (A)

I_B Input current into transducer B (A)

I_i Current at electrical port i (i=1..n) (A)

I_o Current flowing into Z_o^e (A)

I_P Current measurement flowing into cabling (A)

I_S Short circuit current (A)

I_{in} Current flowing into a transducer (A)

J Bessel function, Reciprocity parameter

J_0 Zeroth order Bessel function

J_1 First order Bessel function

K Amplification factor

k Wavenumber (1/m), Electromechanical coupling factor

k_1 Wavenumber in fluid (1/m)

k_2 Wavenumber in solid (1/m)

k_T Thickness electromechanical couple factor

$\mathbf{l}$ Unit length vector (m)

L Inductance (H)

L_p Inductance in parallel (H)

L_s Inductance in series (H)

l Thickness (m)

M Receiving sensitivity

M_{IF} Receiving sensitivity with output current I and input force F (A/N)

M_{IF_B} Blocked-force current receiving sensitivity (A/N)

M_{Iv} Receiving sensitivity with output current I and input velocity v (A/(m/s))

M_{VF} Receiving sensitivity with output voltage V and input force F (V/N)

M_{VF_B} Blocked-force voltage receiving sensitivity (V/N)

M_{Vv} Receiving sensitivity with output voltage V and input velocity v (V/(m/s))

M_{oi} Receiving sensitivity with quantity o as output and quantity i as input

M_{IF}^0 Short-circuit current receiving sensitivity (A/N)

M_{VF}^∞ Open-circuit voltage receiving sensitivity (V/N)

$M_{IF_B}^{0}$ Short-circuit blocked-force current receiving sensitivity (A/N)

$M_{VF_B}^{\infty}$ Open-circuit blocked-force voltage receiving sensitivity (V/N)

$M_{VF_B}^{A}$ Blocked-force receiving sensitivity for transducer A (V/N)

$M_{VF_B}^{A:\infty}$ Open-circuit blocked-force receiving sensitivity for transducer A (V/N)

$M_{V\overline{p}}^{A:\infty}$ Open-circuit receiving sensitivity in terms of pressure $\overline{p}$ (V/Pa)

$M_{VF_B}^{B:\infty}$ Open-circuit blocked-force receiving sensitivity for transducer B (V/N)

$M_{VF_B}^{R:\infty}$ Open-circuit blocked-force receiving sensitivity for transducer R (V/N)

$M_{VF_B}^{T:\infty}$ Open-circuit blocked-force receiving sensitivity for transducer T (V/N)

N Fresnel distance (m)

N_a Fresnel distance with respect to transducer A with radius a (m)

N_b Fresnel distance with respect to transducer B with radius b (m)

$\mathbf{n}$ Normal unit vector

n Turns ratio (A/(m/s) or N/V), Number

n_i Component i of $\mathbf{n}$

p Pressure (Pa)

$\overline{p}$ Average pressure (Pa)

p^a Pressure for solution a (Pa)

p^b Pressure for solution b (Pa)

p_{ave} Average pressure (Pa)

p_{inc} Incident pressure (Pa)

p_{scatt} Scattering pressure (Pa)

Q A parameter appearing in Sittig's model

R Transfer matrix of receiving transducer, Ratio of two impedances

R^c Transfer matrix of cabling in receiving side
R_{11}^c, $R_{12}^c(\Omega)$, $R_{21}^c(1/\Omega)$, R_{22}^c, elements of R^c

R^e Transfer matrix of electrical elements at receiving side
R_{11}^e, $R_{12}^e(\Omega)$, $R_{21}^e(1/\Omega)$, R_{22}^e, elements of R^e

R^G Global transfer matrix of reception process
R_{11}^G(V/N), R_{12}^G(V/(m/s)), R_{21}^G(A/N), R_{22}^G(A/(m/s)), elements of R^G

R^S Transfer matrix of signal conditioning circuit at receiving side
R_{11}^S, $R_{12}^S(\Omega)$, $R_{21}^S(1/\Omega)$, R_{22}^S, elements of R^S

R^T Transfer matrix of receiving transducer

R_{11}^T (V/N), R_{12}^T (V/(m/s)), R_{21}^T (A/N), R_{22}^T (A/(m/s)), elements of R^T

R_s Resistance in series (Ω)

S Surface area (m^2), Strain, Transmitting sensitivity

S_A Surface area of transducer A

S_B Surface area of transducer B

S_R Surface area of receiving transducer

S_T Surface area of transmitting transducer

S_e Surface area of elastic body

S_f Surface area of flaw

S_i Strain component i (i=1..6)

S_{FI} Transmitting sensitivity with output force F and input current I (N/A)

S_{FV} Transmitting sensitivity with output force F and input voltage V (N/V)

S_{FV_i} Transmitting sensitivity with source strength V_i as an input (N/V)

S_{oi} Transmitting sensitivity with quantity o as output and quantity i as input

S_{vI} Transmitting sensitivity with output velocity v and input current I ((m/s)/A)

S_{vV} Transmitting sensitivity with output velocity v and input voltage V ((m/s)/V)

S_{vV_i} Transmitting sensitivity with source strength V_i as an input ((m/s)/V)

S_{FI}^A Transmitting sensitivity of transducer A (N/A)

s System factor (V/Hz)

s^m Measured system factor (V/Hz)

$\mathbf{T}$ Network in terms of transfer matrix

$\mathbf{T}^G$ Global network

$\mathbf{T}_i$ Network i (i=1..n)

T Superscript for transpose, Transfer matrix, Stress (Pa), Time (s)

$T^{(1)}$ Transfer matrix of transmitting cabling
$T_{11}^{(1)}$, $T_{12}^{(1)}$ (Ω), $T_{21}^{(1)}$ (1/Ω), $T_{22}^{(1)}$, elements of $T^{(1)}$

$T^{(2)}$ Transfer matrix of receiving cabling
$T_{11}^{(2)}$, $T_{12}^{(2)}$ (Ω), $T_{21}^{(2)}$ (1/Ω), $T_{22}^{(2)}$, elements of $T^{(2)}$

T^C Transfer matrix of transmitting cabling
T_{11}^C, T_{12}^C (Ω), T_{21}^C (1/Ω), T_{22}^C, elements of T^C

T^P Transfer matrix of backed piezoelectric plate
T_{11}^R (V/N), T_{12}^R (V/(m/s)), T_{21}^R (A/N), T_{22}^R (A/(m/s)), elements of T^P

T^R Transfer matrix of receiving transducer

T_{11}^{R} (V/N), T_{12}^{R} (V/(m/s)), T_{21}^{R} (A/N), T_{22}^{R} (A/(m/s)), elements of T^{R}

T^{T} Transfer matrix of transmitting transducer
T_{11}^{T} (V/N), T_{12}^{T} (V/(m/s)), T_{21}^{T} (A/N), T_{22}^{T} (A/(m/s)), elements of T^{T}

T^{W} Transfer matrix of wear plate
T_{11}^{W} , T_{12}^{W} (N/(m/s)), T_{21}^{W} ((m/s)/N), T_{22}^{W} , elements of T^{W}

T_{i} Stress component i (i=1..6)

T_{max} Maximum time duration (s)

$\mathbf{t}$ Traction (N/m^2)

$\mathbf{t}^{a}$ Traction for solution a (Pa)

$\mathbf{t}^{b}$ Traction for solution b (Pa)

t Time (s), Transfer function

t_0 Time point in a spike-like pulse (s)

t_A Acoustic transfer function

t_G Generation transfer function (N/V)

t_R Reception transfer function (V/N)

t_A^{I} Acoustic transfer function for setup I

t_A^{II} Acoustic transfer function for setup II

t_A^{III} Acoustic transfer function for setup III

u Displacement (m)

u_1 Displacement at port 1 (m)

u_2 Displacement at port 2 (m)

$\mathbf{V}$ Voltage column vector

$\mathbf{V}^{a}$ Voltage column vector for solution a

$\mathbf{V}^{b}$ Voltage column vector for solution b

V Velocity ratio, Voltage (V), Potential (V)

V^{1} Normalized velocity at state 1

V^{2} Normalized velocity at state 2

V^{a} Voltage for solution a

V^{b} Voltage for solution b

V^{m} Voltage measurement containing cabling effect

V^{∞} Open circuit receiving voltage (V)

V_0 Amplitude of electrical impulse (V)

V_{BA} Receiving voltage of transducer A with transducer B firing (V)

V_{BC} Receiving voltage of transducer *C* with transducer *B* firing (V)

V_{CA} Receiving voltage of transducer *A* with transducer *C* firing (V)

V_{CB} Receiving voltage of transducer *B* with transducer *C* firing (V)

V_i Voltage at electrical port *i* (i=1..n)

$V_i(t)$ Source strength of a pulser in time domain (V)

$V_i(\omega)$ Source strength of a pulser in frequency domain (V/Hz)

V_L Receiving voltage across Z_L^c (V)

V_R Receiving voltage (V)

V_{th} Source of Thevenin equivalent circuit (V)

V_∞ Voltage limit at infinite time (V), Open circuit receiving voltage (V)

V_{in}^A Voltage across transducer *A* (V)

V_R^m Voltage measurement across receiving load (V)

V_{CA}^m Voltage measurement of transducer *A* with transducer *C* firing (V)

V_{CB}^m Voltage measurement of transducer *B* with transducer *C* firing (V)

V_{BA}^m Voltage measurement of transducer *A* with transducer *B* firing (V)

$\mathbf{v}$ Particle velocity vector (m/s)

$\mathbf{v}^a$ Particle velocity vector for solution *a* (m/s)

$\mathbf{v}^b$ Particle velocity vector for solution *b* (m/s)

v Lumped velocity (m/s), Particle velocity (m/s)

$\tilde{v}$ Lumped velocity (m/s)

v^a Velocity for solution *a* (m/s)

v^b Velocity for solution *b* (m/s)

v_0 Average velocity, Longitudinal velocity (m/s)

v_1 Velocity at port 1 (m/s)

v_2 Velocity at port 2 (m/s)

v_n Normal velocity (m/s)

v_r Radiation velocity (m/s)

v_T Transmitting velocity (m/s)

v_0^a Average velocity for solution *a* (m/s)

v_0^b Average velocity for solution *b* (m/s)

v_n^a Normal velocity for solution *a* (m/s)

v_n^b Normal velocity for solution *b* (m/s)

X Reaction in KLM model (Ω)

$\mathbf{x}$ Position vector (m)

$\mathbf{x}_S$ Position vector on surface S (m)

x x-coordinate

y y-coordinate

$\mathbf{Z}$ Impedance matrix

$\mathbf{Z}^T$, transpose of $\mathbf{Z}$

$Z_{11}(\Omega)$, Z_{12}(V/(m/s), N/A), Z_{21}(V/(m/s), N/A), Z_{22}(N/(m/s)), elements of $\mathbf{Z}$.

Z Acoustic impedance (N/(m/s)), Electrical impedance (Ω)

Z_a 1-D acoustic impedance (N/(m/s))

Z_0^a Acoustic impedance of piezoelectric plate (N/(m/s))

Z_1^a Acoustic impedance at port 1 (N/(m/s))

Z_2^a Acoustic impedance at port 2 (N/(m/s))

Z_b^a Backing acoustic impedance (N/(m/s))

Z_i^a Internal acoustic impedance (N/(m/s))

Z_L^a Acoustic impedance of semi-infinite medium (N/(m/s))

Z_t^a Transmitting acoustic impedance (N/(m/s))

Z_{in}^a Input acoustic impedance (N/(m/s))

Z_{th}^a Internal acoustic impedance of acoustic Thevenin equivalent circuit (N/(m/s))

Z_r^a Radiation acoustic impedance (N/(m/s))

$Z_r^{B:a}$ Radiation acoustic impedance for transducer B (N/(m/s))

$Z_r^{R:a}$ Radiation acoustic impedance for receiving transducer (N/(m/s))

$Z_r^{T:a}$ Radiation acoustic impedance for transmitting transducer (N/(m/s))

Z_1^e Electrical impedance at port 1 (Ω)

Z_2^e Electrical impedance at port 2 (Ω)

Z_c^e Intrinsic impedance of a cable (Ω)

Z_i^e Internal impedance of a pulser (Ω)

Z_{in}^e Input electrical impedance (Ω)

$Z_{in}^{A:e}$ Input electrical impedance of transducer A (Ω)

$Z_{in}^{B:e}$ Input electrical impedance of transducer B (Ω)

$Z_{in}^{R:e}$ Input electrical impedance of receiving transducer (Ω)

$Z_{in}^{T:e}$ Input electrical impedance of transmitting transducer (Ω)

Z_L^e Electrical load (Ω)

Z_o^e Intrinsic impedance of a cable (Ω), Electrical load impedance (Ω)

Z_s^e Resistance in series in a tuning circuit (Ω)

Z_{th}^e Internal electrical impedance of electrical Thevenin equivalent circuit (Ω)

z z-coordinate, Acoustic specific impedance (Rayl)

z_b Ratio of backing acoustic impedance to crystal acoustic impedance

Specific acoustic impedance of backing

z_t Specific acoustic impedance of piezoelectric plate

z_{wp} Specific acoustic impedance of wear plate

z_m Specific acoustic impedance of propagation medium

α Attenuation factor (1/s)

α_1 First attenuation of a pulser (1/s)

α_2 Second attenuation of a pulser (1/s)

β Dielectric impermittivity (m/F), Efficiency factor (V)

β^p Efficiency factor in terms of pressure (V)

β_r Reception efficiency factor in terms of force (N/V)

β_t Transmission efficiency factor in terms of force (V/N)

β_{ij}^S Dielectic impermittivity components with constant S (i, j=1..3)

β_r^p Reception efficiency factor in terms of pressure (Pa/V)

β_t^p Transmission efficiency factor in terms of pressure (V/Pa)

γ Angle introduced in Sittig's model, Wiener filter constant

ε Permittivity of medium (F/m)

ε_0 Permittivity in free space (F/m)

ε_r Relative permittivity

ε_r^S Relative permittivity with constant S

Φ Turns ratio introduced in Sittig's model (N/V)

ϕ Turns ratio introduced in KLM model (N/V)

μ Permeability of medium (H/m)

μ_0 Permeability in free space (H/m)

μ_r Relative permeability

ρ Density (kg/m^3)

ρ_1 Density of fluid (kg/m^3)

ρ_2 Density of fluid (kg/m^3)

ρ_L Density of semi-infinite medium (kg/m^3)

τ Stress matrix

τ_{ij} Stress components (i, j=1..3) (Pa)

τ_{ij}^a Stress components for solution a (i, j=1..3) (Pa)

τ_{ij}^b Stress components for solution b (i, j=1..3) (Pa)

ω Angular frequency (Rad/s)

ω_0 Antiresonant angular frequency for a crystal

∇ Gradient operator

$\tilde{\nabla}$ Gradient operator in 2-D

ABSTRACT

An ultrasonic nondestructive evaluation (NDE) measurement system is a complex collection of many elements such as the pulser/receiver, the cabling, the transducers, and the material configuration being tested. To completely model an ultrasonic measurement system, a system model, called the *electroacoustic measurement (EAM) model*, was developed. This model allows one to analyze the measurement system at many different levels, ranging from individual details to the entire system itself. The EAM model has been implemented in software using the MATLAB development environment such that one has control over the specification of the detailed system components. On the other hand, the practical use of the EAM model for commercial systems, whose explicit internal construction details are not known, requires that the model be expressed in terms of elements that can either be obtained experimentally or modeled. Thus, the EAM model has also been characterized in terms of a small number of system parameters that can either be explicitly modeled or obtained from purely electrical measurements. This advance is important, since it lays the foundation for new, quantitative transducer characterization procedures and new methods for evaluating and compensating for system variabilities.

CHAPTER 1. INTRODUCTION

An ultrasonic nondestructive evaluation (NDE) measurement system is a complex collection of many elements as shown in Figure 1.1. Each of these elements - the pulser/receiver, the cabling, the transducers, and the material configuration being tested - contributes to the signals that are measured in an NDE test. In order to completely model an ultrasonic measurement system, it is necessary to be able to characterize the contributions of each of these elements in an explicit fashion and develop an overall model of the entire system that describes how these elements are combined. In this thesis, a complete system model of this type is developed, a model called the *electroacoustic measurement (EAM) model*. Our EAM model is written in a general form that we believe is a significant new contribution. This general form allows one to analyze the measurement system at many different levels, ranging from individual details (such as, for example, the transducer crystal) to the entire system itself. The EAM model has also been implemented in software using the MATLAB development environment (see Chapter 7). The usefulness of the EAM model for transducer design purposes is demonstrated (Chapter 8) by examining how the thickness of an adhesive bond layer (between the transducer crystal and a front wear plate) affects the output waveform of the transducer.

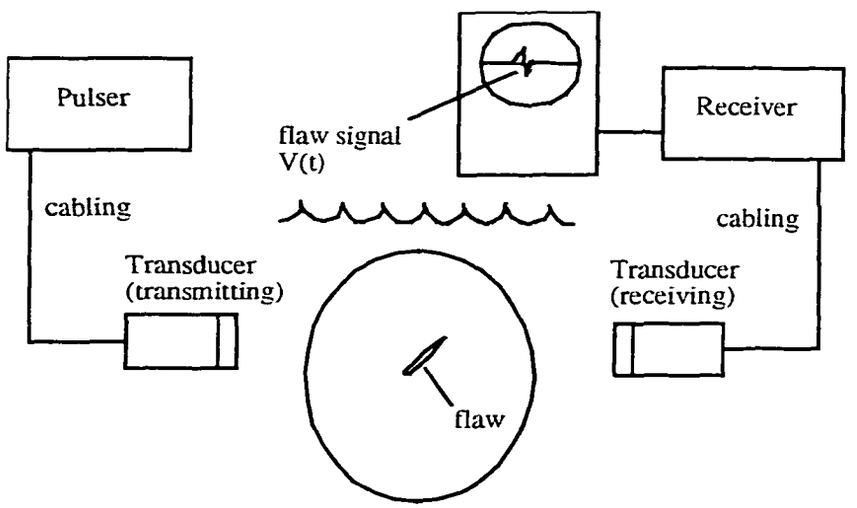

Figure 1.1 An ultrasonic NDE measurement system containing pulser/receiver, cabling, transducers and material configuration being tested.

The EAM model, because it describes all the system elements explicitly, contains numerous parameters that must be specified. For example, in the design studies of Chapter 8, a total of more than 100 parameters were required. For design and optimization studies, where one has control over the specification of the detailed system components, this is not a problem. However, in applying the EAM model to a commercial ultrasonic NDE measurement system, the explicit construction details of many of the elements are not known. Thus, the practical use of the EAM model for commercial systems requires that model be expressed in terms of elements that can either be obtained experimentally or modeled. A second major contribution of this thesis is that we have shown, using the EAM model, that a complete measurement system can be characterized in terms of a small number of system parameters that can either be explicitly modeled or that can be obtained from purely electrical measurements. This advance is important, since it lays the foundation for new, quantitative transducer characterization procedures and new methods for evaluating and compensating for system variabilities.

Because this thesis deals with the complete ultrasonic measurement system, there are many different areas in the literature that we have used. Thus, a traditional overall review of previously published work is not possible. Instead, in this chapter we will describe the pertinent publications that have contributed to the specific work in each subsequent chapter.

1.1 Chapter 2. Transducer Models

The ultrasonic transducers used in a measurement system are complex electromechanical components that play a key role in system performance. Thus, Chapter 2 examines in depth models that can be used to characterize transducer behavior. At the most fundamental level, ultrasonic transducers are devices that convert electrical fields to mechanical (acoustic) fields or vice-versa so that they could be described in terms of a set of coupled electromagnetic and mechanical fields. This type of field description, however, cannot be used practically, so that most transducer models have been based instead on "lumped" parameters such as voltage/current and force/velocity. Using the electromechanical reciprocity for a piezoelectric medium, it is possible to reduce a field model of the transducer to a lumped parameter model, as shown in the pioneering work of Foldy and Primakoff [Foldy and Primakoff, 1945, Primakoff and Foldy, 1947]. In Chapter 2, we have used reciprocity principles to give a new, much "cleaner" reduction from a field

description to a lumped parameter description of a typical immersion ultrasonic transducer. Specifically, we show that all that is needed to perform the reduction are two assumptions:

1) that the fields propagating in the coaxial cable attached to the transducer electrical port can be described by a propagating TEM mode in the cable,

2) that the 1-D force and velocity lumped parameters at the acoustic port are defined consistently in terms of integrals of the underlying pressure and velocity fields at the transducer face.

Once the reduction to lumped parameters is made for a transducer, it is easy to completely characterize the transducer in terms of a two-port network that is modeled by a 2x2 transfer matrix relating voltage/current at the transducer electrical port to force/velocity at the transducer acoustic port. There is a considerable literature available on the properties of two-port networks, much of it found in the area of microwaves, such as the books by Pozar [1998] and Karmel, Colef and Camisa [1998] where a two-port model is often referred to as an ABCD matrix model.

Two port models of an ultrasonic transducer are "black-box" models until the elements of the 2x2 transfer matrix are described explicitly in terms of the underlying transducer components, such as piezoelectric crystal, backing, electrodes, etc. Two popular explicit models of this type that have been developed are the Mason [1964] and KLM [Krimholtz, Leedom, and Matthaei, 1970, Leedom, Krimholtz, and Matthaei 1971] equivalent circuit models (see also the Redwood [1961] model). The Mason and KLM models are actually just two different equivalent circuit representations of a common three-port network model characterized by a 3x3 transfer matrix. The three ports are the transducer electrical port, the acoustic port at the backing end of the transducer piezoelectric crystal, and the acoustic port at the front (output/input) port of the crystal. The derivation of the three port model in Chapter 2 follows closely those given previously in the literature and this three port model is shown to agree with earlier work (see [Auld, 1998, Kino, 1987, and Ristic, 1983]). Once the backing port is connected to a specific type of backing material, the Mason and KLM models reduce to two-port models, where the model can be described by a product of simpler 2x2 transfer matrices, as shown by Sittig [1967, 1969, 1972]. The Sittig model is also given explicitly in Chapter 2. This transducer model is the one used in the thesis since it is in a form that most easily interfaces to the other system components and also is most convenient for describing transducers with facing acoustic layers (on the piezoelectric crystal) as found

in most commercial transducers. Chapter 2 shows that acoustic layers can also be represented by 2x2 transfer matrices.

1.2 Chapter 3. The Generation Process

The key elements involved in the production of ultrasound in an ultrasonic NDE system are the pulser, the cabling, and the (transmitting) transducer (see Figure 1.1). Chapter 3 combines models of the pulser and cabling with a two-port transducer model to describe explicitly the complete generation process. It is shown that this complete process can be characterized by a generation transfer function defined as the ratio of the force output of the transducer to the voltage input of the pulser.

In the generation process, the pulser is a complex set of electrical circuits, whose detailed components are not of particular interest. What is of practical interest is the driving voltage output by the pulser and its electrical impedance. These two quantities can be represented in terms of a simple Thevenin equivalent circuit consisting of an equivalent voltage source and complex electrical impedance, as shown in many electrical engineering texts (see [Hambly, 1997, Oppenheimer, 1984] for example). Chapter 3 uses such a Thevenin equivalent representation of the pulser. Several authors have used other equivalent circuits to also consider the effects the pulser and receiver have on the measured ultrasonic response [Hayward, 1985, 1986, Brown, 2000, Ramos, San Emeterio, Sanz, 2000]. Later (see Chapter 9), it is shown how these equivalent circuit parameters can be measured and how they depend on the energy and damping settings of the pulser. In designing ultrasonic transducers with models the impedance of the cabling and pulser are often ignored and the transducer model is driven directly by a specified voltage "spike" [Panametrics, 1989]. Chapter 3 gives a three parameter model of such a spike that is used later (Chapter 8) to provide the source for a parametric design study.

In the NDE literature there is very little discussion of cabling effects at the frequencies encountered in "normal" testing situations (1-20MHz). This is very unfortunate since it is easy to demonstrate cabling effects in a measurement setup and, as shown in Chapter 9, it is crucial to compensate for cabling effects in transducer characterization studies. In Chapter 3 the cable is modeled as a loss-free transmission line characterized by a 2x2 transfer matrix [Pozar, 1998, Magnusson, 1992, Seshadre, 1971, Balanis, 1989, Staelin, 1994]. As shown in Chapter 9, these transfer matrix elements can also be obtained experimentally by making several electrical measurements under different cable termination conditions.

In the generation of ultrasound, the acoustic output port of the ultrasonic transducer is in contact with a surrounding medium. In the case of an immersion transducer, which is the type discussed in this thesis, the surrounding medium is a fluid. The effects of this fluid loading at the output port can be represented, in a two-port transducer model, as a radiation acoustic impedance, defined as the ratio of the lumped output force of the transducer to the lumped output velocity. This radiation impedance term, Z_r^a, is likely one of the most misinterpreted terms in the ultrasonic literature. Many studies simply take this quantity, without question, as the specific acoustic impedance of a plane wave traveling in the fluid multiplied by the active area of the transducer face, i.e.

$$Z_r^a = \rho_f c_f S \qquad (1.2.1)$$

where ρ_f, c_f are the density and wave speed, respectively, of the fluid, and S is the area of the transducer face. However, an immersion transducer does not generate purely a plane wave so that it is necessary to examine in detail this assumption. As shown by Greenspan [1979], the radiation impedance of a transducer must be obtained by solving for the radiated pressure and then integrating that pressure, suitably weighted over the transducer face by the velocity distribution output of the transducer. Also shown by Greenspan [1979] the resulting radiation impedance is in general frequency dependent. In Chapter 3, and in the article by Schmerr et al [Schmerr, Dang, and Sedov, 1998] we have used Greenspan's results to examine the behavior of the radiation impedance. At the frequencies normally encountered in NDE testing, we found that at the large values of the non-dimensional wave number, *ka*, of typical NDE transducers the radiation impedance is indeed approximately a constant but that in general, for the special types of velocity distributions considered by Greenspan, we have

$$Z_r^a = \alpha \rho_f c_f S \qquad (1.2.2)$$

where $\alpha \neq 1$ unless the transducer acts like a uniform velocity (piston) source. Thus, the expression of Eq. (1.1) commonly used in the literature is correct, but only if *ka* is large enough ($ka > 10$) and the transducer acts like a piston. Furthermore, we found that if Greenspan's model is used to represent a contact transducer radiating into a solid, the assumption of a frequency independent radiation impedance is a questionable assumption at the lower frequencies (1-5 MHz) used in common NDE testing [Schmerr, Dang, and Sedov, 1998].

By combining our models of the pulser, cabling and transducer, it is possible to write an explicit expression for a generation transfer function which characterizes the entire

generation process. The form of the transfer function can be shown to be equivalent to a similar expression derived by Oakley [1997] using equivalent circuits, although a proof of that equivalency has not been included in Chapter 3.

1.3 Chapter 4. The Reception Process

Chapter 4 considers the system elements involved in the reception of ultrasound in a fashion similar to that of Chapter 3 for the generation process. One of the main differences is that on reception, the transducer is driven by "sources" in the form of acoustic wave fields rather than the pulser. It is shown that in a lumped parameter model of the reception process, the so-called blocked force acts as a "voltage" input source in conjunction with an "electrical" impedance represented by the acoustic radiation impedance of the receiving transducer. The acoustic radiation impedance involved in the reception process is the same quantity found in Chapter 3, i.e. it is the radiation impedance of the receiving transducer when it is acting as a transmitter. The blocked force is defined as the force exerted on the receiving transducer when the face of the transducer is held motionless. Many authors assume that the incident and scattered waves at the receiver are plane waves and replace the blocked force source term with a term that is just twice the force generated on the receiver face by the plane incident waves (in the absence of the transducer). In Chapter 4 we have shown that this plane wave assumption is not needed and the blocked force is the appropriate "source" term in general, consistent with the results discussed by Kinsler et al [Kinsler, Frey, Coppens, and Sanders, 1982] in their acoustics textbook (pp. 375-376).

The transducer and cabling involved in the reception process are again modeled in this chapter by 2x2 transfer matrices and the receiver is modeled as an equivalent electrical load, which can be frequency dependent, coupled to a gain (amplification) factor, that can also be a function of frequency in general. When all these elements are combined, an overall reception transfer function is defined in Chapter 4 in a form very similar to that found for the generation transfer function in Chapter 3.

1.4 Chapter 5. Acoustic Wave Propagation and Scattering

The output of the generation process is the total force generated by the transmitting transducer while the input for the reception process is the blocked force present at the receiver. To connect these two lumped parameters it is necessary to consider the 3-D acoustic wave propagation and scattering occurring between the transmitter and receiver. In

this chapter we show how an acoustic transfer function relating the 1-D lumped parameters (blocked force divided by generated force) can be defined from such complex 3-D wave processes. We use general reciprocity principles to obtain this transfer function in a flaw measurement setup in terms of an integral of the acoustic fields over the surface of the flaw. This derivation is a generalization of the mechanical reciprocity relations derived by Schmerr [1998] and the earlier electromechanical relations found by Auld [1979] and Primakoff and Foldy [Foldy and Primakoff, 1945, Primakoff and Foldy, 1947]. If the waves incident on the flaw are assumed to be quasi-plane waves (see [Schmerr, 1998]), then we show that this acoustic transfer function can be written entirely as a product of 1-D transfer function that characterizes the acoustic propagation, attenuation, diffraction, and scattering processes, a result first found by Thompson and Gray [1983] in their seminal work on an ultrasonic measurement model.

In some simple configurations it is possible to obtain the acoustic transfer function explicitly. One important case where this is possible is the calibration setup where two circular, planar piston transducers (of possibly different radii) are placed opposite to each other in a fluid in a configuration where their axes are alligned. An exact expression for the acoustic transfer function for this case is derived in Chapter 5, assuming that we can replace the blocked force by twice the incident force at the receiver. The transfer function for this same configuration has been obtained earlier by Yamada and Fujii [1966] using an infinite series approach, and by Beissner [1981] who employed the Rayleigh-Sommerfeld integral and a clever change of variables. Our derivation is more direct since it uses King's integral representation of the axisymmetric acoustic fields [Harris, 1981] and simply performs the necessary integrations directly. Our results reduce to the much earlier results of Williams [1951] who considered the special case when the radii of the two transducers were equal.

Our two-transducer model is also used in Chapter 5 to examine the influence of the size of the receiving transducer when determining the location of the last on-axis null of the generated wave field. This is an important parametric study since the location of this null is often used to determine experimentally the effective radius of the transmitting transducer [Schmerr, 1998]. Our results show that this null location is indeed very insensitive to the size the receiver used, consistent with a recent study of Goldstein et al made while this thesis was in preparation [Goldstein, Gandhi, and O'Brien, 1998].

1.5 Chapter 6. Transducer Sensitivity

In the expressions derived for the transfer functions in Chapters 3 and 4, the transducer properties appear in terms of four transfer matrix elements. Obtaining all these transfer matrix elements is called complete characterization of the transducer by Sachse and Hsu [1979]. To the best of our knowledge no one has yet demonstrated a practical method for experimentally performing a complete transducer characterization of this type. However, this chapter demonstrates that when a transducer is used in an ultrasonic measurement system it is not necessary to obtain each element in the transducer transfer matrix explicitly. Instead, as shown in section 6.2, one only needs to know three transducer functions: the transducer electrical impedance and acoustic radiation impedance (both of which quantities are defined when the transducer is acting as a transmitter) and the open circuit, blocked force transducer receiving sensitivity. This sensitivity is defined as the voltage measured at the electrical port of the transducer, when it is acting as a receiver, divided by the blocked force at the transducer acoustic port. One should note that in the literature there are a number of different sensitivities that are defined. Some of these definitions use different electrical parameters (e.g. current instead of voltage) or mechanical parameters (e.g. velocity instead of force). Some authors also change the conditions under which the quantities are measured (short circuit rather than open circuit conditions, etc.). A common choice, particularly in the acoustics literature, is to use a sensitivity based on open circuit voltage divided by the average pressure due to the incident waves only (i.e. when the transducer is absent) [Sachse and Hsu, 1979]. As Chapter 6 shows, it is possible to relate all these various sensitivities to the open circuit, blocked force sensitivity, so that in some sense it does not matter which definition of sensitivity one uses. However, it is also shown in Chapter 6 that the open circuit, blocked force sensitivity appears directly in the transfer functions for both the generation and reception processes in an ultrasonic measurement system. Thus, this particular sensitivity appears to be the natural one to choose to use.

As demonstrated in Chapter 3, the acoustic radiation impedance can be obtained directly in terms of a plane wave value if the frequency is high enough and the transducer acts like a piston source. Thus, in this case this transducer parameter can be easily found. Similarly, it is not difficult to perform an electrical measurement to obtain the electrical impedance of the transducer when it is acting as a transmitter. However, the open circuit, blocked force receiving sensitivity is not so easily obtained since its definition involves both mechanical and electrical terms. In the acoustics literature [MacLean, 1940, Wathen-Dunn,

1949, Diestel, 1961, Beatty, 1966, Beatty, Bobber and Phillips, 1966, Bobber, 1966, 1970, Rudnick, 1978, Garrett, 1979, Hill and Egle, 1980, Ludwig and Brendel, 1988, Ge, 1989] it is shown how reciprocity principles and purely electrical measurements involving three transducers can be used to obtain a transducer's open circuit sensitivity. In Chapter 6, this three transducer calibration procedure is generalized to allow one to have a general electrical loading (not open circuit conditions) at the receiving transducer electrical port. This three transducer generalized sensitivity calibration procedure is important for characterizing immersion transducers operating at ultrasonic frequencies since cabling effects are important at these frequencies and open-circuit measurements taken at the ends of the cables are not equivalent to open circuit conditions at the transducer electrical port.

An important contribution of Chapter 6 is to show that the generalized transducer sensitivity can also be obtained using purely electrical measurements and that having this generalized sensitivity one can then use it to obtain the open circuit, blocked force sensitivity parameter that appears in the transfer functions for both the generation and reception processes.

In a three transducer calibration procedure for obtaining the transducer sensitivity, an acoustic parameter appears which is called the reciprocity parameter in the acoustics literature [Simmons and Urick, 1949, Bobber and Sabin, 1961, Bobber, 1966]. In fact, acousticians have defined a number of different reciprocity parameters (plane wave, spherical wave, etc.) in a rather confusing manner. However in Chapter 6 it is shown that the appropriate acoustic parameter in the three transducer calibration method is just the acoustic transfer function defined in Chapter 5. When two transducers in the calibration procedure are far apart, the transmitting transducer looks like a point source (and the receiving transducer like a point receiver) so that the acoustic transfer function becomes essentially the spherical wave reciprocity parameter (we say "essentially" here since the acoustic transfer function and reciprocity factors differ by a constant factor). However, if instead the two transducers are placed very close together, the acoustic transfer function represents instead the plane wave reciprocity parameter. Thus, the acoustic transfer function expression given in Chapter 5 for two aligned transducers in a fluid is the appropriate "reciprocity parameter" when neither the plane wave or spherical wave limits are appropriate and diffraction effects need to be included in the calibration procedure.

Finally, in Chapter 6 an explicit expression is given for a system function which combines the pulser input voltage, the generation transfer function, and the reception transfer

function into one factor that represents all the electrical and electromechanical components of the ultrasonic measurement system. This system function is related directly to the system "efficiency" factor which can be obtained by modeling a calibration setup explicitly [Schmerr, 1998, Schmerr, Song and Zhang, 1984]. One important use of a system efficiency factor has been to extract that part of the measured ultrasonic response related directly to the flaw itself (flaw far field scattering amplitude) [Thompson and Gray, 1983]. This is important since quantitative flaw characterization is best done if effects not related to the flaw are first removed. However, in all these previous applications the system efficiency factor was treated as a "black box" that could only be obtained experimentally. In Chapter 6 the system factor is obtained in a form that expresses it in terms of its underlying components (pulser, receiver, cabling, and transducers). Thus, Chapter 6 changes this "black box" factor into an explicit term whose components can be analyzed and manipulated like all the other components in the measurement system.

1.6 Chapter 7. Electroacoustic Measurement Model

This chapter describes explicit models of all the elements of the EAM model as they were implemented in a MATLAB software package [Hanselman and Littlefield, 1998, MathWorks]. MATLAB was chosen because of its capabilities to program in a high level, matrix-based language, which is a natural environment for implementing the EAM model. MATLAB also contains graphics and GUI-building tools which make it relatively easy to develop highly visual, interactive software [Marchand, 1996, MathWorks]. Chapter 7 provides an overview of the menus, buttons and display windows of the MATLAB-based EAM model and outlines the manner in which all the parameters of the EAM model can be entered and manipulated. The particular acoustic transfer function implemented in the MATLAB package is a special case of the calibration setup considered in Chapter 5, namely two circular piston transducers of equal radius immersed in a fluid where the axes of the two transducers are aligned.

1.7 Chapter 8. Applications of the EAM Model

In this chapter we used the MATLAB-based EAM model described in Chapter 7 to conduct a number of parametric studies. The first study involved the effect that diffraction and impedance changes have on the shape of the output waveform. It is well known that as the separation distance between two aligned transducers increases, the result on the received

waveform is analogous to a differentiation process [Schmerr, 1998]. What is less well known is that reducing the impedance at the receiver also can produce similar differentiation effects. The first study of this chapter describes the underlying theoretical basis for these diffraction and impedance-based effects and demonstrates them explicitly with the MATLAB-based EAM model.

In 1983, Papadakis used a model similar to the EAM model to conduct a series of transducer design studies [Papadakis, 1983]. To help validate our EAM model, we attempted in this chapter to reproduce some of the example output waveforms generated by Papadakis. We were only partially successful in making this comparison. In three of the cases considered by Papadakis our output waveforms were very similar in shape to his but differed in their absolute amplitudes. In two other cases our output waveforms were quite different from those given in [Papadakis, 1983]. These differences are likely due to the fact that we were unable to extract all the needed model parameters from Papadakis' paper, forcing us to substitute reasonable "guesses" in a number of instances.

In 1988, Silk et al [Silk, Bainton and Hillier, 1988] discussed the effect that the thickness of a bonding layer (between the transducer crystal and a facing plate) has on the transducer output response. They found that the transducer output was extremely sensitive to the bond thickness, suggesting that this was a key parameter that needs to be strictly controlled in a transducer design. Thus, in this chapter we also used the EAM model to examine this important parameter. We found that the output waveform was indeed highly affected by the bond line thickness. In fact, as the bond thickness increased from 0.0 mm to just 0.1 mm, the amplitude of the received signal fell by almost an order of magnitude. In addition, as the thickness of the layer increased, the output signal predicted by the EAM model showed the emergence of a large "ringing", which is consistent with the behavior described by Silk et al [Silk, Bainton and Hillier, 1988].

We should note that most of the modeling simulations that have been described in the literature have been for ideal, noise-free systems. Similarly, in the EAM model the only losses that are currently implemented are those due to material attenuation. The electrical and electromechanical elements of the EAM model are all assumed to be free of both losses and noise. However, Oakley [Oakley, 1997] has recently included noise sources in both the transmitting and receiving circuits of a system model similar to the EAM model. Thus, it is possible to extend the present EAM model to handle noise effects and other loss terms explicitly.

1.8 Chapter 9. Characterization of Ultrasonic System Components

The EAM model contains models of all the components of an ultrasonic measurement system and assumes that one has access to all the underlying parameters in each of those components. For system design studies of the type discussed in the last chapter this is a reasonable approach. However, in applying the EAM model to commercial systems, many of these underlying parameters (pulser/receiver electrical circuits, transducer crystal properties, etc.) may not be accessible so that it is important to be able to characterize experimentally the various EAM components. In this chapter, it is demonstrated that all the electrical and electromechanical components of the EAM model can be written entirely in terms of parameters that can be obtained experimentally with purely electrical measurements. The chapter also describes in detail the experimental procedures for characterizing these components. A special voltage/current probe was constructed for many of these measurements, based on a design developed by Barnard et al [Barnard, Dace, Rehbein and Buck, 1997] for conducting acoustic harmonic generation studies. With this probe and other standard electrical measurement setups, the electrical properties needed to characterize the pulser, receiver, and cabling were obtained. The cabling measurements, in particular, showed that at ultrasonic frequencies the cabling transfer matrix is strongly frequency dependent. Thus, cabling effects cannot be ignored when analyzing ultrasonic systems. This is in contrast to acoustic systems operating at, say, 0 – 100kHz, where the cabling passes the signal through the system without modification.

Our specific approach outlined in this chapter for calculating the generalized transducer sensitivity is new but there have been some previous papers in the literature that have determined sensitivities of ultrasonic transducers. Fay, Ludwig, and Reimann [1989], for example, have determined the sensitivity of contact transducers used in pulse-echo setups. Actually, they calculated a product of both transmitting and receiving sensitivities for the transducer, and used several different reference setups (reflection from plane and cylindrical surfaces, direct contact) and a very simple transducer model in their studies. Fay and Reimann [1994] later used similar procedures but with a spherical reference surface as a reflector instead. Brendel and Ludwig [1976] have also used standard acoustic reciprocity principles for analyzing ultrasonic immersion probes. They included correction factors for loading (non-open circuit conditions), diffraction losses, attenuation and a factor to account for differences between the blocked force and twice the incident force on the receiving transducer, but they did not give explicit procedures, as we have, for obtaining such

correction factors. Thus, we believe it is fair to say that we have demonstrated for the first time a complete, explicit procedure for obtaining the sensitivities of ultrasonic immersion transducers and demonstrated how those sensitivity measurements play a fundamental role in the overall ultrasonic system response.

1.9 Chapter 10. Ultrasonic Measurement System Characterization

In this chapter we have combined the measurements of all the components of an ultrasonic system and showed that we could accurately simulate the measured voltage versus time output of a particular ultrasonic NDE measurement system. For this simulation we used the setup considered in previous chapters where two transducers were aligned in a fluid. We also demonstrated in this chapter our ability to synthesize for this setup the system factor as a function of frequency, a result that also agreed well with a direct measurement of this same function through deconvolution procedures [Schmerr, 1998]. To our knowledge, this is the first time that such a complete synthesis of a measured ultrasonic response has been made from measurements of its individual components. Having this capability will give us the ability to characterize and analyze ultrasonic systems in new ways, but further studies of this type are left to future, as discussed in Chapter 11.

1.10 Chapter 11. Summary and Conclusions

In this final chapter we outline the major accomplishments of the thesis. Some places where our modeling work can be extended are described and some suggestions for using this new modeling capability in practical applications are given.

CHAPTER 2. TRANSDUCER MODELS

An ultrasonic transducer is an electromechanical device that transforms electrical energy into mechanical energy, or vice versa. It will be shown in this chapter that models of this transform process can be developed at several levels. At the most fundamental level, the transducer can be described in terms of the electromagnetic and mechanical fields present. This model, while general, is usually not practical to use. However, as shown in section 2.1, if some assumptions are made on the nature of the fields present at the input and output surfaces of the transducer and the transducer is assumed to satisfy reciprocity, the general field model can be reduced to a two-port network model. This two-port network model, replaces the underlying fields with "lumped" input-output parameters such as (voltage, current) and (force, velocity).

Section 2.2 describes some of the important properties of two-port networks as represented in both impedance matrix and transfer matrix forms, and discusses "cascades" of such two-port systems which will be useful later in describing the connection of ultrasonic transducers to other system components, such as cabling.

A different modeling approach is described in section 2.3, where the fields in the transducer are assumed to be one-dimensional disturbances present in a piezoelectric plate. This model leads to a description of the transducer as a three-port model in terms of lumped electrical and mechanical parameters. It is shown that this three-port piezoelectric model can be represented in terms of the two well-known equivalent circuit models called the Mason and KLM models [Mason, 1964, Krimholtz, Leedom and Matthaei, 1970, Selfridge and Gehlbach, 1985].

The three ports present in the models of section 2.3 represent the electrical, acoustical facing, and acoustical backing conditions of the piezoelectric plate. If the acoustical backing conditions for those models are specified, then, as section 2.4 shows, the three-port models reduce to two-port models of the type described in sections 2.1 and 2.2, where the impedance and transfer matrices are known in explicit form. These results are shown to be consistent with a similar model developed by Sittig [1967, 1969, 1972].

Acoustical backings and facings of ultrasonic transducers can involve the presence of several acoustic layers. The wear plate of a contact transducer, for example, is such a layer. Section 2.5 describes these acoustic layers as an acoustic transmission line which can be represented in either equivalent circuit or transfer matrix forms.

2.1 Electromechanical Reciprocity in Transducer Models

A highly idealized model of an ultrasonic transducer is shown in Figure 2.1. Inside the transducer, we assume that electrical, mechanical, and electromechanical fields are present that can be described in general in terms of the fields of linear piezoelectricity. However, at the surface S_1 we assume that the transducer only transfers electrical energy through a connected cable and that at the surface S_2 the transducer only transfers mechanical energy into an adjacent medium. We also assume that there are no electromagnetic or mechanical sources within the transducer itself, i.e. it is a passive device.

On surface S_1, the electromagnetic quantities are the electric field intensity $\mathbf{E}$ and the magnetic field intensity $\mathbf{H}$. On surface S_2, the mechanical quantities are the traction $\mathbf{t}$ and the particle velocity $\mathbf{v}$. The unit normal vector, $\mathbf{n}$, for both of these surfaces is taken as positive outwards.

The reciprocal theorem for a linear piezoelectric medium (see [Schmerr, 1998], for example) can be applied to the conservative transducer system shown in Figure 2.1. Without loss of generality, we can consider $\mathbf{E}$ and $\mathbf{H}$ as input quantities and $\mathbf{t}$ and $\mathbf{v}$ as output quantities. Now consider two solutions: solution a and solution b. In solution a, the field quantities are $\mathbf{E}^a$, $\mathbf{H}^a$, $\mathbf{t}^a$, and $\mathbf{v}^a$. In solution b, the field quantities are $\mathbf{E}^b$, $\mathbf{H}^b$, $\mathbf{t}^b$, and $\mathbf{v}^b$. The reciprocal theorem, thus, gives [Schmerr, 1998],

$$\int_{S_1} \left(\mathbf{E}^b \times \mathbf{H}^a - \mathbf{E}^a \times \mathbf{H}^b\right) \cdot \mathbf{n} dS + \int_{S_2} \left(\mathbf{t}^a \cdot \mathbf{v}^b - \mathbf{t}^b \cdot \mathbf{v}^a\right) dS = 0 . \qquad (2.1.1)$$

First consider the integral of electromagnetic terms in Eq. (2.1.1). Our goal is to express this integral in terms of the corresponding lumped quantities, i.e., the voltage V and the current I imposed on the cable.

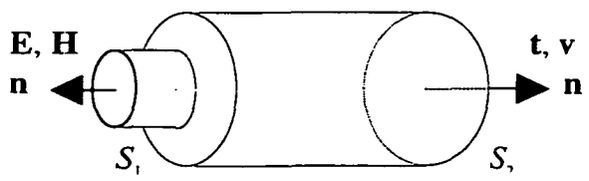

Figure 2.1 Transducer model considered as a conservative system with electromagnetic energy transfer via surface S_1 and mechanical energy transfer via surface S_2.

Generally, a cable can be considered as a transmission line which has two wires: an outer wire c_1 and an inner wire c_2. Assume that the cable is lossless and the inner wire is a perfect conductor. When the outer wire is grounded, the potential on the inner wire is the voltage V. The cross section of a cable is shown in Figure 2.2.

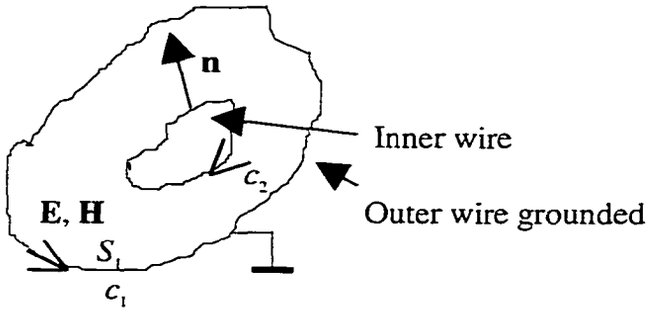

Figure 2.2 Cross section of a general cable with inner and outer wires where TEM wave propagates. The inner wire is a perfect conductor and the outer wire grounded.

We will now show that in order to reduce the electromagnetic integral in Eq.(2.1.1) to equivalent lumped parameters, we only need to make the assumption that the fields in the cable can be described in terms of propagating TEM waves [Balanis, 1989]. For such TEM waves, it can be shown [Seshadre, 1971, Bladel, 1985, Staelin, 1994] that on S_1 the fields satisfy the conditions.

$$\mathbf{E}(x,y,z=0) = -\tilde{\nabla} V(x,y,z=0) \tag{2.1.2}$$

$$\tilde{\nabla} \times \mathbf{H}(x,y,z=0) = 0 \tag{2.1.3}$$

where S_1 and the contours (c_1, c_2) are assumed to lie in the x-y plane ($z=0$) and

$$\tilde{\nabla} = \mathbf{e}_x \frac{\partial}{\partial x} + \mathbf{e}_y \frac{\partial}{\partial y} \tag{2.1.4}$$

is the two dimensional gradient in that plane. On the grounded outer boundary, c_1, $V=0$, while on the inner boundary, c_2, $V(x,y,z=0) = V =$ a constant.

Now consider the following identity

$$\tilde{\nabla} \times (V\mathbf{H}) = V(\tilde{\nabla} \times \mathbf{H}) + (\tilde{\nabla} V) \times \mathbf{H}. \tag{2.1.5}$$

Using Eq. (2.1.2) and Eq. (2.1.3), Eq. (2.1.5) is simplified as

$$\mathbf{E} \times \mathbf{H} = -\tilde{\nabla} \times (V\mathbf{H}). \tag{2.1.6}$$

By applying Eq. (2.1.6), the first term in Eq. (2.1.1) becomes

$$m_1 \equiv \int_{S_1} \left(\mathbf{E}^b \times \mathbf{H}^a - \mathbf{E}^a \times \mathbf{H}^b\right) \cdot \mathbf{n} dS = \int_{S_1} \left[-\tilde{\nabla} \times \left(V^b \mathbf{H}^a\right) + \tilde{\nabla} \times \left(V^a \mathbf{H}^b\right)\right] \mathbf{n} dS. \quad (2.1.7)$$

Thus using the Stoke's theorem in 2-D, we have

$$m_1 \equiv \int_{c_1 + c_2} \left(-V^b \mathbf{H}^a + V^a \mathbf{H}^b\right) \cdot d\mathbf{l} \quad (2.1.8)$$

where c_1 is the boundary of the outer wire and c_2 the boundary of the inner wire. But on c_1 and c_2,

$$V^a\big|_{c_1} = V^b\big|_{c_1} = 0 \quad (2.1.9)$$

$$V^a\big|_{c_2} = V^a \text{ and } V^b\big|_{c_2} = V^b \quad (2.1.10)$$

where V^a and V^b are constants. Therefore, Eq. (2.1.8) is simplified as

$$m_1 \equiv V^a \int_{c_2} \mathbf{H}^b \cdot d\mathbf{l} - V^b \int_{c_2} \mathbf{H}^a \cdot d\mathbf{l}. \quad (2.1.11)$$

From Maxwell-Ampere's law, however, it follows that

$$\int_{c_2} \mathbf{H} \cdot d\mathbf{l} = I \quad (2.1.12)$$

where I is the current flowing into the inner wire, i.e., -**n** direction, by the right hand rule. Thus, Eq. (2.1.11) reduces finally to

$$m_1 \equiv V^a I^b - V^b I^a \quad (2.1.13)$$

or, more explicitly,

$$\int_{S_1} \left(\mathbf{E}^b \times \mathbf{H}^a - \mathbf{E}^a \times \mathbf{H}^b\right) \cdot \mathbf{n} dS = V^a I^b - V^b I^a. \quad (2.1.14)$$

This equation gives the relationship between the electromagnetic field quantities (**E** and **H**) and electrical lumped quantities (V and I) in the representation of energy transfer through the cable connected to a transducer.

Now consider the second integral in Eq. (2.1.1). In an immersion measurement, transducers emit and receive acoustic waves through fluids, usually water. Since there is no shear force in a fluid, the traction takes the form of hydrostatic stress, i.e.,

$$\mathbf{t} = -p\mathbf{n} \quad (2.1.15)$$

where p is the pressure on surface S_2, which is frequency and spatially dependent, and **n** is the outward normal of surface S_2. Then

$$\mathbf{t} \cdot \mathbf{v} = -p\mathbf{n} \cdot \mathbf{v} = -pv_n \quad (2.1.16)$$

where v_n is the normal velocity on surface S_2, which is also frequency and spatially dependent.

The second integral in Eq. (2.1.1) is expressed as

$$m_2 \equiv \int_{S_2} \left(\mathbf{t}^a \cdot \mathbf{v}^b - \mathbf{t}^b \cdot \mathbf{v}^a\right) dS = \int_{S_2} \left(-p^a v_n^b + p^b v_n^a\right) dS . \qquad (2.1.17)$$

In many immersion transducer models, the normal velocity is assumed to be spatially uniform over the surface S_2. However, this assumption is not necessary to arrive at a lumped representation. All that is needed is to assume that the normal velocity can be written in a separable form [Schmerr, Dang and Sedov, 1998]

$$v_n(\mathbf{x}_s, \omega) = v_0(\omega) f(\mathbf{x}_s) \qquad (2.1.18)$$

where $v_0(\omega)$ is a velocity amplitude at frequency ω and $f(\mathbf{x}_s)$ is a spatial distribution function of the position $\mathbf{x}_s$ on the surface S_2. Note that f can be always normalized such that $v_0(\omega)$ is the average velocity, which is the case we will assume henceforth.

Now consider the following integral,

$$\int_{S_2} p v_n dS = \int_{S_2} p(\mathbf{x}_s, \omega) v_0(\omega) f(\mathbf{x}_s) dS . \qquad (2.1.19)$$

This integral can be written as

$$\int_{S_2} p v_n dS = F(\omega) v_0(\omega) \qquad (2.1.20)$$

if we define the "force", $F(\omega)$, to be the weighted pressure integral given by

$$F(\omega) = \int_{S_2} p(\mathbf{x}_s, \omega) f(\mathbf{x}_s) dS . \qquad (2.1.21)$$

Note that only in the case when the normal velocity distribution is uniform ($f = 1$) is this "force" equal to the average pressure multiplied by the area of S_2, as is commonly assumed in transducer models.

Using Eq. (2.1.20), m_2 in Eq. (2.1.17) becomes

$$m_2 \equiv -F^a v_0^b + F^b v_0^a \qquad (2.1.22)$$

or,

$$\int_{S_2} \left(\mathbf{t}^a \cdot \mathbf{v}^b - \mathbf{t}^b \cdot \mathbf{v}^a\right) dS = -F^a v_0^b + F^b v_0^a . \qquad (2.1.23)$$

This equation gives the relationship between the mechanical field quantities ($\mathbf{t}$ and $\mathbf{v}$) and mechanical lumped quantities (F and v) in the representation of energy transfer through the front surface of a transducer.

Using Eqs. (2.1.14) and (2.1.23), the field-based electromechanical reciprocity relationship form Eq. (2.1.1) reduces to the equivalent "lumped" form

$$V^a I^b - V^b I^a = F^a v^b - F^b v^a . \qquad (2.1.24)$$

From now on, the subscripts "0" will be dropped from the normal velocity terms v^a and v^b to simplify the notation.

Consider a set of lumped transducer input-output parameters (V, I, F, v) for a given problem, and two other sets (V^a, I^a, F^a, v^a), (V^b, I^b, F^b, v^b), for two other problems a, and b for the same transducer. Application of Eq. (2.1.24) twice, with the given problem and problem a, and with the given problem and problem b, respectively, then will yield two equations which can be written in the form of either a 2x2 "impedance" matrix or a 2x2 "transfer" matrix. The transfer matrix form, for example, is given by

$$\begin{Bmatrix} V \\ I \end{Bmatrix} = \begin{bmatrix} T_{11} & T_{12} \\ T_{21} & T_{22} \end{bmatrix} \begin{Bmatrix} F \\ v \end{Bmatrix}. \tag{2.1.25}$$

Eq. (2.1.25) shows that our reciprocal transducer model can always be represented by a two-port network, which is usually drawn schematically as a box with input/output "voltages" and "currents" as shown in Figure 2.3

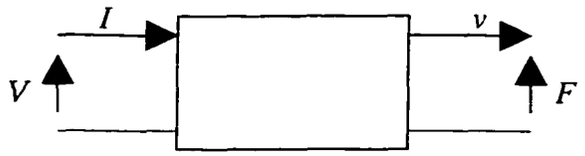

Figure 2.3 An ultrasonic transducer modeled by a two-port network with two pairs of lumped parameters: electric voltage and current (V, I) and mechanical force and velocity (F, v). Note that current goes into and velocity goes out of the network.

The transducer model shown in Figure 2.3 is the one we will use for the transmitting case. For the receiving case, it is convenient to reverse the directions of the current and velocity, a convention we will adopt on the receiver side.

Since a transducer can be modeled by a two-port network, there are many important network theorems that are useful for analyzing the behavior of the transducer. We will derive some of the theorems that will be particularly applicable to our work in the next section.

2.2 Two-Port Network Reciprocity Properties

As shown in the last section the input-output parameters of our reciprocal transducer model can always be represented in terms of a 2x2 matrix, either of the transfer matrix type (as shown) or in an impedance matrix form (as will be discussed shortly). These matrices also possess some particular properties that are a direct consequence of reciprocity.

These properties include that (1) the impedance matrix is symmetric, (2) the determinant of the transfer matrix is unity, and (3) a cascade of reciprocal two-port networks is also reciprocal. Additionally, we will show that the transformation between impedance and transfer matrices is very simple due to the first two properties. The details of these properties are studied in the following three subsections.

2.2.1 Impedance matrix form

When a two-port network is expressed in terms of an impedance matrix, the traditional convention is that the currents flowing into an electric network are considered positive. Thus, in terms of lumped quantities shown in Figure 2.3, one two-port network can be represented by an impedance matrix equation in the form

$$\begin{Bmatrix} V \\ F \end{Bmatrix} = \begin{bmatrix} Z_{11} & Z_{12} \\ Z_{21} & Z_{22} \end{bmatrix} \begin{Bmatrix} I \\ -v \end{Bmatrix} \tag{2.2.1}$$

where $-v$ is the velocity ("current") flowing into the network.

To rewrite the reciprocity expression in Eq. (2.1.24), we define two column vectors,

$$\mathbf{V} = \begin{Bmatrix} V \\ F \end{Bmatrix} \tag{2.2.2}$$

$$\mathbf{I} = \begin{Bmatrix} I \\ -v \end{Bmatrix} \tag{2.2.3}$$

and denote the impedance matrix in Eq. (2.2.1) as

$$[\mathbf{Z}] = \begin{bmatrix} Z_{11} & Z_{12} \\ Z_{21} & Z_{22} \end{bmatrix}. \tag{2.2.4}$$

Then the matrix equation Eq. (2.2.1) is written as

$$\mathbf{V} = [\mathbf{Z}]\mathbf{I}. \tag{2.2.5}$$

Eq. (2.1.24) can be changed from the scalar form,

$$\left[V^a I^b + F^a\left(-v^b\right)\right] - \left[V^b I^a + F^b\left(-v^a\right)\right] = 0 \tag{2.2.6}$$

using Eq. (2.2.2) and Eq. (2.2.3), into the equivalent vector form

$$\mathbf{V}^a \cdot \mathbf{I}^b - \mathbf{V}^b \cdot \mathbf{I}^a = 0. \tag{2.2.7}$$

Putting Eq. (2.2.5) into the above equation, then we have

$$[\mathbf{Z}]\mathbf{I}^a \cdot \mathbf{I}^b - [\mathbf{Z}]\mathbf{I}^b \cdot \mathbf{I}^a = 0. \tag{2.2.8}$$

But, according to the definition of matrix transpose, we have

$$[\mathbf{Z}]\mathbf{I}^b \cdot \mathbf{I}^a = [\mathbf{Z}]^T \mathbf{I}^a \cdot \mathbf{I}^b \tag{2.2.9}$$

so Eq. (2.2.8) can be rewritten as

$$\{[\mathbf{Z}]-[\mathbf{Z}]^T\}\mathbf{I}^a\cdot\mathbf{I}^b=0 \tag{2.2.10}$$

which shows, since $\mathbf{I}^a$ and $\mathbf{I}^b$ are arbitrary, that

$$[\mathbf{Z}]=[\mathbf{Z}]^T. \tag{2.2.11}$$

Therefore, when a transducer is described by an impedance matrix equation, the impedance matrix is symmetric, i.e.,

$$Z_{12}=Z_{21}. \tag{2.2.12}$$

2.2.2 Transfer matrix form

As shown previously, a transfer matrix equation can also be used to describe the transducer model shown in Figure 2.3, which takes the form

$$\begin{Bmatrix} V \\ I \end{Bmatrix}=\begin{bmatrix} T_{11} & T_{12} \\ T_{21} & T_{22} \end{bmatrix}\begin{Bmatrix} F \\ v \end{Bmatrix}. \tag{2.2.13}$$

Here we will show that, in transfer matrix form, reciprocity requires the determinant of the transfer matrix be unity. The proof is as follows.

First, we rewrite Eq. (2.2.13) in the form of Eq. (2.2.1). We find

$$\begin{cases} Z_{11}=T_{11}/T_{21} \\ Z_{12}=(T_{11}T_{22}-T_{12}T_{21})/T_{21} \\ Z_{21}=1/T_{21} \\ Z_{22}=T_{22}/T_{21} \end{cases}. \tag{2.2.14}$$

Symmetry of the impedance matrix (Eq. (2.2.12)) requires that the second equation and the third equation in Eq. (2.2.14) be equal. Therefore,

$$T_{11}T_{22}-T_{12}T_{21}=1 \tag{2.2.15}$$

or,

$$|[\mathbf{T}]\equiv\det[\mathbf{T}]=1. \tag{2.2.16}$$

In Eq. (2.2.13), the electrical quantities are expressed in terms of the mechanical quantities. Using Eq. (2.2.15) or Eq. (2.2.16), Eq. (2.2.13) can be inverted and the mechanical quantities expressed in terms of the electrical quantities as

$$\begin{Bmatrix} F \\ v \end{Bmatrix}=\begin{bmatrix} T_{22} & -T_{12} \\ -T_{21} & T_{11} \end{bmatrix}\begin{Bmatrix} V \\ I \end{Bmatrix}. \tag{2.2.17}$$

From Eqs. (2.2.14)-(2.2.15), inversely, every element in [T] can be expressed in terms of the elements in [Z] as follows

$$\begin{cases} T_{11} = Z_{11}/Z_{12} \\ T_{12} = |[\mathbf{Z}]|/Z_{12} \\ T_{21} = 1/Z_{12} \\ T_{22} = Z_{22}/Z_{12} \end{cases} \tag{2.2.18}$$

where

$$|[\mathbf{Z}]| = Z_{11}Z_{22} - Z_{12}Z_{21}. \tag{2.2.19}$$

Thus, Eq. (2.2.13) can be rewritten as

$$\begin{Bmatrix} V \\ I \end{Bmatrix} = \frac{1}{Z_{12}} \begin{bmatrix} Z_{11} & |[Z]| \\ 1 & Z_{22} \end{bmatrix} \begin{Bmatrix} F \\ v \end{Bmatrix}. \tag{2.2.20}$$

Similarly, from Eqs. (2.2.1), (2.2.14) and (2.2.15), we have

$$\begin{Bmatrix} V \\ F \end{Bmatrix} = \begin{bmatrix} T_{11}/T_{21} & 1/T_{21} \\ 1/T_{21} & T_{22}/T_{21} \end{bmatrix} \begin{Bmatrix} I \\ -v \end{Bmatrix}. \tag{2.2.21}$$

With Eqs. (2.2.20) and (2.2.21), knowing either the impedance matrix or transfer matrix representation, the other representation can be obtained directly.

2.2.3 Cascading transfer matrices

In practice, a transducer is used in combination with other components. For example, a cable is used to connect a transducer to a pulser or receiver. There is also a wear plate attached to the front surface of a transducer. In addition, there might be a tuning circuit attached to the transducer crystal. All of these components can be modeled by reciprocal two-port networks. Therefore, in the ultrasonic generation process and reception process, we typically must consider a cascade of two-port networks (Figure 2.4).

Suppose that there are n two-port networks. Following the convention shown in Figure 2.3, these two-port networks are denoted by $\mathbf{T}_1$, $\mathbf{T}_2$, ..., $\mathbf{T}_n$, respectively, and are shown in Figure 2.4.

For network $\mathbf{T}_i$ ($1 \le i \le n$), its transfer matrix equation is written as, from Eq. (2.2.13),

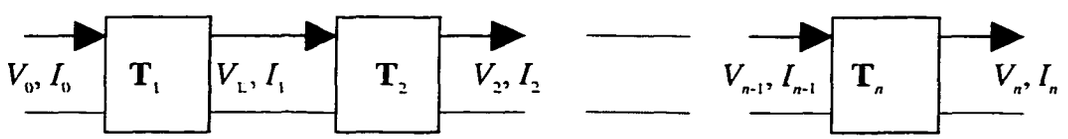

Figure 2.4 Cascade of n reciprocal two-port networks, $\mathbf{T}_1$, $\mathbf{T}_2$, ..., and $\mathbf{T}_n$. The outputs of $\mathbf{T}_i$ are the inputs of $\mathbf{T}_{i+1}$ ($1 \le i < n$).

$$\begin{Bmatrix} V_{i-1} \\ I_{i-1} \end{Bmatrix} = [\mathbf{T}_i] \begin{Bmatrix} V_i \\ I_i \end{Bmatrix}. \tag{2.2.22}$$

Note that, except (V_0, I_0) and (V_n, I_n), (V_i, I_i) with $(1 \le i < n)$ are the outputs of network $\mathbf{T}_i$ and the inputs of $\mathbf{T}_{i+1}$. Repeatedly using Eq. (2.2.22), we have

$$\begin{Bmatrix} V_0 \\ I_0 \end{Bmatrix} = [\mathbf{T}_1][\mathbf{T}_2] \cdot \ldots \cdot [\mathbf{T}_n] \begin{Bmatrix} V_n \\ I_n \end{Bmatrix}. \tag{2.2.23}$$

Thus, if we define a global matrix $[\mathbf{T}^G]$ as

$$[\mathbf{T}^G] = [\mathbf{T}_1][\mathbf{T}_2] \ldots [\mathbf{T}_n] \tag{2.2.24}$$

then Eq. (2.2.23) is written as

$$\begin{Bmatrix} V_0 \\ I_0 \end{Bmatrix} = [\mathbf{T}^G] \begin{Bmatrix} V_n \\ I_n \end{Bmatrix}. \tag{2.2.25}$$

This implies that the cascaded networks in Figure 2.4 can be replaced by a single global two-port network as shown in Figure 2.5.

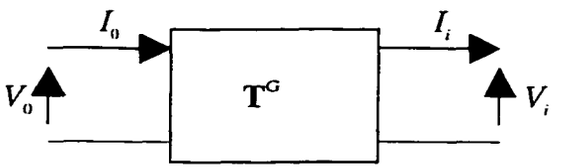

Figure 2.5 Reciprocal global two-port network obtained from the cascade of reciprocal two-port networks shown in Figure 2.4. The global inputs (V_0, I_0) are the inputs of $\mathbf{T}_1$ in Figure 2.4 and the global outputs (V_n, I_n) are the outputs of $\mathbf{T}_n$.

If every two-port network is reciprocal, i.e.,

$$|[\mathbf{T}_i]| = 1 \qquad \text{for } i=1, 2, \ldots, n \tag{2.2.26}$$

then from the property of matrices, we have

$$|[\mathbf{T}^G]| = |[\mathbf{T}_1]| \cdot |[\mathbf{T}_2]| \cdot \ldots \cdot |[\mathbf{T}_n]| = 1 \tag{2.2.27}$$

i.e., the global two-port network is also reciprocal and all the theorems of section 2.2 apply also to this global network. This can also be shown by resorting to the original reciprocal identity of Eq. (2.1.24). In Figure 2.4, we have

$$\begin{cases} V_0^a I_0^b - V_0^b I_0^a = V_1^a I_1^b - V_1^b I_1^a & \text{(for network } \mathbf{T}_1\text{)} \\ V_1^a I_1^b - V_1^b I_1^a = V_2^a I_2^b - V_2^b I_2^a & \text{(for network } \mathbf{T}_2\text{)} \\ \ldots\ldots & \ldots\ldots \\ V_{n-1}^a I_{n-1}^b - V_{n-1}^b I_{n-1}^a = V_n^a I_n^b - V_n^b I_n^a & \text{(for network } \mathbf{T}_n\text{)}. \end{cases} \tag{2.2.28}$$

Adding all of the equations in Eq. (2.2.28) and canceling out all common terms, we have

$$V_0^a I_0^b - V_0^b I_0^a = V_n^a I_n^b - V_n^b I_n^a \quad . \tag{2.2.29}$$

This equation shows that the global network shown in Figure 2.5 is reciprocal.

Therefore, in an ultrasonic measurement system, if all the electrical and electromechanical components satisfy the reciprocal theorem, then the global transfer matrices relating the inputs and outputs in the total generation and reception processes also satisfy the reciprocal theorem.

2.3 1-D Transducer Model

In section 2.1, we showed that if a transducer is modeled as a reciprocal system where (1) a TEM mode carries electrical energy to/from the transducer in an attached cable and (2) the velocity on the transducer face can be written in a separable from, then the transducer can be characterized by a two-port network with one electrical port and one mechanical port. This was a very general result, i.e., no assumptions were made about the explicit nature of the fields within the transducer itself other than that they must be conservative and satisfy reciprocity. As a consequence, the impedance and transfer matrices of the previous section are "black boxes" in that we cannot relate their components to the specific design characteristics of a particular transducer. In this section, we model the field of a piezoelectric transducer directly by considering the transducer to be a piezoelectric plate vibrating in a fundamental thickness mode where the field variations occur in a simple 1-D manner. It will be shown that this 1-D model leads to a representation of the transducer crystal as a three-port network containing an electrical port, a mechanical (output) port and a mechanical (backing) port. In the following section, it will be shown that when the backing port is connected to an acoustical impedance, the three-port model reduces to a two-port system where the impedance and transfer matrices of the previous section can be given in explicit forms.

A three-port electromechanical model also can be represented in equivalent circuit form. See, for example, the Mason equivalent circuit [Mason, 1964], the KLM equivalent circuit [Krimholtz, Leedom, and Matthaei, 1970] and the model derived by Redwood [1961]. Of these models, the Mason equivalent circuit and the KLM equivalent circuit are the two models most commonly used for transducer design purpose [Silk, 1984, Selfridge, 1985]. In

this section, we will derive the Mason equivalent circuit for thickness-mode transducers and show the equivalence of the Mason and KLM circuit models.

2.3.1 Piezoelectric plate as a three-port network

In ultrasonic testing, thickness-mode transducers are widely used. A transducer of this type generally consists of three parts: a protection layer, a piezoelectric plate and a backing material. The key part of a transducer is the piezoelectric plate which converts electric energy into mechanical energy and vice versa. The piezoelectric plate can be characterized by a three-port network.

A typical thickness mode piezoelectric plate is shown in Figure 2.6. The plate thickness is l which is assumed to be much less than the width and length of the plate. The plate expands and contracts in its thickness direction. With the vibration of the plate, its two side surfaces emit acoustic waves in opposite directions. The two side surfaces thus act as two mechanical ports. When the two side surfaces are also plated with thin layers of a conducting material, electrical energy can be imposed on the two surfaces. Electrical leads connected to the plated surfaces then act as the third electrical port.

The piezoelectric plate can transfer energy from its electrical port to its two mechanical ports, or inversely from its mechanical ports to its electrical port. When an electric impulse is imposed on the electrical port, it drives the piezoelectric plate to vibrate and thus emit mechanical waves from the two mechanical ports. On the other hand, when either side surface, or both, of the plate experiences forces, voltage is induced on the electrical port. Such energy transfer phenomenon is the property of the piezoelectric plate.

The piezoelectric plate shown in Figure 2.6 can be abstracted as a three-port network with two pairs of mechanical terminals, which form two mechanical ports and one pair of

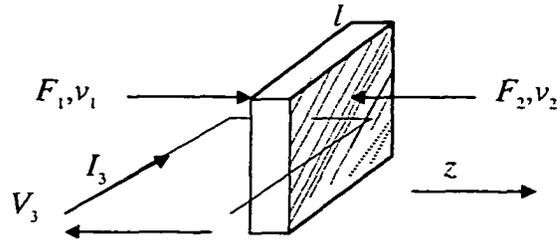

Figure 2.6 A thickness mode piezoelectric plate with the thickness of l which is much less than its width and length.

electrical terminals, which form one electrical port. The three-port network is shown in Figure 2.7. After we obtain the three-port model of the piezoelectric plate, the general principles and theorems for electrical circuits will be used to relate the three-port model to the equivalent Mason and KLM circuit models.

The three-port network contains three pairs of quantities. These quantities are explained as follows. (F_1, v_1) and (F_2, v_2) are two force-velocity pairs at the two mechanical ports, port 1 and port 2, respectively, and (V_3, I_3) are voltage-current pair at the electrical port, port 3. We suppose that the positive particle velocities at the two mechanical ports are inward. These velocities, v_1 and v_2, may be viewed as inward "currents" in the model and the forces, F_1 and F_2, similarly viewed as "voltages" to make it convenient to study the electromechanical phenomenon using purely electrical principles.

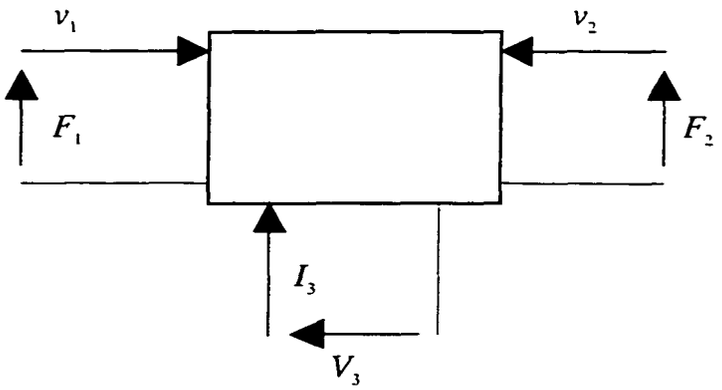

Figure 2.7 Piezoelectric plate abstracted as a three-port network with two mechanical ports and one electrical port.

The electrical equivalent mechanical quantities, (F_1, v_1) and (F_2, v_2), must be carefully related to their corresponding field variables, which in this 1-D model, will be the velocity, $v(z)$, and stress, $T(z)$, where z=0 is defined as the center of the piezoelectric plate (Figure 2.8). Explicitly, the particle velocities v_1 and v_2, and the forces F_1 and F_2, indicated in Figures 2.6 and 2.7 are related to the field variables, $(v(z), T(z))$ at the two side surfaces of a piezoelectric plate by the following relations.

$$v_1 = v(-l/2) \tag{2.3.1}$$

$$v_2 = -v(l/2) \tag{2.3.2}$$

$$F_1 = -AT(-l/2) \tag{2.3.3}$$

$$F_2 = -AT(l/2). \tag{2.3.4}$$

where A is the area of the cross section of the plate and l the thickness.

The above relations are also shown in Figure 2.8. To understand these relations, we must keep in mind that v and T are mechanical field quantities, and (F_1, v_1) and (F_2, v_2) are corresponding "electrical" equivalent quantities. Note that v is positive if it is along the positive z direction. In contrast, v_1 and v_2 are positive if they are both inward. Referring to Figure 2.8, at the left side of the plate, v and v_1 take the same sign (see Eq. (2.3.1)). However, at its right side, v is opposite to v_2 (see Eq. (2.3.2)). The same directions of F_2 and v_2 guarantee that for a 1-D wave traveling in the $+z$ direction at this port, the acoustic impedance in terms of these parameters will be positive. On the other hand, the opposite directions of F_1 and v_1 also guarantee a positive acoustic impedance for a wave traveling in the $-z$ direction at this port. At the electrical port, the voltage drop V_3 is along the $+z$ direction and current I_3 flows into the electrical port.

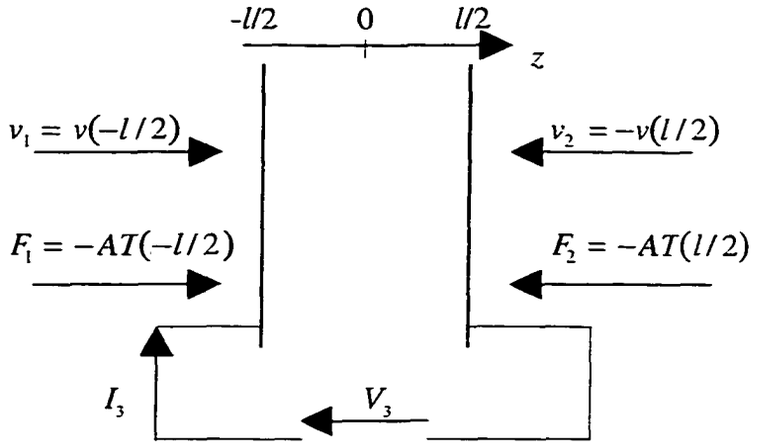

Figure 2.8 Relations between field quantities and their corresponding "electrical" equivalent quantities. This figure also shows the sign convention by which how a piezoelectric plate is transformed into a three-port network.

2.3.2 Equations of a thickness mode piezoelectric

In subsection 2.3.1, a piezoelectric plate (see Figure 2.6) was characterized as a three-port network (see Figure 2.7). Generally, a three-port network can be expressed in terms of the following 3x3 impedance matrix equation which reflects the constitutive relation of a thickness mode piezoelectric.

$$\begin{bmatrix} F_1 \\ F_2 \\ V_3 \end{bmatrix} = \begin{bmatrix} Z_{11} & Z_{12} & Z_{13} \\ Z_{21} & Z_{22} & Z_{23} \\ Z_{31} & Z_{32} & Z_{33} \end{bmatrix} \begin{bmatrix} v_1 \\ v_2 \\ I_3 \end{bmatrix}. \tag{2.3.5}$$

To specify the impedance matrix in Eq. (2.3.5), we need to make some reasonable assumptions. First we assume that the piezoelectric plate is lossless and has a thickness, l, much smaller than its lateral dimensions (see Figure 2.6). Thus the lateral displacements across the plate are ignored. We also assume that the plate is polarized along its thickness direction and that the thickness of the plated layers attached to the plate as electrodes are so thin that their effect on the vibration of the plate can be ignored. We, therefore, only consider the thickness vibration mode of the plate. The poling direction is denoted by z or 3, and the other two lateral directions by 1 and 2. The middle point of the plate is chosen as the origin (see Figure 2.8).

Based on the above assumptions, in the piezoelectric plate, there is only one-dimensional uniform vibration in the z direction. Therefore, only the strain component S_3 is not zero and the others, S_1, S_2, S_4, S_5 and S_6, vanish. When an electric field is imposed on the side surfaces of the plate in the z direction, the only non-zero component of the electric flux density is D_3 while the other two components, D_1 and D_2, vanish.

The equations of the thickness mode piezoelectric plate can be derived from h-type piezoelectric equations [Mason, 1964, Luan, Zhang and Wang, 1990]. Strains and electric flux densities are two independent variables in the h-type piezoelectric equations which are shown as follows:

$$T_h = c_{hk}^D S_k - h_{jh} D_j \tag{2.3.6}$$

$$E_i = -h_{ik} S_k + \beta_{ij}^S D_j \tag{2.3.7}$$

where the subscripts h, k=1, 2, ..., 6 and i, j=1,2,3. T_h are the various stress components and E_i are the electric field components. c_{hk}^D are elastic constants with constant electric flux density, β_{ij}^S dielectric impermeabilities with constant strain and h_{ik} piezoelectric stiffness constants.

The general h-type piezoelectric equations can be greatly simplified by using the assumptions of the thickness mode piezoelectric plate model described previously. Because only quantities related to the thickness direction survive, Eqs. (2.3.6) and (2.3.7) can be rewritten as

$$T_3 = c_{33}^D S_3 - h_{33} D_3 \tag{2.3.8}$$

$$E_3 = -h_{33} S_3 + \beta_{33}^S D_3. \tag{2.3.9}$$

where T_3 and S_3 are the normal stress and normal strain, respectively, in the z-direction.

First we consider the electric effect in the plate. From Eq. (2.3.9), D_3 is expressed as

$$D_3 = \frac{E_3}{\beta_{33}^S} + \frac{h_{33}}{\beta_{33}^S} S_3 . \tag{2.3.10}$$

Since no free charge exists in the plate, the divergence of the electric flux density vector, **D**, is zero, i.e.,

$$\nabla \cdot \mathbf{D} = 0 . \tag{2.3.11}$$

Because D_1 and D_2 are zero, Eq. (2.3.11) implies

$$\frac{\partial D_3}{\partial z} = 0 . \tag{2.3.12}$$

Substituting Eq. (2.3.10) into Eq. (2.3.12), we have

$$\frac{\partial E_3}{\partial z} = -h_{33}\frac{\partial S_3}{\partial z} = -h_{33}\frac{\partial^2 u}{\partial z^2} \tag{2.3.13}$$

where u is the displacement in the z-direction corresponding to the strain $S_3 = \partial u / \partial z$. By integrating Eq. (2.3.13) with respect to z, we find

$$E_3 = -h_{33}\frac{\partial u}{\partial z} + \alpha \tag{2.3.14}$$

where α is a constant to be determined.

The voltage across the piezoelectric plate can be obtained by integrating the electric field along its thickness. Therefore, from Eq. (2.3.14), we obtain the voltage V_3 as

$$V_3 = \int_{-l/2}^{l/2} E_3 dz = -h_{33}\left[u(\frac{l}{2}) - u(-\frac{l}{2})\right] + \alpha l . \tag{2.3.15}$$

Note that there is no negative sign before the integral because the direction from low potential to high potential is in the negative z direction (see Figure 2.8).

According to the sign convention of $u_1 = u(-l/2)$ and $u_2 = -u(l/2)$ similar to $v_1 = v(-l/2)$ and $v_2 = -v(l/2)$ (see Figure 2.8), the constant α is obtained from Eq. (2.3.15) as

$$\alpha = \frac{V_3}{l} - \frac{h_{33}}{l}(u_1 + u_2) . \tag{2.3.16}$$

So that Eq. (2.3.14) can be rewritten in the form

$$E_3 = -h_{33}\frac{\partial u}{\partial z} + \frac{V_3}{l} - \frac{h_{33}}{l}(u_1 + u_2) . \tag{2.3.17}$$

Noting that $S_3 = \partial u / \partial z$ and replacing E_3 in Eq. (2.3.10) by Eq. (2.3.17), we find

$$D_3 = \frac{V_3}{\beta_{33}^S l} - \frac{h_{33}}{\beta_{33}^S l}(u_1 + u_2) . \tag{2.3.18}$$

For harmonic waves of $e^{-i\omega t}$ time dependency, the current flowing into the piezoelectric plate is expressed as

$$I_3 = \frac{\partial D_3}{\partial t} A = -i\omega D_3 A \tag{2.3.19}$$

or, by putting Eq. (2.3.18) into Eq. (2.3.19),

$$I_3 = -i\omega \frac{A}{\beta_{33}^S l} V_3 + \frac{A}{\beta_{33}^S l} h_{33} i\omega (u_1 + u_2) . \tag{2.3.20}$$

This expression for the current I_3 can also be expressed as

$$I_3 = -i\omega C_0 V_3 - n(v_1 + v_2) \tag{2.3.21}$$

where $v_1 = -i\omega u_1$, $v_2 = -i\omega u_2$, and

$$C_0 = \frac{A}{\beta_{33}^S l} \tag{2.3.22}$$

is the so-called clamped capacitance of the plate, and

$$n = h_{33} C_0 \tag{2.3.23}$$

is called the turns ratio of an ideal electromechanical transformer. Both of these quantities will be useful later in discussing equivalent circuit models.

Eq. (2.3.21) is one of the relationships we need that connect the lumped parameters appearing in our three-port model. We now will obtain the other two relations needed.

By ignoring the internal force in the piezoelectric plate, the equation of motion in the plate is written as

$$\nabla \cdot \mathbf{T} = \rho \frac{\partial \mathbf{v}}{\partial t} \tag{2.3.24}$$

where $\mathbf{T}$ is the stress tensor, ρ the density and $\mathbf{v}$ the particle velocity in the plate.

In our 1-D problem, the velocity, v_3, in the z direction is the only non-zero velocity component. Similarly, on a z=constant plane, only the normal stress, T_3, is non-zero. Therefore, Eq. (2.3.24) is simplified to

$$\frac{\partial T_3}{\partial z} = \rho \frac{\partial v}{\partial t} . \tag{2.3.25}$$

Substituting for Eq. (2.3.8) into Eq. (2.3.25) and using Eq. (2.3.12), we have

$$c_{33}^D \frac{\partial S_3}{\partial z} = \rho \frac{\partial v}{\partial t} \tag{2.3.26}$$

or

$$\frac{\partial^2 u}{\partial z^2} = \frac{1}{v_0^2} \frac{\partial^2 u}{\partial t^2} \tag{2.3.27}$$

where

$$v_0 = \sqrt{c_{33}^D/\rho} \tag{2.3.28}$$

is the speed of the longitudinal wave propagating in the piezoelectric plate.

For harmonic waves, we can henceforth omit the common exponential time term of $e^{-i\omega t}$ and write the solution of Eq. (2.3.27) as

$$u = C_1 e^{ikz} + C_2 e^{-ikz} \tag{2.3.29}$$

where C_1 and C_2 are two arbitrary constants to be determined and $k = \omega/v_0$ is the wavenumber.

On the two sides of the plate in Figure 2.8 where $z = \pm l/2$, according to the sign convention (Eqs. (2.3.1) and (2.3.2)), we have

$$u_1 = u(-l/2) = C_1 e^{-ikl/2} + C_2 e^{ikl/2} \tag{2.3.30}$$

$$-u_2 = u(l/2) = C_1 e^{ikl/2} + C_2 e^{-ikl/2}. \tag{2.3.31}$$

In terms of u_1 and u_2, the constants, C_1 and C_2, are expressed as, from Eqs. (2.3.30) and (2.3.31),

$$C_1 = \frac{u_1 e^{-ikl/2} + u_2 e^{ikl/2}}{-2i\sin kl} \tag{2.3.32}$$

$$C_2 = \frac{u_1 e^{ikl/2} + u_2 e^{-ikl/2}}{2i\sin kl}. \tag{2.3.33}$$

Putting Eqs. (2.3.32) and (2.3.33) into Eq. (2.3.29), after some algebra, we write the particle displacement at any point z in the plate as

$$u = \frac{u_1 \sin k(\frac{l}{2} - z) - u_2 \sin k(\frac{l}{2} + z)}{\sin kl}. \tag{2.3.34}$$

Thus the strain is obtained as

$$S_3 = \frac{\partial u}{\partial z} = -k\frac{u_1 \cos(\frac{l}{2} - z) + u_2 \cos(\frac{l}{2} + z)}{\sin kl}. \tag{2.3.35}$$

By taking advantage of the boundary conditions of the plate at $z = \pm l/2$ (see Eqs. (2.3.3) and (2.3.4)) and from Eq. (2.3.8), we write

$$F_1 = -AT(-\frac{l}{2}) = -Ac_{33}^D S_3(-\frac{l}{2}) + Ah_{33}D_3 \tag{2.3.36}$$

$$F_2 = -AT(\frac{l}{2}) = -Ac_{33}^D S_3(\frac{l}{2}) + Ah_{33}D_3. \tag{2.3.37}$$

We first consider the last terms on the right hand sides of Eqs. (2.3.36) and (2.3.37). From Eq. (2.3.18), we have

$$Ah_{33}D_3 = Ah_{33}\left[\frac{V_3}{\beta_{33}^S l} - \frac{h_{33}}{\beta_{33}^S l}(u_1 + u_2)\right]. \tag{2.3.38}$$

Using Eqs. (2.3.22) and (2.3.23), Eq. (2.3.38) is rewritten as

$$Ah_{33}D_3 = nV_3 + \frac{n^2}{i\omega C_0}(v_1 + v_2). \tag{2.3.39}$$

By using Eq. (2.3.21), the above equation can be rewritten as

$$Ah_{33}D_3 = \frac{inI_3}{\omega C_0} = \frac{ih_{33}I_3}{\omega}. \tag{2.3.40}$$

Now consider the first term in Eqs. (2.3.36). From Eq.(2.3.35), we have

$$\begin{aligned} -Ac_{33}^D S_3(-\frac{l}{2}) &= Ac_{33}^D k\frac{u_1\cos kl + u_2}{\sin kl} && (z = -l/2) \\ &= A\rho v_0 \frac{i\omega(u_1\cos kl + u_2)}{i\sin kl} && (c_{33}^D k = \rho v_0 \omega) \\ &= Z_0^a \frac{v_1\cos kl + v_2}{-i\sin kl} && (v = -i\omega u) \end{aligned}$$

or,

$$-Ac_{33}^D S_3\left(-\frac{l}{2}\right) = iZ_0^a v_1\cot kl - \frac{Z_0^a v_2}{i\sin kl} \tag{2.3.41}$$

where $Z_0^a = A\rho v_0$ which is the acoustic impedance of the piezoelectric plate. Following the same procedure as above, for Eq. (2.3.37), we have

$$-Ac_{33}^D S_3\left(\frac{l}{2}\right) = iZ_0^a v_2\cot kl - \frac{Z_0^a v_1}{i\sin kl}. \tag{2.3.42}$$

Substituting Eqs. (2.3.40) and (2.3.41) into Eq. (2.3.36), the force F_1 is given by

$$F_1 = iZ_0^a v_1\cot kl - \frac{Z_0^a v_2}{i\sin kl} - \frac{h_{33}I_3}{i\omega}. \tag{2.3.43}$$

Similarly, substituting Eqs. (2.3.40) and (2.3.42) into Eq. (2.3.37), gives the force F_2 as

$$F_2 = iZ_0^a v_2\cot kl - \frac{Z_0^a v_1}{i\sin kl} - \frac{h_{33}I_3}{i\omega}. \tag{2.3.44}$$

From Eq. (2.3.21), we obtained the voltage, V_3, as

$$V_3 = -\frac{n}{i\omega C_0}(v_1 + v_2) - \frac{I_3}{i\omega C_0} \tag{2.3.45}$$

or, equivalently, using Eq. (2.3.23),

$$V_3 = -\frac{h_{33}}{i\omega}(v_1 + v_2) - \frac{I_3}{i\omega C_0}. \tag{2.3.46}$$

Eqs. (2.3.43), (2.3.44) and (2.3.46) combined form the three equations needed to describe the thickness mode piezoelectric plate in terms of three independent and three dependent variables for the three-port network in Figure 2.7. In the matrix form, these equations are

$$\begin{bmatrix} F_1 \\ F_2 \\ V_3 \end{bmatrix} = i \begin{bmatrix} Z_0^a \cot kl & \dfrac{Z_0^a}{\sin kl} & \dfrac{h_{33}}{\omega} \\ \dfrac{Z_0^a}{\sin kl} & Z_0^a \cot kl & \dfrac{h_{33}}{\omega} \\ \dfrac{h_{33}}{\omega} & \dfrac{h_{33}}{\omega} & \dfrac{1}{\omega C_0} \end{bmatrix} \begin{bmatrix} v_1 \\ v_2 \\ I_3 \end{bmatrix}. \tag{2.3.47}$$

Eq. (2.3.47) specifies every element in the impedance matrix equation shown in Eq. (2.3.5) when a thickness mode piezoelectric plate is considered. It is consistent with the equations described by Kino [1987]. If a thickness mode piezoelectric plate is modeled by a three-port network shown in Figure 2.7, the quantities at the three ports are related in the impedance matrix equation, Eq. (2.3.47). This equation involves the material properties of the piezoelectric material (h_{33}, c_{33}^D, ρ), the geometry of the plate (l, A) and the frequency (ω).

2.3.3 Mason equivalent circuit

In subsection 2.3.2, the set of equations for a thickness mode piezoelectric plate have been derived. The three-port network for the piezoelectric can be completely described by Eq. (2.3.47). Alternatively, the three-port network can be specified by an equivalent circuit. The Mason equivalent circuit is one popular model for this three-port network. In this subsection, using the Kirchhoff voltage law and Kirchhoff current law [Balanis, 1989], the Mason equivalent circuit is derived in detail.

It is difficult to relate the equations of Eq. (2.3.47) to an equivalent circuit directly. Thus, we first rewrite these equations using the following identity

$$\cot kl = \frac{1}{\sin kl} - \tan\frac{kl}{2}. \tag{2.3.48}$$

Eqs. (2.3.41) and (2.3.42) are rewritten as, respectively,

$$-Ac_{33}^D S_3\left(-\frac{l}{2}\right) = \frac{iZ_o^a}{\sin kl}(v_1 + v_2) - iZ_o^a v_1 \tan\frac{kl}{2} \tag{2.3.49}$$

and

$$-Ac_{33}^D S_3\left(\frac{l}{2}\right) = \frac{iZ_o^a}{\sin kl}(v_1 + v_2) - iZ_o^a v_2 \tan\frac{kl}{2}. \tag{2.3.50}$$

By substituting Eqs. (2.3.49) and (2.3.39) into Eq. (2.3.36), and Eqs. (2.3.50) and (2.3.39) into Eq. (2.3.37), the forces, F_1 and F_2, are expressed as

$$F_1 = \left(\frac{iZ_o^a}{\sin kl} + \frac{n^2}{i\omega C_0}\right)(v_1 + v_2) - iZ_o^a v_1 \tan\frac{kl}{2} + nV_3 \tag{2.3.51}$$

$$F_2 = \left(\frac{iZ_o^a}{\sin kl} + \frac{n^2}{i\omega C_0} \right)(v_1 + v_2) - iZ_o^a v_2 \tan\frac{kl}{2} + nV_3. \qquad (2.3.52)$$

Eq. (2.3.21) is also rewritten here as

$$I_3 = -i\omega C_0 V_3 - n(v_1 + v_2). \qquad (2.3.53)$$

In Eqs (2.3.51)-(2.3.53), the "currents" are v_1, v_2 and I_3 and the "voltages" are F_1, F_2 and V_3. The quotation marks are used because (F_1, v_1) and (F_2 v_2) are "electrical" equivalent quantities. In reality, they are mechanical quantities. Applying the Kirchhoff voltage law and Kirchhoff current law, Eqs (2.3.51)-(2.3.53) imply a three-port circuit network which is called the Mason equivalent circuit. The Mason equivalent circuit is shown in Figure 2.9. In the following, how the Mason equivalent circuit is obtained is described in detail.

Eqs. (2.3.51) and (2.3.52) represent the Kirchhoff voltage equations at the two mechanical ports. The voltage drops across the left and right arms in Figure 2.9 are $-iZ_0^a v_1 \tan kl/2$ and $-iZ_0^a v_2 \tan kl/2$, respectively. The voltage drop across the impedance on the middle arm is $iZ_o^a(v_1 + v_2)/\sin kl$. However, the voltage drop across the right side of the electromechanical transformer is not intuitive. The "current" flowing into the right side of the transformer is $v_1 + v_2$ and, thus, the current flowing into the left side of the transformer is $-n(v_1 + v_2)$. Note that the negative sign here shows that the convention of inward currents considered as positive is used. The voltage drop across the negative capacitor is now $n(v_1 + v_2)/i\omega(-C_0)$. Therefore, the voltage drop across the left side of the transformer is $V_3 + n(v_1 + v_2)/i\omega C_0$. Now transform the voltage drop from the left side to the right side of the transformer. Then the voltage drop across the right side of the transformer is written as $nV_3 + n^2(v_1 + v_2)/i\omega C_0$. Collecting all the voltage drops on the two mechanical ports, Eqs. (2.3.51) and (2.3.52) are obtained.

Now considering the electrical port. Recall, the "current" flowing into the left side of the transformer is $-n(v_1 + v_2)$. The current flowing into the positive capacitor is $-i\omega C_0 V_3$. The Kirchhoff current law then gives Eq. (2.3.53).

Here, we should make some remarks about convention. We have chosen to assume harmonic disturbances of the form $e^{-i\omega t}$. Many authors instead assume a time dependency $e^{+j\omega t}$. Simply making the replacement $i \leftrightarrow -j$, however, will allow the use of either convention.

In the Mason equivalent circuit, by using the ideal electromechanical transformer, the mechanical properties (or their electrical analogues) and the electrical properties are largely decoupled. The only link between the two elements is the turns ratio *n* which contains a

piezoelectric constant dominating the energy transfer between the electrical element and the mechanical element. The controversial element is the negative capacitor. No explicit explanation was given when the negative capacitor was introduced by Mason. In the 1980's, several authors, using a series expansion [Zhang, Li and Ying] and feedback systems [Hayward, Macleod and Durrani, 1984], explained independently that the negative capacitor reflects the regeneration of piezoelectricity in the reverberance of the vibration in a piezoelectric plate.

It is convenient to use Mason equivalent circuit to model transducers. Because the equivalent circuit is not different from other circuits used in the electronics field, all principles and theorems in that field can be applied to the Mason equivalent circuit in solving electromechanical problems. As an example application of the Mason equivalent circuit, let's consider the free vibration of a piezoelectric plate.

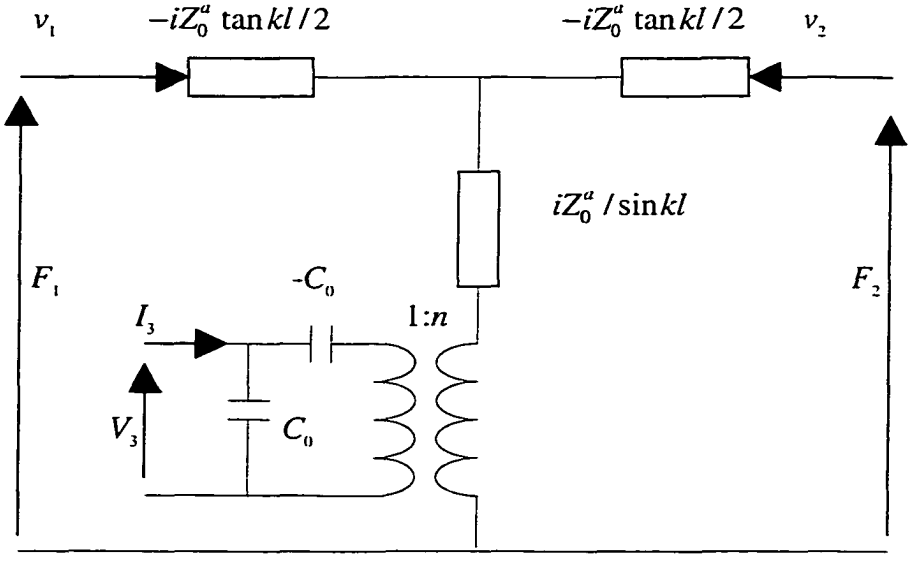

Figure 2.9 Mason equivalent circuit for a three-port network which models a thickness mode piezoelectric plate.

Given a piezoelectric plate, if the two side surfaces of the plate are free, the stresses at these surfaces vanish. Thus the forces F_1 and F_2 at the two mechanical ports in Figure 2.9 go to zero, i.e., the two ports, port 1 and port 2, are shorted. In this special case, the Mason equivalent circuit is simplified as shown in Figure 2.10.

The equivalent impedance on the right side of the electromechanical transformer is obtained as,

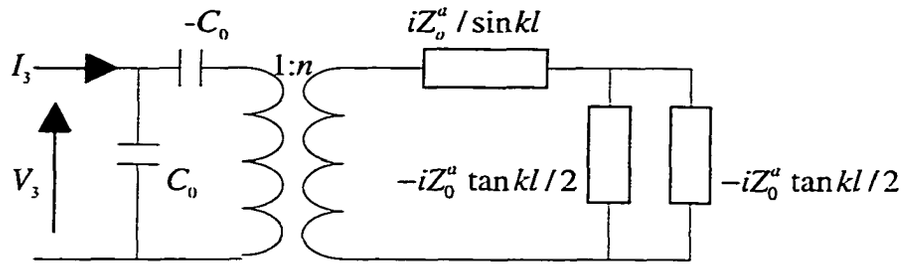

Figure 2.10 Equivalent circuit for the free vibration of a piezoelectric plate.

$$\frac{iZ_o^a}{\sin kl} - \frac{1}{2} iZ_o^a \tan\frac{kl}{2} = i\frac{Z_o^a}{2}\cot\frac{kl}{2}. \tag{2.3.54}$$

If we transfer the right side of the transformer to its left side, Figure 2.10 can be redrawn as shown in Figure 2.11. Thus, the electrical input impedance of the transducer is given as

$$Z_{in}^e = \frac{V_3}{I_3} = \frac{\dfrac{i}{\omega C_0}\left(i\dfrac{Z_0^a}{2n^2}\cot\dfrac{kl}{2} + \dfrac{1}{i\omega C_0}\right)}{i\dfrac{Z_0^a}{2n^2}\cot\dfrac{kl}{2}} \tag{2.3.55}$$

or,

$$Z_{in}^e = \frac{i}{\omega C_0}\left(1 - \frac{2n^2}{\omega C_0 Z_0^a}\tan\frac{kl}{2}\right). \tag{2.3.56}$$

By considering Eqs. (2.3.22) and (2.3.23), Eq. (2.3.56) can be rewritten as

$$Z_{in}^e = \frac{i}{\omega C_0}\left(1 - \frac{h_{33}^2}{c_{33}^D \beta_{33}^S}\frac{\tan(kl/2)}{kl/2}\right). \tag{2.3.57}$$

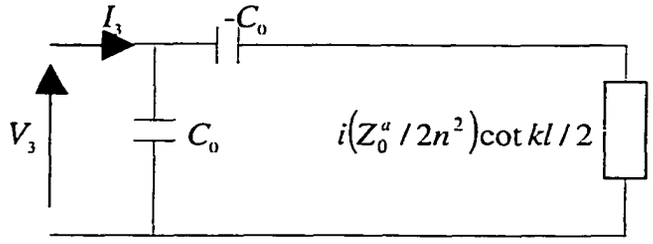

Figure 2.11. Equivalent circuit by eliminating the transformer in Figure 2.10.

Using the electromechanical coupling coefficient for the thickness mode piezoelectric plate, which is expressed as

$$k_T^2 = \frac{h_{33}^2}{c_{33}^D \beta_{33}^S} \tag{2.3.58}$$

therefore, we have

$$Z_{in}^e = \frac{i}{\omega C_0}\left(1 - k_T^2 \frac{\tan(kl/2)}{kl/2}\right). \tag{2.3.59}$$

This result is consistent with those obtained in other works [Luang, Zhang and Wang, 1990, Ristic, 1983].

Eq. (2.3.59) is often used to evaluate the fundamental resonant and antiresonant frequencies of a thickness mode piezoelectric plate.

2.3.4 KLM equivalent circuit

The Mason equivalent circuit is not the only possible circuit that can be used to describe a thickness mode piezoelectric plate. Krimholtz, Leedom and Matthaei illustrated another equivalent circuit for a thickness mode piezoelectric plate [Krimholtz, Leedom and Matthaei, 1970]. The KLM equivalent circuit is shown in Figure 2.12 where

$$\phi = \frac{1}{2M\sin(kl/2)} \tag{2.3.60}$$

$$X = Z_0^a M^2 \sin(kl) \tag{2.3.61}$$

with

$$M = h_{33}/(\omega Z_0^a). \tag{2.3.62}$$

Similar to the Mason equivalent circuit, the KLM equivalent circuit is a three-port network with two mechanical ports and one electrical port. However, the KLM model uses a different way to describe the piezoelectric plate. The mechanical part of the piezoelectric plate is described as an acoustic transmission line with length of l. A lumped electrical network is connected to the midpoint of the acoustic transmission line. Note that the negative capacitor in the Mason model disappears. Using this model, it is convenient to analyze the behavior of a transducer when any other layers are added to the piezoelectric plate because these layers can also be treated as acoustic transmission lines. On the other hand, the lumped electrical network can be used for electrical matching design.

Instead of deriving the KLM equivalent circuit directly, we will prove the equivalence of the Mason model and the KLM model. Note that a thickness mode piezoelectric plate can

be modeled by either the Mason equivalent circuit or the KLM equivalent circuit. Both models show the common 3x3 impedance matrix (Eq. (2.3.47)) for this three-port network. This implies that the two circuit models must be equivalent, and in some sense, interchangeable.

We have shown that the 3x3 impedance matrix of Eq. (2.3.47) leads directly to the Mason equivalent circuit model. Starting from the KLM equivalent circuit and using transfer matrices to describe the transmission lines, our goal is to find the 3x3 impedance matrix for the KLM model and show that it is the same as Eq. (2.3.47).

To begin, choose the quantities with primes at the middle of the transmission line in Figure 2.12. Because the two sides of the middle point are themselves transmission lines

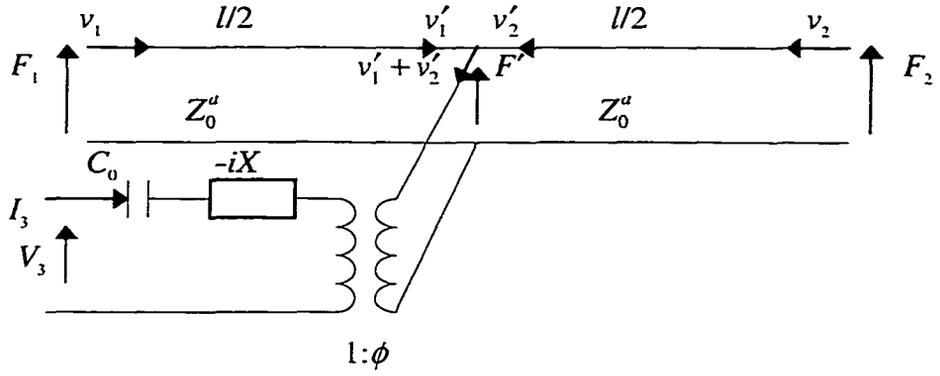

Figure 2.12 KLM equivalent circuit for a thickness mode piezoelectric plate.

with length of $l/2$, respectively, they must satisfy standard transmission line formulae. Thus, their transfer matrix equations are written as

$$\begin{Bmatrix} F' \\ v_1' \end{Bmatrix} = \begin{bmatrix} \cos\frac{kl}{2} & iZ_0^a \sin\frac{kl}{2} \\ i\frac{1}{Z_0^a}\sin\frac{kl}{2} & \cos\frac{kl}{2} \end{bmatrix} \begin{Bmatrix} F_1 \\ v_1 \end{Bmatrix} \tag{2.3.63}$$

$$\begin{Bmatrix} F' \\ v_2' \end{Bmatrix} = \begin{bmatrix} \cos\frac{kl}{2} & iZ_0^a \sin\frac{kl}{2} \\ i\frac{1}{Z_0^a}\sin\frac{kl}{2} & \cos\frac{kl}{2} \end{bmatrix} \begin{Bmatrix} F_2 \\ v_2 \end{Bmatrix}. \tag{2.3.64}$$

Now consider the ideal electromechanical transformer. The voltage V_3 and the current I_3 at the electrical port can be expressed as

$$V_3 = \left[\frac{i}{\omega C_0} - iX\right] I_3 + \frac{1}{\phi} F' \tag{2.3.65}$$

$$I_3 = -\phi(v_1' + v_2'). \tag{2.3.66}$$

Placing Eq. (2.3.62) into Eqs. (2.3.60) and (2.3.61) and then putting those resulting equations into Eqs. (2.3.65) and (2.3.66) gives

$$V_3 = \left[\frac{i}{\omega C_0} - i\frac{Z_0^a h_{33}^2}{(\omega Z_0^a)^2}\right] I_3 + \left(\frac{2h_{33}}{\omega Z_0^a}\sin\frac{kl}{2}\right) F' \tag{2.3.67}$$

$$I_3 = -\left(\frac{\omega Z_0^a}{2h_{33}}\frac{1}{\sin\frac{kl}{2}}\right)(v_1' + v_2'). \tag{2.3.68}$$

Adding the second equations in Eqs. (2.3.63) and (2.3.64), we have

$$v_1' + v_2' = \left(i\frac{1}{Z_0^a}\sin\frac{kl}{2}\right)(F_1 + F_2) + \left(\cos\frac{kl}{2}\right)(v_1 + v_2). \tag{2.3.69}$$

So that placing Eq. (2.3.69) into Eq. (2.3.68) gives

$$I_3 = \left(-i\frac{\omega}{2h_{33}}\right)(F_1 + F_2) - \left(\frac{\omega Z_0^a}{2h_{33}}\cot\frac{kl}{2}\right)(v_1 + v_2). \tag{2.3.70}$$

Then solving for $F_1 + F_2$, we obtain

$$F_1 + F_2 = \left(iZ_0^a \cot\frac{kl}{2}\right)(v_1 + v_2) + i\frac{2h_{33}}{\omega} I_3. \tag{2.3.71}$$

On the other hand, by canceling F' from the first equations in Eqs. (2.3.63) and (2.3.64), we have

$$(F_1 - F_2)\cos\frac{kl}{2} = -(v_1 - v_2)iZ_0^a \sin\frac{kl}{2} \tag{2.3.72}$$

or, in another form,

$$F_1 - F_2 = -(v_1 - v_2)iZ_0^a \tan\frac{kl}{2}. \tag{2.3.73}$$

Solving Eqs. (2.3.71) and (2.3.73) for F_1 and F_2, we have

$$F_1 = i(Z_0^a \cot kl)v_1 + i\left(\frac{Z_0^a}{\sin kl}\right)v_2 + i\frac{h_{33}}{\omega} I_3 \tag{2.3.74}$$

$$F_2 = i\left(\frac{Z_0^a}{\sin kl}\right)v_1 + i(Z_0^a \cot kl)v_2 + i\frac{h_{33}}{\omega} I_3. \tag{2.3.75}$$

In the above derivation, the following identities were used

$$\cot\frac{kl}{2} + \tan\frac{kl}{2} = \frac{2}{\sin kl} \tag{2.3.76}$$

$$\cot\frac{kl}{2} - \tan\frac{kl}{2} = 2\cot kl. \tag{2.3.77}$$

Substituting Eq. (2.3.74) into the first equation of Eq. (2.3.63), and then placing that result into Eq. (2.3.67), we find

$$V_3 = i\frac{h_{33}}{\omega}v_1 + i\frac{h_{33}}{\omega}v_2 + i\frac{1}{\omega C_0}I_3 . \tag{2.3.78}$$

Thus, in summary, from Eqs. (2.3.74), (2.3.75) and (2.3.78), we have altogether

$$\begin{aligned} F_1 &= i\left(Z_0^a \cot kl\right)v_1 + i\left(\frac{Z_0^a}{\sin kl}\right)v_2 + i\frac{h_{33}}{\omega}I_3 \\ F_2 &= i\left(\frac{Z_0^a}{\sin kl}\right)v_1 + i\left(Z_0^a \cot kl\right)v_2 + i\frac{h_{33}}{\omega}I_3 . \\ V_3 &= i\frac{h_{33}}{\omega}v_1 + i\frac{h_{33}}{\omega}v_2 + i\frac{1}{\omega C_0}I_3 \end{aligned} \tag{2.3.79}$$

which are identical to Eq. (2.3.47). Therefore, the equivalence of the two circuits is proved.

Since the Mason and KLM models use different ways to describe the same phenomenon, we will conclude this subsection by making some comparisons.

a. Three-port network

Both the Mason model and the KLM model are three-port models with two mechanical ports and one electrical port. Although the detailed circuits are different in the two models, the three ports are related to each other in the same way in the two models. Therefore, practically speaking, either the Mason or the KLM model can be used in solving electromechanical problems. They are completely equivalent to the same 3x3 impedance matrix so the choice depends only the convenience of using a particular model.

In applications, an ultrasonic transducer is usually described as a two-port network. In section 2.4, we will show that when a backing material is connected to one mechanical port and the other one is used to radiate acoustic waves, our three-port network is reduced to a two-port network. Note that the two-port network can be derived in this manner from either the Mason or the KLM model (or from the 3x3 impedance matrix relation of Eq. (2.3.47)). The resulting equation for the two-port network will be the same or equivalent, regardless of the three-port model we choose to use.

b. Transmission Line

The KLM model is popular because it uses a transmission line concept. In this case, if more layers are added to the two sides of the piezoelectric plate, they can be easily modeled as cascaded acoustic transmission lines.

c. Turns Ratios

In the Mason model, the turns ratio n is a constant which reflects the piezoelectricity of the plate, or the energy transfer between the mechanical part and the electrical part of the piezoelectric plate. In the KLM model, the turns ratio ϕ is dispersive. Besides the piezoelectricity, it also contains some mechanical properties of the plate.

c. Negative Capacitor

The controversial device in the Mason model is its negative capacitor. No satisfactory physical explanation of this component was given until the mid 1980's when it was shown that the negative capacitor reflects the interaction between mechanical and electrical energy in the reverberance of the plate vibrations. No such negative capacitor appears in the KLM model.

d. Lumped electrical devices

In the KLM model, the electrical part is modeled by a lumped network. This lumped element approach makes the KLM model suitable for electrical matching and transducer optimization, and explains its popularity in such applications.

2.4 Backed 1-D Transducer Model

In section 2.1, the transducer was modeled as a reciprocal, two-port network. However, in section 2.3, our model of a piezoelectric plate led to a three-port model. These two models are consistent since, in the fabrication of transducers, a piezoelectric plate is backed by an acoustic material. Thus, one side surface of the plate emits acoustic waves to generate acoustic fields while the other one is connected to the backing which absorbs acoustic waves from the vibrating plate. This process reduces a three-port transducer model to a two-port transducer model where the backing mechanical port is represented in the two-port model through the acoustic impedance of the backing. In this section we will show how to derive the two-port network corresponding to a backed piezoelectric plate.

2.4.1 Two-port electromechanical network

As we have shown, a piezoelectric plate with the thickness of l can be modeled by the Mason equivalent circuit as shown in Figure 2.9. When port 1 is terminated with a backing material with an acoustic impedance, Z_b^a, the Mason equivalent circuit is simplified to the one shown in Figure 2.13. To simplify the notation, the subscripts for the two remaining port quantities are dropped. That is, at the electrical port, the quantities are (V, I) and at the

remaining mechanical port, the quantities are (F, v). The subscripted quantities are retained in this section only as intermediate quantities during our derivation.

The equivalent circuit in Figure 2.13 can be divided into three parts, denoted by (I), (II) and (III) respectively. Part (I) is an electrical part which includes the two clamped capacitors: positive and negative capacitors. Part (II) is the electromechanical transformer with the turns ratio of n. Part (III) includes the acoustic properties of the piezoelectric plate. The three parts are analyzed one by one in the following. In part (I) and part (III), the inward currents or velocities in the three parts are considered as positive.

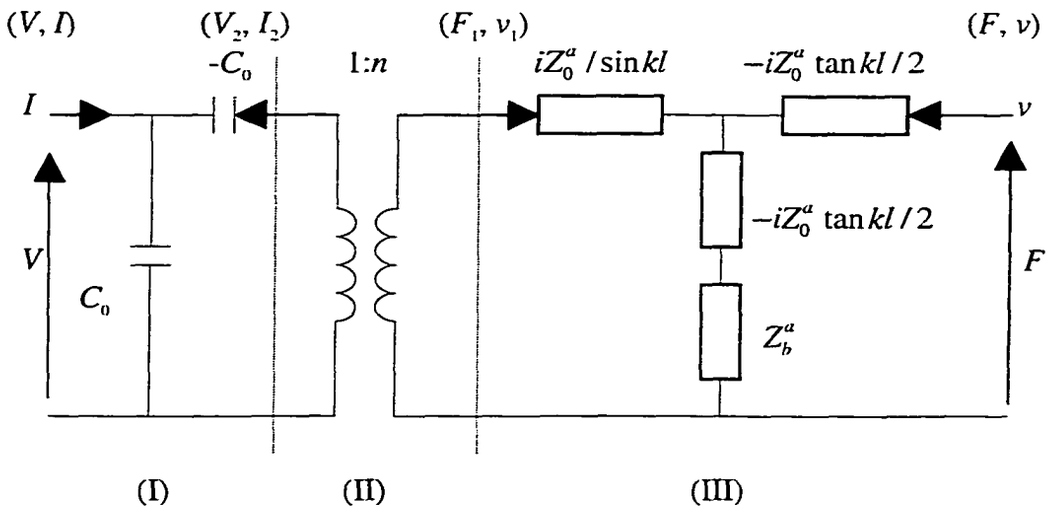

Figure 2.13 Piezoelectric plate considered as a two-port network which is divided into three parts for purpose of analysis convenience. Part (I) is the electrical part, Part (II) the electromechanical transformer and Part (III) the mechanical part.

In part (I), using Kirchhoff voltage law and Kirchhoff current law, we have the following relations

$$I = -I_2 - i\omega C_0 V \tag{2.4.1}$$

$$V = V_2 - I_2/(i\omega C_0). \tag{2.4.2}$$

Putting Eq. (2.4.2) into Eq. (2.4.1), then, gives

$$I = -i\omega C_0 V_2 . \tag{2.4.3}$$

Together, Eq. (2.4.2) and Eq. (2.4.3) form the following transfer relation

$$\begin{Bmatrix} V \\ I \end{Bmatrix} = \begin{bmatrix} 1 & 1/i\omega C_0 \\ -i\omega C_0 & 0 \end{bmatrix} \begin{Bmatrix} V_2 \\ -I_2 \end{Bmatrix}. \tag{2.4.4}$$

In part (II), the electromechanical transformer works as a usual electrical transformer. Thus,

$$F_1 = nV_2 \tag{2.4.5}$$

$$v_1 = -I_2/n\,. \tag{2.4.6}$$

In matrix form, Eq. (2.4.5) and Eq. (2.4.6) give

$$\begin{Bmatrix} V_2 \\ -I_2 \end{Bmatrix} = \begin{bmatrix} 1/n & 0 \\ 0 & n \end{bmatrix} \begin{Bmatrix} F_1 \\ v_1 \end{Bmatrix}. \tag{2.4.7}$$

In part (III), using the Kirchhoff voltage law on the two ports, we have

$$F_1 = iZ_0^a v_1 / \sin kl + \left(Z_b^a - iZ_0^a \tan\frac{kl}{2} \right)(v_1 + v) \tag{2.4.8}$$

$$F = -iZ_0^a v \tan kl/2 + \left(Z_b^a - iZ_0^a \tan\frac{kl}{2} \right)(v_1 + v). \tag{2.4.9}$$

Using Eq. (2.3.48), Eq. (2.4.8) is rewritten as

$$F_1 = \left(Z_b^a + iZ_0^a \cot kl\right)v_1 + \left(Z_b^a - iZ_0^a \tan\frac{kl}{2} \right)v. \tag{2.4.10}$$

Eq. (2.4.9) is also rewritten as

$$F = \left(Z_b^a - iZ_0^a \tan\frac{kl}{2} \right)v_1 + \left(Z_b^a - i2Z_0^a \tan\frac{kl}{2} \right)v. \tag{2.4.11}$$

In matrix form, Eq. (2.4.10) and Eq. (2.4.11) give

$$\begin{Bmatrix} F_1 \\ F \end{Bmatrix} = \begin{bmatrix} Z_b^a + iZ_0^a \cot kl & Z_b^a - iZ_0^a \tan\dfrac{kl}{2} \\ Z_b^a - iZ_0^a \tan\dfrac{kl}{2} & Z_b^a - i2Z_0^a \tan\dfrac{kl}{2} \end{bmatrix} \begin{Bmatrix} v_1 \\ v \end{Bmatrix} \tag{2.4.12}$$

Eq. (2.4.12) gives the impedance matrix relation of the part (III). The corresponding transfer relation can be obtained by using Eq. (2.2.20). After some complex manipulations, the transfer matrix equation for part (III) is written as

$$\begin{Bmatrix} F_1 \\ v_1 \end{Bmatrix} = \frac{1}{Z_b^a - iZ_0^a \tan\dfrac{kl}{2}} \begin{bmatrix} Z_b^a + iZ_0^a \cot kl & \left(Z_0^a\right)^2 + iZ_0^a Z_b \cot kl \\ 1 & Z_b^a - i2Z_0^a \tan\dfrac{kl}{2} \end{bmatrix} \begin{Bmatrix} F \\ -v \end{Bmatrix}. \tag{2.4.13}$$

Incorporating the three parts together, i.e., cascading Eqs. (2.4.4), (2.4.7) and (2.4.13), we have

$$\begin{Bmatrix} V \\ I \end{Bmatrix} = \frac{1}{Z_b^a - iZ_0^a \tan\dfrac{kl}{2}} \begin{bmatrix} 1 & \dfrac{1}{i\omega C_0} \\ -i\omega C_0 & 0 \end{bmatrix} \begin{bmatrix} \dfrac{1}{n} & 0 \\ 0 & n \end{bmatrix} \begin{bmatrix} Z_b^a + iZ_0^a \cot kl & \left(Z_0^a\right)^2 + iZ_0^a Z_b^a \cot kl \\ 1 & Z_b^a - i2Z_0^a \tan\dfrac{kl}{2} \end{bmatrix} \begin{Bmatrix} F \\ -v \end{Bmatrix} \tag{2.4.14}$$

or, more compactly,

$$\begin{Bmatrix} V \\ I \end{Bmatrix} = \frac{1}{Z_b^a - iZ_0^a \tan\frac{kl}{2}} \begin{bmatrix} \frac{1}{n} & \frac{n}{i\omega C_0} \\ \frac{i\omega C_0}{-n} & 0 \end{bmatrix} \begin{bmatrix} Z_b^a + iZ_0^a \cot kl & (Z_0^a)^2 + iZ_0^a Z_b^a \cot kl \\ 1 & Z_b^a - i2Z_0^a \tan\frac{kl}{2} \end{bmatrix} \begin{Bmatrix} F \\ -v \end{Bmatrix}. \tag{2.4.15}$$

This equation specifies the transfer relation of a backed 1-D transducer. The two 2x2 matrices, together with the coefficient before them, finally give an overall 2x2 transfer matrix. It is not difficult to check that Eqs. (2.4.4), (2.4.7) and (2.4.13) satisfy the reciprocal theorem, i.e., Parts (I), (II) and (III) satisfy the reciprocal theorem, respectively. Therefore, the backed 1-D transducer shown in Figure 2.13 also satisfies the reciprocal theorem according to subsection 2.2.3.

To keep consistent with the conventions chosen for expressing the transfer relation of a two-port network, as shown in Figure 2.3, the direction of the transmitting velocity in Figure 2.13 must be changed. That is, the velocity flowing out of the output port must be taken as positive. Thus, the "-" sign before v in Eq. (2.4.15) should be dropped off and Eq. (2.4.15) rewritten as

$$\begin{Bmatrix} V \\ I \end{Bmatrix} = \frac{1}{Z_b^a - iZ_0^a \tan\frac{kl}{2}} \begin{bmatrix} \frac{1}{n} & \frac{n}{i\omega C_0} \\ \frac{i\omega C_0}{-n} & 0 \end{bmatrix} \begin{bmatrix} Z_b^a + iZ_0^a \cot kl & (Z_0^a)^2 + iZ_0^a Z_b^a \cot kl \\ 1 & Z_b^a - i2Z_0^a \tan\frac{kl}{2} \end{bmatrix} \begin{Bmatrix} F \\ v \end{Bmatrix}. \tag{2.4.16}$$

2.4.2 Sittig's model

Sittig has found the transfer matrix equation for a backed 1-D transducer [Sittig, 1967, 1969, 1972] in a form very similar to Eq. (2.4.16). In this subsection, starting from Eq. (2.4.16), Sittig's corresponding model is derived.

If we define an acoustic impedance ratio as

$$z_b = Z_b^a / Z_0^a \tag{2.4.17}$$

then Eq. (2.4.16) can be written as

$$\begin{Bmatrix} V \\ I \end{Bmatrix} = \frac{1}{n} \begin{bmatrix} 1 & \frac{n^2}{i\omega C_0} \\ \frac{i\omega C_0}{-1} & 0 \end{bmatrix} \frac{1}{z_b - i\tan\frac{kl}{2}} \begin{bmatrix} z_b + i\cot kl & Z_0^a(1 + iz_b \cot kl) \\ 1/Z_0^a & z_b - i2\tan\frac{kl}{2} \end{bmatrix} \begin{Bmatrix} F \\ v \end{Bmatrix}. \tag{2.4.18}$$

Multiplying every element in the second matrix and the denominator of the coefficient before it by $-i\sin kl$ gives

$$\begin{Bmatrix} V \\ I \end{Bmatrix} = \frac{1}{nQ}\begin{bmatrix} 1 & \frac{n^2}{i\omega C_0} \\ -i\omega C_0 & 0 \end{bmatrix}\begin{bmatrix} \cos kl - iz_b \sin kl & Z_0^a(z_b \cos kl - i\sin kl) \\ (-iz_b \sin kl)/Z_0^a & 2(\cos kl - 1) - iz_b \sin kl \end{bmatrix}\begin{Bmatrix} F \\ v \end{Bmatrix} \quad (2.4.17)$$

where

$$Q = \cos kl - 1 - iz_b \sin kl\,. \quad (2.4.18)$$

Note that in the derivation of Eq. (2.4.17), the following identity was used

$$-i\tan\frac{kl}{2}\cdot(-i\sin kl) = -\tan\frac{kl}{2}\cdot 2\sin\frac{kl}{2}\cos\frac{kl}{2} = -2\sin^2\frac{kl}{2} = \cos kl - 1\,. \quad (2.4.19)$$

Sittig gave the transfer matrix relation between the input and output for a backed 1-D transducer as follows:

$$\begin{Bmatrix} V \\ I \end{Bmatrix} = \frac{1}{\Phi Q}\begin{bmatrix} 1 & j\Phi^2/\omega C_0 \\ j\omega C_0 & 0 \end{bmatrix}\begin{bmatrix} \cos\gamma + jz_b \sin\gamma & Z_0^a(z_b \cos\gamma + j\sin\gamma) \\ (j\sin\gamma)/Z_0^a & 2(\cos\gamma - 1) + jz_b \sin\gamma \end{bmatrix}\begin{Bmatrix} F \\ v \end{Bmatrix} \quad (2.4.20)$$

where

$$\Phi^2 = \frac{\omega_0 C_0 Z_0^a k_T^2}{\pi} \quad (2.4.21)$$

$$Q = \cos\gamma - 1 + jz_b \sin\gamma \quad (2.4.22)$$

with

$$\gamma = \frac{\pi f}{f_0} \quad (2.4.23)$$

$$\omega_0 = 2\pi f_0 \quad (2.4.24)$$

where f_0 is the fundamental antiresonant frequency of a piezoelectric plate.

Comparing Eq. (2.4.17) with Eq. (2.4.20), it is clear that Sittig used a time dependency of $e^{+j\omega t}$. Thus we need to let $i \to -j$. If we can also prove that

$$\Phi = n \quad (2.4.25)$$

$$\gamma = kl \quad (2.4.26)$$

then the Sittig's model will be identical with the present model.

The fundamental antiresonant frequency of a piezoelectric plate is expressed as

$$f_0 = \frac{v_0}{2l}\,. \quad (2.4.27)$$

Then Eq. (2.4.24) is rewritten as

$$\omega_0 = \pi v_0 / l\,. \quad (2.4.28)$$

Putting Eq. (2.4.28), Eq. (2.3.58) and $Z_0^a = A\rho v_0$ into Eq. (2.4.21), we have

$$\Phi^2 = \frac{\rho v_0^2}{c_{33}^D} C_0 \frac{A}{l\beta_{33}^S} h_{33}^2 . \tag{2.4.29}$$

By the definition of the longitudinal velocity of a piezoelectric (Eq. (2.3.28)) and the definition of the clamped capacitance (Eq. (2.3.22)), Eq. (2.4.29) can be rewritten as

$$\Phi^2 = (h_{33} C_0)^2 . \tag{2.4.30}$$

According to Eq. (2.3.23), Eq. (2.4.25) holds. This shows the turns ratio given by Sittig is the same as that used in the Mason model. Since, using Eq. (2.4.27), we also have

$$\gamma = \frac{\pi f}{f_0} = \frac{2\pi f}{2 f_0} = \frac{2\pi f}{v_0} l . \tag{2.4.31}$$

From the definition of the wavenumber

$$k = \frac{2\pi f}{v_0} \tag{2.4.32}$$

we see that Eq. (2.4.26) holds also.

The two-port network for a backed 1-D transducer in this thesis is therefore equivalent to Sittig's model if we replace i with $-j$, kl with γ and n with Φ. Then Eq. (2.4.17) is changed into Eq. (2.4.20). One characteristic of Sittig's model is that the transfer matrix is expressed only in terms of sine and cosine functions.

We should note some minor errors in Sittig's derivation and results [Sittig, 1969]. Sittig refers to F as a "pressure", but it really is a lumped force, as our derivation shows. Also, the impedance Z_0^a appearing both in our results and in Sittig's is given by $Z_0^a = A\rho v_0$, not by $Z_0^a = \rho v_0$ as stated by Sittig (see Eq. (1) in [Sittig, 1969]).

2.5 Acoustic Transmission Lines

In the fabrication of a transducer, acoustic layers are used to face the piezoelectric plate on either surface. Figure 2.14 shows the configuration of such an ultrasonic transducer. For example, a wear plate or a quarter wave plate could be attached on the front surface of the piezoelectric plate in a transducer. In either case, these plates serve as attached acoustic layers. If the backing is made of a highly absorbing material, then it acts actually as an infinite "half-space" where the waves enter but never return. In this case, the backing can be simply modeled as a plane wave acoustic impedance. If there are some layers between the "half-space" and the piezoelectric plate, those layers act as acoustic transmission lines.

Acoustic layers can also be modeled as a Mason equivalent circuit, a KLM equivalent circuit, or directly from the transfer matrix equations. In this section, the acoustic layers are studied as an acoustic transmission line modeled from all of these viewpoints.

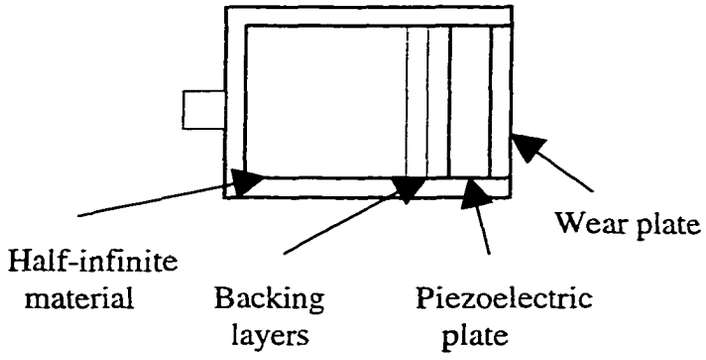

Figure 2.14 Configuration of an ultrasonic transducer with wear plate, piezoelectric plate, backing layers and semi-infinite material.

2.5.1 Mason equivalent circuit for acoustic layers

An acoustic layer has a finite length. It can be considered as the special case of a piezoelectric plate without piezoelectricity. In the Mason equivalent circuit for a piezoelectric plate shown in Figure 2.9, if we let the turns ratio to be zero, the electrical part can be deleted. The equivalent circuit changes to the one describing a usual acoustic layer. Figure 2.15 shows the Mason equivalent circuit for the acoustic layer with length of l and acoustic impedance of Z_0^a. Note that the direction of v_2 has been reversed to correspond to the convention used for transmission lines. It is a typical T-type two-port network used in electrical engineering.

2.5.2 Transfer matrix of an acoustic layer

From the previous subsection, if we let the turns ratio be zero for the piezoelectric plate (Eq. (2.3.47)), we obtain the equations of an acoustic layer (without piezoelectricity) as

$$F_1 = iZ_0^a v_1 \cot kl - i\frac{Z_0^a v_2}{\sin kl} \tag{2.5.1}$$

$$F_2 = i\frac{Z_0^a v_1}{\sin kl} - iZ_0^a v_2 \cot kl \tag{2.5.2}$$

where the sign of v_2 has been changed so that it consistent with the convention used in Figure 2.15. Eq. (2.5.1) and Eq. (2.5.2) show the impedance matrix relations of quantities. Using the matrix transformation relations given in Eq. (2.2.18), the corresponding transfer matrix equation can be written as

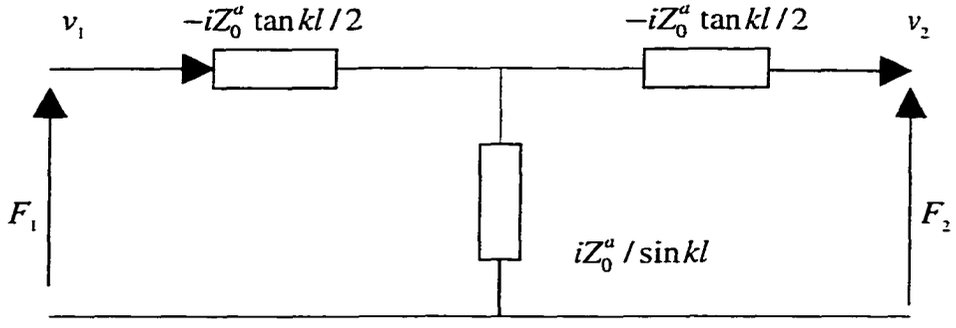

Figure 2.15 Mason equivalent circuit for an acoustic layer with the length of l and acoustic impedance of Z_0^a.

$$\begin{Bmatrix} F_1 \\ v_1 \end{Bmatrix} = \begin{bmatrix} \cos kl & -iZ_0^a \sin kl \\ -i\sin kl / Z_0^a & \cos kl \end{bmatrix} \begin{Bmatrix} F_2 \\ v_2 \end{Bmatrix}. \tag{2.5.3}$$

These two equations represent the same equivalent circuit shown in Figure 2.15 so that Eq. (2.5.3) represents the transfer matrix for the reduced Mason equivalent circuit (see Figure 2.9).

Eq. (2.5.3) is a typical transfer matrix equation of a transmission line. This same transmission line can be obtained by simply taking off the electrical part from the KLM equivalent circuit (see Figure 2.12). The acoustic transmission line characterized by Eq. (2.5.3) is drawn in Figure 2.16 where note that the direction of v_2 is opposite to that of v_2 in the KLM model.

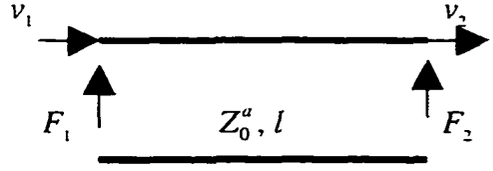

Figure 2.16 Transmission line for an acoustic layer with the length of l and acoustic impedance of Z_0^a.

When several acoustic layers exist, they can be simply cascaded together by multiplying their transfer matrices. As an example of the application of the acoustic transmission line, suppose the port 2 in Figure 2.16 terminates with an acoustic impedance Z_2^a (which could be a "half-space" or the impedance coming from other attached acoustic transmission lines or acoustical elements). Then

$$Z_2^a = \frac{F_2}{v_2}. \tag{2.5.4}$$

Placing Eq. (2.5.4) in Eq. (2.5.3), the input acoustic impedance looking from port 1 in Figure 2.16 then is obtained as

$$Z_1^a = Z_0^a \frac{Z_2^a \cos kl - iZ_0^a \sin kl}{Z_0^a \cos kl - iZ_2^a \sin kl}. \tag{2.5.5}$$

Note that we can follow this same procedure, using the cascading technique, to always replace the backing conditions at the backing port by an equivalent acoustic impedance, Z_b^a, regardless of the number of layers present at the backing side of the piezoelectric crystal. Thus our two-port models of this chapter, where Z_b^a is specified at the backing port, can model many complex backing conditions.

CHAPTER 3. THE GENERATION PROCESS

In an ultrasonic measurement, transducers are generally used in either a pitch-catch mode or a pulse-echo mode. In a pitch-catch mode, one transducer transmits acoustic waves and the other receives the waves. In a pulse-echo mode, only one transducer is used to both transmit and receive acoustic waves. For either mode, it is necessary to consider (1) the conversion processes occurring when the voltage of a pulser is used to drive a transducer, acting as a transmitter of acoustic waves (the generation process) and (2) the conversion processes occurring when a transducer, acting as a receiver, transforms acoustic energy back to electrical energy and transfers that energy to a receiver for amplification (the reception process). In this chapter, the generation process is analyzed. The reception process will be discussed in the next chapter.

As shown in Figure 3.1, the generation process usually includes four components: a pulser, a cable, a transducer and an acoustic medium. The pulser periodically emits spike-like electrical impulses. Its bandwidth is generally very wide so that it can cover all the typical ultrasonic transducer frequencies. The cable connects the transducer to the pulser and carries the spike-like pulses to the transducer. The transducer is an electromechanical energy transformer. It takes the electrical energy from the cable and changes it into mechanical energy in the form of motion (displacement or velocity) at the transducer face. This motion in turn generates waves in the acoustic medium which radiate from the transducer surface. In the following, all these components of the generation process are studied in detail.

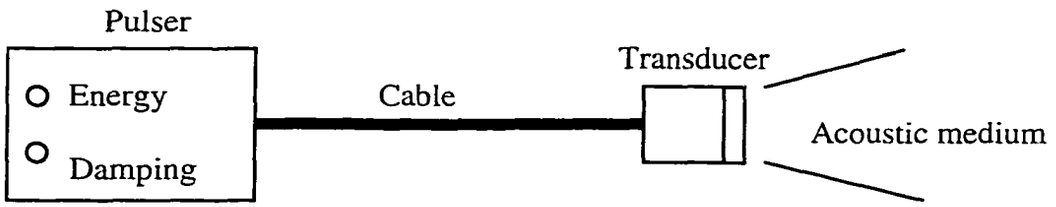

Figure 3.1 The generation process which includes four components: pulser, cable, transducer and acoustic medium.

3.1 Pulser Model

In an ultrasonic measurement, a pulser is an electrical source that emits electrical impulses. These impulses are used to drive an ultrasonic transducer. Usually an electrical impulse is a spike-like negative impulse. In the experimental part of this thesis, a Panametrics 5052PR pulser is used. For this pulser, the width and amplitude of the impulse can be adjusted through energy and damping settings on the front panel of the pulser (see Figure 3.1). For such a pulser, the amplitude of the pulses generated is about several hundred volts and the pulse width is a fraction of a micro second.

The internal structure of an electrical pulser is very complex. It includes many electrical devices which are used to generate an electrical impulse. However, from a modeling standpoint, one only usually cares about the net output properties of the pulser, such as the amplitude of the output signal, the bandwidth, and the internal impedance of the pulser, since these are the factors which control the interactions of the pulser with the cabling and transducer during the generation process. Thus, the pulser can be modeled by a Thevenin equivalent circuit which contains only two components: an electrical source $V_i(\omega)$ and an internal impedance $Z_i^e(\omega)$ in series. The equivalent circuit of the pulser is shown in Figure 3.2. An alternative model of a pulser would be a Norton equivalent circuit. In this thesis, the Thevenin equivalent circuit is chosen. The values of $V_i(\omega)$ and $Z_i^e(\omega)$ in the Thevenin equivalent circuit are obviously functions of the energy and damping settings on the front panel of a pulser (see Figure 3.1).

To describe $V_i(\omega)$ and $Z_i^e(\omega)$ accurately in practice it would be necessary to obtain these parameters experimentally at particular energy and damping settings. However, for simulation purpose, it is useful to also have a simple model of the pulser output so that

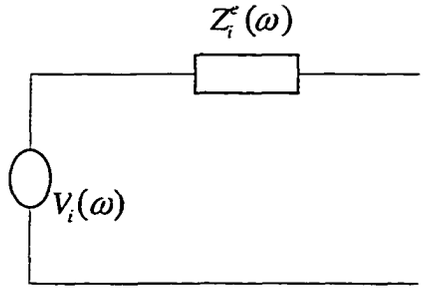

Figure 3.2 An electrical pulser is modeled by the Thevenin equivalent circuit with the source strength of $V_i(\omega)$ and the internal impedance of $Z_i^e(\omega)$ in series.

parametric studies can be performed.

Usually, the output of a pulser is generated by an RC-circuit which has an exponential characteristic response during the process of recharging and discharging. Thus, it is reasonable to choose a simple model which uses two exponential functions. Specifically, we model the impulse by the following function.

$$V_i(t) = \begin{cases} 0 & (t \le 0) \\ -V_\infty\left(1 - e^{-\alpha_1 t}\right) & (0 < t \le t_0) \\ -V_0 e^{-\alpha_2 (t - t_0)} & (t > t_0) \end{cases} \qquad (3.1.1)$$

where α_1 and α_2 are two attenuation factors for the two exponential functions respectively. V_0 is the amplitude of the impulse and V_∞ is an amplitude term appearing in the first exponential function. V_0 and V_∞ are related through the requirement that the pulse be continuous at $t = t_0$. The relationship is

$$V_0 = V_\infty\left(1 - e^{-\alpha_1 t_0}\right). \qquad (3.1.2)$$

The shape of the exponential function given in Eq. (3.1.1) is shown Figure 3.3 when the parameters are chosen as $V_0 = -200V$, $t_0 = 0.2\mu s$, $\alpha_1 = 1 \times 10^6 / s$ and $\alpha_2 = 5 \times 10^6 / s$. Before the pulser emits an impulse ($t < 0$), there is no output. After time t=0, the impulse drops from zero exponentially with attenuation factor α_1. At time $t = t_0 = 0.2\mu s$, it reaches a value of $-V_0$. Then it rises exponentially to zero with attenuation factor α_2.

In the frequency domain, the corresponding spectrum of Eq. (3.1.1) is obtained as

$$V_i(\omega) = \frac{V_\infty}{\alpha_1 - i\omega}\left[e^{-(\alpha_1 - i\omega)t_0} - 1\right] + \frac{V_\infty}{i\omega}\left[e^{i\omega t_0} - 1\right] - \frac{V_0}{\alpha_2 - i\omega} e^{i\omega t_0}. \qquad (3.1.3)$$

The amplitude of the spectrum is drawn in Figure 3.4. For the parameters chosen, there is a peak around 2MHz. Changing energy and damping settings would correspond to changing the model parameters of V_0, t_0, α_1 and α_2, which control the shape of the impulse (Figure 3.3) and the corresponding spectrum (Figure 3.4). However, it is not possible to describe the relationship between pulser settings and these parameters in a simple manner.

3.2 Cabling Model

A cable is used to transmit the electrical signals from the pulser to the transducer (see Figure 3.1). At low frequencies, such as less than 10kHz, which is a range often used in acoustics and underwater sound applications, the cable transmits the electrical pulses without distortion since the length of the cable is much shorter than the characteristic wavelength of

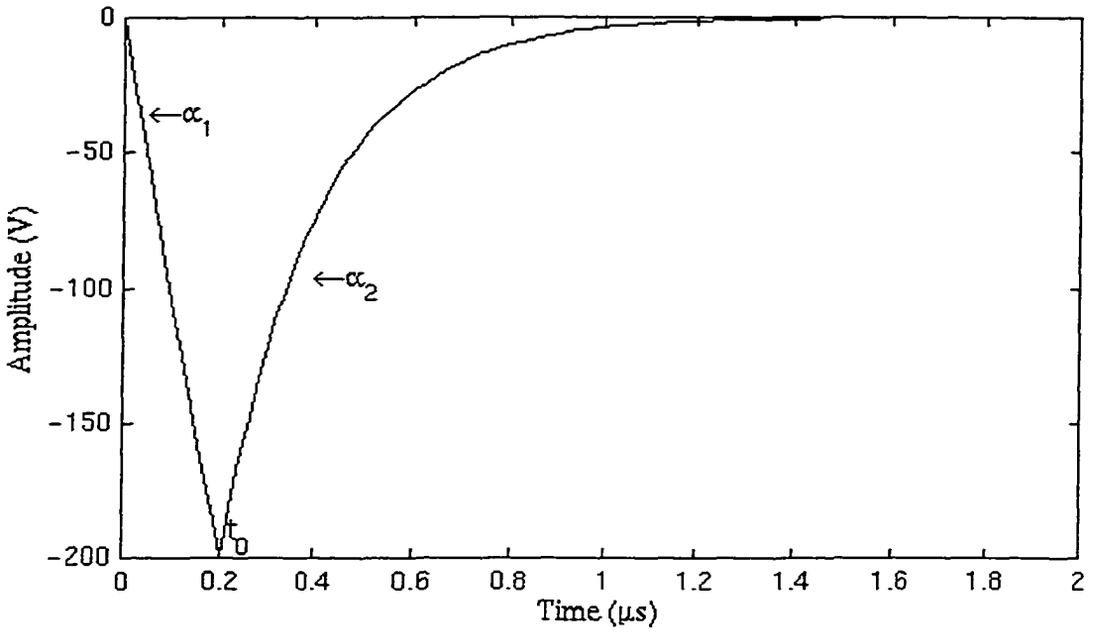

Figure 3.3 The shape of the impulse represented by two exponential functions (see Eq. (3.1.1)) in the time domain with $V_0 = -200\text{V}$, $t_0 = 0.2\mu\text{s}$, $\alpha_1 = 1\times10^6\,/\text{s}$ and $\alpha_2 = 5\times10^6\,/\text{s}$.

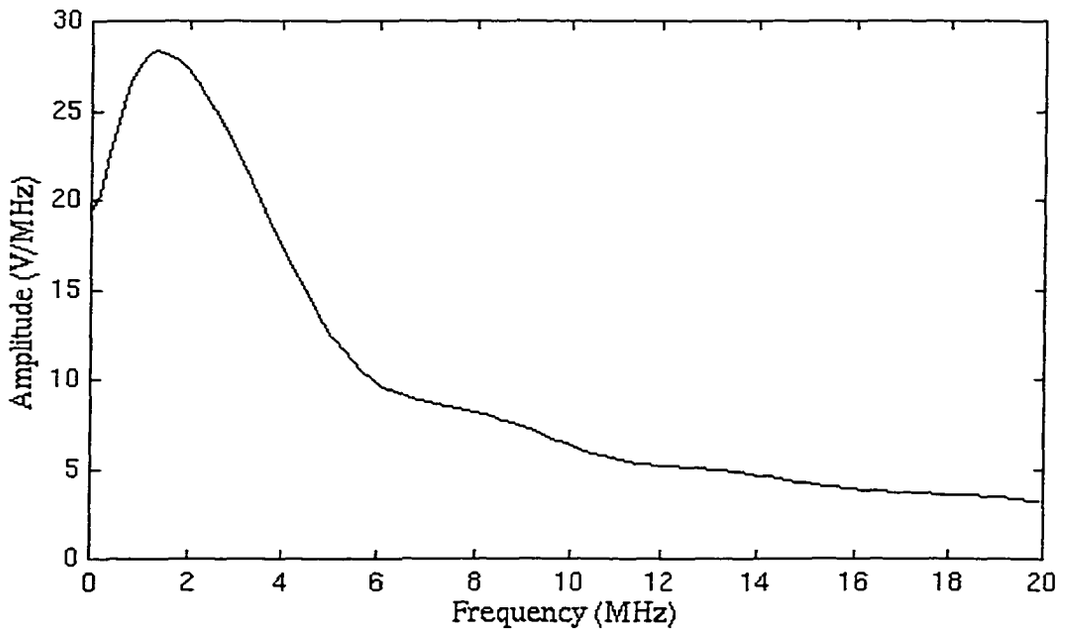

Figure 3.4 Spectrum of the impulse represented by two exponential functions (see Eq. (3.1.3)) in the frequency domain with $V_0 = -200\text{V}$, $t_0 = 0.2\mu\text{s}$, $\alpha_1 = 1\times10^6\,/\text{s}$ and $\alpha_2 = 5\times10^6\,/\text{s}$.

the transmitted pulses. In these cases, the effect of the cable can be neglected. However, in ultrasonic measurements, the frequencies involved are usually no less than 1MHz. In this situation, the cable itself affects the signals transmitted to the transducer, and this cabling effect is frequency dependent. Thus, in most NDE applications, we need to consider the cable effects explicitly.

A cable is usually composed of concentric wires with the outer layer grounded. When only TEM waves are transmitted in a cable, the electromagnetic waves in terms of electric field intensity **E** and magnetic field intensity **H** can be lumped into voltage V and current I (see the discussion in 2.1). As in the description of an acoustic medium layer in section 2.5, a cable can be modeled by either a transmission line model or an equivalent circuit model. In the following, we will describe both of them.

3.2.1 Transmission line model

A transmission line model [Seshadre, 1971, Steaelin, 1994] is commonly used to describe a cable as shown in Figure 3.5. Suppose that the length of the cable is l, its intrinsic impedance is Z_0^e, the input voltage and current are V_1 and I_1, and the output voltage and current are V_2 and I_2. As is usual with transmission line models, the two currents I_1 and I_2 are taken in the same direction. The transfer matrix equation of the cable can easily be shown to be

$$\begin{Bmatrix} V_1 \\ I_1 \end{Bmatrix} = \begin{bmatrix} \cos kl & -iZ_0^e \sin kl \\ -i\sin kl / Z_0^e & \cos kl \end{bmatrix} \begin{Bmatrix} V_2 \\ I_2 \end{Bmatrix} \tag{3.2.1}$$

where $k = \omega / c$ is the space wavenumber of the wave transmitted in the cable with c being the speed of waves transmitted inside the cable.

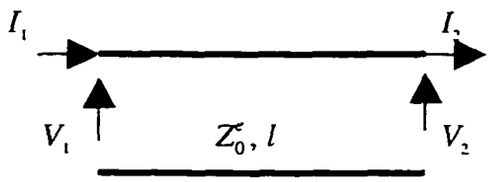

Figure 3.5 Transmission line for a cable with the length of l and intrinsic impedance of Z_0^e, which is characterized by Eq. (3.2.1).

The intrinsic impedance of a cable takes the following form

$$Z_0^e = \sqrt{\frac{\mu}{\varepsilon}} \tag{3.2.2}$$

where μ is the permeability of the cable and ε is the permittivity of the cable. In free space, $\mu = \mu_0 = 4\pi \times 10^{-7}$ H/m and $\varepsilon = \varepsilon_0 = 8.85 \times 10^{-12}$ F/m. For the coaxial cables commonly used in practice, the intrinsic cable impedance is usually set to be 50Ω.

Eq. (3.2.1) shows that when $kl \ll 1$ the transfer matrix reduces to the identity matrix and the cable has no effect ($V_1 = V_2$ and $I_1 = I_2$) as stated before. In all other cases, it is important to keep the frequency dependent terms given in Eq. (3.2.1).

3.2.2 Equivalent circuit model

An equivalent circuit model is another way to describe a cable. To see this, first transform the transfer matrix equation of the cable shown in Eq. (3.2.1) into the corresponding impedance matrix equation by using the relation (2.2.14). The following impedance matrix equation is then obtained:

$$\begin{Bmatrix} V_1 \\ V_2 \end{Bmatrix} = \begin{bmatrix} iZ_0^e \cot kl & iZ_0^e / \sin kl \\ iZ_0^e / \sin kl & iZ_0^e \cot kl \end{bmatrix} \begin{Bmatrix} I_1 \\ -I_2 \end{Bmatrix}. \tag{3.2.3}$$

Using Eq. (2.3.48), Eq. (3.2.3) can be expressed equivalently as

$$V_1 = \left(\frac{iZ_0^e}{\sin kl} \right)(I_1 - I_2) - iZ_0^e I_1 \tan \frac{kl}{2} \tag{3.2.4}$$

$$V_2 = \left(\frac{iZ_0^e}{\sin kl} \right)(I_1 - I_2) + iZ_0^a I_2 \tan \frac{kl}{2}. \tag{3.2.5}$$

But, according to the Kirchhoff voltage law, Eq. (3.2.4) and Eq. (3.2.5) characterizes an equivalent circuit in form of a T-network with three impedances (see Figure 3.6): the left

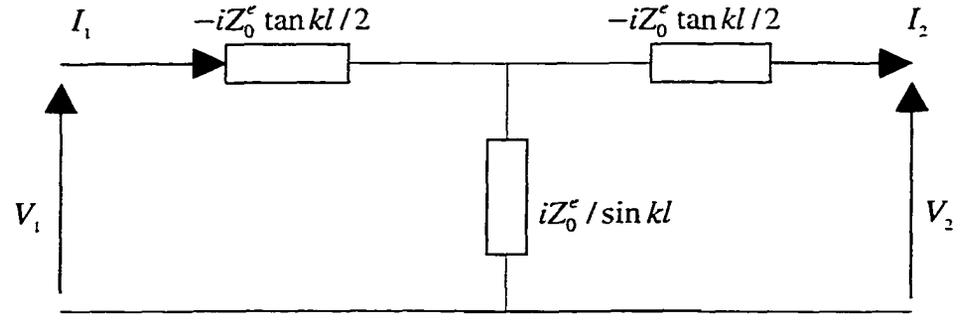

Figure 3.6 Mason equivalent circuit for a cable with the length of l and intrinsic impedance of Z_0^e.

arm and right arm are $-iZ_0^e \tan kl/2$ and the middle arm is $iZ_0^e / \sin kl$. This equivalent circuit for a cable is similar to the Mason equivalent model for an acoustic medium layer discussed in the last chapter because the cable and the acoustic layer both can be modeled as transmission lines.

From the above discussion, a cable can be described by the transmission line model or an equivalent circuit model. In dealing with the problems relevant to cables, choosing which model to use is generally only a matter of convenience.

3.2.3 Impedance of a cable

As a transmission line, a cable can transfer an impedance from one end of the cable to its other end. Suppose that an electrical impedance Z_2^e is connected at the port 2 of the cable shown in Figure 3.5. From the transfer matrix equation of the cable (Eq. (3.2.1)), the electrical impedance at port 1 is obtained as

$$Z_1^e = \frac{V_1}{I_1} = Z_0^e \frac{Z_2^e \cos kl - iZ_0^e \sin kl}{Z_0^e \cos kl - iZ_2^e \sin kl}. \tag{3.2.6}$$

Note that

$$Z_2^e = \frac{V_2}{I_2}. \tag{3.2.7}$$

Figure 3.7 shows how the impedance Z_1^e changes with kl. Generally speaking, for pure resistances Z_2^e and Z_0^e, if $Z_2^e > Z_0^e$, Z_1^e has the characteristic behavior of a capacitance. If $Z_2^e < Z_0^e$, on the other hand, Z_1^e looks like an inductance. If $Z_2^e = Z_0^e$, Z_1^e behaves like a pure resistance and is equal to Z_0^e.

At sufficient low frequency, $kl \to 0$ and Eq. (3.2.6) gives

$$Z_1^e \approx Z_2^e \tag{3.2.8}$$

which shows that the impedance at port 1 of the cable is the same as the impedance at port 2 (see Figure 3.5), i.e., the effect of the cable can be neglected.

For high frequency range, the cable effect should not be ignored. We consider the following three special termination conditions at port 2:

a. Open-circuit

When port 2 is opened, i.e., $Z_2^e \to \infty$, Eq. (3.2.6) is simplified as

$$Z_1^e = iZ_0^e \cot kl. \tag{3.2.9}$$

Because of the finite length of a cable, the impedance of the cable is not infinite. It is expressed as a cotangent function with 90 degrees phase shift.

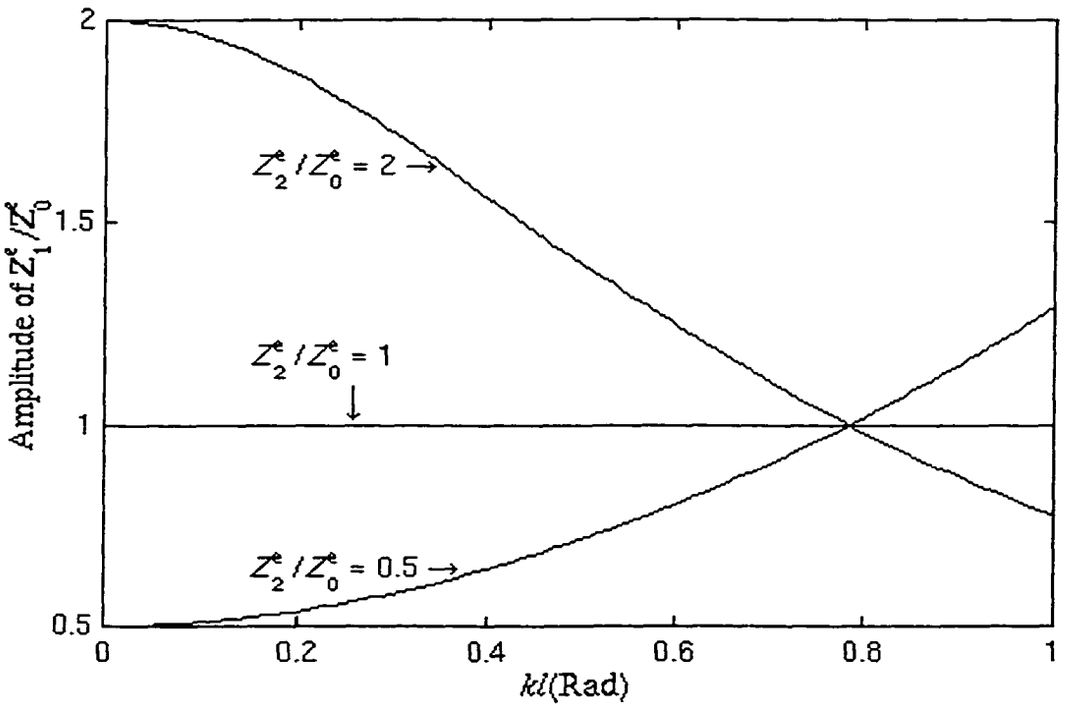

Figure 3.7 Impedances of a cable when the terminated impedance Z_2^e is resistive and is $2Z_0^e$, Z_0^e and $0.5Z_0^e$, respectively, where Z_0^e is also resistive.

b. Short-circuit

When port 2 is shorted, i.e., $Z_2^e \rightarrow 0$, Eq. (3.2.6) is changed into

$$Z_1^e = -iZ_0^e \tan kl. \tag{3.2.10}$$

Again because of the finite length of a cable, the impedance of the cable is not zero. It is expressed as a tangent function with -90 degrees phase shift.

c. Terminated with an impedance equal to cable intrinsic impedance

When port 2 is terminated with an impedance equal to the intrinsic impedance of a cable, i.e., $Z_2^e = Z_0^e$, Eq. (3.2.6) is simplified as

$$Z_1^e = Z_0^e. \tag{3.2.11}$$

The impedance of the cable at port 1 is the same as the intrinsic impedance of the cable. If the intrinsic impedance of a cable is 50Ω, to absorb the reflected wave from one end of the cable due to impedance mismatch, a 50Ω terminator is usually connected at this end.

Figure 3.8 shows the above three cases. The amplitude of the ratio of Z_1^e to Z_0^e for each case is drawn versus kl. These curves show that, aside from the perfect impedance match for

$Z_2^e = Z_0^e$, the effect of cables cannot be neglected. The curves of Figure 3.8 will also be useful later when we measure the properties of a particular cable experimentally.

3.3 Transducer Transfer Function

A transducer used as a transmitter is an electromechanical device which transfers electrical energy to mechanical energy and radiates acoustic waves into an acoustic medium. An important property of a transducer, therefore, is its transfer function which can be defined as the ratio of the force (or velocity) output by the transducer in the acoustic medium to the voltage which drives it. In this section we will use two approaches to obtain the transfer function of a transducer. The first approach is to use the Mason equivalent circuit to derive an explicit expression for the transfer function. The second approach uses a two-port network concept to implicitly give the transfer function.

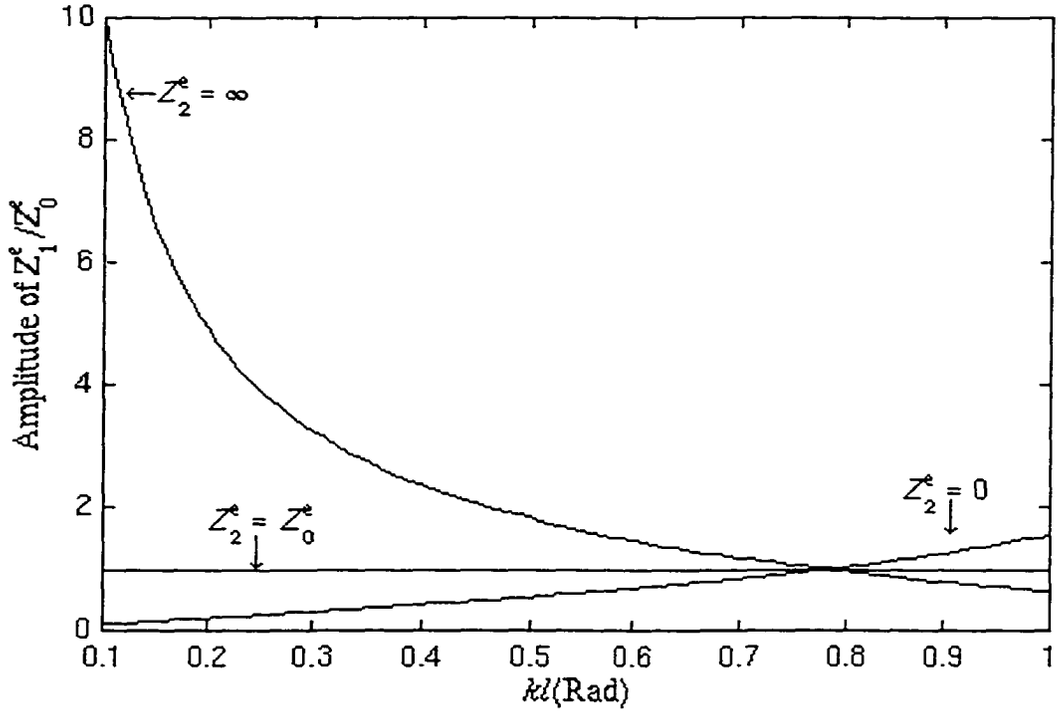

Figure 3.8 Impedances of a cable when one end is opened ($Z_2^e = \infty$), shorted ($Z_2^e = 0$) and terminated with an impedance equal to the intrinsic impedance of the cable ($Z_2^e = Z_0^e$).

3.3.1 Mason equivalent circuit approach

The Mason equivalent circuit for a backed piezoelectric plate is shown in Figure 2.13. To derive its transfer function explicitly, suppose that a voltage source V is connected with the electrical port (see Figure 3.9). During the following derivation, Thevenin's theorem is used to simplify the Mason equivalent circuit.

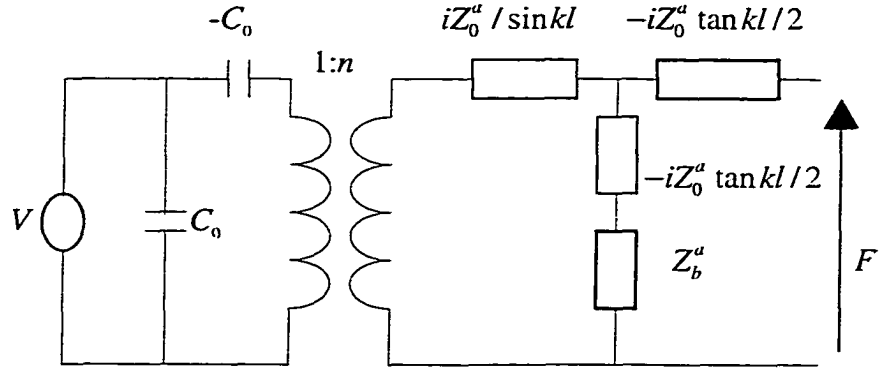

Figure 3.9 Equivalent circuit for a backed piezoelectric plate with the electrical port connected with a voltage source V and the mechanical port radiating acoustic waves.

To eliminate the electromechanical transformer, the voltage source and the two capacitors on the left side of the transformer are shifted to its right side by considering the turns ratio n; the electrical impedance on the left side of the transformer is divided by n^2. Figure 3.10 shows the transferred equivalent circuit.

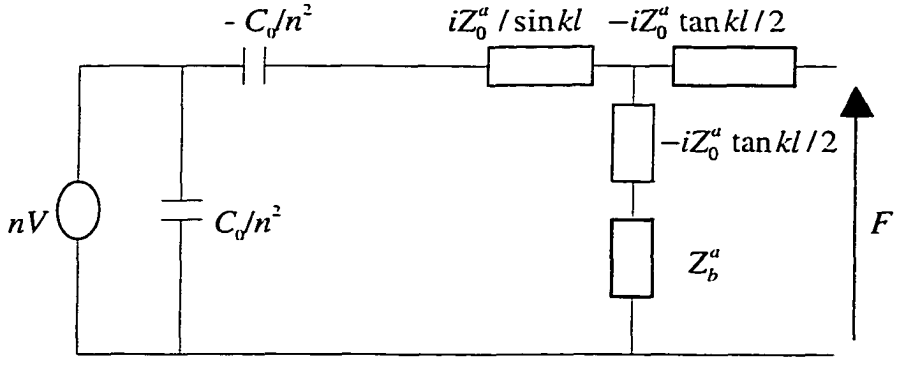

Figure 3.10 Equivalent circuit for a backed piezoelectric plate by eliminating the electromechanical transformer from Figure 3.9.

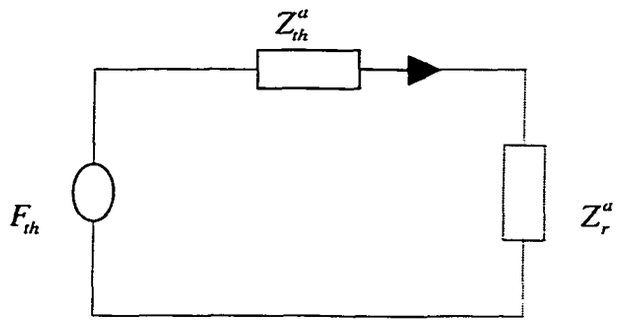

Figure 3.11 Thevenin equivalent circuit for a backed piezoelectric plate shown in Figure 3.10. The acoustic impedance shown by dashed lines is the radiation impedance.

According to Thevenin's theorem, the equivalent circuit in Figure 3.10 can be replaced by a voltage source with the amplitude of F_{th} and an internal impedance of Z_{th}^a in series. The corresponding Thevenin equivalent circuit is shown in Figure 3.11. By shorting the voltage source, nV, in Figure 3.10 and looking from the mechanical port, the internal impedance Z_{th}^a is expressed as

$$Z_{th}^a = -iZ_0^a \tan\frac{kl}{2} + \left(-iZ_0^a \tan\frac{kl}{2} + Z_b^a\right) // \left(\frac{iZ_0^a}{\sin kl} + \frac{n^2}{i\omega C_0}\right) \tag{3.3.1}$$

or,

$$Z_{th}^a = \frac{\left(Z_0^a\right)^2\left(1 - \frac{2n^2}{\omega C_0 Z_0^a}\tan\frac{kl}{2}\right) + iZ_b^a\left(Z_0^a \cot kl - \frac{n^2}{\omega C_0}\right)}{Z_b^a + iZ_0^a \cot kl + \frac{n^2}{i\omega C_0}} \tag{3.3.2}$$

where "//" denotes the two parts on the two sides of it are connected in parallel.

The open-circuit output "voltage" across the mechanical port is obtained as

$$F_{th} = \frac{Z_b^a - iZ_0^a \tan\frac{kl}{2}}{Z_b^a - iZ_0^a \tan\frac{kl}{2} + \frac{iZ_0^a}{\sin kl} + \frac{n^2}{i\omega C_0}} nV \tag{3.3.3}$$

or, using Eq. (2.3.48),

$$F_{th} = \frac{Z_b^a - iZ_0^a \tan\frac{kl}{2}}{Z_b^a + iZ_0^a \cot kl + \frac{n^2}{i\omega C_0}} nV. \tag{3.3.4}$$

When the transducer radiates acoustic waves through the mechanical port into an acoustic medium with the impedance Z_r^a, Z_r^a is connected to the right hand side of the Thevenin equivalent circuit shown in Figure 3.11, and the velocity, therefore, flowing into the load Z_r^a, is written as

$$v = \frac{F_{th}}{Z_{th}^a + Z_r^a}. \tag{3.3.5}$$

Substituting Eqs. (3.3.2) and (3.3.4) into the above equation, we find the particle velocity of the wave transmitted into the load Z_r^a expressed in terms of the electrical source V, the parameters of the piezoelectric plate and the backing.

$$\frac{v}{V} = \frac{\left(Z_b^a - iZ_0^a \tan\frac{kl}{2}\right)n}{Z_r^a Z_b^a + \left(Z_0^a\right)^2\left(1 - \frac{2n^2}{\omega C_0 Z_0^a}\tan\frac{kl}{2}\right) + i\left(Z_b^a + Z_r^a\right)\left(Z_0^a \cot kl - \frac{n^2}{\omega C_0}\right)}. \tag{3.3.6}$$

This is the explicit expression of the transfer function written in terms of the transmitted particle velocity. Correspondingly, the transfer function of the piezoelectric plate in terms of the output force is

$$H_t(\omega) = \frac{Z_r^a v}{V} = \frac{Z_r^a\left(Z_b^a - iZ_0^a \tan\frac{kl}{2}\right)n}{Z_r^a Z_b^a + \left(Z_0^a\right)^2\left(1 - \frac{2n^2}{\omega C_0 Z_0^a}\tan\frac{kl}{2}\right) + i\left(Z_b^a + Z_r^a\right)\left(Z_0^a \cot kl - \frac{n^2}{\omega C_0}\right)}. \tag{3.3.7}$$

Eqs. (3.3.6) and (3.3.7) give the general case with arbitrary acoustic impedance connected to the front and back faces of the piezoelectric plate. By changing the backing acoustic impedance, we can study its effect on the behavior of the transducer function. Figure 3.12 shows the variation $H_t(\omega)$ in the frequency range of from f=0 to f=10MHz, where $\omega = 2\pi f$. The piezoelectric is PZT-5H [Ristic, 1983] and the acoustic medium is water. In this figure, five curves are drawn which corresponds to frequency dependent impedance ratios $z_b = Z_b^a / Z_0^a = 0.1$, 0.4, 1, 2 and 5. By observing these curves, we can draw the following conclusion. If $Z_b^a < Z_0^a$, the piezoelectric plate vibrates like a half-wave resonator, similar to the case when the two mechanical ports are free. There is only one peak from 0-10MHz. If $Z_b^a > Z_0^a$, the piezoelectric plate vibrates like a quarter-wave resonator, similar to the case where one mechanical port free and the other one clamped. There are then two peaks from 0-10MHz. If $Z_b^a = Z_0^a$, the bandwidth of the transducer is the widest.

3.3.2 Transfer matrix model

The transfer function of a backed piezoelectric plate has been derived explicitly using the Mason equivalent circuit in subsection 3.3.1. However, the expression of the transfer function (see Eq. (3.3.7)) does not include cabling effects or an electrical impedance on the driving side, as would be the case with a real pulser driving the transducer, and the output face of the crystal does not include any acoustic layers such as a wear plate. If these factors are included into the Mason model, the explicit expression of the transfer function will become much more complex.

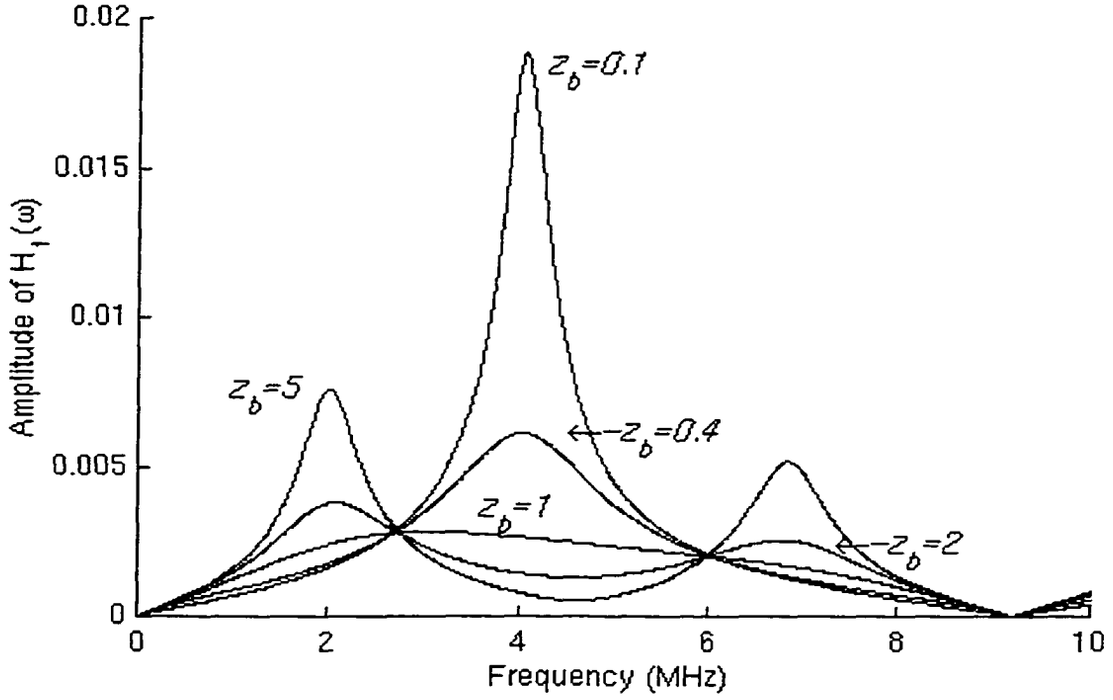

Figure 3.12 Transfer functions for a backed piezoelectric plate. The ratio of backing impedance to piezoelectric impedance, $z_b = Z_b^a / Z_0^a = 0.1$, 0.4, 1, 2 and 5. When $z_b = 0.1$, peak frequency is 4.05MHz. When $z_b = 2$, peak frequencies are 2.10MHz and 6.76MHz.

Such complications, however, can be easily handled if we model the transducer by a two-port network. Even if a wear plate is included at the front surface of the transducer, for example, the whole electromechanical system is still considered as a two-port network. Such a two-port network can be characterized by the following transfer matrix equation.

$$\begin{Bmatrix} V \\ I \end{Bmatrix} = \begin{bmatrix} T_{11}^T & T_{12}^T \\ T_{21}^T & T_{22}^T \end{bmatrix} \begin{Bmatrix} F \\ v \end{Bmatrix}. \qquad (3.3.8)$$

The transfer matrix T^T contains the multiplication of matrices shown in Eq. (2.4.16) and that of the wear plate, if any.

With the help of computers, an explicit expression of the transfer function of a transducer is really not necessary. Its implicit form as defined through products of transfer matrices to obtain the appropriate elements of T^T numerically is enough. From Eq. (3.3.8), if the radiation impedance of the transducer is Z_r^a, i.e.,

$$F/v = Z_r^a. \qquad (3.3.9)$$

The transfer function in terms of the elements of T^T is simply

$$H_t(\omega) = \frac{F}{V} = \frac{Z_r^a}{T_{11}^T Z_r^a + T_{12}^T}. \qquad (3.3.10)$$

3.4 Transducer Radiation Impedance

In many transducer studies in the literature, the radiation acoustic impedance of the transducer at its output face is taken as a constant equal to the specific impedance of a 1-D plane wave multiplied by the active area of the transducer face. However, even if a 1-D model is acceptable for describing the fields in the transducer itself, the same is not true for the acoustic fields the transducer generates. Transducers do not generate in general purely 1-D plane waves, even when the velocity on the face of the transducer is spatially uniform (i.e., a piston source model). As shown in this section, the radiation impedance of the transducer is determined by (1) the type of velocity distribution present on the transducer face and (2) by solving explicitly the acoustic radiation problem to obtain the corresponding radiation force. As we will see, the radiation impedance is generally a function of frequency.

3.4.1 Lumped quantities

If the normal velocity on the surface of a transmitting transducer is not uniform, it can not be directly used in the 1-D Mason equivalent circuit and two-port network models because it is position dependent. Thus, we need to define consistent 1-D force and velocity parameters that can be used with our 1-D transducer models. In Chapter 2, we assumed that the normal velocity $v_n(\mathbf{x}, \omega)$ could be written in separable form in terms of two factors (see Eq. (2.1.18)): one is the average velocity $v(\omega)$ over the surface of the transducer, which is frequency dependent but independent of position, the other is a normalized spatial

distribution function $f(\mathbf{x})$ defined over the transducer surface. The normal velocity then was written as

$$v_n(\mathbf{x},\omega) = v(\omega) f(\mathbf{x}) \tag{3.4.1}$$

where $\mathbf{x}$ is a point on the surface of the transducer. The rate of energy flowing out of the transmitting transducer is therefore

$$\int_S p(\mathbf{x},\omega) v_n(\mathbf{x},\omega) dS = v(\omega) \int_S p(\mathbf{x},\omega) f(\mathbf{x}) dS \tag{3.4.2}$$

where S is the transducer surface area. If we define the radiation force on the surface of the transducer as the weighted integral of the pressure

$$F(\omega) = \int_S p(\mathbf{x},\omega) f(\mathbf{x}) dS \tag{3.4.3}$$

then this energy flow is given by

$$\int_S p(\mathbf{x},\omega) v_n(\mathbf{x}_s,\omega) dS = F(\omega) v(\omega). \tag{3.4.4}$$

Eq. (3.4.4) shows that $F(\omega)$ and $v(\omega)$ are two lumped quantities coming from the two field quantities: pressure $p(\mathbf{x},\omega)$ and normal velocity $v_n(\mathbf{x},\omega)$. In applications of the Mason equivalent circuit and two-port networks, we can consistently use these lumped force and velocity quantities since they produce the same energy transfer as the underlying field quantities.

The velocity function $v(\omega)$ is the average velocity over the transducer surface. This can be shown by using Eq. (3.4.1). Integrating the two sides of Eq. (3.4.1) over the transducer surface, we have

$$\int_S v_n(\mathbf{x},\omega) dS = v(\omega) \int_S f(\mathbf{x}) dS. \tag{3.4.5}$$

But, if $f(\mathbf{x})$ is a normalized function over the transducer surface, i.e.,

$$\frac{1}{S} \int_S f(\mathbf{x}) dS = 1 \tag{3.4.6}$$

Eq. (3.4.5) gives

$$v(\omega) = \frac{1}{S} \int_S v_n(\mathbf{x},\omega) dS \tag{3.4.7}$$

which shows that $v(\omega)$ indeed is the average velocity over the transducer surface.

The lumped force is the integral of the pressure weighted by the velocity distribution function over the surface of the transducer (Eq. 3.4.3). Only if the velocity distribution is uniform, i.e., $f(\mathbf{x}) = 1$, is the lumped force equal to the average pressure on the face of the transducer times the area, i.e.,

$$F(\omega) = \int_S p(\mathbf{x},\omega)dS\,. \tag{3.4.8}$$

Note, however, that there is some arbitrariness in these definitions of lumped parameters. We could have modeled the transducer, for example, as a surface over which we specify the pressure distribution in separable form as

$$p(\mathbf{x},\omega) = \bar{p}(\omega)g(\mathbf{x}) \tag{3.4.9}$$

where $\bar{p}(\omega)$ is the average pressure over the surface of the transducer and $g(\mathbf{x})$ is normalized distribution function such that

$$\frac{1}{S}\int_S g(\mathbf{x})dS = 1\,. \tag{3.4.10}$$

Then we could define a lumped force parameter

$$\tilde{F}(\omega) = \bar{p}(\omega)S \tag{3.4.11}$$

which is always equal to the average pressure multiplied by the area S. In this case, then the rate of energy flowing out of the transducer would become

$$\int_S p(\mathbf{x},\omega)v_n(\mathbf{x}_s,\omega)dS = \tilde{F}(\omega)\tilde{v}(\omega) \tag{3.4.12}$$

where

$$\tilde{v}(\omega) = \frac{1}{S}\int_S v_n(\mathbf{x},\omega)g(\mathbf{x})dS \tag{3.4.13}$$

is a weighted average of the velocity wave field.

Either definition of lumped parameters in principle is acceptable. However, for an immersion transducer radiating into a fluid, the crystal and face plate are much more rigid than the surrounding fluid so that specification of the velocity as in Eq. (3.4.1) appears to be more reasonable from a physical standpoint. For a contact transducer where a thin fluid layer separates the transducer face from an elastic solid, treating the transducer as a pressure source as in Eq. (3.4.9) would seem more appropriate. Here, we will use the average velocity, $v(\omega)$, and weighted force, $F(\omega)$, as our lumped parameters.

We should also note that it is strictly not necessary to make any assumption about either the velocity or pressure on the transducer face to replace a field model with lumped force and velocity parameters. We could equally as well, for example, define an average velocity as shown in Eq. (3.4.7) and the power radiated by the transducer, $P(\omega)$, as

$$P(\omega) = \int_S p(\mathbf{x},\omega)v_n(\mathbf{x},\omega)dS\,. \tag{3.4.14}$$

Then a lumped force, $\hat{F}(\omega)$, could be defined simply as

$$\hat{F}(\omega) = P(\omega)/v(\omega) \tag{3.4.15}$$

and $\left(\hat{F}(\omega), v(\omega)\right)$ would be a consistent pair of lumped parameters since they produce the same power flow as the original fields.

3.4.2 Radiation acoustic impedance

When a transducer radiates acoustic waves directly into an acoustic medium, it is equivalent to connecting an acoustic impedance $Z_r(\omega)$ to the mechanical radiation port such that

$$F(\omega) = Z_r^a(\omega)v(\omega). \tag{3.4.16}$$

From Eq. (3.4.3), the radiation acoustic impedance is obtained as

$$Z_r^a(\omega) = \frac{\int_S f(\mathbf{x})p(\mathbf{x},\omega)dS}{v(\omega)}. \tag{3.4.17}$$

This equation shows that the radiation acoustic impedance is the ratio of the lumped force to the lumped velocity. It is clearly dependent on the velocity distribution function.

If both the velocity and pressure distributions are assumed uniform, then

$$p(\mathbf{x},\omega) = p(\omega) \tag{3.4.18}$$

and

$$f(\mathbf{x}) = 1 \tag{3.4.19}$$

and Eq. (3.4.17) gives

$$Z_r^a(\omega) = \frac{p(\omega)S}{v(\omega)}. \tag{3.4.20}$$

Furthermore, if it is assumed that $p(\omega)$ and $v(\omega)$ are related by the specific impedance of a 1-D plane wave traveling in the acoustic medium,

$$z = \rho c \tag{3.4.21}$$

where ρ is the density of the acoustic medium and c is its longitudinal acoustic velocity, we would find

$$Z_r^a(\omega) = \rho cS = \text{a constant} \tag{3.4.22}$$

as is commonly used in the literature. However, the two assumptions leading to Eq. (3.4.22) are in general both incorrect. First, if we specify a velocity $v_n(\mathbf{x},\omega) = v(\omega)f(\mathbf{x})$ on the transducer face, then the pressure $p(\mathbf{x},\omega)$ is determined by solving a boundary value problem for the radiated waves and we cannot specify the nature of variations of both $v_n(\mathbf{x},\omega)$ and $p(\mathbf{x},\omega)$ simultaneously. Second, in the solution of the radiation problem, the waves

generated are not purely 1-D plane waves so that we do not expect the specific impedance of a plane wave to be appropriate for describing a 3-D diffraction problem.

To see what form $Z_r^a(\omega)$ really takes we must solve a specific radiation problem. Therefore, consider a circular transducer of radius a where the weighting function is only a function of the radial distance, r, from the center of the face of the transducer and takes the following form [Greenspan, 1979]

$$f(\mathbf{x}) = \begin{cases} \dfrac{(n+1)}{\pi a^2}\left(1-\dfrac{r^2}{a^2}\right)^n & (n=0,1,2) \quad (r \le a) \\ 0 & (r > a) \end{cases}. \tag{3.4.23}$$

The value n=0 corresponds to a plane "piston" model, n=1 to a model "simply supported" at $r = a$ and n=2 to a model "clamped" at $r = a$.

a. Piston model (n=0)

For the piston model where n=0 in Eq. (3.4.23), Greenspan derived the acoustic radiation impedance of the transducer. This impedance normalized by the plane wave acoustic impedance was given as

$$\frac{Z_r^a(\omega)}{\rho c S} = 1 - \frac{1}{ka}\left\{J_1(2ka) - iH_1(2ka)\right\} \tag{3.4.24}$$

where $S = \pi a^2$ is the surface area of the transducer, $J_1(x)$ the first order Bessel function and $H_1(x)$ the first order Struve function which is given as [Gradshteyn and Ryzhik, 1980]

$$H_1(x) = \frac{2x}{\pi}\int_0^1 \sqrt{1-t^2}\sin(xt)dt. \tag{3.4.25}$$

For high frequency, i.e., $ka \to \infty$, from Eq. (3.4.24), it is easy to show that

$$Z_r^a(\omega) = \rho c S. \tag{3.4.26}$$

This equation shows that at sufficient high frequency, the acoustic radiation impedance of a piston transducer indeed is equal to the product of the specific impedance of the radiation medium and the surface area of the transducer, as often assumed.

b. Simply-supported model (n=1)

For the simply-supported model where n=1 in Eq. (3.4.23), Greenspan also gave the normalized acoustic radiation impedance as

$$\frac{Z_r^a(\omega)}{\rho c S} = \frac{4}{3}\left\{1 - \frac{3}{(ka)^5}\left[F_1(2ka) + iF_2(2ka)\right]\right\} \tag{3.4.27}$$

with

$$F_1(y) = (10 - y^2)J_1(y) - 5yJ_0(y) - y^3/8 \tag{3.4.28}$$

$$F_2(y) = (y^2 - 10)H_1(y) + 5yH_0(y) - 10y^2/3\pi \tag{3.4.29}$$

where $J_0(x)$ is the zeroth order Bessel function and $H_0(x)$ the zeroth order Struve function which is given as [Gradshteyn and Ryzhik, 1980]

$$H_0(x)=\frac{2}{\pi}\int_0^1 \frac{\sin(xt)}{\sqrt{1-t^2}}dt. \tag{3.4.30}$$

For high frequency, i.e., $ka \to \infty$, the limit of Eq. (3.4.27) can be obtained, but now we find

$$Z_r^a(\omega)=\frac{4}{3}\rho cS. \tag{3.4.31}$$

This equation shows that at high frequency, the acoustic radiation impedance of the simply supported case is a constant but that constant is not just ρcS as in the piston case.

c. Clamped model (n=2)

For the clamped model where n=2 in Eq. (3.4.23), Greenspan again found the normalized acoustic radiation impedance as

$$\frac{Z_r^a(\omega)}{\rho cS}=\frac{9}{5}\left\{1-\frac{20}{(ka)^9}\left[F_1'(2ka)+iF_2'(2ka)\right]\right\} \tag{3.4.32}$$

with

$$F_1'(y)=AJ_1(y)+BJ_0(y)-\frac{y^5}{16}-\frac{y^7}{768} \tag{3.4.33}$$

$$F_2'(y)=-AH_1(y)-BH_0(y)+\frac{14y^4}{15\pi}-\frac{168y^2}{\pi} \tag{3.4.34}$$

where

$$A=y^4-91y^2+504$$
$$B=14y\left(y^2-18\right).$$

For high frequency, i.e., $ka \to \infty$, again, Eq. (3.4.32) yields

$$Z_r^a(\omega)=\frac{9}{5}\rho cS. \tag{3.4.35}$$

Once more at high frequency, the acoustic radiation impedance of the clamped case does not agree with a simple 1-D plane wave value.

The acoustic radiation impedances for the three cases are given in Figure 3.13 versus the non dimensional frequency, ka. The impedances are normalized by $V\rho cS$ with V=1 for a piston model, V=4/3 for a simply-supported model and V=9/5 for a clamped model.

In Figure 3.13, the solid line shows the normalized impedance for a piston model (n=0), the long dashed line shows the normalized impedance for a simply-supported model (n=1) and the short dashed line shows the normalized impedance for a clamped model (n=2). For ka>10, these normalized impedance curves all asymptote to a constant of 1. Thus, for all

practical purposes for $ka>10$, the radiation impedances all are equal to their constant high frequency limits.

Typically, in ultrasonic NDE, transducers radiating into water often have ka values of 100 or greater so that we expect that in such cases it will be in general a good approximation to assume that the radiation impedance is a constant. However, as our discussion has just shown, this constant is not necessarily just equal to the product of the specific impedance of the acoustic medium and the surface area of the transducer. Note that if we use the fluid model of Greenspan to describe the radiation of a contact transducer into an elastic solid, then the ka values are typically much smaller and we cannot expect $Z_r^a(\omega)$ to be constant.

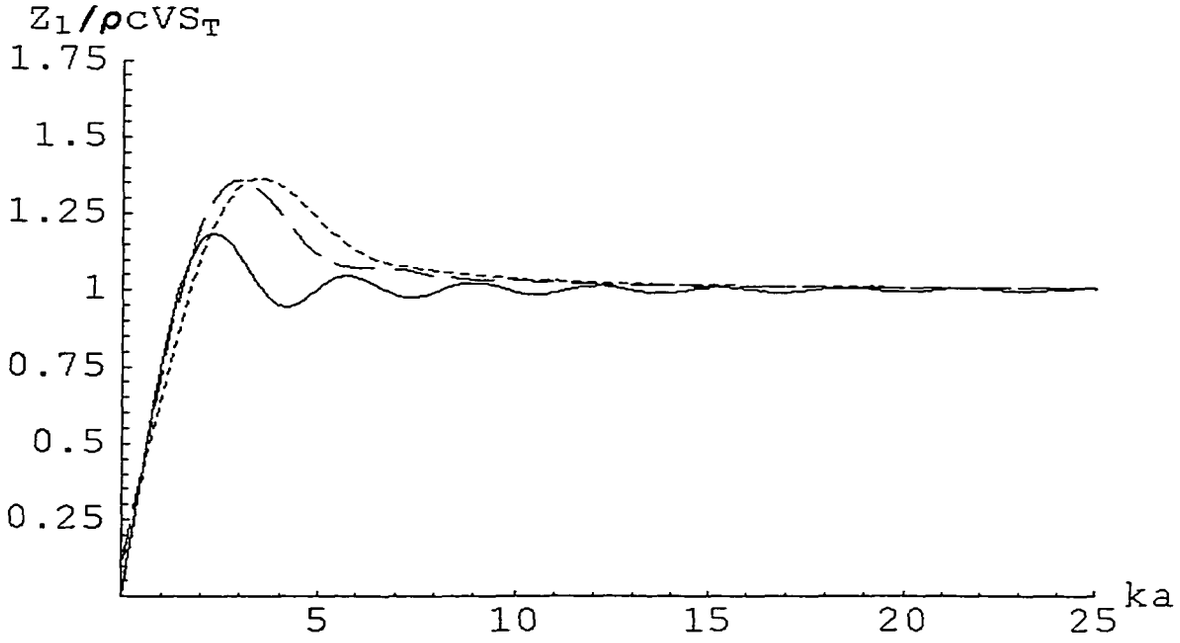

Figure 3.13 Normalized radiation acoustic impedance versus non-dimensional wave number ka for a piston model (n=0, solid line), a simply-supported model (n=1, long dashes) and a clamped model (n=2, short dashes).

3.5 Generation Process Transfer Function

In this chapter, the generation process was divided into four components: pulser, cable, transducer and acoustic medium (Figure 3.1). In Section 3.1, the pulser was modeled by a Thevenin equivalent circuit (Figure 3.2). In Section 3.2, the cable was modeled by a

transmission line (Figure 3.5). In Section 3.3, the transducer is modeled by a transfer matrix. In Section 3.4, the acoustic medium was replaced by a radiation acoustic impedance. Collecting all of these components, the entire generation process is modeled by the diagram shown in Figure 3.14.

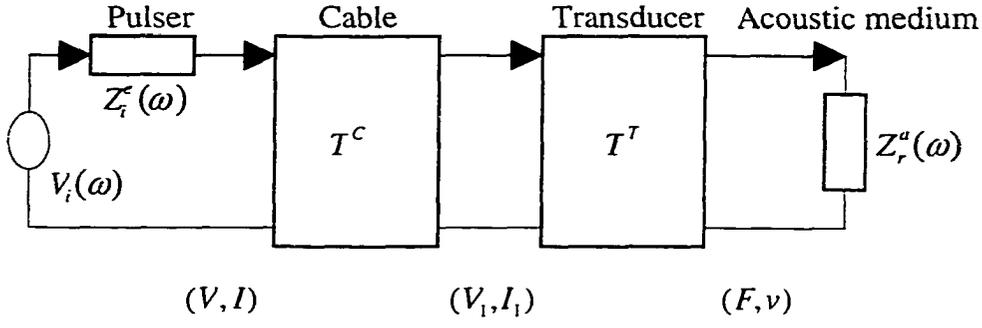

Figure 3.14 The generation process model where the pulser modeled by a Thevenin equivalent circuit, the cable by a transmission line, the transducer by a transfer matrix and the acoustic medium by the radiation acoustic impedance.

The transfer matrices of the cable and the transducer form the global transfer matrix for the generation process. From Eq. (3.2.1), the cable transfer matrix equation is written as

$$\begin{Bmatrix} V \\ I \end{Bmatrix} = \begin{bmatrix} T_{11}^{C} & T_{12}^{C} \\ T_{21}^{C} & T_{22}^{C} \end{bmatrix} \begin{Bmatrix} V_1 \\ I_1 \end{Bmatrix}. \tag{3.5.1}$$

From Eq. (3.3.8), the transducer transfer matrix equation is written as

$$\begin{Bmatrix} V_1 \\ I_1 \end{Bmatrix} = \begin{bmatrix} T_{11}^{T} & T_{12}^{T} \\ T_{21}^{T} & T_{22}^{T} \end{bmatrix} \begin{Bmatrix} F \\ v \end{Bmatrix}. \tag{3.5.2}$$

Putting Eq. (3.5.2) into Eq. (3.5.1) gives

$$\begin{Bmatrix} V \\ I \end{Bmatrix} = \begin{bmatrix} T_{11}^{C} & T_{12}^{C} \\ T_{21}^{C} & T_{22}^{C} \end{bmatrix} \begin{bmatrix} T_{11}^{T} & T_{12}^{T} \\ T_{21}^{T} & T_{22}^{T} \end{bmatrix} \begin{Bmatrix} F \\ v \end{Bmatrix}. \tag{3.5.3}$$

Letting

$$\left[T^{G}\right] = \begin{bmatrix} T_{11}^{G} & T_{12}^{G} \\ T_{21}^{G} & T_{22}^{G} \end{bmatrix} = \begin{bmatrix} T_{11}^{C} & T_{12}^{C} \\ T_{21}^{C} & T_{22}^{C} \end{bmatrix} \begin{bmatrix} T_{11}^{T} & T_{12}^{T} \\ T_{21}^{T} & T_{22}^{T} \end{bmatrix} \tag{3.5.4}$$

then $\left[T^{G}\right]$ is called the global transfer matrix for the generation process. Eq. (3.5.3) is written as

$$\begin{Bmatrix} V \\ I \end{Bmatrix} = \begin{bmatrix} T_{11}^{G} & T_{12}^{G} \\ T_{21}^{G} & T_{22}^{G} \end{bmatrix} \begin{Bmatrix} F \\ v \end{Bmatrix}. \tag{3.5.5}$$

Eq. (3.5.5) shows that the combined effect of the cable and transducer is modeled by a global transfer matrix $[T^G]$. In fact, if there are any other components between the pulser and the acoustic medium that can be modeled by two-port networks, those two-port networks can also be reduced to a single two-port network characterized by a global transfer matrix. The strategy is to cascade all the component transfer matrices as discussed in subsection 2.2.3. If every component is reciprocal, the global transfer matrix is also reciprocal.

Using Eq. (3.5.5), the generation process shown in Figure 3.14 is simplified to the network of Figure 3.15.

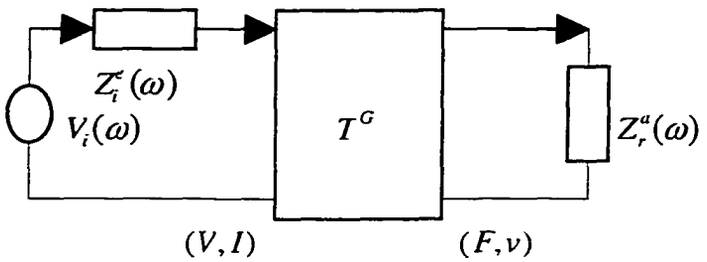

Figure 3.15 The generation process model with the global matrix used to replace all the two-port networks between the pulser and the acoustic medium.

The transmitting sensitivity of the entire generation process can be obtained from Figure 3.15. On the two sides of the global two-port network, the following equations hold.

$$V_i(\omega) = V + IZ_i^e(\omega) \tag{3.5.6}$$

$$F = vZ_r^a(\omega). \tag{3.5.7}$$

From Eq. (3.5.5), we have

$$\frac{V}{I} = \frac{T_{11}^{G}F + T_{12}^{G}v}{T_{21}^{G}F + T_{22}^{G}v}. \tag{3.5.8}$$

Using Eq. (3.5.7), Eq. (3.5.8) is rewritten as

$$\frac{V}{I} = \frac{T_{11}^{G}Z_r^a(\omega) + T_{12}^{G}}{T_{21}^{G}Z_r^a(\omega) + T_{22}^{G}}. \tag{3.5.9}$$

Canceling out current I from Eq. (3.5.6) and Eq. (3.5.9) gives

$$V_i(\omega) = V\left(1 + \frac{T_{21}^{G}Z_r^a(\omega) + T_{22}^{G}}{T_{11}^{G}Z_r^a(\omega) + T_{12}^{G}} Z_i^e(\omega)\right). \tag{3.5.10}$$

The first equation in Eq. (3.5.5) is expressed as

$$V = FT_{11}^{G} + vT_{12}^{G}. \tag{3.5.11}$$

Considering Eq. (3.5.7), Eq. (3.5.11) becomes

$$V = v\left(Z_r^a(\omega)T_{11}^{G} + T_{12}^{G}\right). \tag{3.5.12}$$

Putting Eq. (3.5.12) into Eq. (3.5.10), we have

$$V_i(\omega) = v\left[\left(Z_r^a(\omega)T_{11}^{G} + T_{12}^{G}\right) + \left(T_{21}^{G}Z_r^a(\omega) + T_{22}^{G}\right)Z_i^e(\omega)\right] \tag{3.5.13}$$

or,

$$\frac{v(\omega)}{V_i(\omega)} = \frac{1}{\left(Z_r^a(\omega)T_{11}^{G} + T_{12}^{G}\right) + \left(T_{21}^{G}Z_r^a(\omega) + T_{22}^{G}\right)Z_i^e(\omega)}. \tag{3.5.14}$$

Eq. (3.5.14) gives a velocity based transfer function which describes the entire generation system. The transmitting velocity is expressed in terms of the source parameters, global transfer matrix parameters and the acoustic medium parameter. Given all the parameters of the generation process, the radiation velocity is obtained from Eq. (3.5.14).

If the transfer function of the generation system is expressed instead in terms of the transmitting force, $F = F_t$, then using Eq. (3.5.7), we have

$$t_G(\omega) = \frac{F_t(\omega)}{V_i(\omega)} = \frac{Z_r^a(\omega)}{\left(Z_r^a(\omega)T_{11}^{G} + T_{12}^{G}\right) + \left(T_{21}^{G}Z_r^a(\omega) + T_{22}^{G}\right)Z_i^e(\omega)}. \tag{3.5.15}$$

CHAPTER 4. THE RECEPTION PROCESS

Like the generation process described in the last chapter, the reception process in an ultrasonic measurement system contains four components: an acoustic medium in front of the receiving transducer, a receiving transducer, cabling, and a receiver. The components of the entire reception process are shown in Figure 4.1. The effects of the cable discussed in section 3.2 apply to the cable here also, so they need not be considered again. However, the other components are discussed in detail.

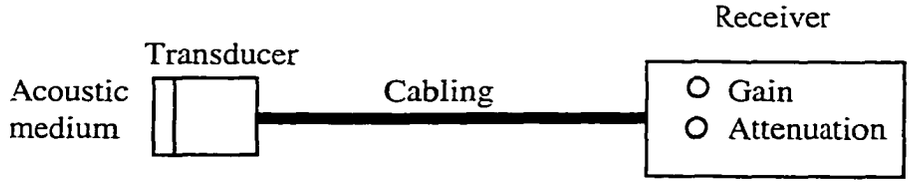

Figure 4.1 Reception process which includes four components: acoustic medium, transducer, cabling and receiver.

4.1 Incident Acoustic Waves

Consider the case where acoustic waves are incident on a receiving transducer, as shown in Figure 4.2. These waves could come from a flaw or from another transducer. In either case the waves are generally not plane waves and are not propagating normal to the transducer surface (although in practice if the receiving transducer is oriented to maximize the received signal the assumption that the transducer normal is along the incoming wave direction may be correct). When the incoming waves strike the transducer, a part of these waves is scattered from the transducer surface and part is transmitted into the transducer and converted to electrical energy. The sum of the incident, scattered, and transmitted waves will generate a velocity field, $\mathbf{v}(\mathbf{x},\omega)$, on the face of the transducer. We can decompose our original problem (Figure 4.2) into two separate problems as shown in Figure 4.3(a) and (b). In problem one (Figure 4.3(a)), the incident waves strike the transducer with its face blocked, i.e. the surface velocity is identically zero. In problem two (Figure 4.3(b)), the incident wave is absent but now the transducer radiates (like a transmitter) with the same velocity distribution, $\mathbf{v}(\mathbf{x},\omega)$, as is generated by all the waves present in Figure 4.2. Furthermore, if we assume that the motion of the transducer in this reception mode has the same separable

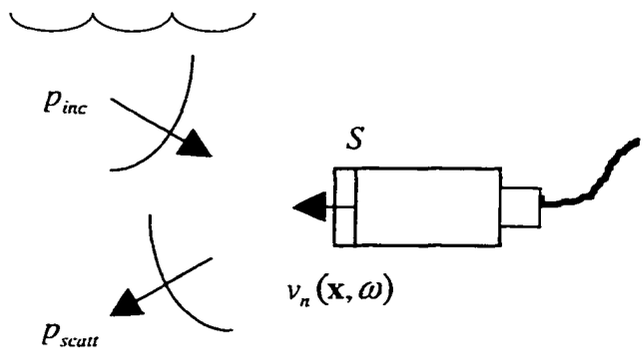

Figure 4.2 Incident and scattered waves at a receiving transducer which has a normal velocity $v_n(\mathbf{x},\omega)$ on its surface S.

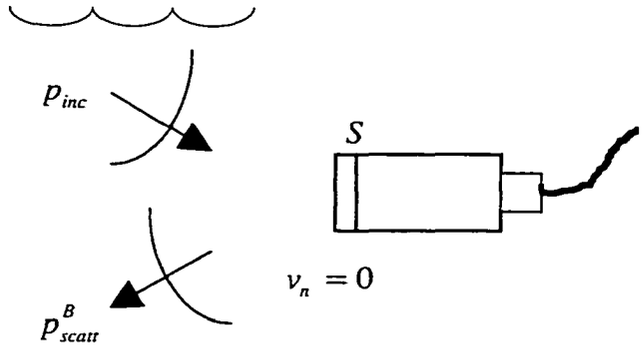

Figure 4.3 (a) Incident and scattered waves at a "blocked" transducer when $v_n = 0$ on its surface S.

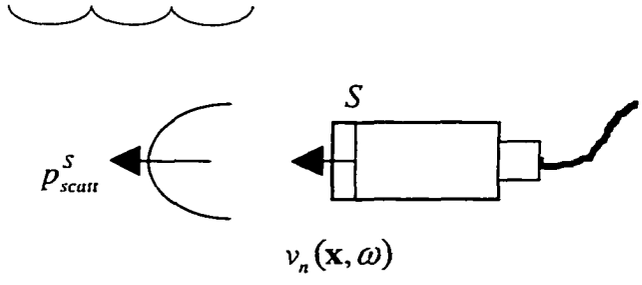

Figure 4.3 (b) The "scattered" waves generated by a surface normal velocity, $v_n(\mathbf{x},\omega)$, of the face of the transducer which is identical to the normal velocity in Figure 4.2.

form as found when this transducer is used as a transmitter then $\mathbf{v}(\mathbf{x},\omega) = v_n(\mathbf{x},\omega)\mathbf{n}$, where $\mathbf{n}$ is the unit outward normal to the transducer surface, and we have

$$v_n(\mathbf{x},\omega) = v(\omega) f(\mathbf{x}). \tag{4.1.1}$$

Under these assumptions, we can again define a lumped force at the transducer face in terms of a weighted pressure integral, as in the generation process. Now consider this force, which for our original problem is given by

$$F(\omega) = \int_S [p_{inc}(\mathbf{x},\omega) + p_{scatt}(\mathbf{x},\omega)] f(\mathbf{x}) dS. \tag{4.1.2}$$

The total scattered waves in Figure 4.2 can be decomposed into the waves scattered from the blocked transducer, Figure 4.3(a), and the waves "scattered" by the velocity distribution of Fig 4.3(b), i.e.

$$p_{scatt}(\mathbf{x},\omega) = p^B_{scatt}(\mathbf{x},\omega) + p^S_{scatt}(\mathbf{x},\omega) \tag{4.1.3}$$

where $p^B_{scatt}(\mathbf{x},\omega)$ is the pressure on the surface of the blocked transducer of problem one and $p^S_{scatt}(\mathbf{x},\omega)$ is the pressure due to the waves generated by the velocity distribution "source" of problem two. Then the lumped "blocked force" of problem one, $F_B(\omega)$, is given by

$$F_B(\omega) = \int_S [p^B_{scatt}(\mathbf{x},\omega) + p_{inc}(\mathbf{x},\omega)] f(\mathbf{x}) dS \tag{4.1.4}$$

and the lumped force for problem two is

$$F_S(\omega) = \int_S p^S_{scatt}(\mathbf{x},\omega) f(\mathbf{x}) dS = Z^a_r(\omega) v(\omega) \tag{4.1.5}$$

where, based on our assumptions, $Z^a_r(\omega)$ is the same radiation impedance present when the transducer is acting as a transmitter. Combining Eqs. (4.1.2), (4.1.4) and (4.1.5), using Eq. (4.1.3), we thus find

$$F(\omega) = F_B(\omega) + Z^a_r(\omega) v(\omega). \tag{4.1.6}$$

Equation (4.1.6) shows that in general at the receiving face of the transducer, the input conditions in terms of the lumped force and velocity parameters can be considered to be a blocked "voltage" source, $F_B(\omega)$, in series with an acoustic impedance, $Z^a_r(\omega)$. Thus, at the input side of a 1-D transducer model we have the input conditions shown in Figure 4.4.

Many transducer modeling studies derive the input conditions for a receiver under much more restrictive assumptions. Typically, it is assumed that the incident wave is a 1-D plane wave and that the interactions with the transducer face can be treated as if that plane wave is at normal incidence to an infinite planar interface. Under those assumptions the total force and velocity at the interface, $F(\omega)$ and $v(\omega)$, are given by

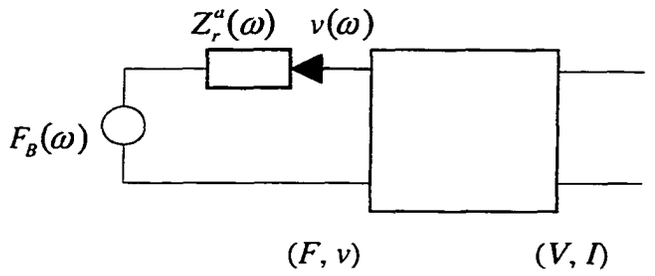

Figure 4.4 Lumped force and velocity conditions on the input side of a 1-D transducer model consistent with the fields present.

$$F(\omega) = F_{inc}(\omega) + F_{reflt}(\omega) \tag{4.1.7}$$

$$v(\omega) = -\frac{F_{inc}(\omega)}{Z_a} + \frac{F_{reflt}(\omega)}{Z_a} \tag{4.1.8}$$

where $F_{inc}(\omega)$ is the force at the interface due to the incident plane wave, $F_{reflt}(\omega)$ is the corresponding force for the reflected wave, and $Z_a = \rho c S$ is the 1-D plane wave acoustic impedance for the fluid surrounding the receiver multiplied by the transducer surface area. Eliminating the force of the reflected waves from these two equations, we find

$$F(\omega) = 2F_{inc}(\omega) + Z_a(\omega)v(\omega). \tag{4.1.9}$$

Comparing Eq. (4.1.9) with Eq. (4.1.6), we see that in a 1-D model the blocked force is given by

$$F_B(\omega) = 2F_{inc}(\omega) \tag{4.1.10}$$

and the radiation impedance is replaced by the 1-D plane wave value. This leads to the input conditions in a 1-D transducer model shown in Figure 4.5, a result that commonly is used in the literature.

Either Eq. (4.1.6) or Eq. (4.1.9) shows that the force acting on the transducer face, $F(\omega)$, is not equal to the blocked force, in general. However, if we know the input impedance of the entire receiving system (transducer, cabling, and receiver), $Z_{in}^a(\omega)$, then the Thevenin equivalent circuit of Figure 4.6 gives the relations

$$F(\omega) - F_B(\omega) = Z_r^a(\omega)v(\omega) \tag{4.1.11}$$

$$F(\omega) = -Z_{in}^a(\omega)v(\omega) \tag{4.1.12}$$

which can be combined to yield

$$F(\omega) = \frac{Z_{in}^a(\omega)}{Z_r^a(\omega) + Z_{in}^a(\omega)} F_B(\omega) \tag{4.1.13}$$

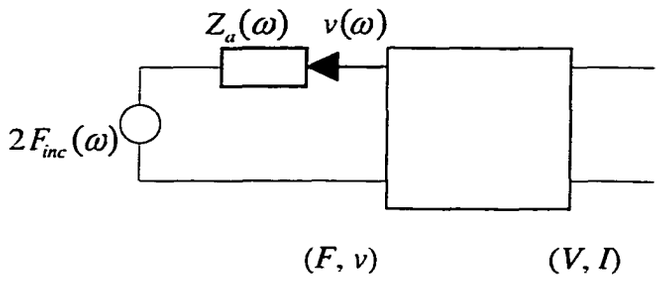

Figure 4.5 Lumped force and velocity conditions on the input side of a 1-D transducer model where the acoustic waves are modeled as 1-D plane waves traveling parallel to the surface normal of the transducer surface.

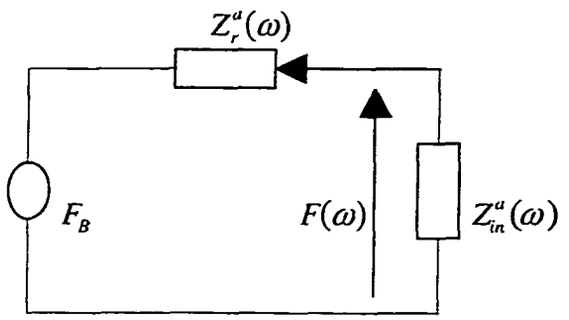

Figure 4.6 Thevenin equivalent circuit for the normal incidence acoustic system shown in Figure 4.4. The source strength is F_B and the internal impedance is the acoustic medium carrying the incident acoustic waves.

which gives the relationship between the blocked force and the force acting on the transducer face.

4.2 Receiving Transducer

A receiving transducer accepts acoustic waves at its mechanical port and outputs electrical signals at its electrical port. Similar to the transmitting transducer, a receiving transducer can be modeled either by a Mason equivalent circuit or by a 2x2 transfer matrix network. Again, we will use both approaches to analyze the behavior of the receiving transducer.

4.2.1 Mason equivalent circuit approach

The Mason equivalent circuit of a receiving transducer is shown in Figure 4.7 where the receiving transducer is composed of a thickness mode piezoelectric plate and a backing material with an acoustic impedance of Z_b^a.

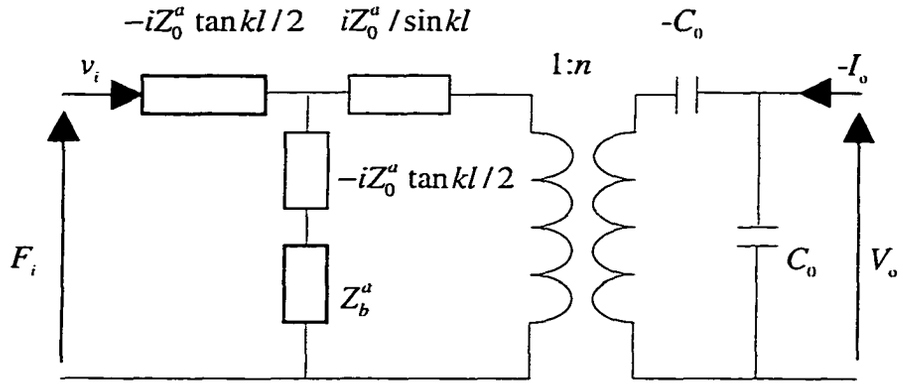

Figure 4.7 Equivalent circuit for the receiving transducer composed of a piezoelectric plate and a backing material. It is a two-port network with the mechanical port on the left side to receive acoustic waves and the electrical port on the right side to output electrical signals.

The energy flow in the receiving transducer is opposite to that found in the transmitting transducer. This is reflected in Figure 4.7 where input and output "current" (v_i, I_0) flow from the "force side" of the circuit to the "current side".

In this subsection, the equivalent circuit shown in Figure 4.7 will be used to derive explicit expression for both the input acoustic impedance of the receiving transducer and its transfer function.

4.2.1.1 Input acoustic impedance

To discuss the input impedance of the receiving transducer, it is necessary to specify termination conditions of the electrical port of that transducer, which in an ultrasonic measurement may be a function of the cabling and receiver properties. Thus, as mentioned previously, the input impedance is really a property of the entire receiving system, not just the transducer itself. With this in mind, we will continue to call quantities such as Z_{in}^a in Figure 4.6 the input impedance of the receiving transducer.

Equation (4.1.13) showed that, given the blocked force on the transducer, the total force $F(\omega)$ sensed by the transducer can be found if the input impedance of the receiving transducer and its radiation impedance are both known. We have already discussed the radiation impedance in section 3.4. Here we will consider the input impedance. Note that the total force $F(\omega)$ has been relabeled as F_i in Figure 4.7 so that (force, velocity) inputs are (F_i, v_i), respectively, and the (voltage, current) outputs are (V_0, I_0), respectively.

We will assume that the transducer of Figure 4.7 is terminated by an electrical impedance, Z_o^e, at the electrical port. If we then eliminate the electromechanical transformer of Figure 4.7, we arrive at the equivalent circuit shown in Figure 4.8.

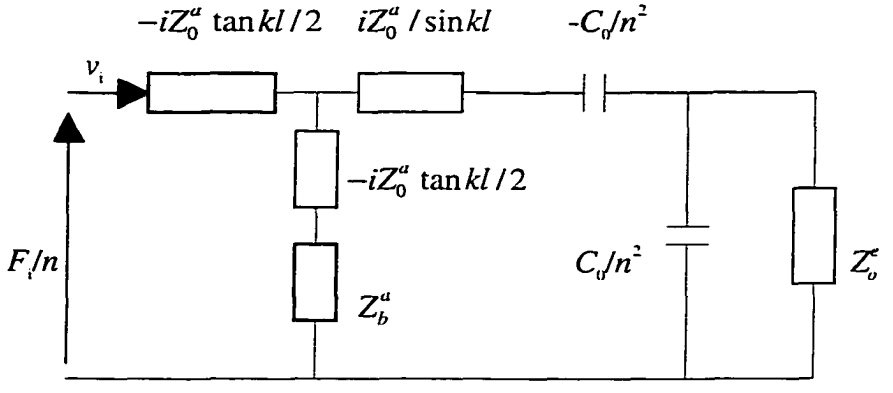

Figure 4.8 Equivalent circuit by connecting an electrical impedance of Z_o^e at the electrical port in Figure 4.7 and eliminating the electromechanical transformer.

The input acoustic impedance of a receiving transducer is then expressed as

$$Z_{in}^a = \frac{F_i}{v_i}. \tag{4.2.1}$$

Looking from the left side of the circuit shown in Figure 4.8, the input acoustic impedance is

$$Z_{in}^a = -iZ_0^a \tan\frac{kl}{2} + \left(Z_b^a - iZ_0^a \tan\frac{kl}{2}\right) // \left(\frac{iZ_0^a}{\sin kl} + \frac{n^2}{i\omega C_0} + n^2 Z_o^e // \frac{n^2}{-i\omega C_0}\right) \tag{4.2.2}$$

or,

$$Z_{in}^a = -iZ_0^a \tan\frac{kl}{2} + \left(Z_b^a - iZ_0^a \tan\frac{kl}{2}\right) // \left(\frac{iZ_0^a}{\sin kl} + \frac{n^2}{i\omega C_0} + \frac{n^2 Z_o^e}{1 - i\omega C_0 Z_o^e}\right). \tag{4.2.3}$$

Again, "//" denotes that the two parts on the two sides of this symbol are connected in parallel.

Using Eq. (2.3.48) and explicitly deriving Z_{in}^a from the condition specified in Eq. (4.2.3), we find

$$Z_{in}^a = \frac{(Z_0^a)^2\left(1-\frac{2n^2}{\omega C_0 Z_0^a}\tan\frac{kl}{2}\right)+iZ_b^a\left(Z_0^a\cot kl-\frac{n^2}{\omega C_0}\right)+\frac{n^2 Z_v^e Z_b^a}{1-i\omega C_0 Z_v^e}\left(1-i2\tan\frac{kl}{2}\right)}{Z_b^a+iZ_0^a\cot kl+\frac{n^2}{i\omega C_0}+\frac{n^2 Z_v^e}{1-i\omega C_0 Z_v^e}}. \tag{4.2.4}$$

It is interesting to note that, if we let $Z_v^e = 0$, Eq. (4.2.4) is simplified as

$$Z_{in}^a = \frac{(Z_0^a)^2\left(1-\frac{2n^2}{\omega C_0 Z_0^a}\tan\frac{kl}{2}\right)+iZ_b^a\left(Z_0^a\cot kl-\frac{n^2}{\omega C_0}\right)}{Z_b^a+iZ_0^a\cot kl+\frac{n^2}{i\omega C_0}} \tag{4.2.5}$$

which is the same as the internal impedance (see Eq. (3.3.2)) of the equivalent circuit in the generation process shown in Figures 3.10 and 3.11. This conclusion comes from the reciprocity of the transducer. In fact, letting $Z_v^e = 0$ in Figure 4.5 and shorting the source in Figure 3.10, the two equivalent circuits are the same.

Another important fact is that, letting the turns ratio of the electromechanical transformer, n, be zero, Eq. (4.2.4) simplifies to

$$Z_{in}^a = Z_0^a\frac{Z_0^a+iZ_b^a\cot kl}{Z_b^a+iZ_0^a\cot kl} \tag{4.2.6}$$

which is equivalent to Eq. (2.5.5). In this case, the receiving transducer can be considered as an acoustic transmission line terminated with an impedance Z_b^a.

4.2.1.2 Receiving transfer functions

Similar to the generation process (see Chapter 3), the transfer function of the reception process can be derived by use of a Thevenin equivalent circuit. Consider the equivalent circuit for a receiving transducer shown in Figure 4.7. The input force F_i at the mechanical port is replaced by a force source and we transpose the left side of the electromechanical transformer to its right side. All impedances on the left side of the transformer thus are divided by n^2 and the force source F_i is divided by n. The new equivalent circuit is shown in Figure 4.9.

According to the Thevenin theorem, the equivalent circuit shown in Figure 4.9 can be replaced by a Thevenin equivalent circuit which has an equivalent voltage source V_{th} and an internal electrical impedance Z_{th}^e. The Thevenin equivalent circuit for the receiving transducer is shown as solid lines in Figure 4.10. These two quantities are obtained as

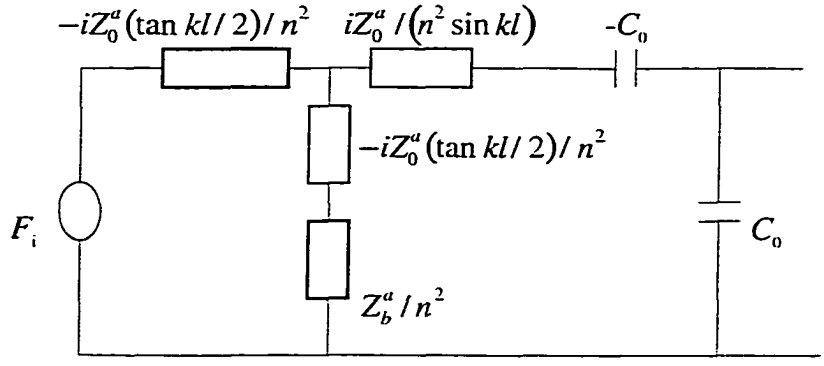

Figure 4.9 Equivalent circuit for the receiving transducer by transposing the left side of the electromechanical transformer to its right side shown in Figure 4.7. The input force F_i is replaced by a force source.

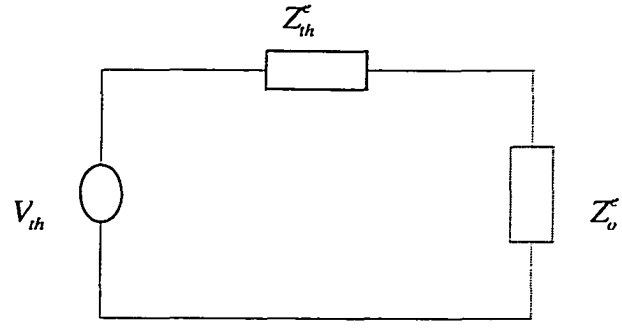

Figure 4.10 Thevenin equivalent circuit for the receiving transducer whose equivalent circuit is shown in Figure 4.9. The electrical load connected to the electrical port of the transducer is Z_o^e.

$$V_{th} = \frac{nF_i}{\omega C_0 Z_0^a} \frac{\left(Z_b^a - iZ_0^a \tan\frac{kl}{2}\right)\sin kl}{\left(Z_b^a - iZ_0^a \tan\frac{kl}{2}\right)\cos kl - iZ_0^a \tan\frac{kl}{2}} \tag{4.2.7}$$

and

$$Z_{th}^e = \frac{-1}{i\omega C_0}\left[1 - \frac{1}{\omega C_0 Z_0^a} \frac{n^2 \sin kl\left(Z_b^a - i2Z_0^a \tan\frac{kl}{2}\right)}{\left(Z_b^a - iZ_0^a \tan\frac{kl}{2}\right)\cos kl - iZ_0^a \tan\frac{kl}{2}}\right]. \tag{4.2.8}$$

When an electrical impedance, Z_o^e, is connected at the electrical port, the voltage at the electrical port can be obtained from Figure 4.10 as

$$V_o = \frac{Z_o^e}{Z_{th}^e + Z_o^e} V_{th}. \tag{4.2.9}$$

Putting Eq. (4.2.7) into Eq. (4.2.9), the transfer function of the receiving transducer can then be found as

$$H_r(\omega) = \frac{V_o}{F_i} = \frac{Z_o^e}{Z_{th}^e + Z_o^e} \frac{nF_i}{\omega C_0 Z_0^a} \frac{\left(Z_b^a - iZ_0^a \tan\frac{kl}{2}\right)\sin kl}{\left(Z_b^a - iZ_0^a \tan\frac{kl}{2}\right)\cos kl - iZ_0^a \tan\frac{kl}{2}} \tag{4.2.10}$$

where Z_{th}^e is expressed in Eq. (4.2.8).

If we want to express the transfer function as the ratio of receiving voltage to the blocking force, we have to resort to Eq. (4.1.13). The transfer function is then expressed as

$$H_r'(\omega) = \frac{V_o}{F_B} = \frac{F_i}{F_B} \cdot \frac{V_o}{F_i}. \tag{4.2.11}$$

So from Eqs. (4. 1.13) and (4.2.10), we obtain

$$H_r'(\omega) = \frac{Z_{in}^a}{Z_i^a + Z_{in}^a} \frac{Z_o^e}{Z_{th}^e + Z_o^e} \frac{nF_i}{\omega C_0 Z_0^a} \frac{\left(Z_b^a - iZ_0^a \tan\frac{kl}{2}\right)\sin kl}{\left(Z_b^a - iZ_0^a \tan\frac{kl}{2}\right)\cos kl - iZ_0^a \tan\frac{kl}{2}} \tag{4.2.12}$$

where Z_{th}^e and Z_{in}^a are given by Eq. (4.2.8) and Eq. (4.2.4), respectively.

4.2.2 Transfer matrix approach

It is complex to derive the explicit expressions of input acoustic impedance and transfer functions of a receiving transducer even when configuration of the transducer is very simple, as found here where only a piezoelectric plate and a backing material are considered. It is expected that if more elements are involved in the receiving transducer, the explicit expressions would become prohibitively complex. This was also found to be the case in Chapter 3 when we considered the generation process. However, there we showed that a two-port transfer matrix approach could easily handle additional complexities without difficulty. The same is true here for the reception process.

Thus, consider the two-port network for a receiving transducer shown in Figure 4.11. It is natural to choose the directions of current and velocity in the energy transfer direction, i.e., the direction from mechanical port to electrical port. Note that the equivalent circuit shown previously in Figure 4.7 was such a two-port network with explicit equivalent electrical elements inside the "black box" shown in Figure 4.11.

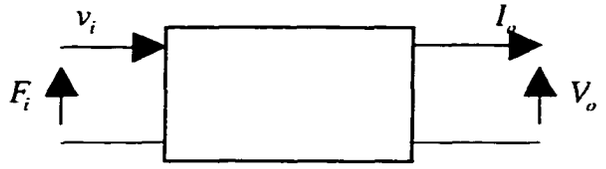

Figure 4.11 Two-port network for a receiving transducer whose elements inside the box are shown in Figure 4.7.

Similar to Eq. (3.3.8), when the receiving transducer is used as a transmitting transducer, its transfer matrix equation is written as

$$\begin{Bmatrix} V_o \\ -I_o \end{Bmatrix} = \begin{bmatrix} T_{11}^R & T_{12}^R \\ T_{21}^R & T_{22}^R \end{bmatrix} \begin{Bmatrix} F_i \\ -v_i \end{Bmatrix} \tag{4.2.13}$$

where the negative signs show that the directions of current and velocity in reception process are assumed opposite to those in generation process of the transducer.

If we absorb the negative signs into the transfer matrix in Eq. (4.2.13), then we have the transfer matrix equation for the reception process of the receiving transducer given as

$$\begin{Bmatrix} V_o \\ I_o \end{Bmatrix} = \begin{bmatrix} T_{11}^R & -T_{12}^R \\ -T_{21}^R & T_{22}^R \end{bmatrix} \begin{Bmatrix} F_i \\ v_i \end{Bmatrix}. \tag{4.2.14}$$

Note that T_{11}^R, T_{12}^R, T_{21}^R and T_{22}^R here are still the elements of the transfer matrix when the receiving transducer is used a transmitter.

To derive the input acoustic impedance of a receiving transducer, we need to express the mechanical quantities (F_i, v_i) in terms of electrical quantities (V_o, I_o), i.e., we need to invert the transfer matrix in Eq. (4.2.14). Because the receiving transducer is reciprocal (see Eqs. (2.2.13) and (2.2.17)), we have

$$\begin{Bmatrix} F_i \\ v_i \end{Bmatrix} = \begin{bmatrix} T_{22}^R & T_{12}^R \\ T_{21}^R & T_{11}^R \end{bmatrix} \begin{Bmatrix} V_o \\ I_o \end{Bmatrix} \tag{4.2.15}$$

which is very similar to Eq. (4.2.13) except for the interchange of T_{11}^R and T_{22}^R.

If the receiving transducer is now terminated with an electrical load of Z_o^e, V_o and I_o are related through

$$\frac{V_o}{I_o} = Z_o^e. \tag{4.2.16}$$

From Eq. (4.2.15), the input acoustic impedance of a receiving transducer then is written simply as

$$Z_{in}^a = \frac{F_i}{v_i} = \frac{T_{22}^R + Z_o^e T_{12}^R}{T_{21}^R + Z_o^e T_{11}^R}. \tag{4.2.17}$$

By using Eq. (4.2.17), the receiving transfer function of a receiving transducer can also be derived from Eq. (4.2.14). In fact, Eq. (4.2.17) and the first equation in Eq. (4.2.14) give

$$H_r(\omega) = \frac{V_o}{F_i} = T_{11}^R - Z_{in}^a T_{12}^R . \qquad (4.2.18)$$

4.3 Ultrasonic Receiver

Like the pulser, an ultrasonic receiver is a rather complex circuit network, but for model purposes, we will represent the receiver as a receiving load, Z_o^e, and an amplification factor $K(\omega)$, as shown in Figure 4.12. Both Z_o^e and $K(\omega)$ are in general functions of the settings chosen for controls on the pulser/receiver (damping and gain, for example) and both are in general frequency-dependent. An ultrasonic system receiver could be part of a pulser/receiver (such as is the case for the 5052PR from Panametrics which we used in our experimental work), or it could be a separate instrument. In either case, the purpose of the receiver is to amplify the signals and (possibly) filter them.

A simple representation of a receiver like the Panametrics 5052PR was shown in Figure 4.1 where there are two controls labeled Gain and Attenuation. Together, these controls allow a range of various amplification settings.

Ideally, the input electrical impedance of the receiver should be infinite so that the receiver can receive signals with as large amplitude as possible. In this ideal case, the receiver would receive the open-circuit voltage from the receiving transducer. However, in

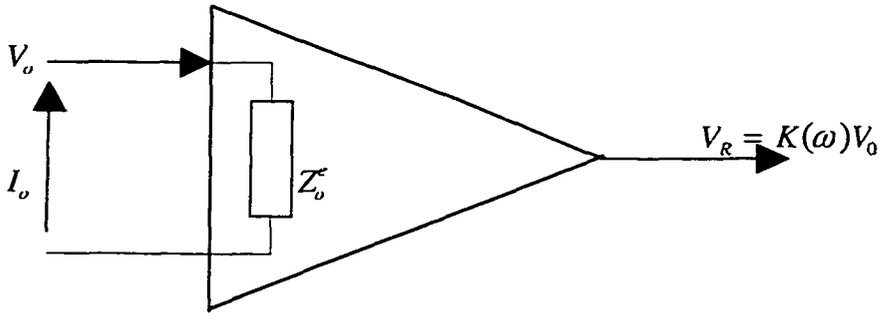

Figure 4.12 Electrical receiver modeled by the input electrical impedance Z_o^e and the amplification factor $K(\omega)$ controlled by Gain and Attenuation buttons shown in Figure 4.1.

practice, the input electrical impedance of a receiver is finite and we need to know the value of its input impedance to completely derive the reception process.

From Figure 4.12, if we can measure the input voltage V_o and output voltage V_R, the amplification factor is written as

$$K = \frac{V_R}{V_o}. \tag{4.3.1}$$

Furthermore, if we can measure the input current I_o, the receiving load is written as

$$Z_o^e = \frac{V_o}{I_o}. \tag{4.3.2}$$

4.4 Reception Process Transfer Function

The entire reception process of an ultrasonic measurement was shown schematically in Figure 4.1. Generally this process contains four elements: acoustic medium, cable, transducer and receiver. This reception process can be modeled by the collection of two-port networks shown in Figure 4.13.

From Eq. (4.2.15), the transfer matrix of the receiving transducer is written as

$$\begin{Bmatrix} F_i \\ v_i \end{Bmatrix} = \begin{bmatrix} T_{22}^R & T_{12}^R \\ T_{21}^R & T_{11}^R \end{bmatrix} \begin{Bmatrix} V_1 \\ I_1 \end{Bmatrix}. \tag{4.4.1}$$

Similar to Eq. (4.4.1), the transfer matrix of a cable can be written as

$$\begin{Bmatrix} V_1 \\ I_1 \end{Bmatrix} = \begin{bmatrix} T_{22}^C & T_{12}^C \\ T_{21}^C & T_{11}^C \end{bmatrix} \begin{Bmatrix} V_o \\ I_o \end{Bmatrix}. \tag{4.4.2}$$

Note that T_{11}^C, T_{12}^C, T_{21}^C and T_{22}^C are again the elements of the transfer matrix of the cable when it is used in generation process where the transfer matrix equation was written as

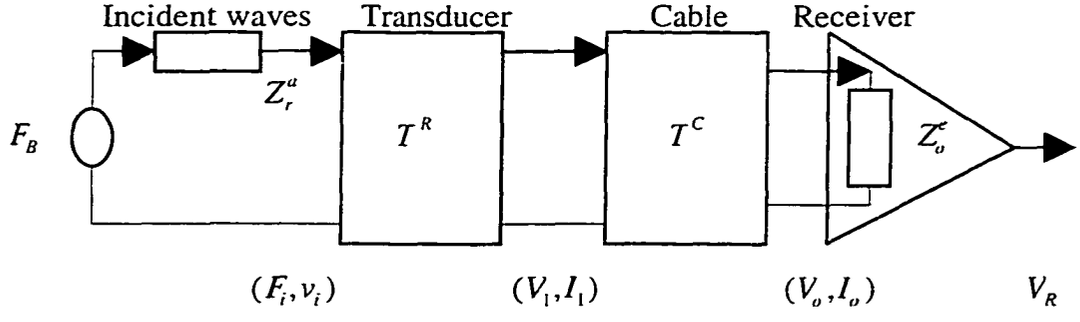

Figure 4.13 Reception process model which includes four components: incident acoustic waves, receiving transducer, cable and electrical receiver.

$$\begin{Bmatrix} V_o \\ -I_o \end{Bmatrix} = \begin{bmatrix} T_{11}^C & T_{12}^C \\ T_{21}^C & T_{22}^C \end{bmatrix} \begin{Bmatrix} V_1 \\ -I_1 \end{Bmatrix} \tag{4.4.3}$$

with the negative signs showing that the direction of current in reception process is opposite to that of the generation process. However, because a cable is a completely symmetric device, $T_{11}^C = T_{22}^C$ and there is no difference between Eq. (4.4.2) and Eq. (4.4.3).

Putting Eq. (4.4.2) into Eq. (4.4.1) gives

$$\begin{Bmatrix} F_i \\ v_i \end{Bmatrix} = \begin{bmatrix} T_{22}^R & T_{12}^R \\ T_{21}^R & T_{11}^R \end{bmatrix} \begin{bmatrix} T_{22}^C & T_{12}^C \\ T_{21}^C & T_{11}^C \end{bmatrix} \begin{Bmatrix} V_o \\ I_o \end{Bmatrix}. \tag{4.4.4}$$

If we now define a global transfer matrix, $[R^G]$, as

$$[R^G] = \begin{bmatrix} R_{22}^G & R_{12}^G \\ R_{21}^G & R_{22}^G \end{bmatrix} = \begin{bmatrix} T_{22}^R & T_{12}^R \\ T_{21}^R & T_{11}^R \end{bmatrix} \begin{bmatrix} T_{22}^C & T_{12}^C \\ T_{21}^C & T_{11}^C \end{bmatrix}. \tag{4.4.5}$$

Eq. (4.4.4) becomes simply

$$\begin{Bmatrix} F_i \\ v_i \end{Bmatrix} = \begin{bmatrix} R_{22}^G & R_{12}^G \\ R_{21}^G & R_{11}^G \end{bmatrix} \begin{Bmatrix} V_o \\ I_o \end{Bmatrix}. \tag{4.4.6}$$

Eq. (4.4.6) shows that the effect of the receiving transducer and that of the cable can be combined into the global matrix $[R^G]$. In fact, no matter how many two-port networks there are between the incident waves and the receiver, the cascade of these networks gives a global two-port network. As in the generation process, if each network in the cascade is reciprocal, the global transfer matrix is also reciprocal.

Using Eq. (4.4.6), the reception process shown in Figure 4.13 can be simplified as the diagram shown in Figure 4.14 where the global two-port network replaces the cable and transducer.

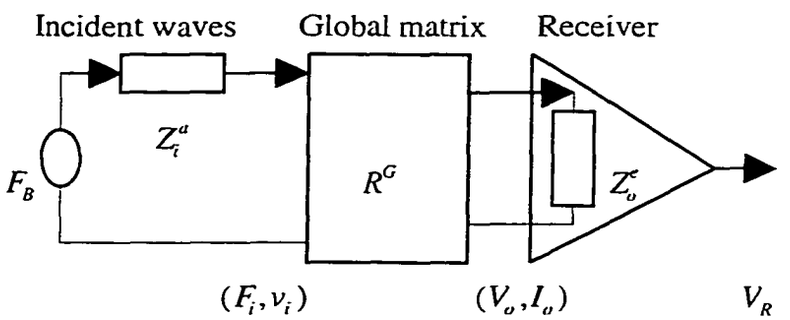

Figure 4.14 Reception process model with the global matrix to replace all the two-port networks between the incident waves and the receiver.

The transfer function for the reception process can be obtained from Figure 4.14. On the two sides of the global two-port network, the following equations hold.

$$F_B = F_i + v_i Z_i^a \tag{4.4.7}$$

$$V_o = I_o Z_o^e . \tag{4.4.8}$$

From Eq. (4.4.6), we have

$$\frac{F_i}{v_i} = \frac{R_{22}^G V_o + R_{12}^G I_o}{R_{21}^G V_o + R_{11}^G I_o} . \tag{4.4.9}$$

Using Eq. (4.4.8), Eq. (4.4.9) can be rewritten as

$$\frac{F_i}{v_i} = \frac{R_{22}^G Z_o^e + R_{12}^G}{R_{21}^G Z_o^e + R_{11}^G} . \tag{4.4.10}$$

Then eliminating velocity v_i from Eq. (4.4.7) and Eq. (4.4.10) gives

$$F_B = F_i \left(1 + \frac{R_{21}^G Z_o^e(\omega) + R_{11}^G}{R_{22}^G Z_o^e(\omega) + R_{12}^G} Z_r^a(\omega) \right) . \tag{4.4.11}$$

The first equation in Eq. (4.4.6) is expressed as

$$F_i = V_o R_{22}^G + I_o R_{12}^G \tag{4.4.12}$$

so that considering Eq. (4.4.8), Eq. (4.4.12) becomes

$$F_i = I_o \left(Z_o^e(\omega) R_{22}^G + R_{12}^G \right) . \tag{4.4.13}$$

Putting Eq. (4.4.13) into Eq. (4.4.11), we have

$$F_B = I_o \left[\left(Z_o^e(\omega) R_{22}^G + R_{12}^G \right) + \left(R_{21}^G Z_o^e(\omega) + R_{11}^G \right) Z_r^a(\omega) \right] \tag{4.4.14}$$

and solving for I_o gives

$$I_o = \frac{F_B}{\left(Z_o^e(\omega) R_{22}^G + R_{12}^G \right) + \left(R_{21}^G Z_o^e(\omega) + R_{11}^G \right) Z_r^a(\omega)} \tag{4.4.15}$$

or,

$$I_o = \frac{F_B}{\left(Z_r^a(\omega) R_{11}^G + R_{12}^G \right) + \left(R_{21}^G Z_r^a(\omega) + R_{22}^G \right) Z_o^e(\omega)} . \tag{4.4.16}$$

Using Eq. (4.4.8), the voltage then also is given as

$$V_o = \frac{F_B Z_o^e(\omega)}{\left(Z_r^a(\omega) R_{11}^G + R_{12}^G \right) + \left(R_{21}^G Z_r^a(\omega) + R_{22}^G \right) Z_o^e(\omega)} . \tag{4.4.17}$$

Now, considering the amplification factor $K(\omega)$ of the receiver, the transfer function, $t_R(\omega)$, of the entire reception process is obtained, using Eq. (4.3.1), as

$$t_R(\omega) = \frac{V_R(\omega)}{F_B(\omega)} = \frac{Z_o^e(\omega) K(\omega)}{\left(Z_r^a(\omega) R_{11}^G + R_{12}^G \right) + \left(R_{21}^G Z_r^a(\omega) + R_{22}^G \right) Z_o^e(\omega)} . \tag{4.4.18}$$

Eq. (4.4.18) shows that the receiving transfer function is expressed in terms of the receiver parameters, the global transfer matrix parameters and the radiation impedance of the receiving transducer.

Open-circuit and unamplified received voltage measurements are often discussed in the literature. From Eq. (4.4.18), if we let $Z_o^e(\omega) \to \infty$ and set $K(\omega)=1$, then the open-circuit voltage is given as

$$V_R(\omega) = \frac{F_B(\omega)}{R_{21}^G Z_i^a(\omega) + R_{22}^G}. \tag{4.4.19}$$

CHAPTER 5. ACOUSTIC WAVE PROPAGATION AND SCATTERING

In the previous two chapters, we derived transfer functions that described both the generation and reception processes. In the generation process, for example, we obtained the transfer function $t_G(\omega) = F_t(\omega) / V_i(\omega)$ (Eq. (3.5.15)) relating the output force of the transmitting transducer, $F_t(\omega)$, to the Thevenin equivalent input voltage of the pulser, $V_i(\omega)$. Similarly, in the reception process, we obtained the transfer function $t_R(\omega) = V_R(\omega) / F_B(\omega)$ (Eq. (4.4.18)) in terms of the measured output (received) voltage, $V_R(\omega)$, and the blocked force, $F_B(\omega)$, at the face of the receiving transducer. Thus, if we can find an expression for the transfer function relating the blocked force to the output force, i.e. $t_A(\omega) = F_B(\omega) / F_t(\omega)$, we will have a model for the entire ultrasonic measurement system, since the input and output voltages could then be directly related as

$$V_R(\omega) = t_R(\omega) t_A(\omega) t_G(\omega) V_i(\omega). \tag{5.1}$$

The acoustic transfer function $t_A(\omega)$ is a function of all the 3-D acoustic and elastic wave propagation and scattering processes that occur between the transmitting and receiving transducers. Thus, in general it must be calculated from the underlying 3-D wave fields for each specific problem. However, in the case where the ultrasonic measurement system is used to obtain a flaw response, the reciprocal theorem can be used to obtain $t_A(\omega)$ in terms of the wave fields at the surface of the flaw, a result that has been very useful in modeling flaw inspection problems [Schmerr, 1998].

In this chapter, we will obtain the acoustic transfer function $t_A(\omega)$ for an ultrasonic flaw measurement system and also derive the acoustic transfer function for the specific case where two unfocused transducers, one sending and one receiving ultrasound, are aligned along their axes in a fluid. The latter problem is an important configuration because of its use in calibration experiments, as will be seen in later chapters.

5.1 Ultrasonic Flaw Measurement and Reciprocity

Several authors have previously considered the problem of how to represent the 3-D wave propagation and scattering effects present in an ultrasonic flaw measurement system in terms of lumped 1-D input and output parameters that could be measured. Auld, for example, used the general reciprocal relations for a piezoelectric medium to relate the fields surrounding a flaw to electrical transmission coefficients that describe the signals present in

the receiving cable [Auld, 1979]. Schmerr, on the other hand, used purely mechanical reciprocity principles to relate the fields surrounding the flaw to the incident fields present at the face of the receiver [Schmerr, 1998]. Neither of those approaches are directly useful to us because as the above discussion showed, we need to obtain the ratio of the blocked force at the receiver to the output force of the transmitter. Certainly, with some additional assumptions, we could modify either Auld's or Schmerr's results to obtain $t_A(\omega)$, but we will show that such additional assumptions are unnecessary and we can directly obtain a general expression for the acoustic transfer function in terms of the fields surrounding a flaw using reciprocity principles.

Figure 5.1 shows a general immersion pitch-catch testing setup where two transducers are used to interrogate a flaw in an elastic solid. Although in practice transient pulses are present in such a test, as done previously we will assume that all the acoustic and elastic waves are harmonic in nature with an $\exp(-i\omega t)$ time dependency term, a term that will henceforth not be written explicitly for the field and lumped quantities. In using the reciprocal theorem we will consider the geometry of Figure 5.1 for three different cases (which we will refer to as "states"). In state one, the transmitting transducer, T, is firing and the flaw (S_f) is present. In state two, the receiver, R, is firing and the flaw is absent $(S_f = 0)$. In state three, the transmitter, T, is firing and the flaw is again absent $(S_f = 0)$. Field quantities present in state one, therefore, will be written as $f^1(\mathbf{x},\omega|\, T;S_f)$, where the notation means that the transmitter, T, is acting as the generator of waves in the presence of the flaw. Similarly, field quantities in state two will be written as $f^2(\mathbf{x},\omega|\, R;S_f=0)$ (the receiver, R, is generating waves and the flaw is absent), and in state three as $f^3(\mathbf{x},\omega|\, T;S_f=0)$ (the transmitter, T, is generating waves, and the flaw is again absent). Here the field quantity f could be any field variable such as pressure, a velocity component, stress component, etc. For economy of notation, in some of the following derivations, the arguments of the field quantities will not be given explicitly but will be understood implicitly by the superscript on the field quantity, which indicates the state in which that quantity is calculated. For example, we may write $f^3 \equiv f^3(\mathbf{x},\omega|\, T;S_f=0)$.

First consider the fluid medium in Figure 5.1 and two general states, a, and b, which could be, for example, any of the three states mentioned previously. The transducer "active" surfaces, S_T and S_R, and the surface of the elastic body being inspected, S_e, are the only

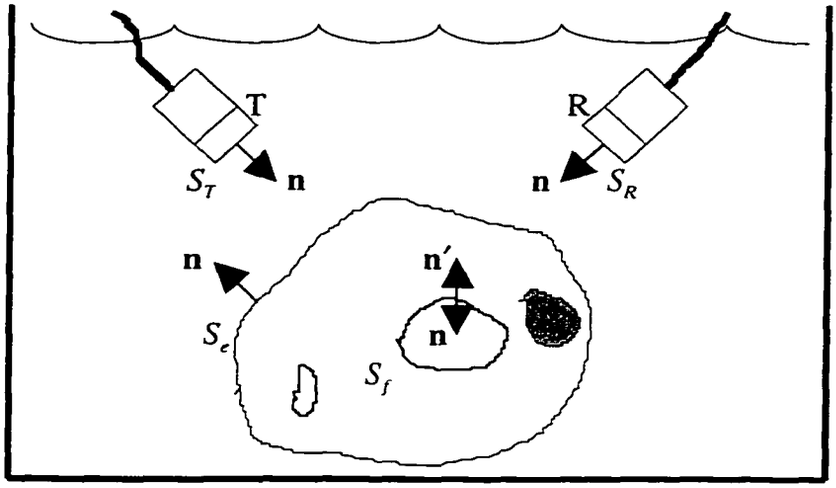

Figure 5.1 A general immersion pitch-catch testing setup where two transducers are used to interrogate a flaw in an elastic solid.

surfaces adjacent to the fluid which are not assumed rigid in both states a and b so the reciprocal theorem for the fluid can be written as

$$\int_{S_T}\left[p^a(\mathbf{x},\omega)v_n^b(\mathbf{x},\omega)-p^b(\mathbf{x},\omega)v_n^a(\mathbf{x},\omega)\right]dS+\int_{S_R}\left[p^a(\mathbf{x},\omega)v_n^b(\mathbf{x},\omega)-p^b(\mathbf{x},\omega)v_n^a(\mathbf{x},\omega)\right]dS$$
$$+\int_{S_e}\left[p^a(\mathbf{x},\omega)v_n^b(\mathbf{x},\omega)-p^b(\mathbf{x},\omega)v_n^a(\mathbf{x},\omega)\right]dS=0 \tag{5.1.1}$$

But, since the shear stresses are zero on the surface of the elastic body and the normal stress and normal velocity are continuous, we have

$$\int_{S_e}\left[p^a(\mathbf{x},\omega)v_n^b(\mathbf{x},\omega)-p^b(\mathbf{x},\omega)v_n^a(\mathbf{x},\omega)\right]dS$$
$$=-\int_{S_e}\left[\tau_{ij}{}^a(\mathbf{x},\omega)v_i^b(\mathbf{x},\omega)n_j-\tau_{ij}{}^b(\mathbf{x},\omega)v_i^a(\mathbf{x},\omega)n_j\right]dS \tag{5.1.2}$$

Thus, Eq. (5.1.1) becomes, in abbreviated notation

$$\int_{S_T}\left[p^a v_n^b-p^b v_n^a\right]dS+\int_{S_R}\left[p^a v_n^b-p^b v_n^a\right]dS$$
$$=\int_{S_e}\left[\tau_{ij}{}^a v_i^b n_j-\tau_{ij}{}^b v_i^a n_j\right]dS \tag{5.1.3}$$

In the elastic solid, regardless of whether a flaw exists or not, we can also write a reciprocal theorem relating integrals over the surface S_e and the surface, S_f, (which is the actual flaw surface when the flaw is present) as

$$\int_{S_e}\left[\tau_{ij}{}^{a}v_i^b n_j - \tau_{ij}{}^{b}v_i^a n_j\right]dS + \int_{S_f}\left[\tau_{ij}{}^{a}v_i^b n_j - \tau_{ij}{}^{b}v_i^a n_j\right]dS = 0. \qquad (5.1.4)$$

Integrals over all other surfaces in the elastic body vanish if those surfaces do not contain any active sources and satisfy the same boundary conditions for both states a and b. If we place Eq. (5.1.4) into Eq. (5.1.3) and replace the normal $\mathbf{n}$ on the surface S_f by a normal $\mathbf{n}'$ which acts outward from that surface into the solid (Figure 5.1), we find

$$\begin{aligned}&\int_{S_T}\left[p^a v_n^b - p^b v_n^a\right]dS + \int_{S_R}\left[p^a v_n^b - p^b v_n^a\right]dS \\ &= \int_{S_f}\left[\tau_{ij}{}^{a}v_i^b n_j' - \tau_{ij}{}^{b}v_i^a n_j'\right]dS\end{aligned} \qquad (5.1.5)$$

Applying Eq. (5.1.5) to states one and two, as defined previously, gives

$$\begin{aligned}&\int_{S_T}\left[p^1 v_n^2 - p^2 v_n^1\right]dS + \int_{S_R}\left[p^1 v_n^2 - p^2 v_n^1\right]dS \\ &= \int_{S_f}\left[\tau_{ij}{}^{1}v_i^2 n_j' - \tau_{ij}{}^{2}v_i^1 n_j'\right]dS\end{aligned} \qquad (5.1.6)$$

Similarly, applying Eq. (5.1.5) to states three and two, since both of these states satisfy the same conditions within S_f (the flaw is absent in both cases), we have

$$\int_{S_T}\left[p^3 v_n^2 - p^2 v_n^3\right]dS + \int_{S_R}\left[p^3 v_n^2 - p^2 v_n^3\right]dS = 0. \qquad (5.1.7)$$

Subtracting Eq. (5.1.7) from Eq. (5.1.6) then yields

$$\begin{aligned}&\int_{S_T}\left[\Delta p^f v_n^2 - p^2 \Delta v_n^f\right]dS + \int_{S_R}\left[\Delta p^f v_n^2 - p^2 \Delta v_n^f\right]dS \\ &= \int_{S_f}\left[\tau_{ij}{}^{1}v_i^2 n_j' - \tau_{ij}{}^{2}v_i^1 n_j'\right]dS\end{aligned} \qquad (5.1.8)$$

where

$$\begin{aligned}\Delta p^f &= p^1\left(\mathbf{x},\omega\middle|T;S_f\right) - p^3\left(\mathbf{x},\omega\middle|T;S_f=0\right) \\ \Delta v_n^f &= v_n^1\left(\mathbf{x},\omega\middle|T;S_f\right) - v_n^3\left(\mathbf{x},\omega\middle|T;S_f=0\right)\end{aligned} \qquad (5.1.9)$$

These pressure and velocity differences represent the pressure and velocity scattered from the flaw due to the transmitter T firing since both the incident waves generated by T and any waves which do not interact with the flaw are contained in both states one and three, and thus are canceled out.

Consider now the integral on the transmitter surface, S_T, in Eq. (5.1.8). The pressure and velocity terms, p^2 and v_n^2, come from waves generated in state two when the receiver is firing. Thus, like the difference terms, which come from the scattered flaw signals, these terms contain only waves incident on the transmitter from sources other than the transmitter itself. If, as we have done before, we assume that the velocity of the waves arriving at T can be written in separable form, then we can define lumped average velocity terms, $v_T^f(\omega), v_T^2(\omega)$, through

$$\begin{aligned} \Delta v_n^f &= v_T^f(\omega) f(\mathbf{x}) \\ v_n^2 &= v_T^2(\omega) f(\mathbf{x}) \end{aligned} \tag{5.1.10}$$

and corresponding lumped force terms as

$$\begin{aligned} F_T^f(\omega) &= \int_{S_T} \Delta p^f f(\mathbf{x}) dS \\ F_T^2(\omega) &= \int_{S_T} p^2 f(\mathbf{x}) dS \end{aligned} \tag{5.1.11}$$

Similarly, on the face of the receiver we have

$$\begin{aligned} \Delta v_n^f &= v_R^f(\omega) g(\mathbf{x}) \\ v_n^2 &= v_R^2(\omega) g(\mathbf{x}) \end{aligned} \tag{5.1.12}$$

and the corresponding force terms

$$\begin{aligned} F_R^f(\omega) &= \int_{S_R} \Delta p^f g(\mathbf{x}) dS \\ F_R^2(\omega) &= \int_{S_R} p^2 g(\mathbf{x}) dS \end{aligned} \tag{5.1.13}$$

Placing Eqs. (5.1.10)–(5.1.13) into Eq. (5.1.8), we find

$$\begin{aligned} &\left[F_T^f(\omega) v_T^2(\omega) - F_T^2(\omega) v_T^f(\omega)\right] + \left[F_R^f(\omega) v_R^2(\omega) - F_R^2(\omega) v_R^f(\omega)\right] \\ &= \int_{S_f} \left[\tau_{ij}^1 v_i^2 n_j' - \tau_{ij}^2 v_i^1 n_j'\right] dS \end{aligned} \tag{5.1.14}$$

On the transmitter, both the fields coming from the difference terms and the fields coming from state two see the same input impedance, $Z_{in}^{T:a}(\omega)$, which is due to the transmitting transducer and attached cabling, pulser, and etc. Thus

$$\begin{aligned} F_T^f(\omega) &= -Z_{in}^{T:a}(\omega) v_T^f(\omega) \\ F_T^2(\omega) &= -Z_{in}^{T:a}(\omega) v_T^2(\omega) \end{aligned} \tag{5.1.15}$$

where the minus signs exist because a positive velocity is taken outwards from the transducer. When Eq. (5.1.15) is placed in Eq. (5.1.14), the first set of terms in brackets in that equation vanish. On the face of the receiver, however, we have

$$F_R^f(\omega) = -Z_{in}^{R:a}(\omega)v_R^f(\omega)$$
$$F_R^2(\omega) = -Z_r^{R:a}(\omega)v_R^2(\omega) \qquad (5.1.16)$$

where $Z_{in}^{R:a}(\omega)$ is the input impedance seen at the receiver by all the scattered waves coming from the flaw and $Z_r^{R:a}(\omega)$ is the radiation impedance of the receiver when it acts as a transmitter in state two. With these relations, Eq. (5.1.14) becomes

$$F_R^f(\omega)v_R^2(\omega)\left[\frac{Z_{in}^{R:a}(\omega)+Z_r^{R:a}(\omega)}{Z_{in}^{R:a}(\omega)}\right] = \int_{S_f}\left[\tau_{ij}^1 v_i^2 n_j' - \tau_{ij}^2 v_i^1 n_j'\right]dS. \quad (5.1.17)$$

But the total received force at the receiver from the flaw signals times the impedance terms in Eq. (5.1.17) is just the blocked force at the receiver due to the waves from the flaw (see Eq. (4.1.13) in Chapter 4), which we will call simply $F_B(\omega)$. Eq. (5.1.17) then shows that finally

$$F_B = \frac{1}{v_R^2(\omega)}\int_{S_f}\left[\tau_{ij}^1 v_i^2 n_j' - \tau_{ij}^2 v_i^1 n_j'\right]dS \qquad (5.1.18)$$

or, returning to our more explicit notation,

$$F_B = \frac{1}{v_R^2(\omega)}\int_{S_f}\left[\tau_{ij}^1(\mathbf{x},\omega \mid T;S_f)v_i^2(\mathbf{x},\omega \mid R;S_f=0)\right.$$
$$\left.-\tau_{ij}^2(\mathbf{x},\omega \mid R;S_f=0)v_i^1(\mathbf{x},\omega \mid T;S_f)\right]n_j'(\mathbf{x})dS \qquad (5.1.19)$$

Since in state one the force at the face of the transmitting transducer, which was written in Eq. (5.1) as $F_t(\omega)$, is related to the lumped velocity term in that state, $v_T^1(\omega)$, by the relation $F_t(\omega) = Z_r^{T:a}(\omega)v_T^1(\omega)$, Eq. (5.1.18) shows that the acoustic transfer function, $t_A(\omega)$, in Eq. (5.1) is given by

$$t_A(\omega) \equiv \frac{F_B(\omega)}{F_t(\omega)} = \frac{1}{Z_r^{T:a}(\omega)v_T^1(\omega)v_R^2(\omega)}\int_{S_f}\left[\tau_{ij}^1(\mathbf{x},\omega \mid T;S_f)v_i^2(\mathbf{x},\omega \mid R;S_f=0)\right.$$
$$\left.-\tau_{ij}^2(\mathbf{x},\omega \mid R;S_f=0)v_i^1(\mathbf{x},\omega \mid T;S_f)\right]n_j'(\mathbf{x})dS. \qquad (5.1.20)$$

Eqs. (5.1.19) and (5.1.20) are very general results, since they are based primarily on assumptions of linearity and reciprocity of the ultrasonic measurement system. These equations yield the relationship we need to describe the acoustic propagation and scattering elements of the measurement system in terms of the lumped parameters that appear in Eq. (5.1). Schmerr has previously derived a relationship similar to Eq. (5.1.18), also based on mechanical reciprocity principles [Schmerr, 1998], where it was found that

$$2F_{inc}(\omega) = \frac{1}{v_R^2(\omega)}\int_{S_f}\left[\tau_{ij}^1 v_i^2 n_j' - \tau_{ij}^2 v_i^1 n_j'\right]dS. \qquad (5.1.21)$$

In Eq. (5.1.21), $F_{inc}(\omega)$ is the force incident on the receiver due to the flaw signals in the absence of the receiver. Since the presence of the receiver alters the acoustic fields in its vicinity, it is not possible to use Eq. (5.1.21) consistently without some additional assumptions. For example, if the incident and scattered waves at the face of the receiving transducer are assumed to be 1-D plane waves propagating parallel to the normal of the transducer face, $2F_{inc}$ is just the blocked force and Eqs. (5.1.21) and (5.1.18) are identical. However, our derivation has shown that such additional assumptions are unnecessary. It is the blocked force that is the force term that naturally appears in the acoustic transfer function (or, equivalently, the total force $F_R^I(\omega)$ at the receiver as found in Eq. (5.1.17), which also takes into account the presence of the receiving transducer).

If the waves incident on the flaw are assumed to be quasi-plane waves (paraxial assumption), it is possible to also write the acoustic transfer function entirely in terms of lumped 1-D elements (see Thompson and Gray for the original derivation [Thompson and Gray, 1983] as well as [Schmerr, 1998]). In this case, it is found that

$$\frac{1}{v_T^1(\omega)v_R^2(\omega)}\int_{S_f}\left[\tau_{ij}{}^1 v_i^2 n_j' - \tau_{ij}{}^2 v_i^1 n_j'\right]dS = V^1(\omega)V^2(\omega)A(\omega)\left[\frac{4\pi\rho_2 c_2}{-ik_2}\right] \qquad (5.1.22)$$

where $V^1(\omega)$ represents a normalized velocity incident on the flaw in state one (transmitter firing), $V^2(\omega)$ is a corresponding normalized incident velocity for state two (receiver firing), $A(\omega)$ represents the plane wave far field scattering amplitude of the flaw, ρ_2 is the density of the elastic solid surrounding the flaw, and c_2 and k_2 are the wave speed and wave number, respectively, for the waves incident on the flaw in state two. One of the important aspects of Eq. (5.1.22) is that the effects of the flaw on the ultrasonic measurement are separated explicitly from the other components. This fact permits practical implementation of many parametric flaw inspection studies.

The quantity appearing in the left side of Eq. (5.1.22) represents a 1-D lumped acoustic impedance that characterizes all the acoustic propagation and scattering elements in an ultrasonic flaw measurement system. Thus, Eq. (5.1.22) could be interpreted as giving this acoustic impedance, $Z_A^a(\omega)$, as

$$Z_A^a(\omega) = V^1(\omega)V^2(\omega)A(\omega)\left[\frac{4\pi\rho_2 c_2}{-ik_2}\right] \qquad (5.1.23)$$

and the acoustic transfer function, $t_A(\omega)$, could be written in terms of this acoustic impedance as

$$t_A(\omega)=\frac{Z_A^a(\omega)}{Z_r^{T:a}(\omega)}. \qquad (5.1.24)$$

5.2 The Acoustic Transfer Function for a Calibration Configuration

In the previous section the acoustic transfer function in an ultrasonic measurement system was obtained in a form suitable specifically for a flaw measurement system. However, one can use Eq. (5.1) for any ultrasonic measurement system where one can obtain an explicit expression for $t_A(\omega)$. In this section we will model the acoustic transfer function for the problem where the waves in a fluid from a circular, planar (unfocused) piston transducer of radius a are received by another circular planar transducer of radius b in a configuration where the axes of the two transducers are aligned (Figure 5.2). This is an important setup that is used in many calibration studies, including those discussed in the next chapter.

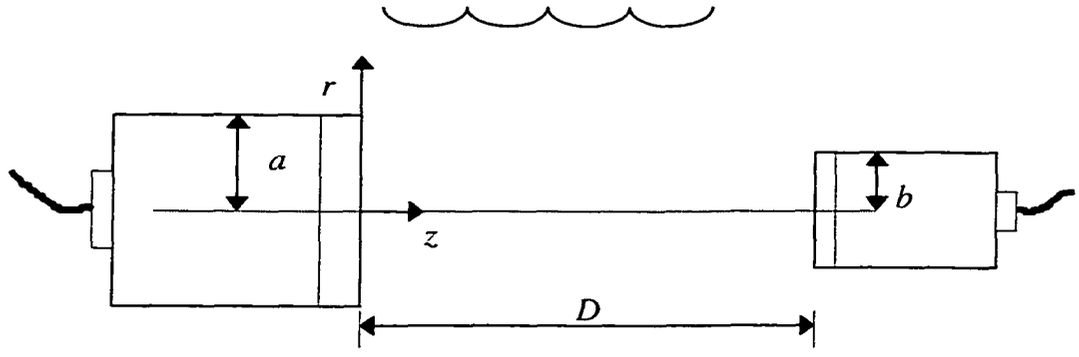

Figure 5.2 Two circular transducers with radii of a and b in an immersion test.

The starting point for this model is a representation of the pressure generated by a circular piston transducer of radius a as a superposition of harmonic cylindrical waves (for $\exp(-i\omega t)$ time dependency) in the form [King, 1934]

$$p(\mathbf{x},\omega)=\omega\rho_1 v_0(\omega)a\int_{p_\rho=0}^{p_\rho=\infty}\frac{J_0(p_\rho r)J_1(p_\rho a)}{\sqrt{k_1^2-p_\rho^2}}\exp\left[i\sqrt{k_1^2-p_\rho^2}\,z\right]dp_\rho \qquad (5.2.1)$$

where ρ_1 is the density of the fluid, $k_1=\omega/c_1$ is the wave number, and $v_0(\omega)$ is the uniform velocity on the transducer surface. Because of symmetry, the pressure in the fluid is only a function of the distance, z, from the transducer face along the central axis, and the radius, r, from that axis. If this pressure is averaged over the radius, b, of another transducer located

along the z-axis at the distance, D, then the average pressure times the area of the receiver is the total force incident on the receiver, F_{inc}, given by

$$F_{inc}(\omega)=2\pi\omega\rho_1 v_0(\omega)a\int_{r=0}^{b}\int_{p_\rho=0}^{p_\rho=\infty}\frac{J_0(p_\rho r)J_1(p_\rho a)}{\sqrt{k_1^2-p_\rho^2}}\exp\left[i\sqrt{k_1^2-p_\rho^2}D\right]dp_\rho rdr. \quad (5.2.2)$$

But

$$\int_0^b J_0(p_\rho r)rdr=\frac{bJ_1(p_\rho b)}{p_\rho} \quad (5.2.3)$$

so that we have

$$F_{inc}(\omega)=2\pi\omega\rho_1 v_0(\omega)ab\int_{p_\rho=0}^{p_\rho=\infty}\frac{J_1(p_\rho a)J_1(p_\rho b)}{p_\rho\sqrt{k_1^2-p_\rho^2}}\exp\left[i\sqrt{k_1^2-p_\rho^2}D\right]dp_\rho. \quad (5.2.4)$$

However, from [Gradshteyn and Ryzhik, 1980]

$$\int_0^\pi\frac{\sin^2 x\,J_1\left(\sqrt{\alpha^2+\beta^2+2\alpha\beta\cos x}\right)}{\sqrt{\alpha^2+\beta^2+2\alpha\beta\cos x}}dx=\pi\frac{J_1(\alpha)}{\alpha}\frac{J_1(\beta)}{\beta} \quad (5.2.5)$$

so we find

$$J_1(p_\rho a)J_1(p_\rho b)=\frac{abp_\rho}{\pi}\int_0^\pi\frac{\sin^2 x\,J_1\left(p_\rho\sqrt{a^2+b^2+2ab\cos x}\right)}{\sqrt{a^2+b^2+2ab\cos x}}dx \quad (5.2.6)$$

which, when placed into Eq. (5.2.4), gives

$$F_{inc}(\omega)=2\omega\rho_1 a^2b^2\int_0^\pi\sin^2 x\left\{\int_0^\infty\frac{J_1\left(p_\rho\sqrt{a^2+b^2+2ab\cos x}\right)}{\sqrt{a^2+b^2+2ab\cos x}}\frac{\exp\left[i\sqrt{k_1^2-p_\rho^2}D\right]}{\sqrt{k_1^2-p_\rho^2}}dp_\rho\right\}dx. \quad (5.2.7)$$

The inner integral in Eq. (5.2.7) can be performed since

$$\int_0^\infty\frac{J_1(p_\rho K)\exp\left[i\sqrt{k_1^2-p_\rho^2}D\right]}{\sqrt{k_1^2-p_\rho^2}}dp_\rho=\frac{1}{k_1K}\left\{\exp[ik_1D]-\exp\left[ik_1\sqrt{D^2+K^2}\right]\right\} \quad (5.2.8)$$

(Eq. (5.2.8) can be easily shown by comparing the expression for the on-axis pressure obtained by setting $r=0$ in Eq. (5.2.1) with the known exact result for this same pressure given by $p(r,z,\omega)\big|_{r=0}=\rho_1 c_1 v_0(\omega)\left\{\exp(ik_1z)-\exp\left(ik_1\sqrt{z^2+a^2}\right)\right\}$ in many references) so that

$$F_{inc}(\omega)=2\rho_1 c_1 v_0(\omega)a^2b^2\int_0^\pi\frac{\sin^2 x}{a^2+b^2+2ab\cos x}\left\{\exp[ik_1D]-\exp\left[ik_1\sqrt{D^2+a^2+b^2+2ab\cos x}\right]\right\}dx. \quad (5.2.9)$$

The first integral in Eq. (5.2.9) can be performed exactly since [Gradshteyn and Rhyzhik, p. 379, 1980]

$$\int_0^{\pi} \frac{\sin^2 x}{p+q\cos x}\,dx = \frac{\pi p}{q^2}\left[1-\sqrt{1-\frac{q^2}{p}}\right] \tag{5.2.10}$$

which gives

$$\int_0^{\pi} \frac{\sin^2 x}{a^2+b^2+2ab\cos x}\,dx = \begin{cases} \dfrac{\pi}{2a^2} & a \geq b \\ \dfrac{\pi}{2b^2} & b \geq a \end{cases}. \tag{5.2.11}$$

Using this result for the first integral in Eq. (5.2.9) and rewriting the second integral in terms of $u = x/2$, then using the trigonometric identity $\cos x = 2\cos^2 u - 1$, we have

$$F_{inc}(\omega) = \rho_1 c_1 v_0(\omega)\left\{\Theta \exp[ik_1 D]\right.$$
$$\left. -16a^2b^2 \int_0^{\pi/2} \frac{\sin^2 u \cos^2 u}{(a-b)^2+4ab\cos^2 u} \exp\left[ik_1\sqrt{D^2+(a-b)^2+4ab\cos^2 u}\right]du\right\} \tag{5.2.12}$$

where

$$\Theta = \begin{cases} \pi b^2 & a \geq b \\ \pi a^2 & b \geq a \end{cases}. \tag{5.2.13}$$

If one takes the blocked force, $F_B(\omega)$, at the receiving transducer to be equal to $2F_{inc}(\omega)$ and at the transmitter assume the radiation impedance is its high frequency limit, i.e., $Z_r^a(\omega) = \rho_1 c_1 \pi a^2$, then in terms of the total force radiated by the transmitter, $F_t(\omega) = Z_r^a(\omega) v_0(\omega)$, the acoustic transfer function is given explicitly as

$$t_A(\omega) = \frac{F_B(\omega)}{F_t(\omega)} = \frac{2}{\pi a^2}\left\{\Theta \exp[ik_1 D]\right.$$
$$\left. -16a^2b^2 \int_0^{\pi/2} \frac{\sin^2 u \cos^2 u}{(a-b)^2+4ab\cos^2 u} \exp\left[ik_1\sqrt{D^2+(a-b)^2+4ab\cos^2 u}\right]du\right\}. \tag{5.2.14}$$

5.2.1 Special cases

Consider first the case where the radii of the transmitter and receiver are the same, i.e. $a = b$. Then the acoustic transfer function simplifies to

$$t_A(\omega) = 2\left\{\exp[ik_1 D] - \frac{4}{\pi}\int_0^{\pi/2} \sin^2 u \exp\left[ik_1\sqrt{D^2+4a^2\cos^2 u}\right]du\right\}. \tag{5.2.15}$$

For this same case, the average pressure on the receiver, $p_{ave}(\omega) = F_{inc}(\omega)/\pi a^2$, is given by

$$p_{ave}(\omega) = \rho_1 c_1 v_0(\omega)\left\{\exp[ik_1 D] - \frac{4}{\pi}\int_0^{\pi/2} \sin^2 u \exp\left[ik_1\sqrt{D^2+4a^2\cos^2 u}\right]du\right\}$$
$$= \rho_1 c_1 v_0(\omega)\exp[ik_1 D]D_p(\omega, a, D) \tag{5.2.16}$$

which is a result that was originally obtained by Williams [1951] to study diffraction corrections (i.e. deviations from plane wave results) contained in the D_p coefficient. Rogers and Van Buren [1974] later showed that this diffraction coefficient could be obtained at high frequencies in a purely analytical form.

It is also interesting to examine this average pressure for the limiting case $b << a, D$. From Eq. (5.2.12) we find

$$p_{ave}(\omega)\big|_{b<<a} = \rho_1 c_1 v_0(\omega)\left\{\exp[ik_1 D] - \frac{16}{\pi}\int_0^{\pi/2} \sin^2 u\cos^2 u \exp\left[ik_1\sqrt{D^2+a^2}\right]du\right\} \tag{5.2.17}$$
$$= \rho_1 c_1 v_0(\omega)\left\{\exp[ik_1 D] - \exp\left[ik_1\sqrt{D^2+a^2}\right]\right\}$$

which is just the expression for the on-axis pressure from the piston transducer [Schmerr, 1998]. Note that if instead we had taken $a << b, D$ we would find from Eq. (5.2.12) in exactly the same fashion

$$p_{ave}(\omega)\big|_{a<<b} = \rho_1 c_1 v_0(\omega)\frac{a^2}{b^2}\left\{\exp[ik_1 D] - \exp\left[ik_1\sqrt{D^2+b^2}\right]\right\}. \tag{5.2.18}$$

Also, for the general case of two transducers where $a \neq b$, we can consider the far field limit where $D >> a, b$. Then from Eq. (5.2.12) the average received pressure is

$$p_{ave}(\omega) = \frac{\rho_1 c_1 v_0(\omega)}{\pi b^2}\exp[ik_1 D]\left\{\Theta - 16a^2b^2\right.$$
$$\left.\cdot\int_0^{\pi/2} \frac{\sin^2 u\cos^2 u}{(a-b)^2+4ab\cos^2 u}\exp\left[ik_1\sqrt{D^2+(a-b)^2+4ab\cos^2 u} - ik_1 D\right]du\right\}. \tag{5.2.19}$$

But, to first order

$$\exp\left[ik_1\sqrt{D^2+(a-b)^2+4ab\cos^2 u} - ik_1 D\right] \cong 1 + \frac{ik_1\left[a^2+b^2+4ab\cos^2 u\right]}{2D} \tag{5.2.20}$$

so

$$p_{ave}(\omega)=\frac{\rho_1 c_1 v_0(\omega)}{\pi b^2}\exp[ik_1 D]\left\{\Theta-16a^2b^2\int_0^{\pi/2}\frac{\sin^2 u\cos^2 u}{(a-b)^2+4ab\cos^2 u}du\right.$$
$$\left.-\frac{16ik_1a^2b^2}{2D}\int_0^{\pi/2}\sin^2 u\cos^2 u\,du\right\}. \tag{5.2.21}$$

Each of these integrals have appeared previously and can be done exactly since

$$16a^2b^2\int_0^{\pi/2}\frac{\sin^2 u\cos^2 u}{(a-b)^2+4ab\cos^2 u}du=2a^2b^2\int_0^{\pi}\frac{\sin^2 x}{a^2+b^2+2ab\cos x}=\Theta \tag{5.2.22}$$

and

$$\int_0^{\pi/2}\sin^2 u\cos^2 u\,du=\frac{\pi}{16}. \tag{5.2.23}$$

Thus, the first two terms inside the curly braces of Eq. (5.2.21) cancel, leaving

$$p_{ave}(\omega)\Big|_{D>>a,b}=\frac{-i\omega\rho_1 v_0(\omega)a^2}{2}\frac{\exp(ik_1D)}{D} \tag{5.2.24}$$

which is identical with the far field on-axis pressure generated by the transmitting transducer.

5.2.2 Simulation results

In subsection 5.2.1, analytical results for four special cases were obtained, namely, $a=b$, $b<<a$, $a<<b$ and $D>>a,b$. Here we will numerically evaluate the average receiving pressure and more explicitly study those four cases and others.

Dividing the area of transducer B, πb^2, Eq. (5.2.12) then gives the average receiving pressure as

$$p_{ave}(\omega)=\rho_1 c_1 v_0(\omega)\left\{\frac{\Theta}{\pi b^2}\exp[ik_1D]-\frac{16a^2}{\pi}\right.$$
$$\left.\cdot\int_0^{\pi/2}\frac{\sin^2 u\cos^2 u}{(a-b)^2+4ab\cos^2 u}\exp\left[ik_1\sqrt{D^2+(a-b)^2+4ab\cos^2 u}\right]du\right\}. \tag{5.2.25}$$

If this average pressure is normalized by $\rho_1 c_1 v_0(\omega)$, then we obtain

$$\frac{p_{ave}(\omega)}{\rho_1 c_1 v_0(\omega)}=\frac{\Theta}{\pi b^2}\exp[ik_1D]-$$
$$\frac{16a^2}{\pi}\int_0^{\pi/2}\frac{\sin^2 u\cos^2 u}{(a-b)^2+4ab\cos^2 u}\exp\left[ik_1\sqrt{D^2+(a-b)^2+4ab\cos^2 u}\right]du\Bigg\} \tag{5.2.26}$$

which is the non-dimensional from we will use for all of our numerical studies.

For purpose of simulation, we will let transducer A be a half-inch (12.7mm) diameter planar transducer. Therefore, its radius is a=6.35mm. The radius of transducer B, b, will be determined by specifying the desired ratio b/a. We will take the frequency f=5MHz and let the acoustic medium between transducer A and transducer B be water with wave speed c_1=1500m/s. The near field distance of transducer A for this case, therefore, is

$$N_a = \frac{a^2 f}{c_1} = 0.1344\text{m}. \qquad (5.2.27)$$

The definite integral in Eq. (5.2.26) was evaluated using quadrature method whose function is built-in Matlab. The function used was quad8 which uses an adaptive recursive Newton-Cotes panel rule to find the area under the graph of the kernel function in Eq. (5.2.26), that is, the definite integral [MathWorks].

Figure 5.3 shows the amplitude of normalized pressure versus normalized distance D/N_a when b/a=0, 0.02, 0.04, 0.06, 0.08 and 0.1, respectively. From that figure it follows, for b/a ratios $\leq$0.1, the positions of the first peak and the first null do not change very much, but the amplitude of the peak decreases and that of the null increases. Since the location of the first null in particular is often used in experimentally determining parameters such as the equivalent radius of a transducer [Schmerr, 1998], these results demonstrate that the null location is not very sensitive to the averaging process inherent in measuring the on-axis response with a small receiver. This is in agreement with similar results obtained by Goldstein et al [Goldstein, Gandhi, and O'Brien, 1998].

Figure 5.4 shows the amplitude of the normalized pressure versus normalized distance D/N_a when b/a= 0.1, 0.25, 0.5, 0.75, 1, 1.5, 2, 3, 4, and 5. From these curves, one sees that with increasing b/a ratios the first peak and the first null move farther away from the transmitter A. The amplitude of the first peak decreases monotonically. On the other hand, the amplitude of the first null increases until b/a=0.45, then it decreases monotonically. When the normalized distance D/N_a is very large, all curves come together and decrease with D/N_a. This corresponds to the far field on-axis pressure distribution (see Eq. (5.2.24)). For the lowest of the curves in Figure 5.4 (b/a=5.0) it is interesting to note that the amplitude received is nearly constant over a wide range of distances up to approximately $D/N_a = 10$. This behavior in turn implies that in this setup for a given distance of separation between the two transducers there is a range of frequencies over which the diffraction effects of the setup is characterized by a constant. This fact has been noted by Jiang and Apfel [1991] who

suggested that this type of setup could be used to perform material attenuation measurements without the need to compensate for frequency dependent diffraction corrections.

Figure 5.5 examines the behavior of the first peak and the first null for large *b/a* ratios. The solid lines show the behavior for the first peak and the dashed lines show the behavior for the first null. The upper figure illustrates the movements of the first peak and the first null. With increasing *b/a*, the peak and null both move farther away from transducer A. The lower figure illustrates the change of amplitudes of the first peak and the first null. For *b/a*>1, both amplitudes decreases with increasing *b/a* and the two amplitudes are very close.

Finally, Figure 5.6 separately shows the normalized average pressures when *b/a*=1, 0 and 50. When *b/a*=1 (the upper figure), we have the special case often used in the literature to study diffraction corrections (Eq. (5.2.16)) and this figure agrees with those correction factors [Khimunin, 1972].

When *b/a*=0 (the middle figure), the normalized average pressure is just the on-axis pressure given by Eq. (5.2.17). The first peak is at $D / N_a = 1$ with the amplitude of 2. The first null is at $D / N_a = 0.5$ with the amplitude of 0.

When *b/a*=50 (the lower figure), the normalized average pressure is much like the one shown for *b/a*=0. However, the distance is normalized by N_b where

$$N_b = 50^2 N_a = 336\text{m}$$

for transducer B. The first peak is at $D / N_b = 1$ with the amplitude of 2×10^{-4}, which comes, as can be seen from Eqs. (5.2.17) and (5.2.18), by computing

$$2(a / b)^2 = 2 \times 10^{-4}.$$

The first null again is at $D / N_b = 0.5$ with the amplitude of 0. This behavior is not unexpected since it is a demonstration of the reciprocity of the received pressure at a point due to a transducer (*b/a*=0) and the received pressure at a transducer due to a point source (b/a≈50).

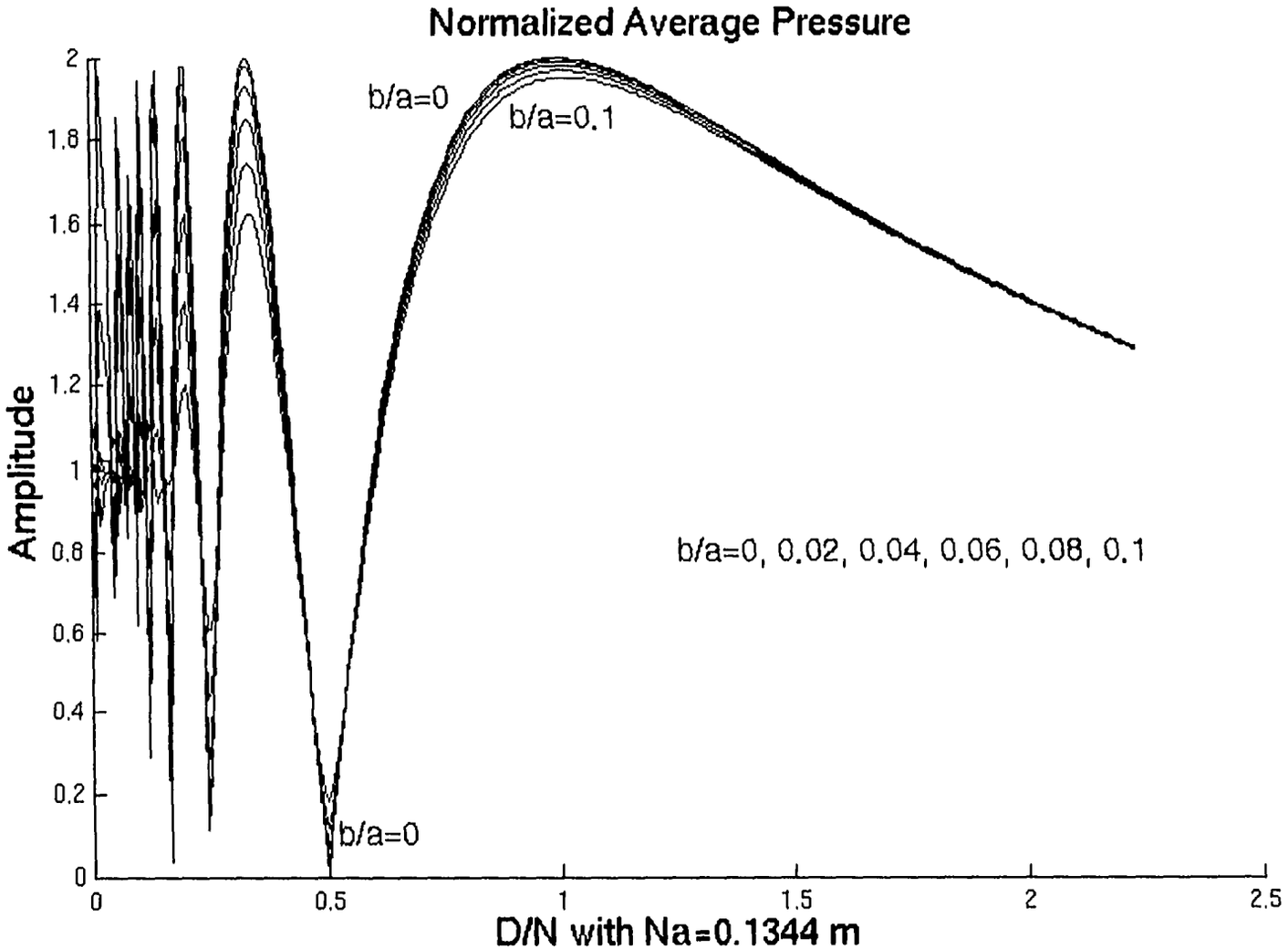

Figure 5.3 Amplitude of normalized pressure versus normalized distance D/Na when *b/a*=0, 0.02, 0.04, 0.06, 0.08 and 0.1.

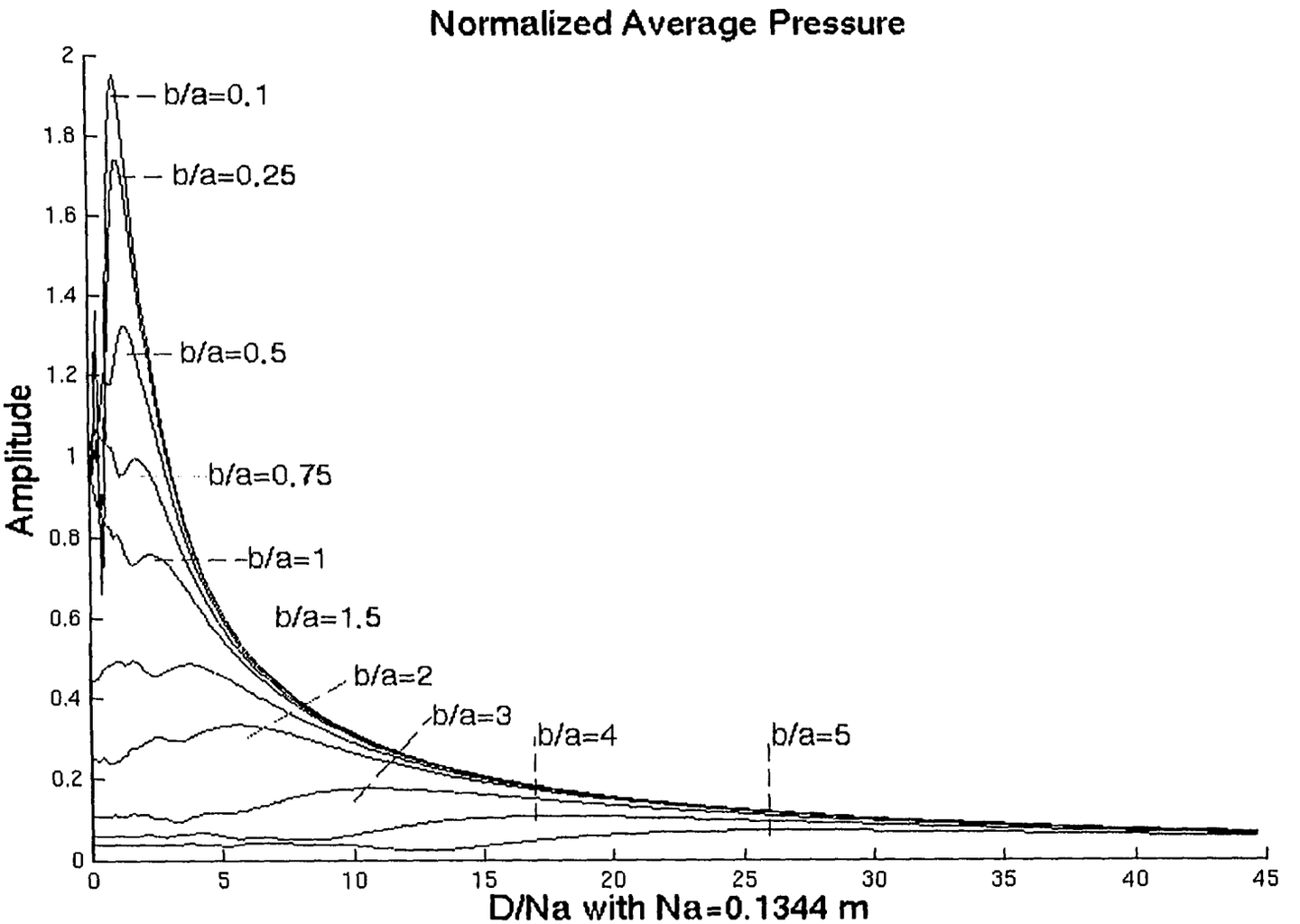

Figure 5.4 Amplitude of normalized pressure versus normalized distance D/Na when b/a=0.1, 0.25, 0.5, 0.75, 1, 1.5, 2, 3, 4, and 5.

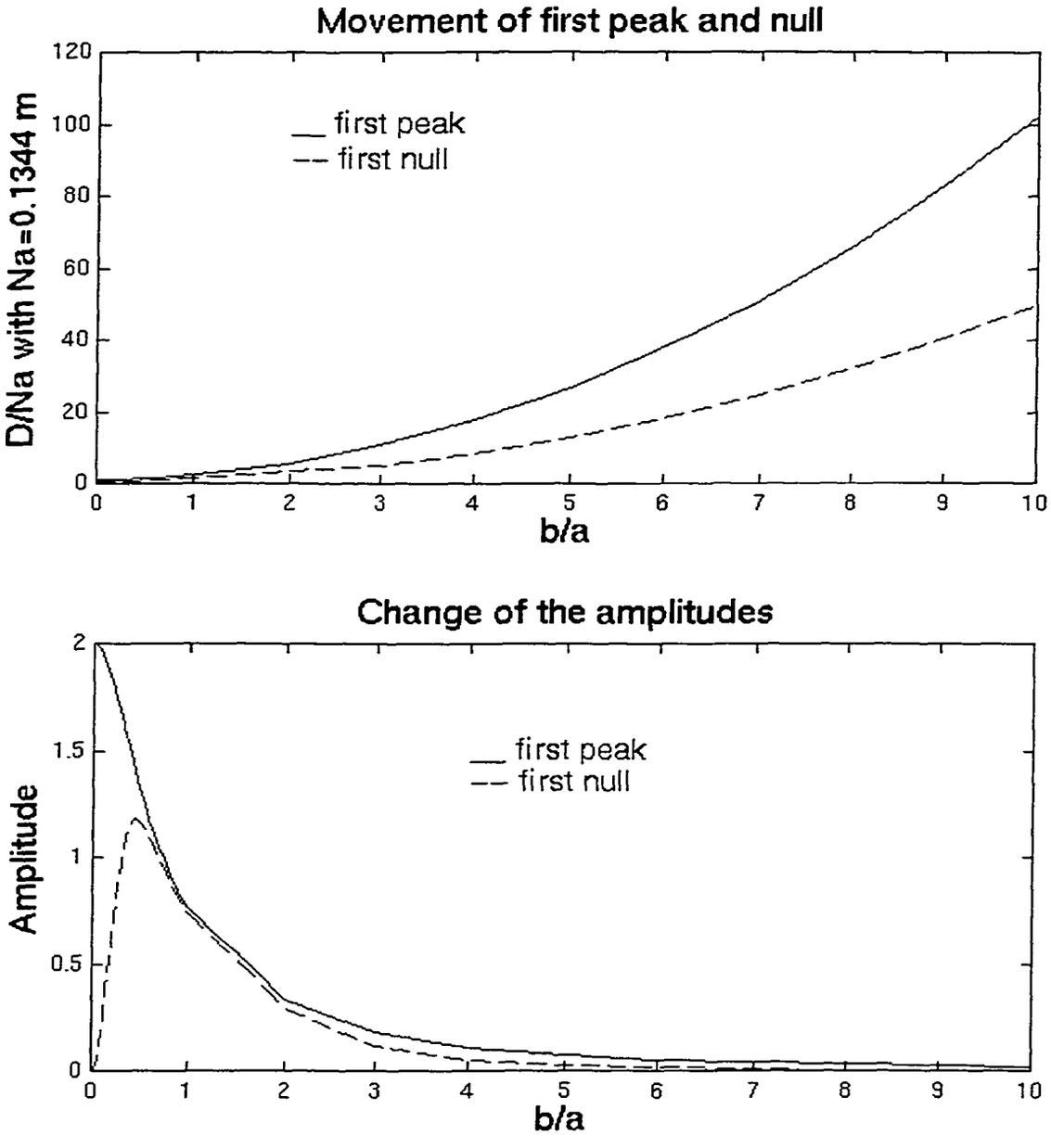

Figure 5.5 The upper figure illustrates the movements of the first peak and the first null with the increment of *b/a*. The lower figure illustrates the change of the amplitudes of the first peak and the first null with the increment of *b/a*.

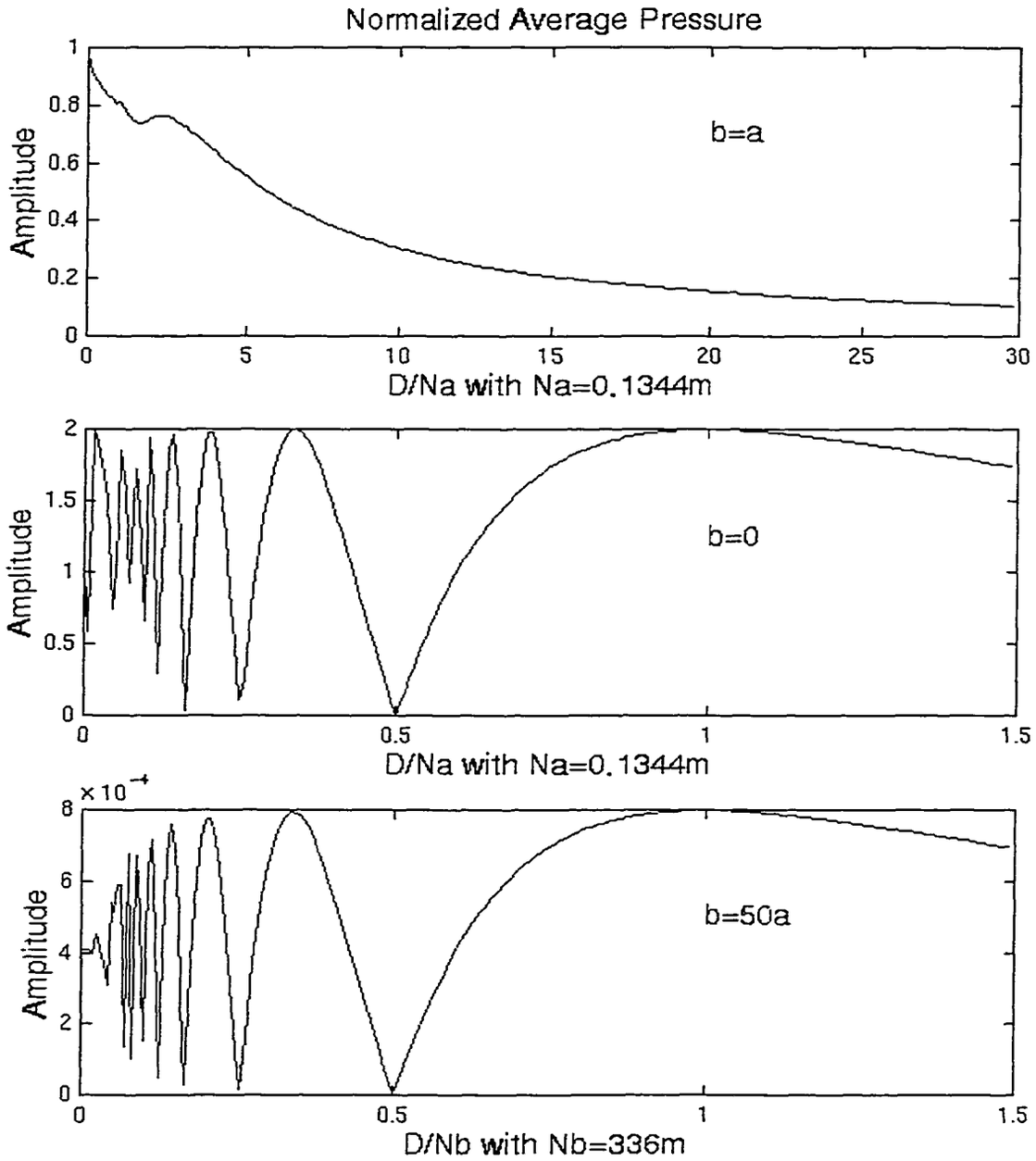

Figure 5.6 The upper figure shows the normalized average pressures when b/a=1. The first peak and the first null are very close. The middle figure shows the normalized average pressures when b/a=0. The distance is normalized by N_a=0.1344m. The lower figure shows the normalized average pressures when b/a=50. The distance is normalized by N_b=336m.

CHAPTER 6. TRANSDUCER SENSITIVITY

In the previous chapters we have shown that the entire ultrasonic measurement system can be characterized in terms of three transfer functions representing the generation, receiving, and acoustic propagation/scattering processes present. The transducers used in the measurement are of course very important parts of those processes. Transducers are also some of the most complex elements in the measurement process since they involve coupled electrical and mechanical inputs/outputs which make them difficult to characterize experimentally. When modeled as a two-port network, one way to characterize a transducer would be to find explicitly all the elements of its 2x2 transfer matrix. Sachse and Hsu [1979] refer to obtaining all the transfer matrix elements as "complete characterization" of the transducer. They suggest that a series of experimental mechanical and electrical measurements can, in principle, determine all the transfer matrix elements. To our knowledge, a practical experimental procedure for obtaining such a complete characterization has never been accomplished.

However, it will be shown in this chapter that the transfer functions, $t_G(\omega)$ and $t_R(\omega)$, both depend on the properties of the transducer only through three lumped parameters – the acoustic radiation impedance of the transducer when it is acting as a transmitter, the input electrical impedance of the transducer when it is also acting as a transmitter, and a quantity called the open-circuit sensitivity of the transducer, which is defined in a configuration where the transducer acts as a receiver. Furthermore, it will be shown that the latter two of these parameters can be related to quantities that can be obtained by electrical measurements only.

Thus, transducer sensitivity is an important parameter that will be discussed extensively in this chapter. In section 6.1 we will outline the various sensitivities that can be defined and their corresponding physical meanings and dimensions. In section 6.2 we will show that an open-circuit receiving sensitivity is the key parameter that appears naturally in the generation and reception transfer functions together with the transducer input impedance. In section 6.3, it is demonstrated how this open-circuit receiving sensitivity can in principle be obtained experimentally in a three-transducer measurement process that only involves electrical measurements. In sections 6.4 and 6.5 we define other generalized receiving and transmitting sensitivities and discuss their relationship to the open-circuit receiving sensitivity defined in section 6.2. Finally, in section 6.6 we will relate the transfer functions, sensitivities, and

impedance parameters of this thesis to other quantities such as the system "efficiency" factors defined previously in the literature.

6.1 Sensitivity Definitions

Sensitivity is defined as the ratio of one output quantity to one input quantity. For a transducer, an electromechanical device characterized by a two-port network, there are two pairs of quantities: force-velocity, (F,v), and voltage-current, (V,I). During the reception process, the input quantities are the force-velocity pair, (F,v), and the output quantities the voltage-current pair, (V,I). On the other hand, during generation process, the input quantities are the voltage-current pair, (V,I), and the output quantities the force-velocity pair, (F,v).

Transmitting sensitivity is defined as the ratio of an output mechanical quantity to an input electrical quantity. The transmitting sensitivity is called the speaker response in acoustics literature and is denoted as S_{oi}. The letter o in the subscript denotes one of the output quantities, (F,v), and the letter i one of the input quantities, (V,I). The transmitting sensitivity S_{oi} takes four forms as follows:

$S_{FV} = F/V$ transmitting voltage sensitivity with the unit of (N/V)

$S_{FI} = F/I$ transmitting current sensitivity with the unit of (N/A)

$S_{vV} = v/V$ transmitting voltage sensitivity with the unit of ((m/s)/V)

$S_{vI} = v/I$ transmitting current sensitivity with the unit of ((m/s)/A)

Similarly, the receiving sensitivity is defined as the ratio of an output electrical quantity to an input mechanical quantity. In the acoustics literature the receiving sensitivity is called the microphone response and is denoted as M_{oi}. The letter o in the subscript denotes one of the output quantities, (V,I), and the letter i one of the input quantities, (F,v). The receiving sensitivity M_{oi} takes four forms as follows:

$M_{VF} = V/F$ receiving voltage sensitivity with the unit of (V/N)

$M_{IF} = I/F$ receiving current sensitivity with the unit of (A/N)

$M_{Vv} = V/v$ receiving voltage sensitivity with the unit of (V/(m/s))

$M_{Iv} = I/v$ receiving current sensitivity with the unit of (A/(m/s))

There are many sensitivities of the types listed above that can be specified because in practice it is necessary to define a sensitivity under specific output or input conditions. For example, we often encounter receiving sensitivities under either open-circuit or short-circuit conditions. We will put a superscript "∞" to denote an open-circuit sensitivity and a

superscript "0" to denote a short-circuit sensitivity. For example, M_{VF}^{∞} is an open-circuit receiving voltage sensitivity and M_{IF}^{0} is a short-circuit receiving current sensitivity.

6.2 Transfer Functions and Transducer Parameters

In modeling the generation process, the transfer function relating the output force and Thevenin equivalent driving voltage of the pulser was obtained in Chapter 3 in the form (see Figure 6.1)

$$t_G(\omega)=\frac{F_t(\omega)}{V_i(\omega)}=\frac{Z_r^a(\omega)}{\left(Z_r^a(\omega)T_{11}^G+T_{12}^G\right)+\left(Z_r^a(\omega)T_{21}^G+T_{22}^G\right)Z_i^e(\omega)}. \qquad (6.2.1)$$

Similarly, the transfer function describing the reception process was found in Chapter 4 as (see Figure 6.2)

$$t_R(\omega)=\frac{V_R(\omega)}{F_B(\omega)}=\frac{Z_o^e(\omega)K(\omega)}{\left(Z_r^a(\omega)R_{11}^G+R_{12}^G\right)+\left(Z_r^a(\omega)R_{21}^G+R_{22}^G\right)Z_o^e(\omega)}. \qquad (6.2.2)$$

To characterize both these transfer functions completely, it is necessary to know all the elements of the global transfer matrices, T^G and R^G. These global matrices contain implicitly the transfer elements of the transducer.

In the generation process (Figure 6.1), we can separate the total global transfer matrix into a transfer matrix, T^e, which represents all the electrical elements (cabling etc.) between the pulser and the transducer, and the transducer transfer matrix itself, T^T. We find

$$\begin{bmatrix} T_{11}^G & T_{12}^G \\ T_{21}^G & T_{22}^G \end{bmatrix}=\begin{bmatrix} T_{11}^e & T_{12}^e \\ T_{21}^e & T_{22}^e \end{bmatrix}\begin{bmatrix} T_{11}^T & T_{12}^T \\ T_{21}^T & T_{22}^T \end{bmatrix}. \qquad (6.2.3)$$

On the output side of the generation process model, the total force, F_t, and the velocity, v, were related through the acoustic radiation impedance of the transducer, i.e. $F_t = Z_r^a(\omega)v$. Thus,

$$\begin{Bmatrix} V \\ I \end{Bmatrix}=\begin{bmatrix} T_{11}^G & T_{12}^G \\ T_{21}^G & T_{22}^G \end{bmatrix}\begin{Bmatrix} F_t \\ v \end{Bmatrix}=\begin{bmatrix} T_{11}^G & T_{12}^G \\ T_{21}^G & T_{22}^G \end{bmatrix}\begin{Bmatrix} Z_r^a v \\ v \end{Bmatrix} \qquad (6.2.4)$$

and, hence

$$\begin{bmatrix} T_{11}^G & T_{12}^G \\ T_{21}^G & T_{22}^G \end{bmatrix}\begin{Bmatrix} Z_r^a v \\ v \end{Bmatrix}=\begin{bmatrix} T_{11}^e & T_{12}^e \\ T_{21}^e & T_{22}^e \end{bmatrix}\begin{bmatrix} T_{11}^T & T_{12}^T \\ T_{21}^T & T_{22}^T \end{bmatrix}\begin{Bmatrix} Z_r^a v \\ v \end{Bmatrix} \qquad (6.2.5)$$

or, equivalently, canceling out a common term, v, on both sides,

$$\begin{Bmatrix} \left(Z_r^a T_{11}^G+T_{12}^G\right) \\ \left(Z_r^a T_{21}^G+T_{22}^G\right) \end{Bmatrix}=\begin{bmatrix} T_{11}^e & T_{12}^e \\ T_{21}^e & T_{22}^e \end{bmatrix}\begin{Bmatrix} \left(Z_r^a T_{11}^T+T_{12}^T\right) \\ \left(Z_r^a T_{21}^T+T_{22}^T\right) \end{Bmatrix}. \qquad (6.2.6)$$

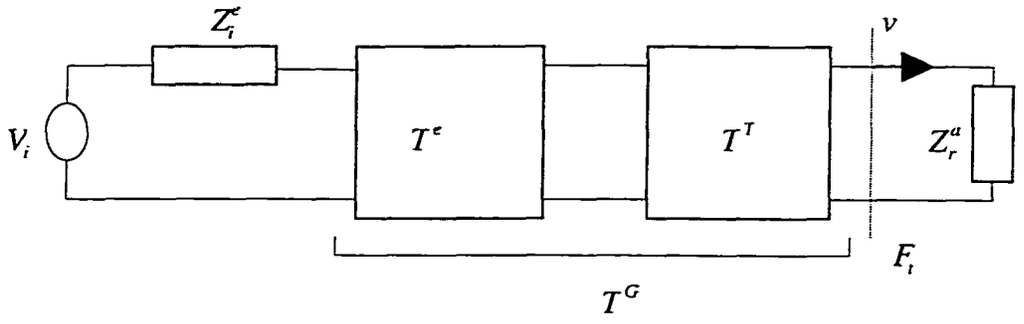

Figure 6.1 The generation process with the global transfer matrix T^G separated into the transducer matrix, T^T, and the other electrical components, T^e. Z_r^a here is the radiation acoustic impedance of the transmitter.

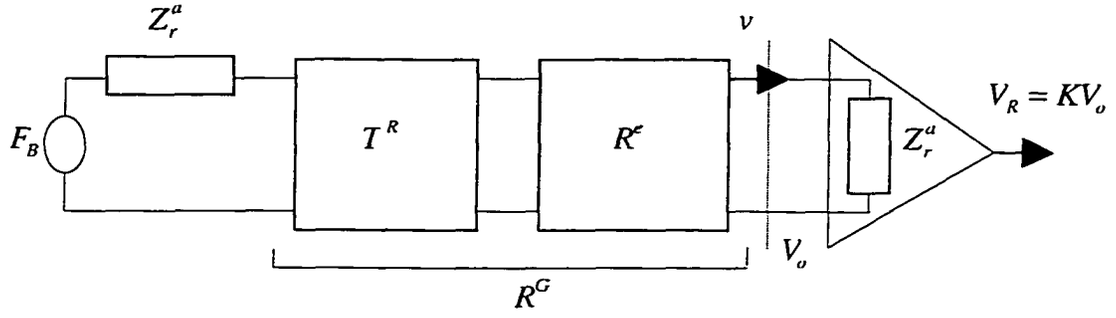

Figure 6.2 The reception process with the global transfer matrix R^G separated into the transducer matrix, T^R, and the other electrical components, R^e. Z_r^a here is the radiation acoustic impedance of the receiver.

The terms on the left side of Eq. (6.2.6) are just those terms that appear in the expression for the transfer function describing the generation process. Thus, Eq. (6.2.6) shows that these transfer matrix terms depend on the transducer only through the corresponding terms given on the right side of Eq. (6.2.6). We will now show that these two terms can be written in terms of the transducer's input impedance and the transducer's receiving sensitivity.

To see this, first consider the transducer when it acts as a transmitter (Figure 6.3) radiating into the fluid. We have

$$\begin{Bmatrix} V \\ I \end{Bmatrix} = \begin{bmatrix} T_{11}^T & T_{12}^T \\ T_{21}^T & T_{22}^T \end{bmatrix} \begin{Bmatrix} Z_r^a v \\ v \end{Bmatrix} \tag{6.2.7}$$

so that its input electrical impedance, $V / I = Z_{in}^{T:e}(\omega)$, is given by

$$Z_{in}^{T:e}(\omega)=\frac{Z_r^a T_{11}^T+T_{12}^T}{Z_r^a T_{21}^T+T_{22}^T}. \tag{6.2.8}$$

Now, consider this same transducer, acting as a receiver (Figure 6.4). We have

$$\begin{Bmatrix} F_i \\ v_i \end{Bmatrix}=\begin{bmatrix} T_{22}^T & T_{12}^T \\ T_{21}^T & T_{11}^T \end{bmatrix}\begin{Bmatrix} V \\ I \end{Bmatrix} \tag{6.2.9}$$

where note we have taken the velocity, v_i, as "flowing" into the transducer, and the current, I, is taken flowing out, as in Chapter 4. If we measure the output voltage, $V = V^{\infty}$, under open-circuit conditions ($I = 0$), then we find from Eq. (6.2.9)

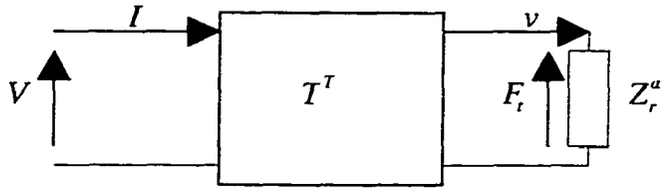

Figure 6.3 The transducer acting as a transmitter where Z_r^a is the radiation acoustic impedance of the transducer.

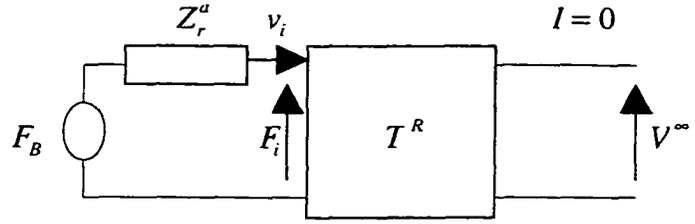

Figure 6.4 The same transducer of Figure 6.3 acting as a receiver (thus Z_r^a is the same as in Figure 6.3) under open-circuit conditions.

$$\begin{aligned} F_i &= T_{22}^T V^{\infty} \\ v_i &= T_{21}^T V^{\infty} \end{aligned} \tag{6.2.10}$$

so that in terms of the blocked force, F_B, which acts as the source term in Figure 6.4, we have

$$\begin{aligned} F_B &= Z_r^a v_i + F_i \\ &= \left(Z_r^a T_{21}^T + T_{22}^T\right)V^{\infty}. \end{aligned} \tag{6.2.11}$$

Eq. (6.2.11) defines a transducer sensitivity, $M_{VF_B}^{T:\infty} = V^{\infty} / F_B$, given by

$$M_{VF_B}^{T:\infty}(\omega)=\frac{1}{\left(Z_r^a T_{21}^T+T_{22}^T\right)} \tag{6.2.12}$$

where, to be specific, $M_{VF_B}^{\infty}$ is the open-circuit, blocked-force receiving sensitivity of the transducer.

Combining Eqs. (6.2.12), (6.2.8) and (6.2.6), we find

$$\begin{Bmatrix} Z_r^a T_{11}^G + T_{12}^G \\ Z_r^a T_{21}^G + T_{22}^G \end{Bmatrix} = \begin{bmatrix} T_{11}^e & T_{12}^e \\ T_{21}^e & T_{22}^e \end{bmatrix} \begin{Bmatrix} Z_{in}^{T:e} / M_{VF_B}^{T:\infty} \\ 1/M_{VF_B}^{T:\infty} \end{Bmatrix} \tag{6.2.13}$$

so that generation transfer function, Eq. (6.1), can be rewritten as

$$t_G(\omega) = \frac{F_t(\omega)}{V_i(\omega)} = \frac{Z_r^{T:a}(\omega) M_{VF_B}^{T:\infty}}{\left[Z_{in}^{T:e}(\omega) T_{11}^e + T_{12}^e\right] + \left[Z_{in}^{T:e}(\omega) T_{21}^e + T_{22}^e\right] Z_i^e(\omega)} \tag{6.2.14}$$

where we have written $Z_r^{T:a}(\omega) \equiv Z_r^a(\omega)$ to show explicitly this is the radiation acoustic impedance for the transmitting transducer T (below it will be important to distinguish it from the similar impedance of the receiving transducer).

Equation (6.2.14) is an important result, since it shows that the effect of the transmitting transducer, T, on the generation process can be characterized entirely in terms of three transducer parameters – the transducer input electrical impedance, $Z_{in}^{T:e}(\omega)$, the open-circuit, blocked-force receiving sensitivity, $M_{VF_B}^{T:\infty}(\omega)$, and the radiation acoustic impedance, $Z_r^{T:a}(\omega)$. As we have seen in Chapter 3, the radiation acoustic impedance can often be replaced by its explicit high frequency limit. As will be shown shortly, both the transducer input impedance and the open-circuit sensitivity terms appearing in Eq. (6.2.14) can be obtained explicitly through particular electrical measurements. Since all the other elements appearing in Eq. (6.2.14) can also be obtained from electrical measurements, Eq. (6.2.14) provides a means for characterizing the entire generation process by purely electrical means.

In exactly the same fashion, the receiving transducer response can be separated out from the other components in the reception process and the transfer function, Eq. (6.2.2) written in terms of the receiving transducer input impedance, sensitivity, and radiation acoustic impedance. Since the details are identical to those just described for the transmitting transducer, we simply write the end result, i.e.

$$t_R(\omega) = \frac{Z_o^e(\omega) K(\omega) M_{VF_B}^{R:\infty}}{\left[Z_{in}^{R:e}(\omega) R_{11}^e + R_{12}^e\right] + \left[Z_{in}^{R:e}(\omega) R_{21}^e + R_{22}^e\right] Z_o^e(\omega)} \tag{6.2.15}$$

where $Z_{in}^{R:e}$ is the input impedance of the receiving transducer (when acting as a transmitter), $M_{VF_B}^{R:\infty}(\omega)$ is the open-circuit, blocked-force receiving sensitivity of the receiving transducer, and R^e is the transfer matrix representing all the electrical elements existing between the receiving transducer and the pulser (see Figure 6.2), whose individual terms appear in Eq.(6.2.15). The radiation acoustic impedance of the receiving transducer, $Z_r^{R:a}(\omega)$, does not

appear explicitly in Eq. (6.2.15), but is contained implicitly in the determination of the sensitivity of the receiver, as will be shown shortly.

6.3 Three-transducer Calibration

As seen in the last section, the open-circuit, blocked-force receiving sensitivity appears naturally in describing the generation and reception processes. Unlike the transducer input impedance, which is defined in terms of electrical terms (voltage/current), this sensitivity involves a ratio of electrical and mechanical terms so that it is not obvious that one can obtain this parameter by purely electrical measurements. In this section, we will show that through the use of three transducers used in simple calibration setups, this sensitivity of the transducer can be obtained.

The three-transducer calibration setups, labeled I, II, and III, are shown in Figure 6.5. The acoustic transfer functions for these three setups are assumed known and are given as t_A^I, t_A^{II}, t_A^{III}, respectively. In practice, for simplicity, we may wish to make all three acoustic transfer functions the same, but for generality we will not make that assumption here. We will let transducer A be the transducer whose open-circuit, blocked-force sensitivity we wish to determine. Transducers B and C will be two other transducers whose own explicit transfer matrices need not be known.

In setup I, transducer C fires from a given excitation source and transducer A is the receiver. In setup II, transducer C fires from the same excitation source and transducer B is the receiver. In setup III, transducer B fires and transducer A again is the receiver. A fourth setup, setup IV, is also shown in Figure 6.5. While this fourth setup shown in Figure 6.5 is not needed to obtain the sensitivity of transducer A, it can be used as a reciprocity check, as will be shown later.

It is assumed that certain electrical measurements are made in each of the three setups, I, II, and III. These measurements are the open-circuit receiving voltage in setup I, V_{CA}^{∞}, the open-circuit receiving voltage in setup II, V_{CB}^{∞}, and the current driving transducer B in setup III, I_B, together with the resulting open-circuit voltage, V_{BA}^{∞}, in that setup.

Consider first setup I. We can write the measured open-circuit voltage, V_{CA}^{∞}, in this setup as

$$\begin{aligned} V_{CA}^{\infty}(\omega) &= \frac{V_{CA}^{\infty}(\omega)}{F_B(\omega)} \frac{F_B(\omega)}{F_t(\omega)} \frac{F_t(\omega)}{V_i(\omega)} V_i(\omega) \\ &= M_{VF_B}^{A;\infty}(\omega) t_A^I(\omega) t_G(\omega) V_i(\omega) \end{aligned} \qquad (6.3.1)$$

Similarly, for the open-circuit voltage, V_{CB}^{∞}, measured in setup II

$$V_{CB}^{\infty}(\omega) = \frac{V_{CB}^{\infty}(\omega)}{F_B(\omega)} \frac{F_B(\omega)}{F_t(\omega)} \frac{F_t(\omega)}{V_i(\omega)} V_i(\omega)$$
$$= M_{VF_B}^{B:\infty}(\omega) t_A^{II}(\omega) t_G(\omega) V_i(\omega) \qquad (6.3.2)$$

where the transfer function, t_G, and the input voltage, V_i, are assumed to be the same as in setup I, i.e. both setups are carried out under exactly the same conditions (pulser settings, cables, etc.). Taking the ratio of Eqs. (6.3.1) and (6.3.2), we obtain

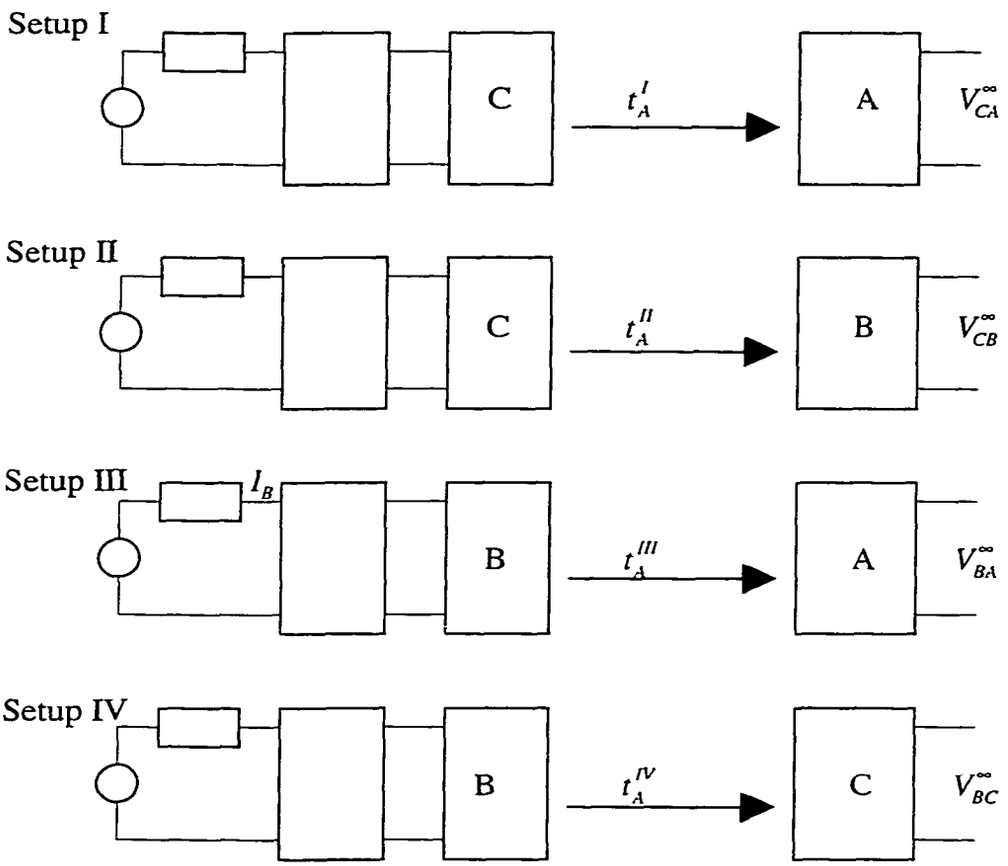

Figure 6.5 Three-transducer calibration setups. Setups I, II and III are used to measure the open-circuit, blocked force receiving sensitivity $M_{VF_B}^{A:\infty}(\omega)$ of transducer A. Setup IV is used for reciprocity check.

$$\frac{V_{CA}^{\infty}(\omega)}{V_{CB}^{\infty}(\omega)} = \frac{M_{VF_B}^{A:\infty}(\omega)}{M_{VF_B}^{B:\infty}(\omega)} \frac{t_A^{I}(\omega)}{t_A^{II}(\omega)}. \tag{6.3.3}$$

For setup III, consider transducer B, which is now the transmitter. In terms of its transfer matrix, T^B, we have the voltage and current driving the transducer V_B and I_B given as

$$\begin{Bmatrix} V_B \\ I_B \end{Bmatrix} = \begin{bmatrix} T_{11}^B & T_{12}^B \\ T_{21}^B & T_{22}^B \end{bmatrix} \begin{Bmatrix} F_t \\ F_t / Z_r^{B:a} \end{Bmatrix} \tag{6.3.4}$$

where $Z_r^{B:a}(\omega)$ is the radiation acoustic impedance of transducer B. From Eq. (6.3.4) it follows then that

$$\begin{aligned} I_B &= \left(Z_r^{B:a} T_{21}^B + T_{22}^B\right) \frac{F_t}{Z_r^{B:a}} \\ &= \frac{1}{M_{VF_B}^{B:\infty}} \frac{F_t}{Z_r^{B:a}} \end{aligned} . \tag{6.3.5}$$

Solving for the sensitivity of transducer B, we find

$$\begin{aligned} M_{VF_B}^{B:\infty}(\omega) &= \frac{F_t(\omega)}{Z_r^{B:a}(\omega) I_B(\omega)} \\ &= \frac{F_t(\omega)}{F_B(\omega)} \frac{F_B(\omega)}{V_{BA}^{\infty}(\omega)} \frac{V_{BA}^{\infty}(\omega)}{Z_r^{B:a}(\omega) I_B(\omega)} \\ &= \frac{1}{t_A^{III}(\omega)} \frac{1}{M_{VF_B}^{A:\infty}(\omega)} \frac{V_{BA}^{\infty}(\omega)}{Z_r^{B:a}(\omega) I_B(\omega)} \end{aligned} . \tag{6.3.6}$$

Placing Eq. (6.3.3) into Eq. (6.3.6) gives

$$\frac{V_{CA}^{\infty}(\omega)}{V_{CB}^{\infty}(\omega)} = \left(M_{VF_B}^{A:\infty}(\omega)\right)^2 \frac{t_A^{I}(\omega) t_A^{III}(\omega)}{t_A^{II}(\omega)} \frac{Z_r^{B:a}(\omega) I_B(\omega)}{V_{BA}^{\infty}(\omega)} \tag{6.3.7}$$

which can be solved for the open-circuit, blocked-force receiving sensitivity of transducer A in the form

$$M_{VF_B}^{A:\infty}(\omega) = \sqrt{\frac{V_{CA}^{\infty}(\omega) V_{BA}^{\infty}(\omega)}{V_{CB}^{\infty}(\omega) I_B(\omega)} \frac{t_A^{II}(\omega)}{Z_r^{B:a}(\omega) t_A^{I}(\omega) t_A^{III}(\omega)}}. \tag{6.3.8}$$

Eq. (6.3.8) gives the sensitivity of A in terms of measurable voltages and currents and acoustic quantities that are assumed to be known.

For the special case where all the acoustic transfer functions are the same, i.e. $t_A^{I} = t_A^{II} = t_A^{III} \equiv t_A$, Eq. (6.3.8) reduces to the simpler form

$$M_{VF_B}^{A:\infty}(\omega) = \sqrt{\frac{V_{CA}^{\infty}(\omega) V_{BA}^{\infty}(\omega)}{V_{CB}^{\infty}(\omega) I_B(\omega)} \frac{1}{Z_r^{B:a}(\omega) t_A(\omega)}}. \tag{6.3.9}$$

6.3.1 Reciprocity check

In Figure 6.5 we showed a setup IV that can be used in conjunction with setup II to serve as a check that reciprocity is satisfied for these two configurations. Figure 6.6 shows general input and output voltages and currents in these two setups. Since there are a pair of inputs and outputs in both of these setups, we can define a two-port transfer function, T^S relating these inputs/outputs. If these two setups satisfy reciprocity, then from Figure 6.6 we should have for setup II

$$\begin{Bmatrix} V'_C \\ I'_C \end{Bmatrix} = \begin{bmatrix} T^S_{11} & T^S_{12} \\ T^S_{21} & T^S_{22} \end{bmatrix} \begin{Bmatrix} V'_{CB} \\ I'_{CB} \end{Bmatrix} \tag{6.3.10}$$

and for setup IV

$$\begin{Bmatrix} V'_B \\ I'_B \end{Bmatrix} = \begin{bmatrix} T^S_{22} & T^S_{12} \\ T^S_{21} & T^S_{11} \end{bmatrix} \begin{Bmatrix} V'_{BC} \\ I'_{BC} \end{Bmatrix} \tag{6.3.11}$$

where in obtaining Eq. (6.3.11) we have used the fact that the directions of the currents in setup II are opposite from those of setup IV, and that the transfer matrix T^s is reciprocal, i.e., $\det(T^S) = 1$. It follows from Eqs. (6.3.10) and (6.3.11) that if we take open-circuit conditions at the receiver in both of these setups ($I'_{CB} = I'_{BC} = 0$) that the received open-circuit voltages, V^{∞}_{CB} and V^{∞}_{BC}, are related to the driving currents through

$$\begin{aligned} I'_C &= T^S_{21} V^{\infty}_{CB} \\ I'_B &= T^S_{21} V^{\infty}_{BC} \end{aligned} \tag{6.3.12}$$

Eq. (6.3.12) shows that if reciprocity is satisfied, we must have

$$I'_C(\omega) V^{\infty}_{BC}(\omega) = I'_B(\omega) V^{\infty}_{CB}(\omega) \tag{6.3.13}$$

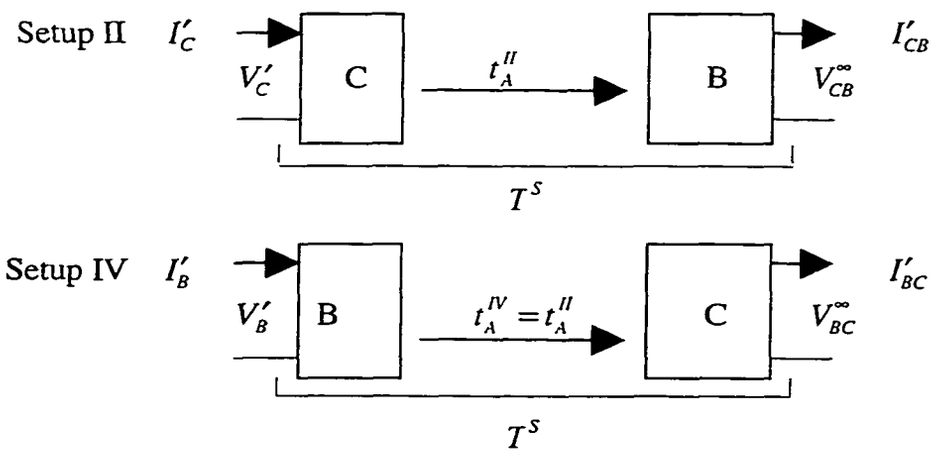

Figure 6.6 Reciprocity check using setups II and IV where the acoustic transfer functions are identical in both setups.

which is a check that can be made by making measurements of the quantities appearing in Eq. (6.3.13).

6.3.2 Reciprocity parameter

In the acoustics literature, the open-circuit receiving sensitivity of a transducer A is defined in terms of the ratio of the open-circuit receiving voltage to the average pressure, $\overline{p}$, in the incident wave, $M_{V\overline{p}}^{A:\infty}$. This quantity can be related to our open-circuit, blocked-force receiving sensitivity if we assume the incident waves are plane waves normal to the transducer surface and the velocity is uniform across the transducer surface so that we have $F_B = 2F_{inc} = 2\overline{p}S_A$, where S_A is the surface area of the transducer. We find, in our notation

$$M_{V\overline{p}}^{A:\infty}(\omega) = 2S_A M_{VF_B}^{A:\infty}(\omega). \tag{6.3.14}$$

Note that the sensitivity $M_{V\overline{p}}^{A:\infty}$ has the units of V/Pa. In the acoustics literature [MacLean, 1940, Bobber, 1966], this sensitivity factor is expressed in the form similar to Eq. (6.3.9) given by

$$M_{V\overline{p}}^{A:\infty}(\omega) = \sqrt{\frac{V_{CA}^{\infty}(\omega)V_{BA}^{\infty}(\omega)J(\omega)}{V_{CB}^{\infty}(\omega)I_B(\omega)}} \tag{6.3.15}$$

where J is called the reciprocity parameter. Comparing Eqs. (6.3.15) and (6.3.9) through the use of Eq. (6.3.14), then shows that J is given by

$$J(\omega) = \frac{4S_A^2}{Z_r^{B:a}(\omega)t_A(\omega)}. \tag{6.3.16}$$

However, in the acoustics literature, it is normally assumed that the radiation impedance is given by its high frequency value, in which case we have

$$J(\omega) = \frac{4S_A^2}{\rho c S_B\, t_A(\omega)} \tag{6.3.17}$$

in terms of the density, ρ, and wave speed, c of the fluid and the area, S_B, of transducer B.

It is also common in acoustics to take as the calibration setups I, II, and III to involve two equal area circular piston transducers whose axes are aligned and separated by a distance, D. In this case the reciprocity parameter is given by

$$J(\omega) = \frac{4S}{\rho c t_A(\omega)}. \tag{6.3.18}$$

This is also a special case of the configuration discussed in Chapter 5, where an exact integral expression was obtained for the acoustic transfer function t_A. However, in the paraxial approximation, this integral expression can be reduced to an explicit analytical form given by [Schmerr, 1998].

$$t_A(\omega) = 2\exp(ikD)\left[1 - \exp\left(ika^2 / D\right)\left\{J_0\left(ka^2 / D\right) - iJ_1\left(ka^2 / D\right)\right\}\right] \quad (6.3.19)$$

where k is the wave number and a is the radius of the transducers. Now, consider the case where the two transducers are very close so that $ka^2 / D >> 1$. Then since the Bessel functions both go to zero in this limit, to first order we have

$$t_A(\omega) \cong 2\exp(ikD) \quad (6.3.20)$$

and the reciprocity parameter becomes

$$J(\omega) = \frac{2S}{\rho c}\exp(-ikD) \quad (6.3.21)$$

which is called plane wave calibration [Trott, 1962, Chertock, 1962, Garrett, 1979] in the acoustics literature. On the other hand, when $D >> a$, we have $J_0\left(ka^2 / D\right) \cong 1$, $J_1\left(ka^2 / D\right) \cong ka^2 / 2D$ and $\exp\left(ika^2 / D\right) = 1 + ika^2 / D$ so that placing these approximations into Eq. (6.3.19), to first order we find

$$t_A(\omega) \cong -\frac{ika^2}{D}\exp(ikD) \quad (6.3.22)$$

so in terms of the wavelength $\lambda = 2\pi / k$, with $S = \pi a^2$ Eq.(6.3.18) for the reciprocity parameter becomes

$$J(\omega) = \frac{2i\lambda D}{\rho c}\exp(-ikD) \quad (6.3.23)$$

which is called spherical wave calibration in the acoustics literature [MacLean, 1940, Trott, 1962, Chertock, 1962, Bobber, 1966]. Thus, Eq. (6.3.19) provides the generalization needed for a calibration setup where the transducers are not in either the very near field where a plane wave result is valid or in the far field where the transducers act as point sources and a spherical wave limit is appropriate.

6.4 Generalized Sensitivities

In the previous sections we have seen that the open-circuit, blocked-force receiving sensitivity is the transducer parameter that appears naturally in modeling the generation and reception transfer functions and is a sensitivity that can be related directly to electrical measurements in a calibration setup. However, as indicated in section 6.1, other sensitivities can be defined and it is useful to consider their relationship to the open-circuit, blocked-force receiving sensitivity.

6.4.1 Generalized receiving sensitivities

The generalized receiving voltage sensitivity of a receiving transducer is defined as the ratio of the receiving voltage across an arbitrary electrical impedance to the blocked force on the front surface of a receiving transducer. It has the unit of V/N. Similarly, the generalized receiving current sensitivity of a receiving transducer is defined as the ratio of the receiving current through an arbitrary electrical impedance to the blocked force on the front surface of a receiving transducer. It has the unit of A/N.

Following a procedure similar to the derivation of the receiving transfer function for the general reception process (which is in terms of a V_R / F_B ratio), we can express an generalized receiving current sensitivity (see Figure 6.7) as

$$M_{IF_B} = \frac{I_0}{F_B} = \frac{1}{\left(Z_o^e(\omega)T_{22}^{\mathrm{R}} + T_{12}^{\mathrm{R}}\right) + \left(T_{21}^{\mathrm{R}} Z_o^e(\omega) + T_{11}^{\mathrm{R}}\right) Z_r^a(\omega)} \tag{6.4.1}$$

which is similar to Eq. (4.4.16), and a generalized receiving voltage sensitivity as

$$M_{VF_B} = \frac{V_0}{F_B} = \frac{Z_o^e(\omega)}{\left(Z_o^e(\omega)T_{22}^{\mathrm{R}} + T_{12}^{\mathrm{R}}\right) + \left(T_{21}^{\mathrm{R}} Z_o^e(\omega) + T_{11}^{\mathrm{R}}\right) Z_r^a(\omega)} \tag{6.4.2}$$

which is similar to Eq. (4.4.17).

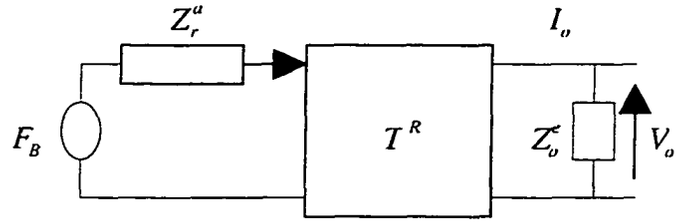

Figure 6.7 A receiving transducer with a loading impedance, Z_o^e, at its electrical terminals.

The generalized receiving voltage sensitivity can be reduced to the open-circuit voltage sensitivity by taking $Z_o^e \to \infty$, i.e.,

$$\lim_{Z_o^e \to \infty} M_{VF_B} = \frac{1}{T_{22}^{\mathrm{R}} + T_{21}^{\mathrm{R}} Z_r^a(\omega)} = M_{VF_B}^{\infty}. \tag{6.4.3}$$

Similarly, the generalized receiving current sensitivity can be reduced to the short-circuit current sensitivity by taking $Z_o^e \to 0$ in Eq. (6.4.1), i.e.,

$$\lim_{Z_o^e \to 0} M_{IF_B} = \frac{1}{T_{12}^{\mathrm{R}} + T_{11}^{\mathrm{R}} Z_r^a(\omega)} = M_{IF_B}^{0}. \tag{6.4.4}$$

Because we have (Figure 6.7)

$$V_0 = Z_0^e I_0 \tag{6.4.5}$$

the generalized receiving voltage sensitivity and the generalized receiving current sensitivities are related to each other by

$$M_{VF} = M_{IF} Z_o^e. \tag{6.4.6}$$

Similarly, the open-circuit and short-circuit sensitivities are related through an impedance since from Eqs. (6.4.3), (6.4.4), and (6.2.8)

$$\frac{M_{VF_B}^{\infty}}{M_{IF_B}^{0}} = \frac{Z_r^a T_{11}^R + T_{12}^R}{Z_r^a T_{21}^R + T_{22}^R} = Z_{in}^{R:e} \tag{6.4.7}$$

where $Z_{in}^{R:e}$ is the input electrical impedance of the receiver when it is acting as a transmitter.

The generalized receiving voltage sensitivity can also be expressed as a function of the open-circuit voltage sensitivity and appropriate impedances. To see this, first rewrite Eq. (6.4.2) as

$$M_{VF_B} = \frac{Z_o^e}{\left(T_{22}^R + Z_r^a T_{21}^R\right) Z_o^e + \left(T_{12}^R + Z_r^a T_{11}^R\right)}. \tag{6.4.8}$$

Using Eqs. (6.4.3) and (6.4.4), we can rewrite Eq. (6.4.8) as

$$M_{VF_B} = \frac{Z_o^e M_{VF_B}^{\infty}}{Z_o^e + M_{VF_B}^{\infty} / M_{IF_B}^{0}} \tag{6.4.9}$$

and using Eq. (6.4.7) then gives

$$M_{VF_B} = \frac{Z_o^e M_{VF_B}^{\infty}}{Z_o^e + Z_{in}^{R:e}}. \tag{6.4.10}$$

This equation, relating the generalized receiving voltage sensitivity and the open-circuit voltage sensitivity, will be very useful in experimental measurements, as will be discussed in the next section.

6.4.2 Measuring generalized receiving voltage sensitivity

In an ultrasonic measurement, it is difficult to satisfy the open-circuit condition at a receiving transducer. Usually, a cable is used to connect the receiving transducer to a monitor such as an oscilloscope, receiver or data acquisition circuit board. Even a very short cable (for example, 2cm long) would affect the receiving voltage at the high frequency range present in ultrasonic tests because when one end of the cable is opened, the input impedance at the other end is still not infinite. In this case, it is useful to measure the generalized receiving sensitivity M_{VF_B} for a transducer and then use Eq. (6.4.10) to solve for the open-circuit voltage sensitivity $M_{VF_B}^{\infty}$.

In this subsection, three-transducer calibration procedure described in section 6.3 is modified to measure the generalized receiving sensitivity.

To begin, we first derive the relationship between the open-circuit voltage and the voltage measured across a finite electrical load. We can replace the receiving transducer by a Thevenin equivalent circuit, using the Thevenin theorem, as shown in Figure 6.8. From the Thevenin theorem it follows that the Thevenin voltage, V_0, is given by

$$V_0 = \frac{F_B}{Z_r^a T_{21}^R + T_{22}^R} \tag{6.4.11}$$

and the Thevenin equivalent impedance is given by

$$Z_{in}^{R:e} = \frac{Z_r^a T_{11}^R + T_{12}^R}{Z_r^a T_{21}^R + T_{22}^R} \tag{6.4.12}$$

which is just the input electrical impedance of the receiver when it is acting as a transmitter.

From Figure 6.8, the open-circuit receiving voltage can be expressed as

$$V^{\infty} = V\left(1 + \frac{Z_{in}^{R:e}}{Z_o^e}\right). \tag{6.4.13}$$

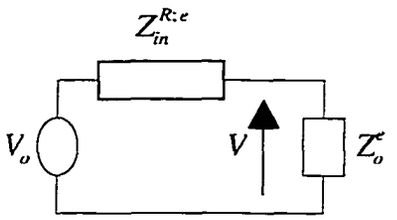

Figure 6.8 Thevenin equivalent circuit of a receiving transducer with Thevenin equivalent voltage source, V_o, and impedance, $Z_{in}^{R:e}$, which is just the input impedance of the receiving transducer where it acts as a transmitter. Z_o^e is the electrical load.

Now, assume the same receiving load, Z_0^e, is connected to the receiving transducers in all Setups in Figure 6.5. Let the voltages across Z_o^e in Setups I, II, and III be V_{CA}, V_{CB} and V_{BA}. Using Eq. (6.4.13), the open-circuit receiving voltages in all the setups can be evaluated respectively.

In Setup I, the open-circuit receiving voltage from transducer A is

$$V_{CA}^{\infty} = V_{CA}\left(1 + \frac{Z_{in}^{A:e}}{Z_o^e}\right) \tag{6.4.14}$$

where $Z_{in}^{A:e}$ is the input electrical impedance of transducer A when it transmits acoustic waves into the acoustic medium.

In Setup II, the open-circuit receiving voltage from transducer B is

$$V_{CB}^{\infty} = V_{CB}\left(1+\frac{Z_{in}^{B:e}}{Z_o^e}\right) \tag{6.4.15}$$

where $Z_{in}^{B:e}$ is the input electrical impedance of transducer B when it transmits acoustic waves into the acoustic medium.

In Setup III, the open-circuit receiving voltage from transducer A is

$$V_{BA}^{\infty} = V_{BA}\left(1+\frac{Z_{in}^{A:e}}{Z_o^e}\right). \tag{6.4.16}$$

Using Eq. (6.4.10), the open-circuit receiving voltage sensitivity is expressed as

$$M_{VF_B}^{A:\infty} = M_{VF_B}^{A}\left(1+\frac{Z_{in}^{A:e}}{Z_o^e}\right). \tag{6.4.17}$$

Substituting Eqs. (6.4.14)-(6.4.17) into Eq. (6.3.8), then

$$M_{VF_B}^{A}\left(1+\frac{Z_{in}^{A:e}}{Z_o^e}\right) = \sqrt{\frac{V_{CA}\left(1+\frac{Z_{in}^{A:e}}{Z_o^e}\right)V_{BA}\left(1+\frac{Z_{in}^{A:e}}{Z_o^e}\right)}{I_B V_{CB}\left(1+\frac{Z_{in}^{B:e}}{Z_o^e}\right)}\cdot\frac{t_A^{II}}{Z_r^a t_A^I t_A^{III}}} \tag{6.4.18}$$

which simplifies to

$$M_{VF_B}^{A} = \sqrt{\frac{V_{CA}V_{BA}}{I_B V_{CB}\left(1+Z_{in}^{B:e}/Z_o^e\right)}\cdot\frac{t_A^{II}}{Z_r^a t_A^I t_A^{III}}}\,. \tag{6.4.19}$$

Eq. (6.4.19) is an important result since it shows that the generalized sensitivity can be determined directly through electrical measurements and then, through Eq. (6.4.17) used to obtain the open-circuit sensitivity that appears naturally in all our measurement model terms. For acoustic systems which involve much lower frequencies than NDE applications, the open-circuit sensitivity is easy to determine, but for NDE tests the sensitivity must usually be found under a known load impedance that is not infinite.

6.4.3 Generalized transmitting sensitivities

The generation process is depicted in Figure 3.14 in Chapter 3. It includes four components: the pulser, the cabling, the transducer and the acoustic medium. To study the behavior of the transmitting transducer, we will replace the elements driving the transducer by the equivalent source and impedance terms shown in Figure 6.9. The radiation acoustic

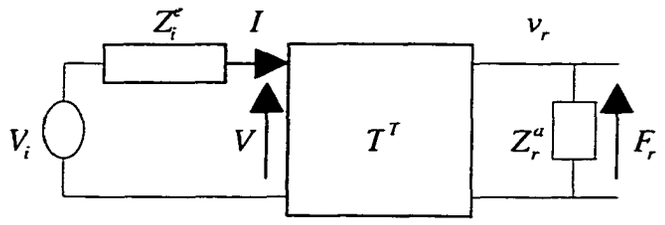

Figure 6.9 A transmitting transducer with a source voltage V_i and electrical impedance, Z_i^e, at its driving terminals and radiation acoustic impedance, Z_r^a, at its output terminals.

impedance of the transducer is Z_r^a. The equivalent source has the source strength of V_i and an internal electrical impedance of Z_i^e. The input pair of voltage-current into the transducer are (V, I) and the output pair of force-velocity are (F_r, v_r).

The transmitting transducer is characterized by its transfer matrix T^T which is written as

$$[T^T] = \begin{bmatrix} T_{11}^T & T_{12}^T \\ T_{21}^T & T_{22}^T \end{bmatrix} \tag{6.4.20}$$

and the corresponding matrix equation is written as (see Eq. (3.5.5))

$$\begin{Bmatrix} V \\ I \end{Bmatrix} = \begin{bmatrix} T_{11}^T & T_{12}^T \\ T_{21}^T & T_{22}^T \end{bmatrix} \begin{Bmatrix} F_r \\ v_r \end{Bmatrix}. \tag{6.4.21}$$

The boundary condition on the left side of the transducer shown in Figure 6.9 is expressed as

$$V_i = V + IZ_i^e \tag{6.4.22}$$

and the boundary condition on the right side of the transducer is written as

$$F_r = v_r Z_r^a. \tag{6.4.23}$$

Similar to the definition of the receiving sensitivity, the source strength V_i is taken here as the input quantity. Note that this is not the input voltage V directly driving the transducer. The source strength V_i is equal to the input voltage V only if the equivalent electrical impedance is equal to zero. The output quantities are the force and velocity (F_r, v_r).

The generalized transmitting force sensitivity of a transmitting transducer is defined as the ratio of the transmitting force into radiation acoustic medium to the source strength of the pulser that drives the transducer. It has the unit of N/V and is denoted by S_{FV_i}. Similarly, the generalized transmitting velocity sensitivity of a transmitting transducer can also be defined

as the ratio of the transmitting velocity into radiation acoustic medium to the source strength. It has the unit of (m/s)/V and is denoted by S_{vV_t}.

Following the similar procedure to our derivation of the transmitting transfer function for a general generation process, it is not difficult to derive the generalized transmitting sensitivities of a transducer. For example, the generalized transmitting force sensitivity is obtained as

$$S_{FV_t} = \frac{F_r(\omega)}{V_i(\omega)} = \frac{Z_r^a(\omega)}{\left(Z_r^a(\omega)T_{11}^T + T_{12}^T\right) + \left(T_{21}^T Z_r^a(\omega) + T_{22}^T\right)Z_i^e(\omega)} \qquad (6.4.24)$$

and the generalized transmitting velocity sensitivity is

$$S_{vV_t} = \frac{v_r(\omega)}{V_i(\omega)} = \frac{1}{\left(Z_r^a(\omega)T_{11}^T + T_{12}^T\right) + \left(T_{21}^T Z_r^a(\omega) + T_{22}^T\right)Z_i^e(\omega)}. \qquad (6.4.25)$$

Certainly, following the discussion about the open-circuit and short-circuit receiving sensitivities, we can also discuss the sensitivities when $Z_r^a \to \infty$ and $Z_r^a \to 0$. However these conditions do not normally occur in NDE tests ($Z_r^a \to \infty$ corresponds to the case where the front surface of the transmitting transducer is clamped or does not move and $Z_r^a \to 0$ the case where its front surface is free). Therefore we will not describe explicitly those special cases.

The generalized transmitting force sensitivity can also be expressed as a function of its receiving voltage sensitivity. Let's consider S_{FV_t}. Suppose that the transducer receives acoustic waves from the acoustic medium with the acoustic impedance of Z_r^a. Its open-circuit , blocked-force sensitivity is, from Eq. (6.4.3),

$$M_{VF_B}^{\infty} = \frac{1}{T_{22}^T + Z_r^a T_{21}^T} \qquad (6.4.26)$$

and its short-circuit current , blocked-force sensitivity is, from Eq. (6.4.4),

$$M_{IF_B}^{0} = \frac{1}{Z_r^a T_{11}^T + T_{12}^T}. \qquad (6.4.27)$$

Replacing the transfer matrix elements in Eq. (6.4.24) with Eqs. (6.4.26) and (6.4.27) the transmitting voltage sensitivity becomes

$$S_{FV_t} = \frac{Z_r^a(\omega)}{\frac{1}{M_{IF_B}^0} + \frac{Z_i^e(\omega)}{M_{VF_B}^{\infty}}}. \qquad (6.4.28)$$

Using Eq. (6.4.7), Eq. (6.4.28) reduces to

$$S_{FV_t}(\omega) = \frac{Z_r^a(\omega)M_{VF_B}^{\infty}(\omega)}{\left(Z_{in}^{T:e}(\omega) + Z_i^e(\omega)\right)} \qquad (6.4.29)$$

where $Z_{in}^{T:e}$ is the input electrical impedance of the transmitter.

Equation (6.4.29) shows that the transmitting sensitivity of a transducer is related with its receiving sensitivity when the transducer works in the same acoustic medium as both transmitter and receiver. If the open-circuit receiving sensitivity of a transducer is known, its transmitting sensitivity can be obtained by using Eq. (6.4.29) provided that the input electrical impedance of the transmitter, the equivalent internal electrical impedance at the driving end of the transmitter, and the radiation acoustic impedance of the transmitter are known.

6.4.4 Reciprocal relations between receiving and transmitting quantities

A transducer can be used as a transmitting transducer or a receiving transducer. There are a number of relationships between the input and output quantities of the transducer during the generation process and reception process that we will discuss in this subsection.

In the generation process shown in Figure 6.9, we have

$$F_r = Z_r^a v_r \tag{6.4.30}$$

and

$$V_i = I\left(Z_{in}^e + Z_i^e\right) \tag{6.4.31}$$

where Z_{in}^e (=V/I) is the input electrical impedance of the transducer. Thus, the generalized transmitting voltage sensitivity is

$$S_{FV_i} = \frac{F_r}{V_i} = \frac{Z_r^a}{\left(Z_{in}^e + Z_i^e\right)} \frac{v_r}{I}. \tag{6.4.32}$$

In the reception process shown in Figure 6.7 with $Z_0^e = \infty$, the open-circuit voltage is V^∞ and the blocked-force is F_B. The open-circuit receiving voltage sensitivity is expressed as

$$M_{VF_B}^\infty = \frac{V^\infty}{F_B}. \tag{6.4.33}$$

Recall from Eq. (6.4.29) that

$$S_{FV_i} = \frac{Z_r^a}{\left(Z_{in}^e + Z_i^e\right)} \frac{V^\infty}{F_B}. \tag{6.4.34}$$

Equating Eqs. (6.4.32) and (6.4.34) gives

$$\frac{v_r}{I} = \frac{V^\infty}{F_B} \tag{6.4.35}$$

which is a reciprocal relationship between input – output quantities during the generation and reception processes.

On the other hand, Eq. (6.4.31) can be written as using $Z_{in}^e = V / I$

$$V_i = V\left(Z_{in}^e + Z_i^e\right) / Z_{in}^e. \tag{6.4.36}$$

Then the generalized transmitting voltage sensitivity can be expressed instead in the form

$$S_{FV_i} = \frac{F_r}{V_i} = \frac{Z_r^a Z_{in}^e}{\left(Z_{in}^e + Z_i^e\right)} \frac{v_r}{V}. \tag{6.4.37}$$

In the reception process shown in Figure 6.7 with $Z_0^e = 0$, the short-circuit current is I_s and the blocked force is F_B. The short-circuit receiving current sensitivity is expressed as

$$M_{IF_B}^0 = \frac{I_s}{F_B}. \tag{6.4.38}$$

Then using Eq. (6.4.7), Eq. (6.4.29) is rewritten as

$$S_{FV_i} = \frac{Z_r^a Z_{in}^e M_{IF_B}^0}{\left(Z_{in}^e + Z_i^e\right)} = \frac{Z_r^a Z_{in}^e}{\left(Z_{in}^e + Z_i^e\right)} \frac{I_s}{F_B}. \tag{6.4.39}$$

Equating Eqs. (6.3.39) and (6.4.37) gives another input-output relationship, namely

$$\frac{v_r}{V} = \frac{I_s}{F_B}. \tag{6.4.40}$$

Furthermore, from Eqs. (6.4.40) and (6.4.35), we have the additional relationships

$$F_B v_r = V^\infty I = V I_s. \tag{6.4.41}$$

6.5 Relations between Sensitivities

The definitions of various sensitivities were listed in section 6.1. Because these sensitivities share the same transfer matrix which specifies an ultrasonic transducer, they have to be related with each other. In this section we will summarize those relationships.

We will take the open-circuit voltage, blocked-force receiving sensitivity, $M_{VF_B}^\infty$, as the reference sensitivity and express all other sensitivities in terms of it. Some of these relations have already been derived (for example, Eq. (6.4.29), which was just derived, was one of them)). From the definitions of the sensitivities, it is straightforward to derive similar expressions relating them to $M_{VF_B}^\infty$. We find:

$$M_{VF_B} = \frac{Z_o^e M_{VF_B}^\infty}{Z_o^e + Z_{in}^e} \tag{6.5.1}$$

$$M_{IF_B} = \frac{M_{VF_B}^\infty}{Z_o^e + Z_{in}^e} \tag{6.5.2}$$

$$M_{V_r} = \frac{Z_r^a + Z_{in}^a}{Z_o^e + Z_{in}^e} Z_o^e M_{VF_B}^\infty \tag{6.5.3}$$

$$M_{Iv} = \frac{Z_r^a + Z_{in}^a}{Z_o^e + Z_{in}^e} M_{VF_B}^{\infty} \tag{6.5.4}$$

$$S_{FV_i} = \frac{Z_r^a M_{VF_B}^{\infty}}{Z_{in}^e + Z_i^e} \tag{6.5.5}$$

$$S_{FI} = Z_r^a M_{VF_B}^{\infty} \tag{6.5.6}$$

$$S_{vV_i} = \frac{M_{VF_B}^{\infty}}{Z_{in}^e + Z_i^e} \tag{6.5.7}$$

$$S_{vI} = M_{VF_B}^{\infty}. \tag{6.5.8}$$

In these equations, five impedances are involved. They are

Z_o^e, the electrical impedance as a load for a receiving transducer

Z_i^e, the equivalent electrical impedance at the driving end of a transmitter

Z_{in}^e, the input electrical impedance of a transducer acting as a transmitter

Z_r^a, the radiation acoustic impedance of the transducer

Z_{in}^a, the input acoustic impedance of a transducer when it acts a receiver.

6.6 Sensitivities, System Functions, and System Efficiency Factors

We have expressed the voltage output, $V_R(\omega)$, of the entire ultrasonic measurement system in terms of three transfer functions, t_G, t_R and t_A, and the Thevenin equivalent input pulser voltage, $V_i(\omega)$, as

$$V_R(\omega) = t_G(\omega) t_R(\omega) t_A(\omega) V_i(\omega). \tag{6.6.1}$$

We could combine all the electrical and electromechanical terms in Eq. (6.6.1) into one "system" function, $s(\omega) = t_G(\omega) t_R(\omega) V_i(\omega)$, and write the output voltage as

$$V_R(\omega) = s(\omega) t_A(\omega) \tag{6.6.2}$$

which has the advantage of separating out the electromechanical and acoustic elements of the entire system. In terms of transducer sensitivities, from Eqs. (6.2.14) and (6.2.15) we have

$$s(\omega) = \frac{Z_r^{T:a}(\omega) M_{VF_B}^{T:\infty}}{\left(Z_{in}^{T:e} T_{11}^e + T_{12}^e\right) + \left(Z_{in}^{T:e} T_{21}^e + T_{22}^e\right) Z_i^e(\omega)} \frac{Z_o^e K M_{VF_B}^{R:\infty}}{\left(Z_{in}^{R:e} R_{11}^e + R_{12}^e\right) + \left(Z_{in}^{R:e} R_{21}^e + R_{22}^e\right) Z_o^e} V_i(\omega). \tag{6.6.3}$$

In a pulse-echo setup, where the sending and receiving transducers are the same and the same cabling is shared on the transmission and reception processes, Eq. (6.6.3) becomes

$$s(\omega) = \frac{Z_r^{T:a}(\omega) M_{VF_B}^{T:\infty}}{\left(Z_{in}^{T:e} T_{11}^e + T_{12}^e\right) + \left(Z_{in}^{T:e} T_{21}^e + T_{22}^e\right) Z_i^e(\omega)} \frac{Z_o^e K M_{VF_B}^{T:\infty}}{\left(Z_{in}^{T:e} T_{11}^e + R_{12}^e\right) + \left(Z_{in}^{T:e} T_{21}^e + T_{22}^e\right) Z_o^e} V_i(\omega). \tag{6.6.4}$$

Although this pulse-echo system response is proportional to the square of the transducer sensitivity, it is not proportional to the square of the other terms appearing in the denominator, as some authors assume, unless we have $Z_0^e = Z_i^e$. This system function is similar to the system "efficiency" factor [Schmerr,1998]. There, the system response for an immersion setup was written in the form

$$V_R(\omega) = \beta_r^p(\omega)\beta_t^p(\omega)F^p(\omega)V_i(\omega) \tag{6.6.5}$$

where we have placed a "p" superscript on the quantities described above to emphasize that they involve pressure and not force, as we will see. For example, the receiving "efficiency" factor, β_r^p, has the dimensions of voltage divided by pressure and is defined as

$$\beta_r^p(\omega) = \frac{V_R(\omega)}{p_{ave}(\omega)} \tag{6.6.6}$$

where $V_R(\omega)$ is the output voltage and p_{ave} is the average incident pressure at the location of the receiving transducer in its absence. If we recall that the receiving transfer function, t_R, was defined in terms of V_R and the blocked voltage, F_B, by $t_R = V_R / F_B$, and use the high frequency relation for a piston transducer $F_B = 2F_{inc} = 2p_{ave}S_R$, where S_R is the area of the receiving transducer, then from Eq. (6.6.6) it follows that

$$\beta_r^p(\omega) = 2S_R t_R(\omega). \tag{6.6.7}$$

Similarly, the transmitting "efficiency", β_t^p, was defined as

$$\beta_t^p(\omega) = \frac{\rho c v_T(\omega)}{V_i(\omega)} \tag{6.6.8}$$

where ρ and c are density and wave speed of the fluid, and $v_T(\omega)$ is the average velocity on the face of the transmitting transducer. This "efficiency" factor, we see, has the dimensions of pressure divided by voltage. If we again recall that the transfer function, t_G, was defined as $t_G = F_t / V_i$ and use the high frequency result for a piston transducer, namely $F_t = \rho c S_T v_T(\omega)$, we see that

$$\beta_t^p(\omega) = \frac{t_G(\omega)}{S_T} \tag{6.6.9}$$

where S_T is the area of the transmitting transducer. Finally, the acoustic term in Eq. (6.6.5), F^p, was defined as the dimensionless pressure ratio

$$F^p(\omega) = \frac{p_{ave}(\omega)}{\rho c v_T(\omega)}. \tag{6.6.10}$$

In contrast, our acoustic transfer function, t_A, was given as $t_A = F_B / F_t$ so we have

$$F^p(\omega) = \frac{S_T}{2S_R} t_A(\omega). \tag{6.6.11}$$

Thus, in terms of a total system "efficiency" factor, $\beta^p(\omega) = \beta_r^p(\omega)\beta_t^p(\omega)V_i(\omega)$, we have

$$V_R(\omega) = \beta^p(\omega)F^p(\omega) \tag{6.6.12}$$

and, consequently

$$\begin{aligned} s(\omega) &= \frac{S_T}{2S_R}\beta_r^p(\omega)\beta_t^p(\omega)V_i(\omega) \\ &= \frac{S_T}{2S_R}\beta^p(\omega) \end{aligned} \tag{6.6.13}$$

CHAPTER 7. ELECTROACOUSTIC MEASUREMENT MODEL

In the previous chapters we have developed models of every element in an ultrasonic measurement system. These models can be combined to produce what we call an electroacoustic measurement (EAM) model. We have implemented the EAM model in software using the commercial package MATLAB. This software was developed to (1) provide an environment where the effects of various parameters on a measured signal could be studied in a quantitative manner and (2) to allow the user to examine the behavior of the components of the system in the frequency domain (and, in some cases, in the time domain as well).

This chapter describes the MATLAB EAM model in detail. Section 7.1 outlines the components of the EAM model as they are implemented in MATLAB and gives a breakdown of all the components in block-diagram form. Section 7.2 describes the underlying input parameters needed for each of those components. Section 7.3 outlines the graphical user interface of the MATLAB code and the manner in which input and output parameters are selected. Finally, Section 7.4 lists some of the current limitations of the EAM modeling software.

7.1 The Elements of the Electroacoustic Measurement Model

The MATLAB implementation of the EAM model is broken into components that differ somewhat from the components as they were described in the previous chapters. Therefore, we will outline those differences here. Figure 7.1 illustrates the components of the overall EAM model as implemented in MATLAB. The generation process is characterized by a transfer function, $\beta_t(\omega)$, while the acoustic and scattering processes are modeled by an acoustic "configuration factor", $F(\omega)$. The reception process is characterized by a transfer function, $\beta_r(\omega)$, and both the generation and reception processes are combined with the input voltage, $V_i(\omega)$, in terms of an overall system "efficiency" factor, $\beta(\omega)$. The electrical output voltage, $V_0(\omega)$, is therefore given as

$$V_0(\omega) = \beta(\omega)F(\omega) \tag{7.1.1}$$

where the "efficiency" factor is expressed as

$$\beta(\omega) = \beta_t(\omega)\beta_r(\omega)V_i(\omega). \tag{7.1.2}$$

In terms of our previous components, we see that β_t plays the same role as the generation transfer function, t_G, and β_r plays the same role as the reception transfer function, t_R, while the configuration factor, F, is analogous to the acoustic transfer function, t_A. The overall system "efficiency" factor, β, is similar to overall system function, s, defined previously (see Eq. 6.6.2). The explicit relationships between all these parameters is as follows:

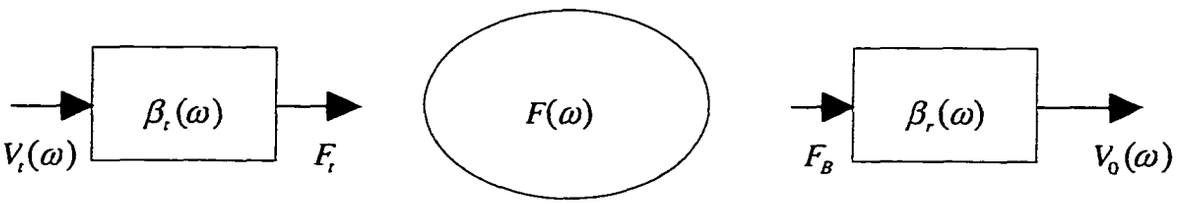

Figure 7.1 An electroacoustic measurement model split into the generation process characterized by $\beta_t(\omega)$, the reception process by $\beta_r(\omega)$ and the acoustic field by $F(\omega)$.

The generation process transfer function is defined as the ratio of the total force generated at transducer face to the Thevenin equivalent source voltage of the pulser, i.e.

$$\beta_t(\omega)=\frac{F_t(\omega)}{V_t(\omega)} \tag{7.1.3}$$

The reception process transfer function is defined as the ratio of the receiver output voltage to the total force, F_{inc}, present in the waves incident on the receiving transducer in the absence of that transducer, i.e.

$$\beta_r(\omega)=\frac{V_0(\omega)}{F_{inc}(\omega)}. \tag{7.1.4}$$

Finally, the configuration factor is given as the ratio of the incident force in Eq. (7.1.4) to the output force in Eq. (7.1.3) so we have

$$F(\omega)=\frac{F_{inc}(\omega)}{F_t(\omega)}. \tag{7.1.5}$$

Comparing Eq. (7.1.3) with our previous definition of the generation transfer function (Eq. (3.5.15)) we see they are identical so that

$$\beta_t(\omega)=t_G(\omega). \tag{7.1.6}$$

In comparing Eq. (7.1.4) with our previous definition of the receiving transfer function (Eq. (4.4.18)), if we make the 1-D assumption that the blocked force is just equal to twice the force in the incident waves, i.e. $F_B = 2F_{inc}$, then

$$\beta_r(\omega) = 2t_R(\omega). \tag{7.1.7}$$

Similarly, since the acoustic transfer function, $t_A(\omega)$, was also given in terms of the blocked force (see Eq. (5.1.20)), from Eq. (7.1.5) the configuration factor is

$$F(\omega) = \frac{t_A(\omega)}{2}. \tag{7.1.8}$$

Finally, comparing the overall system "efficiency" factor of Eq. (7.1.2) with the system transfer function, $s(\omega)$, of Eq. (6.6.2), we find

$$\beta(\omega) = 2\, s(\omega). \tag{7.1.9}$$

Figure 7.2 gives an overall block diagram description of the EAM model as implemented in MATLAB in terms of the parameters just discussed. As Figure 7.2 shows, the EAM model can either give the output "voltage", $V_0(\omega)$, or the corresponding time domain voltage, $V_0(t)$, since these are simply related through the Fourier transform and its inverse, i.e.

$$V_0(\omega) = \int_{-\infty}^{+\infty} V_0(t)\exp(i\omega t)dt \tag{7.1.10}$$

and

$$V_0(t) = \frac{1}{2\pi}\int_{-\infty}^{+\infty} V_0(\omega)\exp(-i\omega t)d\omega. \tag{7.1.11}$$

7.1.1 Generation process transfer function

The generation process transfer function used here is defined in Eq. (7.1.3). From Eq. (7.1.6), this is identical to the transfer function defined in Chapter 3 (Eq. (3.1.5) given

$$\beta_t(\omega) = \frac{Z_r^a(\omega)}{\left(Z_r^a(\omega)T_{11}^G + T_{12}^G\right) + \left(T_{21}^G Z_r^a(\omega) + T_{22}^G\right)Z_i^e(\omega)} \tag{7.1.12}$$

where T_{11}^G, T_{12}^G, T_{21}^G and T_{22}^G are the four elements of the global generation transfer matrix $\left[T^G\right]$.

The global generation transfer matrix $\left[T^G\right]$ lumps all the two-port networks between the source and the acoustic medium in the generation process (see Figure 3.14). In our MATLAB EAM model, there are three two-port networks which are (1) the two-port network for cabling,

$$\left[T^C\right] = \begin{bmatrix} T_{11}^C & T_{12}^C \\ T_{21}^C & T_{22}^C \end{bmatrix} \tag{7.1.13}$$

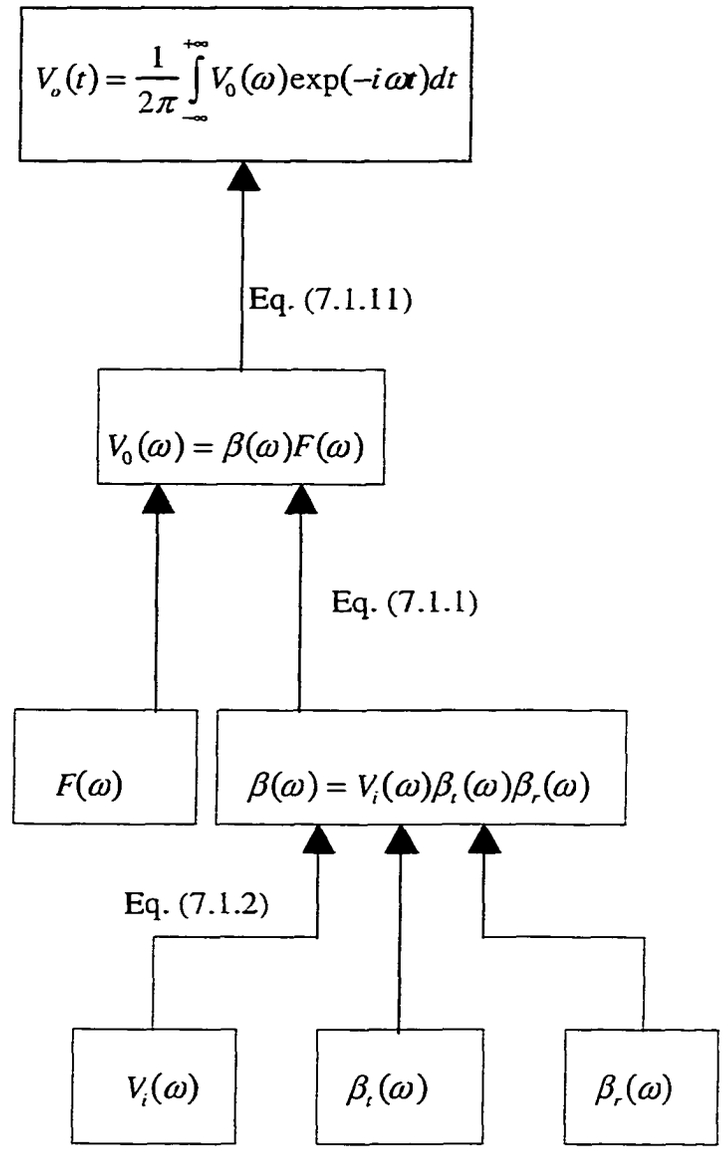

Figure 7.2 The block diagram for the electroacoustic measurement model where $V_i(\omega)$ is the source strength, $\beta_t(\omega)$ the transfer function for transmission, $\beta_r(\omega)$ the transfer function for reception, $F(\omega)$ the configuration factor, $\beta(\omega)$ the system efficiency factor, $V_o(\omega)$ the output voltage in frequency domain and $V_o(t)$ the output wave form.

(2) the two-port network for signal conditioning

$$[T^S]=\begin{bmatrix} T_{11}^S & T_{12}^S \\ T_{21}^S & T_{22}^S \end{bmatrix} \tag{7.1.14}$$

and (3) the two-port network for the transmitting transducer

$$[T^T]=\begin{bmatrix} T_{11}^T & T_{12}^T \\ T_{21}^T & T_{22}^T \end{bmatrix}. \tag{7.1.15}$$

Then the global transfer matrix $[T^G]$ is expressed as

$$[T^G]=[T^C][T^S][T^T]=\begin{bmatrix} T_{11}^G & T_{12}^G \\ T_{21}^G & T_{22}^G \end{bmatrix}. \tag{7.1.16}$$

The block diagram for the evaluation of the generation process transfer function is shown in Figure 7.3. Note that the radiation impedance of the transducer is taken to be just the 1-D plane wave impedance of the acoustic medium multiplied by the area of the transmitting transducer.

7.1.2 Reception process transfer function

The reception process transfer function defined in Eq. (7.1.4) is related to our previous definition of this transfer function in Chapter 4 through Eq. (7.1.7). From Eq. (4.4.18), therefore, we have

$$\beta_r(\omega)=\frac{2Z_o^e(\omega)K(\omega)}{\left(Z_i^a(\omega)R_{11}^G+R_{12}^G\right)+\left(R_{21}^G Z_i^a(\omega)+R_{22}^G\right)Z_o^e(\omega)} \tag{7.1.17}$$

where R_{11}^G, R_{12}^G, R_{21}^G and R_{22}^G are the four elements of the global receiving matrix $[R^G]$.

The global receiving matrix $[R^G]$ lumps all the two-port networks between the source and the acoustic medium in the reception process (see Figure 4.13). In the MATLAB EAM model, there are three two-port networks which are (1) the two-port network for cabling,

$$[R^C]=\begin{bmatrix} R_{11}^C & R_{12}^C \\ R_{21}^C & R_{22}^C \end{bmatrix} \tag{7.1.18}$$

(2) the two-port network for signal conditioning

$$[R^S]=\begin{bmatrix} R_{11}^S & R_{12}^S \\ R_{21}^S & R_{22}^S \end{bmatrix} \tag{7.1.19}$$

and (3) the two-port network for the receiving transducer

$$[R^T]=\begin{bmatrix} R_{11}^T & R_{12}^T \\ R_{21}^T & R_{22}^T \end{bmatrix}. \tag{7.1.20}$$

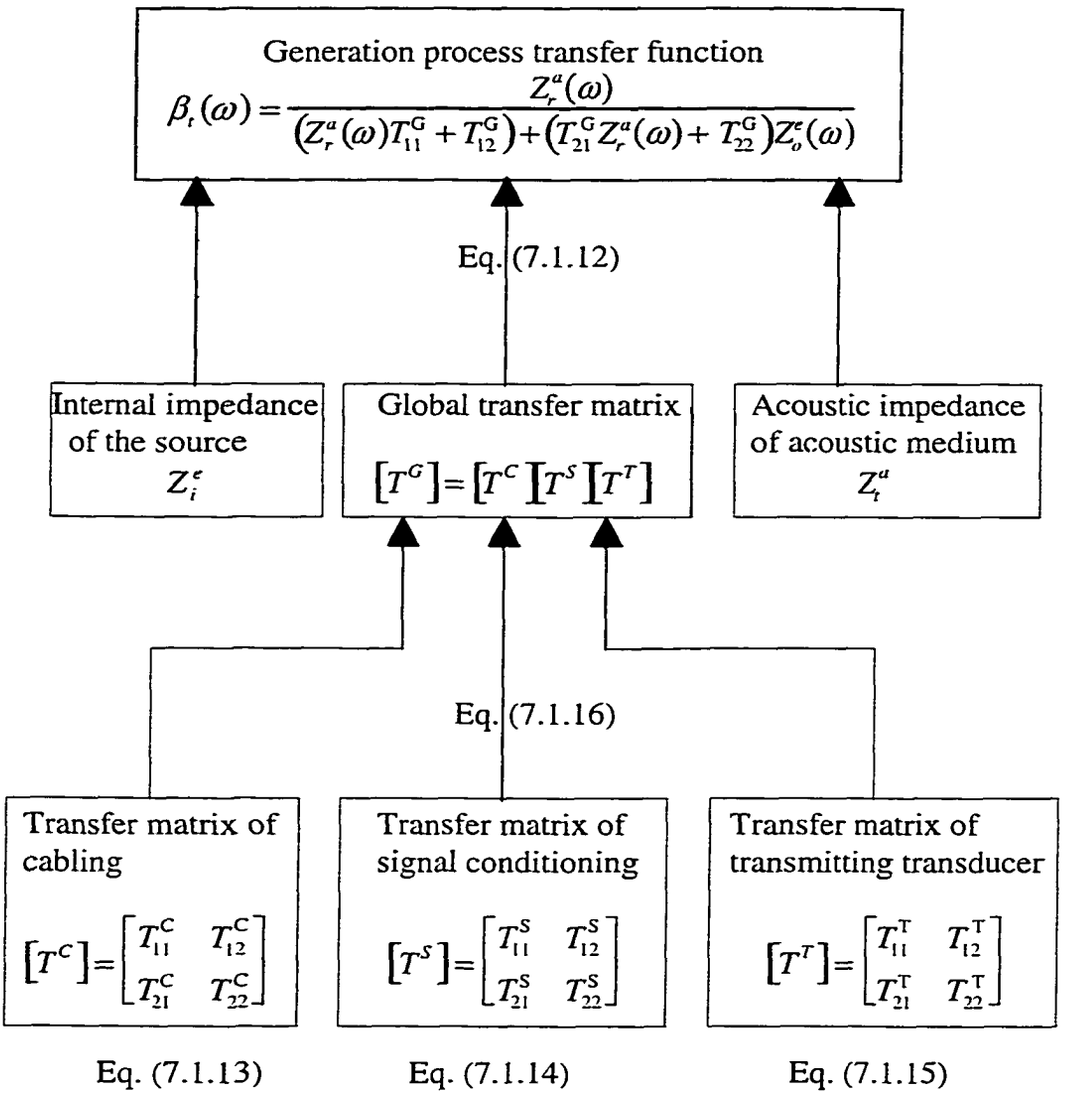

Figure 7.3 The block diagram for the transfer function $\beta_t(\omega)$ for transmission where Z_i^e is the internal electrical impedance of the source strength, Z_t^a the acoustic impedance of the acoustic medium, $[T^G]$ the global transfer matrix of the transmission process and $[T^C]$, $[T^S]$ and $[T^T]$ the transfer matrices for cabling, signal conditioning circuit and transmitting transducer.

Then the global transmitting matrix $[R^G]$ is expressed as

$$[R^G]=[R^C][R^S][R^T]=\begin{bmatrix} R_{11}^G & R_{12}^G \\ R_{21}^G & R_{22}^G \end{bmatrix}. \qquad (7.1.21)$$

For convenience, the elements of these matrices are taken to be those which form the transfer matrices during the generation process.

The block diagram for the evaluation of the reception process transfer function is shown in Figure 7.4. Since it is assumed in the MATLAB EAM model that the acoustic medium is the same at both the transmitter and receiver and that the area of the receiving transducer is the same as that of the transmitter, the radiation impedance on reception is taken in the same form as during generation.

7.1.3 Transducer

A transducer can be used to either receive acoustic waves or transmit acoustic waves. The receiving transducer and the transmitting transducer both have the same basic structure shown in Figure 7.5(a). This structure is composed of three parts: a piezoelectric plate, a wear plate and backing [Papadakis, 1971, Martin and Sigelmann, 1975, Sigelmann, 1977, Lewis, 1980]. In the EAM model, the wear plate can consist of 0-5 layered acoustic plates. The backing can also consist of 0-5 layered acoustic plates terminated with one half-infinite acoustic medium. The block diagram of an entire transducer structure is shown in Figure 7.5(b).

If the transfer matrix of the multi-layered wear plate is

$$[T^W]=\begin{bmatrix} T_{11}^W & T_{12}^W \\ T_{21}^W & T_{22}^W \end{bmatrix} \qquad (7.1.22)$$

and the transfer matrix of the backed piezoelectric plate is

$$[T^P]=\begin{bmatrix} T_{11}^P & T_{12}^P \\ T_{21}^P & T_{22}^P \end{bmatrix} \qquad (7.1.23)$$

then the transfer matrix of the transducer is

$$[T^T]=[T^P][T^W]=\begin{bmatrix} T_{11}^T & T_{12}^T \\ T_{21}^T & T_{22}^T \end{bmatrix}. \qquad (7.1.24)$$

Note that the properties of the backing, however, are implicitly contained in $[T^P]$ and appear explicitly in that transfer matrix in terms of the backing acoustic impedance, Z_b (see Figure 7.5(b)). If the transducer is a receiving transducer, the transfer matrix $[T^T]$ in the above equation should be replaced by $[R^T]$.

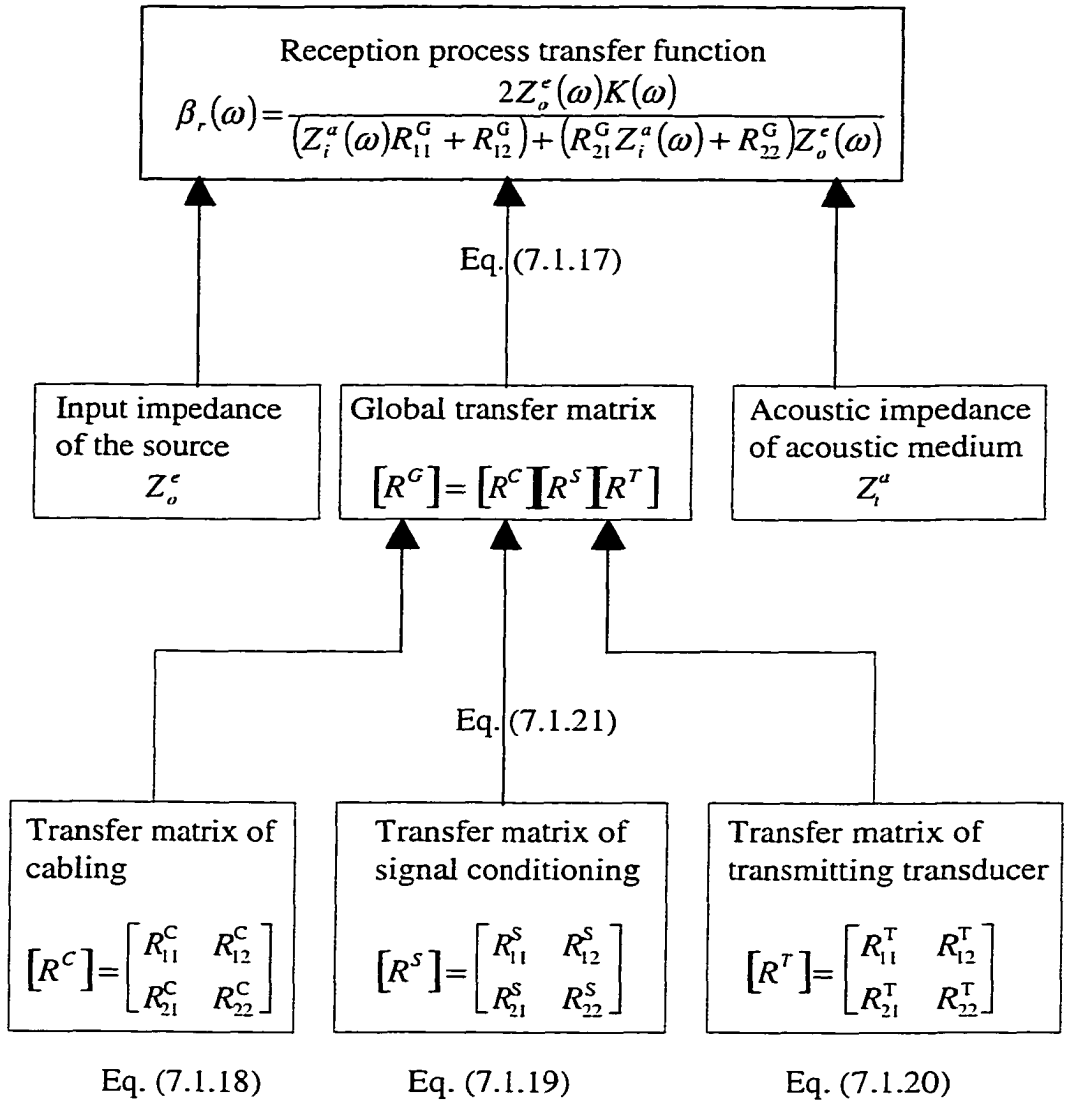

Figure 7.4 The block diagram for the transfer function $\beta_r(\omega)$ for reception where Z_o^e is the input electrical impedance of the receiver, Z_i^a the acoustic impedance of the acoustic medium, $[R^G]$ the global transfer matrix of the reception process and $[R^C]$, $[R^S]$ and $[R^T]$ the transfer matrices for cabling, signal conditioning circuit and receiving transducer.

7.2 Input Parameters

Because of the complexity of the EAM model, there are many input parameters needed to define the entire ultrasonic system. In this section we will describe all of the input parameters.

7.2.1 The pulser

In the MATLAB EAM model the pulser is modeled by a Thevenin equivalent circuit with an internal electrical impedance Z_i^e and a source strength of $V_i(\omega)$ (see Figure 3.2). The source voltage has the shape shown in Figure 3.3, which is defined by a time constant, t_0, and two slopes, α_1 and α_2. The equation of the voltage strength is shown in Eq. (3.1.3). All of the input parameters needed to model the pulser are therefore:

V_0, the amplitude of the source strength with the unit of V
α_1, attenuation factor 1 with the unit of 1/s
α_2, attenuation factor 2 with the unit of 1/s
t_0, time of the first part with the unit of s
Z_i^e, pulser internal electrical impedance with the unit of Ω

7.2.2 The receiver

The receiver is modeled by an input electrical impedance, Z_o^e, and an amplification factor, $K(\omega)$, as show in Figure 4.12. In the MATLAB EAM model, the amplification factor $K(\omega) = 1$, so that only the impedance is needed. Thus there is only one input parameter for the receiver,

Z_o^e, the input electrical impedance with the unit of Ω

7.2.3 The cabling

The cabling is modeled by a transmission line (see Figure 3.5). The transfer matrix of the cabling is written as

$$[T^C] = \begin{bmatrix} \cos kl & -iZ_c^e \sin kl \\ -i\sin kl / Z_c^e & \cos kl \end{bmatrix} \tag{7.2.1}$$

with the intrinsic impedance of the cable

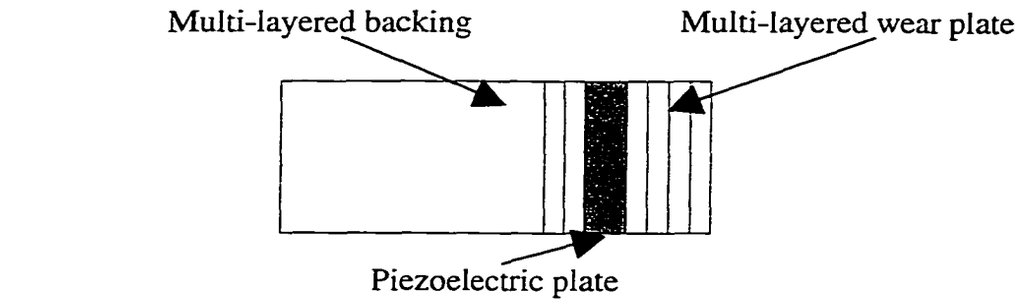

(a)

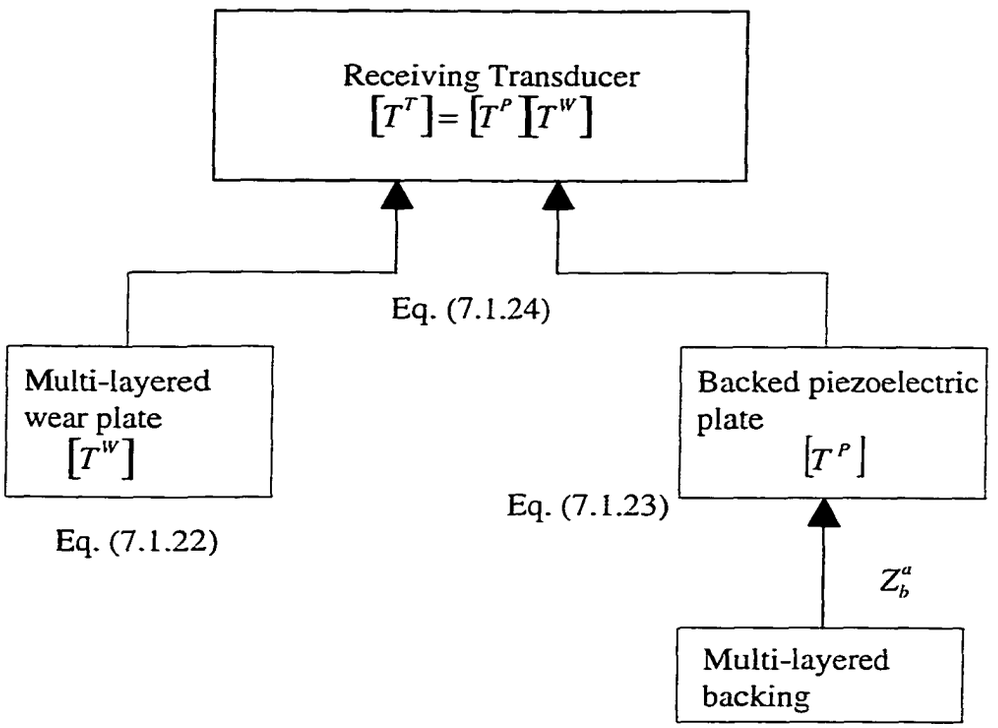

(b)

Figure 7.5 Transducer. (a) The structure of the transducer and (b) The block diagram for the transfer matrix of the transducer. $[T^T]$ is the transfer matrix of the transducer, $[T^W]$ the transfer matrix of the wear plate and $[T^P]$ the transfer matrix of the backed piezoelectric plate.

$$Z_c^e = \sqrt{\frac{\mu_r \mu_0}{\varepsilon_r \varepsilon_0}} \tag{7.2.2}$$

where $\mu_0 = 4\pi \times 10^{-7}$ H/m and $\varepsilon_0 = 8.85 \times 10^{-12}$ F/m. The input parameters of a cable are listed in the following:

ε_r, the relative permittivity
μ_r, the relative permeability
l, the length of the cabling with the unit of m

For these inputs, the intrinsic impedance of the cable can be derived using Eq. (7.2.2). The velocity of electromagnetic wave in the cable can also be obtained since

$$v_0 = \sqrt{\frac{1}{\mu_r \mu_0 \varepsilon_r \varepsilon_0}}. \tag{7.2.3}$$

The wavenumber in Eq. (7.2.1) is

$$k = 2\pi f / v_0 \tag{7.2.4}$$

where f is the frequency. This parameter is known once the frequency is specified (which is done elsewhere in the model).

7.2.4 The acoustic layers

In our electroacoustic measurement model, acoustic layers are used in making the backing and wear plates. One acoustic layer is considered as an acoustic transmission line. Its transfer matrix is written as (see Eq. (2.5.3))

$$[T^a] = \begin{bmatrix} \cos kl & -iZ_0^a \sin kl \\ -i\sin kl / Z_0^a & \cos kl \end{bmatrix}. \tag{7.2.5}$$

The wear plate is formed by multiple acoustic layers. Using the matrix multiplication of transfer matrices as shown in Eq. (2.2.23), the overall transfer matrix of the wear plate is formed, where each layer transfer matrix takes the form of Eq. (7.2.5).

Similarly, the transfer matrix of each layer in a multiple layered backing takes the form of Eq. (7.2.5) and can be multiplied together to form an overall matrix, $[T^B]$. When the semi-infinite backing layer is added, the overall effect is equivalent to an acoustic impedance

$$Z_b^a = \frac{Z_L^a T_{11}^B + T_{12}^B}{Z_L^a T_{21}^B + T_{22}^B} \tag{7.2.6}$$

where Z_L^a is the acoustic impedance of the semi-infinite backing layer.

The input parameters for each acoustic layer are

ρ, the density of the layer with the unit of kg/m^3
c, the velocity of the acoustic layer with the unit of m/s
l, the thickness of the acoustic layer with the unit of m
S, the cross section area of the acoustic layer with the unit of m^2

Note that the area, S, is the same for all layers and equal to the area of the transducer.

The acoustic impedance of the semi-infinite backing layer is

$$Z_L^a = \rho_L c_L S. \tag{7.2.7}$$

So its input parameters are

ρ_L, the density with the unit of kg/m^3
c_L, the velocity with the unit of m/s
S, the cross section area with the unit of m^2

7.2.5 The signal conditioning circuits

Signal conditioning circuits are often used for tuning transducers. The basic structure of the signal conditioning circuit contained in the MATLAB EAM model is shown in Figure 7.6.

The transfer matrix equation for this circuit is

$$\begin{Bmatrix} V_1 \\ I_1 \end{Bmatrix} = \begin{bmatrix} 1 & Z_2 \\ 1/Z_3 & 1+Z_2/Z_3 \end{bmatrix} \begin{Bmatrix} V_2 \\ I_2 \end{Bmatrix} \tag{7.2.8}$$

where

$$Z_2 = -i\omega L_s + R_s \tag{7.2.9}$$

$$Z_3 = \frac{-i\omega L_p}{1-\omega^2 L_p C_p}. \tag{7.2.10}$$

The MATLAB EAM model allows for three basic types of matching networks:

Type 1: $L_p = \infty$ and $C_p = 0$ (i.e., without L_p and C_p)

This leads to

$$Z_3 \to \infty \tag{7.2.11}$$

and the corresponding transfer matrix is

$$[T^S] = \begin{bmatrix} 1 & Z_2 \\ 0 & 1 \end{bmatrix}. \tag{7.2.12}$$

Type 2: In this case all the elements shown in Figure 7.6 are present.

The transfer matrix takes the form

$$[T^S]=\begin{bmatrix}1 & Z_2\\ 1/Z_3 & 1+Z_2/Z_3\end{bmatrix}. \tag{7.2.13}$$

Type 3: $L_p=\infty$ (i.e., without L_P)

This leads to

$$Z_3=\frac{i}{\omega C_p} \tag{7.2.14}$$

where again the corresponding matrix takes the form of Eq. (7.2.13).

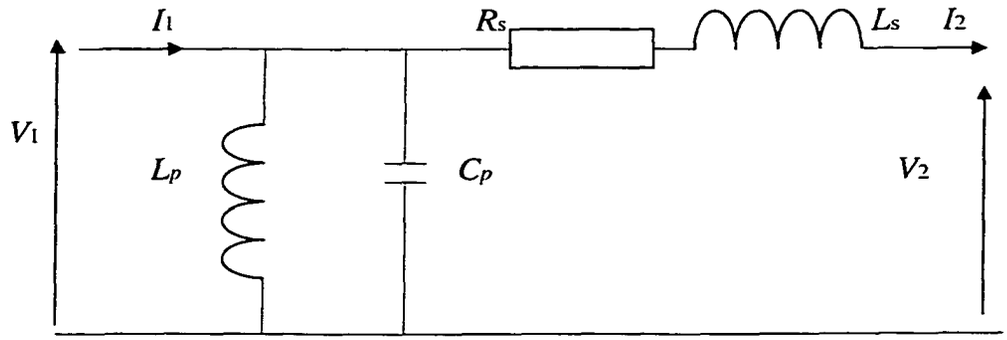

Figure 7.6 Signal conditioning circuit which has another two types by taking out L_P or L_P and C_P.

The input parameters of the signal conditioning circuit are therefore

R_S, the resistance in series with the unit of Ω
L_S, the inductance in series with the unit of H
L_P, the inductance in parallel with the unit of H (if it is not infinite)
C_P, the capacitance in Parallel with the unit of F (if it is not zero)

7.2.6 The piezoelectric plate

One face of a piezoelectric plate is backed by a backing material whose equivalent impedance Z_b^a is obtained from Eq. (7.2.6) and the other face radiates acoustic waves into the acoustic field or receives the waves from the acoustic field. The transfer matrix of the backed piezoelectric plate is written as, from Eq. (2.4.16),

$$[T^P]=\frac{1}{Z_b^a-iZ_0^a\tan\frac{kl}{2}}\begin{bmatrix}\frac{1}{n} & \frac{n}{i\omega C_0}\\ \frac{i\omega C_0}{in} & 0\end{bmatrix}\begin{bmatrix}Z_b^a+iZ_0^a\cot kl & \left(Z_0^a\right)^2+iZ_0^aZ_b^a\cot kl\\ 1 & Z_b^a-i2Z_0^a\tan\frac{kl}{2}\end{bmatrix} \tag{7.2.15}$$

where Z_0^a is the acoustic impedance of the piezoelectric plate and l its thickness.

The basic input parameters of the piezoelectric plate are:

ρ, the density of the plate with the units of kg/m^3
c^E, the stiffness with constant electric field intensity E with the units of Pa
ε_r^S, the relative dielectric constant with constant strain S
e, the piezoelectric stress constant with the units of C/m^2
l, the thickness of the plate with the units of m
S, the surface of the plate with the units of m^2

The derived quantities from the above parameters are:

C_0, the clamped capacitance, with the units of F, given by

$$C_0 = \varepsilon_r^s \varepsilon_0 S / l. \tag{7.2.16}$$

n, the turns ratio of the electromechanical transformer, with the units of N/V, given by

$$n = \frac{eS}{l}. \tag{7.2.17}$$

v_0, the velocity of acoustic waves inside of the plate, with the units of m/s, given by

$$v_0 = \sqrt{\frac{c^E + e^2/\varepsilon_r^S \varepsilon_0}{\rho}}. \tag{7.2.18}$$

Z_0^a, the acoustic impedance of the plate, with the units of N/(m/s), given by

$$Z_0^a = \rho v_0 S. \tag{7.2.19}$$

7.2.7 The configuration factor

The configuration factor is dependent on the acoustic field between the transmitting and receiving transducers. Thus it depends on the particular inspection problem and transducers being modeled. In the MATLAB EAM model, we have used the configuration factor for the case where a circular piston transducer radiates into a fluid waves that are received by an equal area piston transducer where the axes of the two transducers are aligned. This is a common calibration setup and the one where, in the paraxial approximation, the configuration factor can be given in explicit form as (see Eq. (6.3.19))

$$F = \left[1 - \exp\left(ika^2 / D\right)\left\{J_0\left(ka^2 / D\right) - iJ_1\left(ka^2 / D\right)\right\}\right]\exp(ikD) \tag{7.2.20}$$

where D is the distance between the two transducers, a the transducer radius, and k the wave number of the acoustic field.

The input parameters needed to compute the configuration factor are:

ρ, the density of water path with the unit of kg/m^3
c, the wave velocity of water path with the unit of m/s
D, the distance between two transducers with the unit of m
a, the radius of the two transducers with the unit of m

The derived quantities from the above parameters are:

S, the surface area of transducers with the unit of m^2, given by

$$S = \pi a^2. \tag{7.2.21}$$

Z_t^a and Z_i^a the acoustic impedances of water path in front of the transmitting and receiving transducer with the unit of N/(m/s), which are given by

$$Z_t^a = Z_i^a = \rho c S. \tag{7.2.22}$$

and are also the values used for calculating the transmitting and receiving radiation impedances.

7.2.8 Other quantities

In our EAM model, we need to give all the transfer matrices as functions of frequencies, for a discrete set of frequencies. Thus the frequency range and number of sampling points need to be set before modeling. These input parameters used for this specification are:

$f_{\min}$, the minimum frequency with the unit of Hz
$f_{\max}$, the maximum frequency with the unit of Hz
N, the number of frequency points

From the above parameters, we can then derive:

Δf , the frequency interval between discrete frequencies, in units of Hz, given by

$$\Delta f = \frac{f_{\max} - f_{\min}}{N}. \tag{7.2.23}$$

$T_{\max}$, the total time duration of corresponding time interval, in units of seconds, given by

$$T_{\max} = \frac{1}{\Delta f}. \tag{7.2.24}$$

7.3 EAM Model Implementation

7.3.1 General description

An EAM model is a model of an ultrasonic measurement system that explicitly incorporates all the elements of the measurement process, including the electrical and electomechanical components. The components of this model were implemented in the commercial software package, MATLAB. A MATLAB-based graphical user interface (GUI) was also developed to allow a user to specify transducer properties, electrical conditions at the sending and receiving transducers, etc., and to calculate and display quantities such as the 2x2 transducer transfer matrix (as a function of frequency), the system efficiency factor (also as a function of frequency), and the received time domain waveform.

The software was developed on an SGI workstation and written purely in the MATLAB 5.0 language. MATLAB was used because it combines powerful computation capabilities as well as convenient GUI-building tools. The modeling program's name is EAM.

When EAM runs, it loads the most recently stored data as the default parameters which describe the basic components for the EAM model. Based on these parameters, the transfer matrices of two-port networks for transducers, cabling, signal conditioning circuits and etc. are computed. The global transmitting and receiving matrices, the transfer functions for transmission and reception, overall efficiency factor, waveform and etc. are also computed. The user can then use the GUI to

a. Change parameters for any basic components in the EAM model

b. Save these parameters into a data file

c. Load another data file which contains a set of parameters used for an EAM model

d. Display curves for quantities of source, transmission process, reception process, configuration, output spectrum, transmitting force in the frequency domain, and transmitting force and output waveform in the time domain

e. Zoom, rotate and shift the curves.

The graphical user interface for the EAM model is shown in Figure 7.7. The basic five parts of that interface are shown in Figure 7.8. They are the Menu bar, the Parameter window, the Parameter buttons, the Result window and the Result buttons. These five parts are described in the following.

7.3.2 The Menu bar

The menu bar is on the top of the GUI of Figure 7.7 and is shown separately in Figure 7.9. There are five pull-down submenus which are: P/R, Transmission, Reception, Configuration, and Display. The first four are used to set the input parameters for the basic components of the EAM model and the last one is used to display modeling results. Note that in addition to these EAM menus, the three standard MATLAB pull-down submenus are also available as shown in Figure 7.7.

When one item in a pull-down menu is chosen, the parameters listed under this item are shown in the Parameter window. A user can change these parameters accordingly.

a. The P/R submenu

The P/R submenu is a pull-down menu which contains the items setting the input parameters for the pulser and receiver. These items are the Exponential source, $V_i(\omega)$, the Pulser internal impedance, Z_i^e, and the Receiver impedance, Z_o^e, and are shown in Figure 7.10. When one item is clicked, the parameters listed under it are shown in a Parameter window.

b. The Transmission submenu

The transmission submenu (Figure 7.11) is a pull-down menu which contains the items for setting the input parameters for the transmission process. This submenu shows labels for each of the three two-port networks that form the global transfer matrix for transmission. They are: Cabling, SigCond (standing for signal conditioning circuit), and Transducer. There are three types of signal conditioning circuits definable, as has been discussed in 7.2.5. The transducer specification is divided into three parts: one for the Crystal (the piezoelectric plate), one for the Backing and one for the Front (wear plate). The Backing can have up to five layers. The default backing is Layer 1 which is a semi-infinite material. Similarly Front allows the specification of 0-5 layers. The default is no wear plate, i.e., the number of layers for Front is zero. In defining these multi-layered media, a user must first choose the Number of layers which is the first item on the submenu (Figure 7.11). If, for example, the Number of layers is set to 2, then the labels for Layer 1 and Layer 2 are darkened and the others are grayed. A user can then only set parameters for the darkened layers.

c. The Reception submenu

The Reception submenu is also a pull-down menu which contains the items for setting the input parameters for the reception process (Figure 7.12). This submenu shows labels for the three two-port networks which form the global transfer matrix for reception. They are:

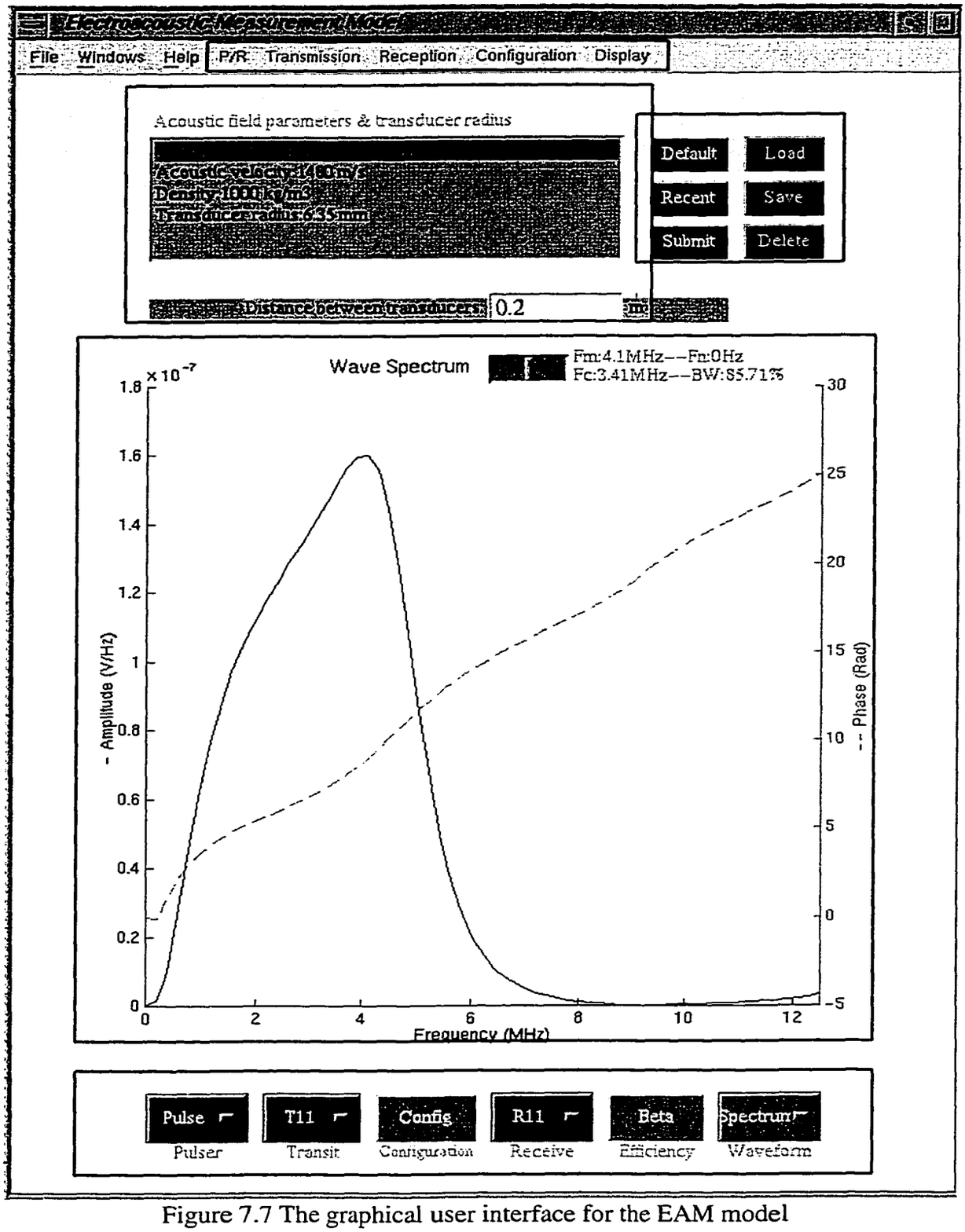

Figure 7.7 The graphical user interface for the EAM model which is divided into five parts which are shown the five block boxes.

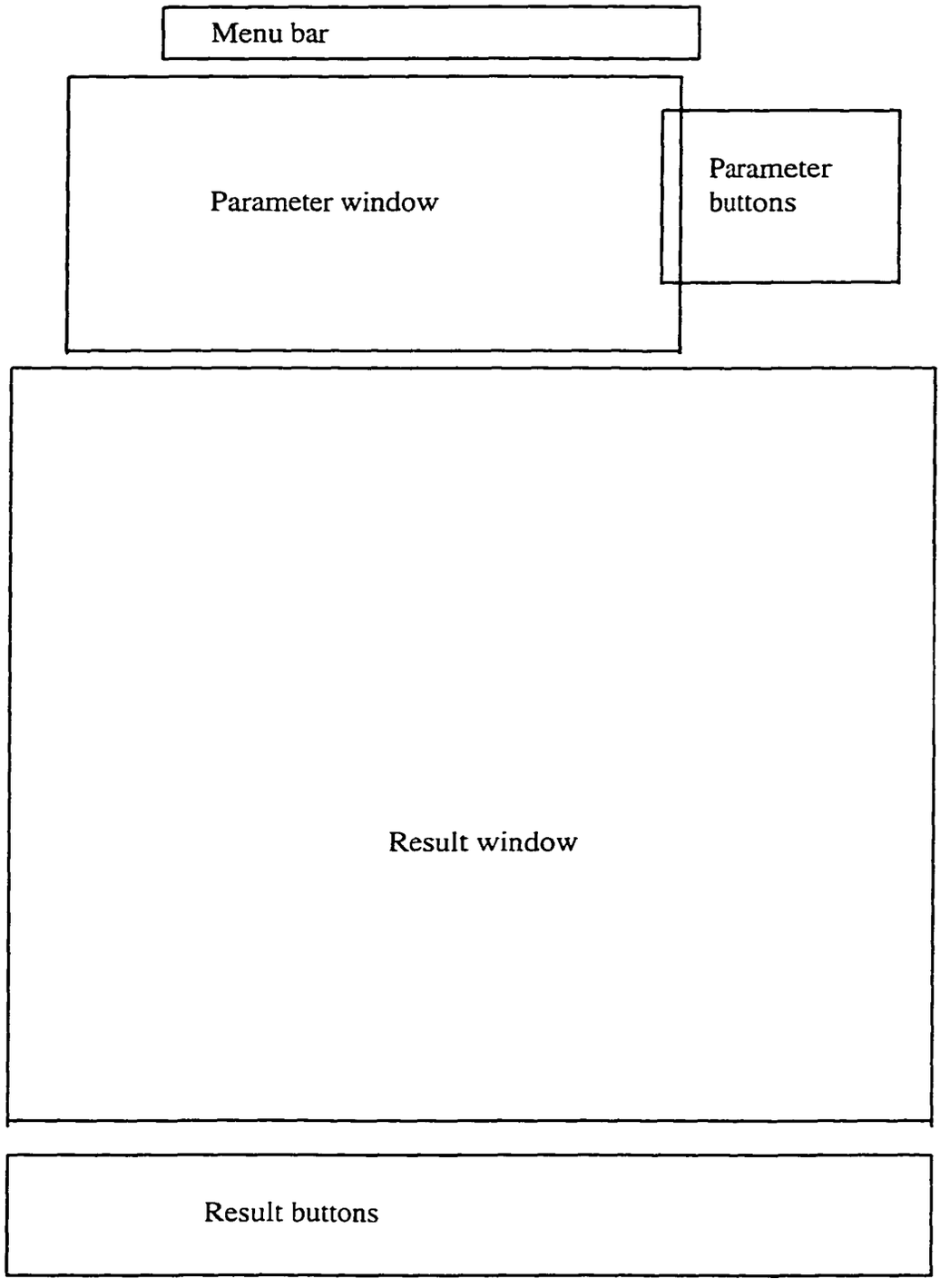

Figure 7.8 The graphical user interface for EAM model is divided into five parts: are Menu bar, Parameter window, Parameter buttons, Result window and Result buttons

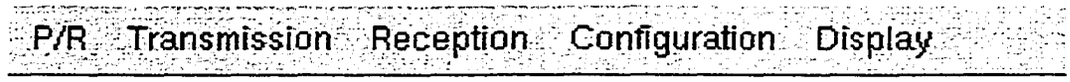

Figure 7.9 Menu bar contains five pulldown submenus: P/R for pulser/receiver, Transmission for transmission process, Reception for reception process, Configuration for acoustic field.

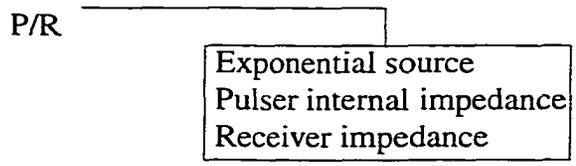

Figure 7.10 P/R submenu contains three items: Exponential source, Pulser internal impedance and Receiver impedance.

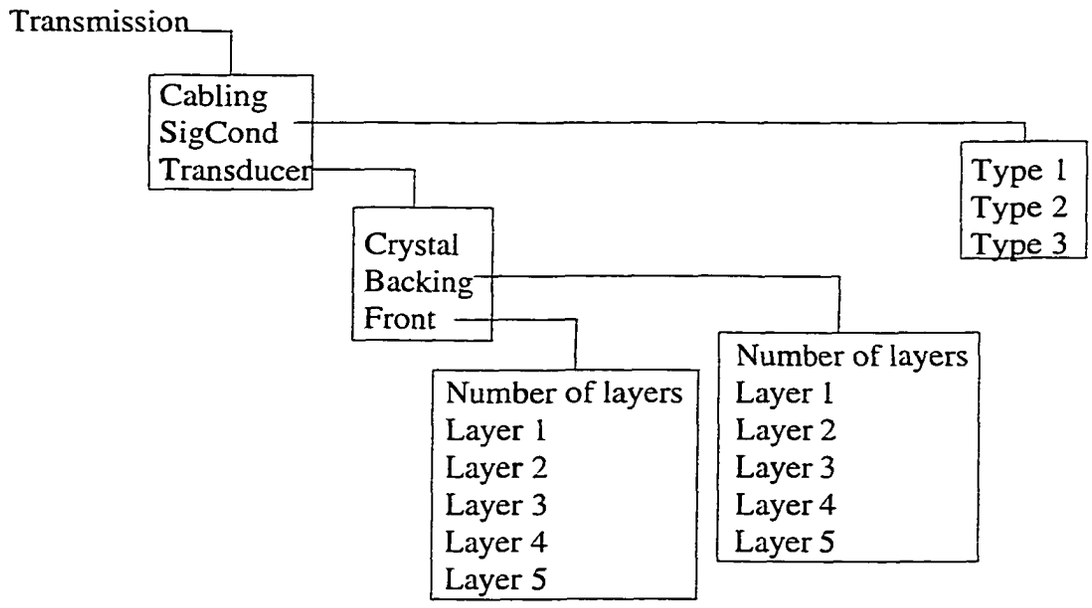

Figure 7.11 Cascading structure of the Transmission submenu.

Cabling, SigCond (standing for signal conditioning circuit), and Transducer. All of these items are the same as those in the Transmission submenu so that we do not need to go into further detail in describing them.

Our EAM model can be used to deal with a pulse-echo mode setup. Although we

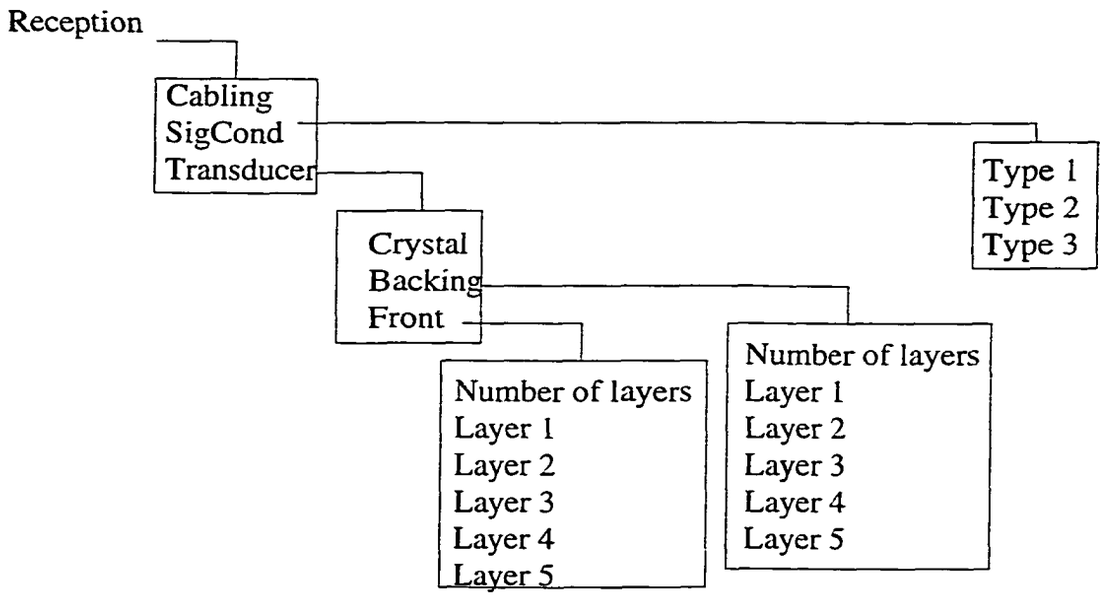

Figure 7.12 Cascading structure of the Reception submenu.

consider explicitly a pitch-catch measurement setup in our modeling if we set all the parameters for every component in the reception process equal to those used in transmission process, we are then modeling the pulse-echo response for the configuration factor where an ideal reflector (e.g. a rigid planar surface) is located at a distance D/2 from a single transducer (which acts as both sender and receiver).

d. The Configuration submenu

The Configuration submenu is a pull-down menu which contains the items that set the input parameters for the configuration factor and other parameters. These parameters are described in subsections 7.2.7 and 7.2.8. The structure of the Configuration submenu is depicted in Figure 7.13.

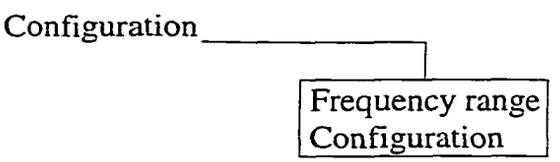

Figure 7.13 Structure of the Configuration submenu.

e. The Display submenu

The Display submenu is a pull-down menu which contains the list of output items that can be computed and displayed. These outputs are shown in the Result window either in the time domain or the frequency domain. The cascading structure of the Display submenu is shown in Figure 7.14.

There are six choices listed in the display submenu: Transmission, Reception, Source, Eff-Factor (efficiency factor), Conf-Factor (configuration factor) and Waveform. Most of the results listed in this submenu also can be selected by the Result buttons (see Figure 7.7) which will be discussed later.

Transmission includes the four elements of the global transmitting matrix $[T]$, T_{11}, T_{12}, T_{21} and T_{22}, BetaT, the transfer function for transmission, $\beta_t(\omega)$, SigCond, the signal conditioning circuit, Pressure(T), the transmitting pressure in the time domain and Pressure(F), the transmitting pressure in the frequency domain.

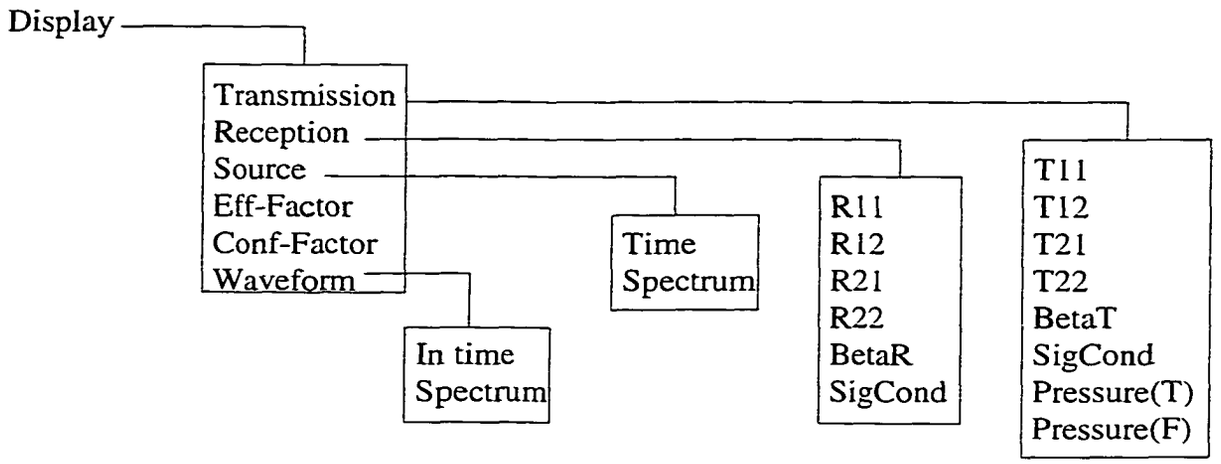

Figure 7.14 Structure of the Display submenu which displays the figures of results.

In a similar fashion, the Reception submenu includes choices for the four elements of the global transmitting matrix $[R]$, R_{11}, R_{12}, R_{21} and R_{22}, BetaR, the transfer function for reception, $\beta_r(\omega)$, and SigCond, the signal conditioning circuit.

The submenu Source allows one to display the curves of driving pulse in time domain (Time) and frequency domain (Spectrum).

The submenu Conf-Factor presents the configuration factor of the acoustic field between two planar transducers in the frequency domain.

Finally, the submenu Waveform gives two choices: the curves of the output signal in time domain (In time) and the output spectrum (Spectrum).

7.3.3 The Parameter window

The parameter window is under the Menu bar described in the above subsection (Figure 7.7). Two examples of the Parameter window are shown in Figure 7.15. As we will see, the Parameter window works in conjunction with the Parameter buttons.

The Parameter window is a list box which shows two types of information: parameters and data files. When an item under the Menu bar is pressed, the Parameter window shows all the corresponding parameters with their descriptions and units (see Figure 7.15(a)). When a file manipulation button (Load, Save or Delete, which will be described in detail later) is pressed, the names of source data files containing all predefined parameters are listed in the Parameter window (see Figure 7.15(b)).

At the top of the parameter window is the general description of the items listed in the window (Figure 7.15(a)). At the bottom of the window is a modifiable line. When the Parameter window shows parameters and if one line is clicked, this line is chosen and is repeated in the modifiable line. Within the modifiable line, one can change the value of one parameter (Figure 7.15(a)). When the Parameter window shows data files, if one file name is clicked, it similarly is shown in the modifiable line (Figure 7.15(b)). In the EAM program, a data file name has three parts: a prefix of "data", a suffix of ".dat", and a middle part between them that is modifiable by the user.

Note that data1.dat and data2.dat are two default data files which are not modifiable by users although they can be chosen. However, they can be modified by operating system commands outside the program.

By default, the first item in the Parameter window is always chosen unless one clicks on another item in the window.

7.3.4 The Parameter buttons

The Parameter buttons are on the right side of the Parameter window. There are six buttons grouped into two columns. Each column has three buttons. The buttons on the left column are used to manipulate parameters and those on the right column to manipulate data files containing parameters. The Parameter buttons are shown in Figure 7.16 and are described in the following in detail.

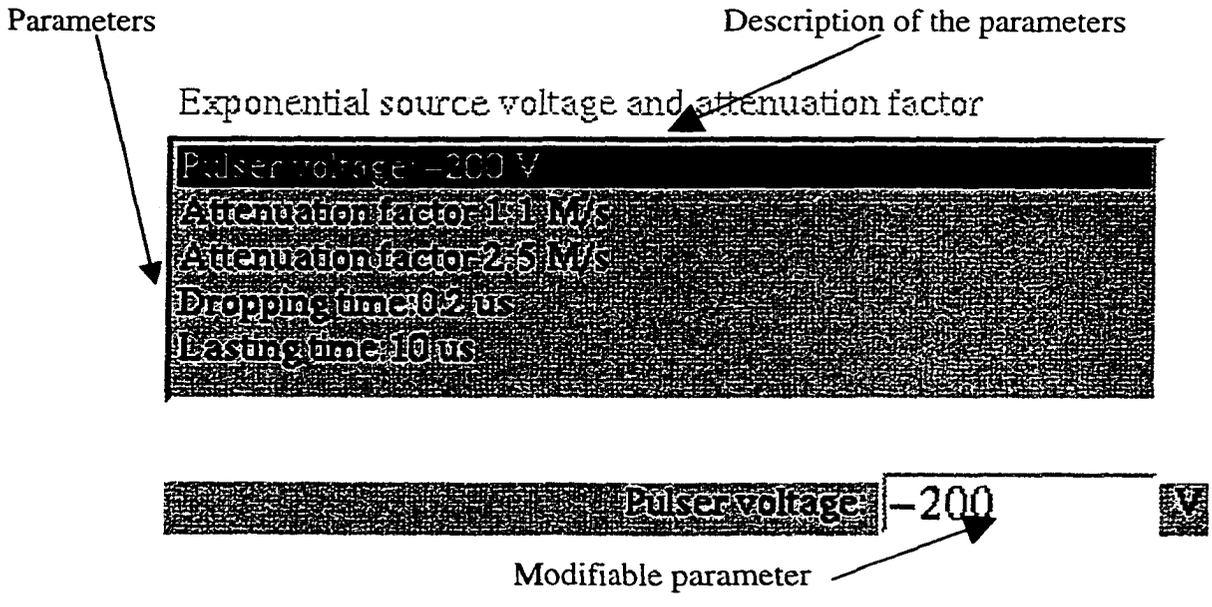

(a)

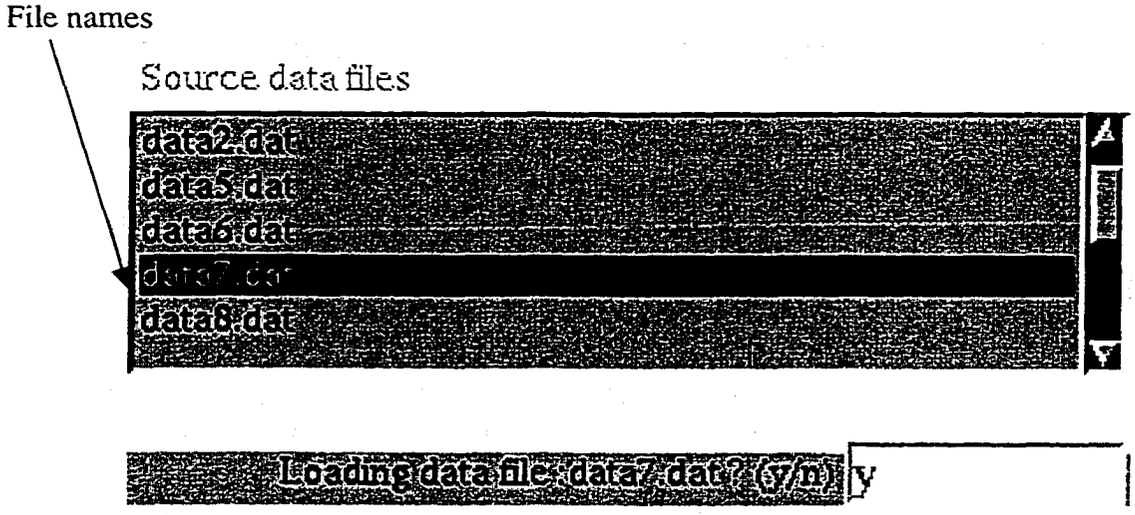

(b)

Figure 7.15 Parameter window shows (a) parameters when one item in Menu bar is chosen or (b) data file names when Load, Save or Delete button is pressed. On the top of the widow is the general description of the parameters or data files. At the bottom of the window is a modifiable line used to modify one parameter or take user's response.

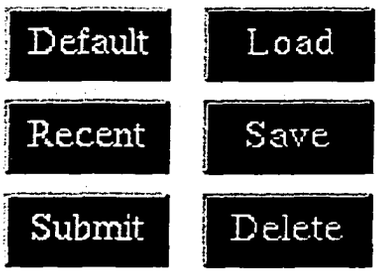

Figure 7.16 Parameter buttons divided into two columns. The left column contains three buttons used to manipulate parameters and the right column contains three buttons used to manipulate data files.

a. The Default button

Whenever this button is pressed, the default data file, data1.dat is loaded into memory, together with the result data files calculated from data1.dat. In fact, when the EAM model starts, data1.dat is automatically loaded as a default case. One could modify parameters based on data1.dat to define a new set of input parameters.

b. The Recent button

When the EAM model runs, the most recently modified parameters together with any unchanged values are stored in data2.dat. Whenever the Recent button is pressed, data2.dat is loaded into memory, together with the corresponding result data computed from data2.dat. Therefore, data2.dat and its result data files always keep track of the most recently calculated model.

c. The Submit button

When one has finished modifying parameters, pressing the Submit button computes the results and stores the current predefined parameters into data2.dat and the calculated results into result data files.

d. The Load button

The Load button lists all the stored data file names into the Parameter window. The first data file is chosen as default. If one wants to choose anther data file, click the file name in the Parameter window. The file name is blackened. Shown in the modifiable line is a question asking whether the chosen data file is to be loaded in the modifiable line (see Figure

7.15(b)). If so, put the cursor on the modifiable line by clicking it and then presses return. The program loads the chosen data file, stores its parameters into data2.dat, computes the results and saves them into result data files. Then one could show curves by pressing Result buttons.

e. The Save button

The Save button lists all the data file names already existing in the disk and asks for a new data file name in which one can save the current parameters. The new file name is specified on the modifiable line. It has a prefix of "data" and a suffix of ".dat". The user-defined middle part is taken from the modifiable line and should be numbers, letters or "_". However, the default files, data1.dat and data2.dat can not be overwritten so one should not try to save parameters into either data1.dat or data2.dat.

f. The Delete button

The Delete button lists all the existing files in the Parameter window and asks whether one wants to delete a data file on the modifiable line. First, one chooses a data file from the Parameter window by blackening it. Second, one clicks on the editable part of the modifiable line to make sure deletion and then presses return. The two data files, data1.dat and data2.dat, can not be removed because they are default data files.

7.3.5 The Result window

The Result window is the largest window on the interface. It mainly shows the curves calculated from the model parameters. An example Result window is shown in Figure 7.17. This window can show curves in both the time and the frequency domains. When a curve in the time domain is displayed, the x-axis denotes the time in microseconds and the y- axis its amplitude. When a curve in the frequency domain is displayed, the x-axis denotes the frequency in MHz, the left y-axis its amplitude (a curve drawn in a black solid line) and the right y-axis its phase (a curve drawn in a red dashed line). Besides showing results, it could also show the signal conditioning circuits when SigCond item in Display submenu is chosen. Figure 7.18 illustrates the third type of tuning circuit. The following description is appropriate for the Result window showing curves (Figure 7.17).

On the top of the Result window, there are the title of the Result window, a slider and a small window. The small window shows the parameters calculated from the curves in the Result window. When a curve is in the time domain, the maximum and minimum amplitudes of the curve presented (Max and Min) are displayed in this small window together

with their occurring times. From these values one could calculate, for example, the peak-peak value of the displayed waveform. When a curve is in the frequency domain, the small window shows the frequency with maximum amplitude (Fm), the frequency with minimum amplitude (Fn), the center frequency (Fc) and the bandwidth (BW) computed from the

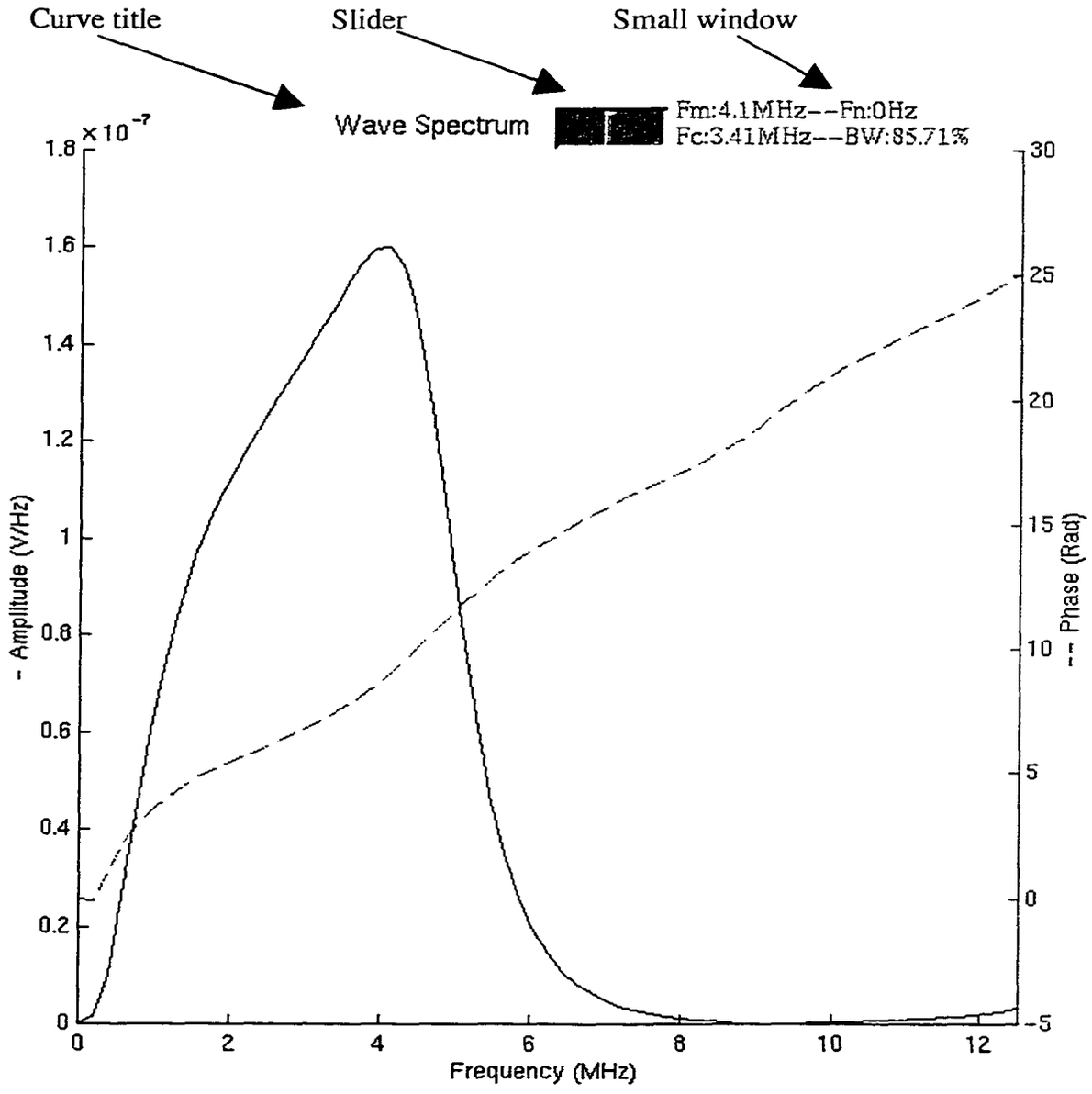

Figure 7.17 Result window shows curves in the time and frequency domains or figures of signal condition circuits.

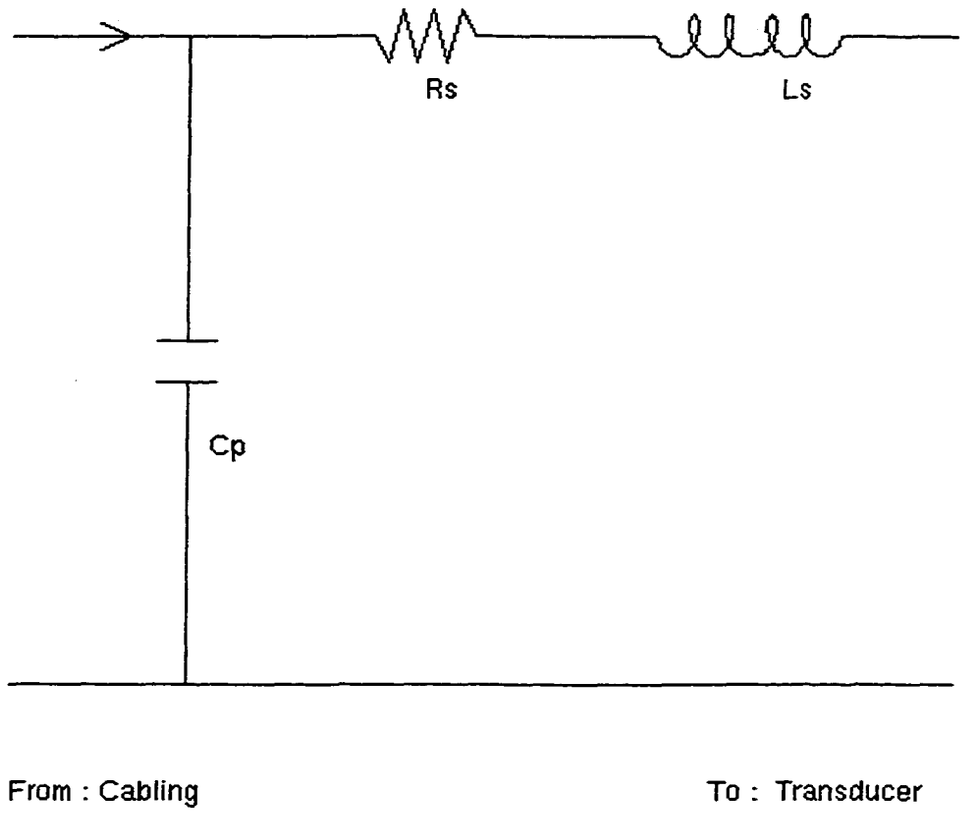

Figure 7.18 Result window shows the third type of signal conditioning circuit.

frequencies at the half-power points. If either of the half-power points is out of the current figure window, Fc and BW are not computed and the words of "Fc: & BW: Not Available" are shown.

The slider is used to rotate or move the curve in the Result window to the left or right. The middle bar corresponds to the middle of the current curve and always returns to the middle after an action is finished. If the middle bar is dragged to the Left, this moves the curve to the left. Similarly, if the middle bar is dragged to the right, this moves the curve to the right. Furthermore, a click on the left trough of the slider moves the curve 10% to the left, and a click on the right trough moves the curve 10% to the right.

The slider is used to perform a "circular shift" of curves in the time domain, i.e., when a part of the curve is shifted out of the window, it is appended to the other side of the window. However, for curves in frequency domain, the slider is just used to shift the curve to the left or right.

In the Result window, the left mouse button can be used to zoom the curve shown. One first moves the mouse cursor into the Result window. Clicking the left button of the mouse on the white area in the window then enlarges the current curve by a factor of 2 from the left margin. This feature allows one to "zoom-in" on a curve to see more detail. Clicking the left button of the mouse on the black curve displayed in the window reduces that current curve by a factor of 2 to the left margin. This feature gives a "zoom-out" capability to see a larger picture. If the current curve can not be doubled or halved, the zoom features generated by these buttons do not work. Note that combining the slider and mouse button down functions allows complex rotation, shifting and zooming of curves.

7.3.6 The Result buttons

The Result buttons are displayed under the Result window (Figure 7.7). They are shown separately in Figure 7.19. These buttons are divided into two groups: two pushdown buttons, titled Configuration and Efficiency, and four menu buttons, titled Pulser, Transit, Receive, and Waveform. The structure of the menu buttons are also shown in Figure 7.19. When an item is chosen with these buttons, the corresponding result curve is shown in the Result window. Note that the functions defined on these buttons are duplicated by some items under the Display submenu.

The six Result buttons are described as follows:

a. Pulser is a menu button containing two items: Pulse and Spectrum. The Pulse item selects the input impulse from the pulser to the transmitting transducer for display. The Spectrum item selects the spectrum of input impulse for display instead.

b. Transit is a menu button containing five items: T11, T12, T21, T22 which are the four components of the global transmitting transfer matrix, and BetaT which is the generation transfer function, $\beta_t(\omega)$.

c. Configuration is a pushdown button which displays the configuration factor of the acoustic field. Currently it only takes the form shown in Eq. (7.2.20).

d. Receive is a menu button including five items: R11, R12, R21, R22 which are the four components of the global receiving transfer matrix, and BetaR which is the receiving transfer function, $\beta_r(\omega)$.

e. Efficiency is a pushdown button which gives the overall "efficiency" factor for the entire transit-receive system (see Eq. (7.1.2)).

f. Waveform is a menu button containing two items: Wave which displays the received waveform at the receiver and Spectrum which shows the spectrum of the receiving waveform.

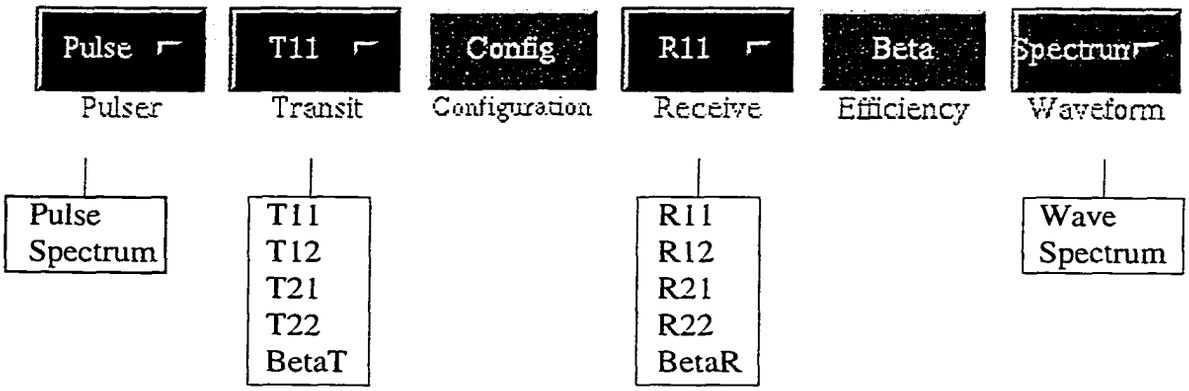

Figure 7.19 Result buttons which are two pushdown buttons (Configuration and Efficiency) and four menu buttons.

7.4 Model Limitations

The EAM model as implemented in MATLAB provides the basis for conducting a wide range of parametric studies. Nevertheless, the model does have a number of limitations. These include:

a. the configuration factor is currently implemented only for the simple two piston transducer calibration setup described in Chapter 5.

b. the attenuation of the fluid in this calibration setup is not currently modeled.

c. the backing and facing acoustic layers are limited to a maximum of five each, and attenuation in these layers is also not modeled.

d. only three types of tuning circuits are available in the model.

e. the cables are modeled as ideal transmission lines whose losses are neglected.

f. electrical and acoustic sources of noise are neglected.

g. pulser and receiver impedances are modeled only as purely resistive elements.

h. the acoustic radiation impedances of both transducers are taken as frequency independent values appropriate for modeling piston transducers at high frequencies.

If the EAM program were to be turned into a commercial transducer modeling software package, many of these limitations would have to be removed. However, as a research and demonstration tool, even with these limitations, the MATLAB-based EAM model is both powerful and versatile.

CHAPTER 8. APPLICATIONS OF EAM MODEL

The complete electroacoustic measurement (EAM) model was described in the last chapter and the MATLAB software implementation of that model discussed. The EAM model allows a user to change essentially any parameter in an ultrasonic measurement system and quantitatively estimate the effects of that change. In this chapter we will use the MATLAB code to conduct a number of numerical studies for the configuration shown in Figure 8.1 where two axially collinear transducers are placed in a simple pitch-catch setup. In section 8.1 we will describe the "differentiation effects" that occur for such a setup due to beam diffraction effects and/or changes in the impedance at the receiver and use the MATLAB EAM code to model those effects. In section 8.2 we will use the EAM model to quantitatively evaluate the influence that a bonding layer between the transducer crystal and front wear plate has on the ultrasonic response. In section 8.3 we will examine the consistency of our EAM model simulations with some previous modeling studies of Papadakis [1983].

8.1 Diffraction-based and Impedance-based Differentiation Effects

It is well known [Schmerr, 1998] that if the face of a piston transducer radiating into a fluid is driven impulsively, in the far field the on-axis pressure response of the transducer is proportional to a derivative (in time) of the input impulse. This differentiation effect can also be observed in the voltage versus time output of the setup shown in Figure 8.1 when the distance, D, is changed from very small to very large values. Similarly, if the distance, D, is fixed but the receiving impedance, Z_o^e, is changed from very large to very small values, the changes of the output voltage time domain waveform appear similar to differentiation. Differentiation effects due to both distance and impedance changes can be easily observed experimentally and they can be explained with the aid of our EAM model as follows.

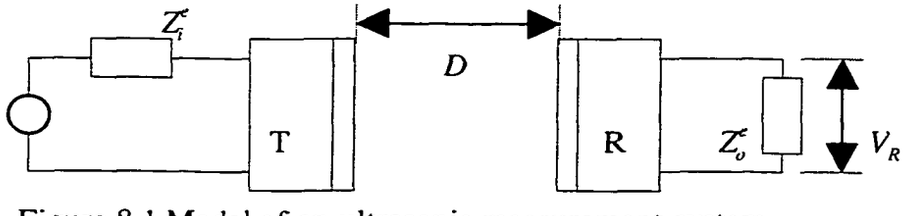

Figure 8.1 Model of an ultrasonic measurement system.

8.1.1 Differentiation due to diffraction

The configuration factor, F, for the setup of Figure 8.1 (which is one half the acoustic transfer function discussed earlier) can, at high frequencies, be obtained in the purely analytical form $F(\omega) = \exp(ikD)\tilde{F}(\omega)$ (see Eq. (7.2.20)) where

$$\tilde{F}(\omega) = \left[1 - \exp(ix)\{J_0(x) - iJ_1(x)\}\right] \tag{8.1.1}$$

and $x = ka^2 / D$. For a small transducer separation distance $(D << a)$ we have $x \to \infty$. However, for large x the Bessel functions have the asymptotic behavior

$$J_\nu(x) \approx \sqrt{\frac{2}{\pi x}} \cos\left(x - \frac{\nu\pi}{2} - \frac{\pi}{4}\right) \tag{8.1.2}$$

where $\nu = 0$ or 1, so that we obtain

$$\tilde{F}(\omega)\Big|_{D<<a} \cong 1. \tag{8.1.3}$$

On the other hand, for a large separation between transducers $(D >> a)$, $x \to 0$ and we have

$$\begin{aligned} J_0(x) &\cong 1 \\ J_1(x) &\cong x/2 \\ \exp(ix) &\cong 1 + ix \end{aligned} \tag{8.1.4}$$

which, when placed into Eq. (8.1.1), give

$$\tilde{F}(\omega)\Big|_{D>>a} = -ix/2. \tag{8.1.5}$$

Since the output voltage in Figure 8.1 is proportional to F, we see that (neglecting the phase term change due to $\exp(ikD)$ which only causes a time shift of the response in the time domain)

$$V_R(\omega)\Big|_{D>>a} = -i\omega \frac{a^2}{2Dc} V_R(\omega)\Big|_{D<<a} \tag{8.1.6}$$

where c is the wave speed in the medium separating the two transducers. Since multiplication by a factor $-i\omega$ in the frequency domain is equivalent to differentiation in the time domain, Eq. (8.1.6) shows that apart from a scaling factor (due to beam spread), beam diffraction effects indeed produce a differentiation effect as the distance D changes. Of course, the differentiation effect is only strictly true when going from very small to very large distances where Eq. (8.1.3) and Eq. (8.1.5) are valid. In Figure 8.2 we plot the magnitude of the configuration factor F in between these limits, showing the transition in behavior of that factor from a constant to a linearly increasing function of frequency which is characteristic of differentiation.

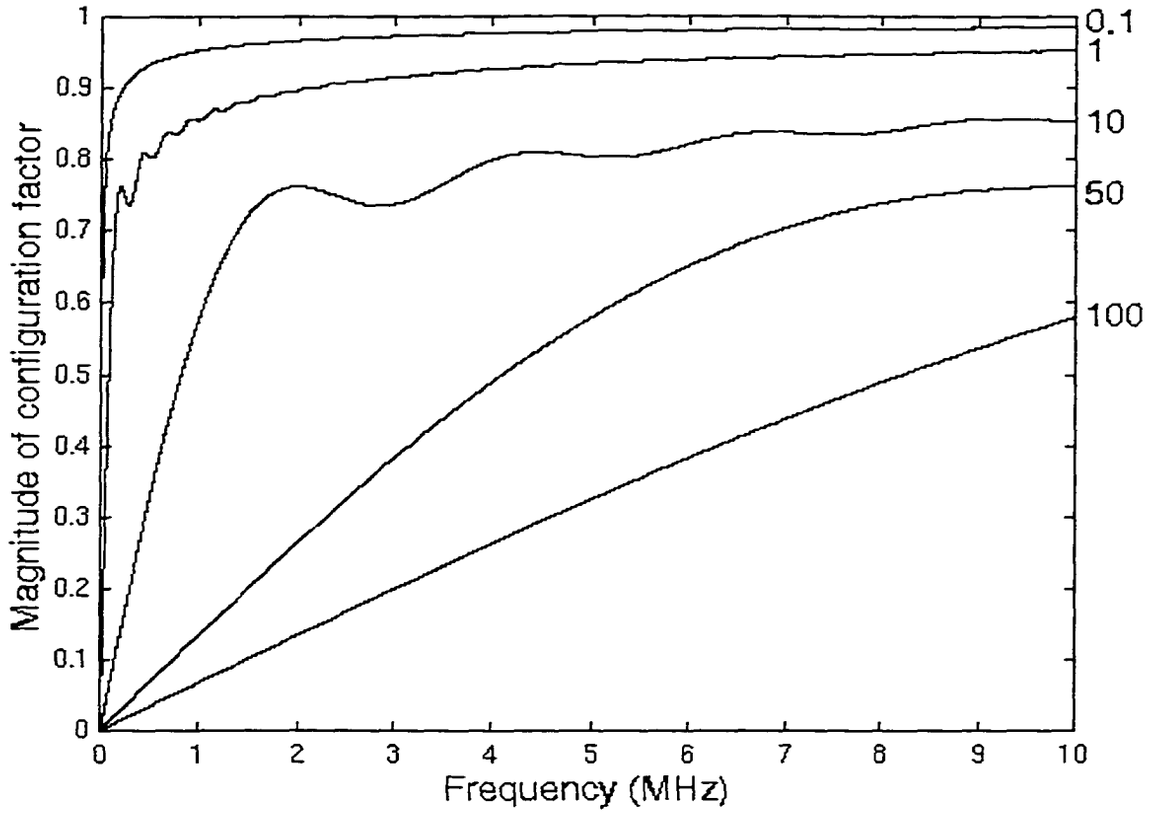

Figure 8.2 Magnitude of configuration factor showing characteristic of differentiation when $D/2a$=0.1, 1, 10, 50 and 100.

8.1.2 Differentiation due to impedance changes

Consider now the case where in Figure 8.1 we keep the distance, D, fixed, but allow the receiving impedance, Z_o^e, to vary. As shown in Chapter 4, we can replace the receiving transducer by a Thevenin equivalent circuit (see Figure 4.10) which for convenience is repeated here (Figure 8.3). In Chapter 4 we found that

$$V_R(\omega) = \frac{Z_o^e}{Z_{th}^e(\omega) + Z_o^e} V_{th}(\omega) \tag{8.1.7}$$

where, recall (Eq. (4.2.7))

$$V_{th}(\omega) = \frac{nF_i(\omega)}{\omega C_0 Z_0^a} \frac{\left[Z_b^a - iZ_0^a \tan(ikl/2)\right]\sin kl}{\left[Z_b^a - iZ_0^a \tan(ikl/2)\right]\cos kl - iZ_0^a \tan(ikl/2)} \tag{8.1.8}$$

and (from Eq. (4.2.8))

$$Z_{th}^e(\omega) = \frac{-1}{i\omega C_0} A(\omega) \tag{8.1.9}$$

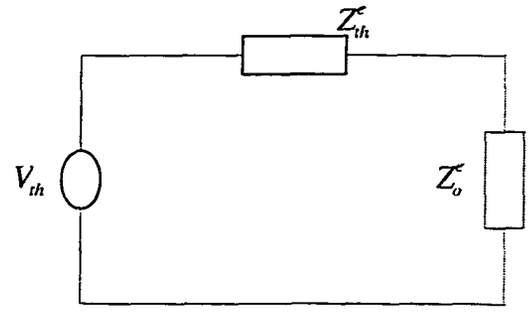

Figure 8.3 Thevenin equivalent circuit for the receiving transducer. The electrical load connected to the electrical port of the transducer is Z^e_o.

with

$$A(\omega)=1-\frac{1}{\omega C_0 Z_0^a}\frac{n^2\sin kl\left[Z_b^a-iZ_0^a\tan(ikl/2)\right]}{\left[Z_b^a-iZ_0^a\tan(ikl/2)\right]\cos kl-iZ_0^a\tan(ikl/2)}. \qquad (8.1.10)$$

For a very large receiving impedance, $Z^e_o \to \infty$ and from Eq. (8.1.7) we obtain

$$V_R(\omega)\big|_{Z^e_o\to\infty}=V_{th}(\omega). \qquad (8.1.11)$$

Conversely for a very small receiving impedance, $Z^e_o \to 0$ and Eq. (8.1.7) gives

$$V_R(\omega)\big|_{Z^e_o\to 0}=-i\omega\frac{C_0 Z^e_o}{A(\omega)}V_{th}(\omega). \qquad (8.1.12)$$

But for many piezoelectric crystals the $A(\omega)$ term is nearly a constant. For example, for a PZT crystal plate with thickness of 0.5mm, acoustic impedance of 4370N/(m/s), velocity of 4600m/s, turns ratio of 5.9A/(m/s), clamped capacitance of 3.3×10^{-9} F and a backing of epoxy and tungsten powder mixture with acoustic impedance of 4100N/(m/s), Figure 8.4 shows that over most ultrasonic frequencies $A(\omega)\equiv 1$ so that when this is the case Eq. (8.1.11) and Eq. (8.1.12) combine to give

$$V_R(\omega)\big|_{Z^e_o\to 0}\equiv -i\omega\left(C_0 Z^e_o\right)V_R(\omega)\big|_{Z^e_o\to\infty} \qquad (8.1.13)$$

which shows that again apart from a scaling factor going from a very high to a very low receiving impedance condition produces a differentiation effect.

Schmerr, Dang and Sedov [1998] have described these effects of distance and impedance changes on simulated waveforms by using an explicit model of the entire measurement process of Figure 8.1. Similarly, we can use the MATLAB implementation of the EAM model to illustrate these differentiation effects. For example, consider the transducers made from the crystal whose parameters are shown in the title of Figure 8.4

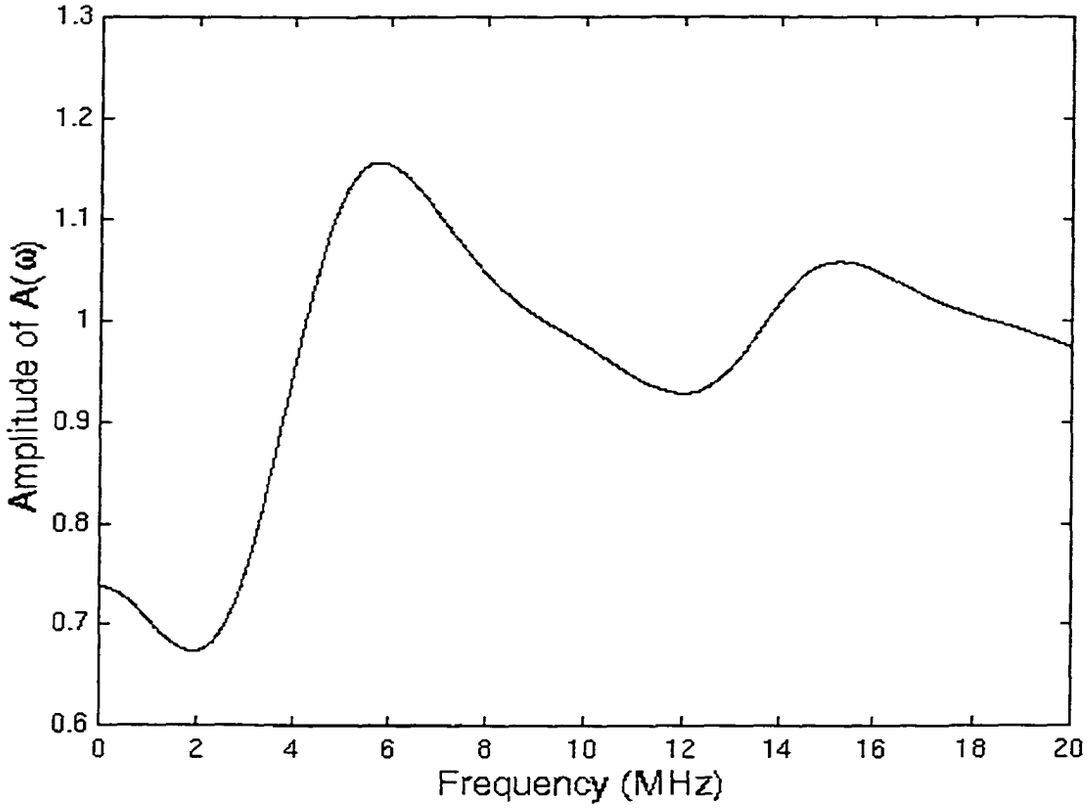

Figure 8.4 Amplitude of term $A(\omega)$ shown in Eq. (8.1.10) when the parameters of a PZT crystal plate are chosen as: thickness of 0.5mm, acoustic impedance of 4370N/(m/s), velocity of 4600m/s, turns ratio of 5.9A/(m/s), and clamped capacitance of 3.3×10^{-9} F and the parameter of the backing is the mixture of epoxy and tungsten powder with acoustic impedance of 4100N/(m/s).

and a water medium. The received waveform is shown in Figure 8.5 for D= 0.001m and $Z_o^e = 100\,k\Omega$. The "single cycle" shape of the waveform in Figure 8.5 is changed to the "one and a half" cycle waveform of Figure 8.6 when D is increased significantly to D = 1m and the impedance is held at $Z_o^e = 100\,k\Omega$, which is what is expected from diffraction-based differentiation effects. Similarly, Figure 8.7 shows a "one and a half cycle" waveform generated when the distance is the same as for the case of Figure 8.5 and the impedance is decreased to $Z_o^e = 1\,\Omega$, corresponding to an impedance-based differentiation effect.

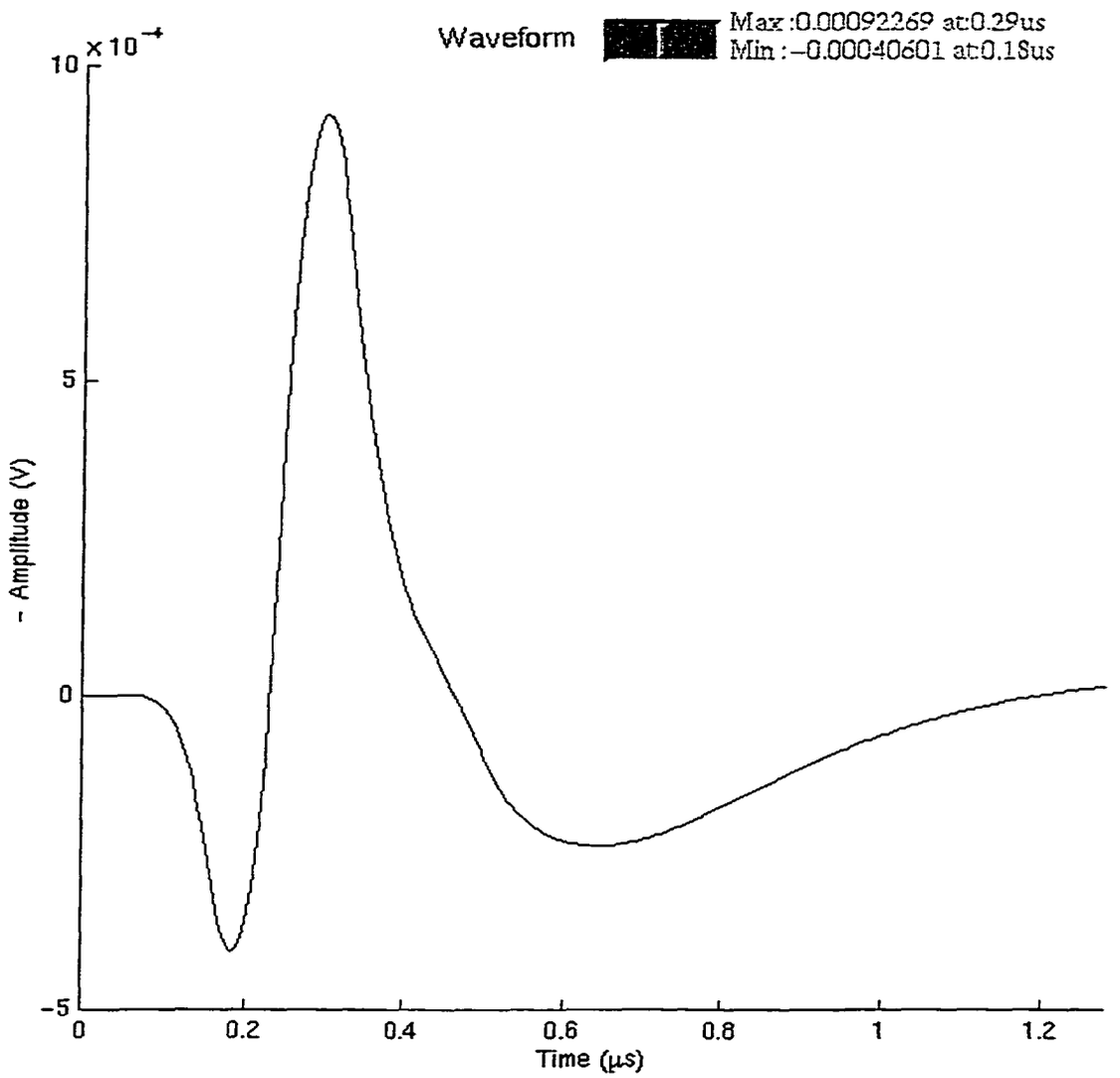

Figure 8.5 The receiving waveform for small D and large Z_o^e with D=0.001m and $Z_o^e = 100k\Omega$.

8.2 Bond Thickness Effects

Papadakis has used a model similar to our EAM model to analyze the effects of different parameters on transducer response [Papadakis, 1983]. For example, he conducted parametric studies where the impedance of the backing material, the electromechanical coupling factor, and the input pulse length were varied. In the next section we will compare some results obtained with the EAM model with those of Papadakis. In this section we will

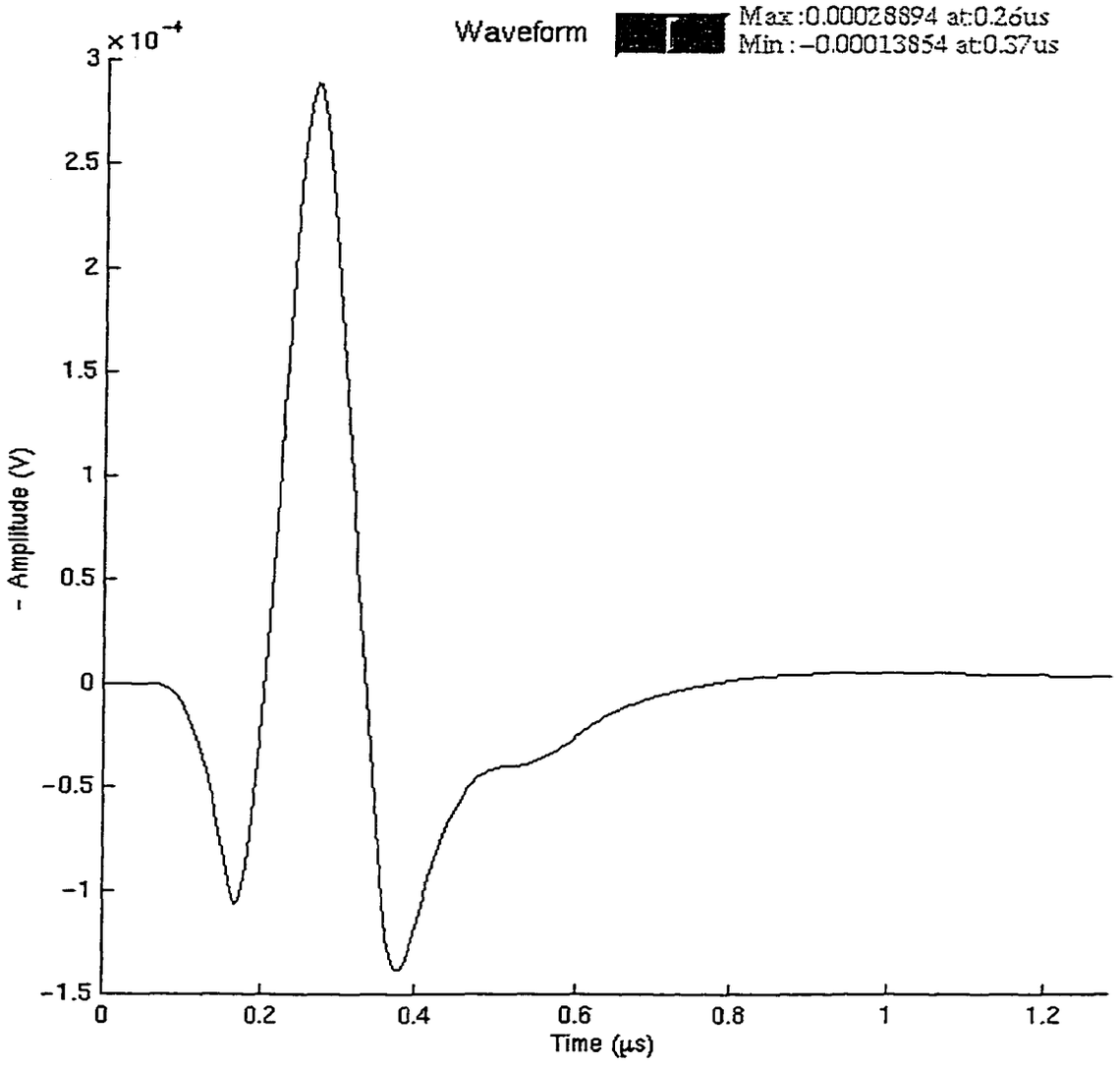

Figure 8.6 The receiving waveform for large D and large Z_o^e with D=1m and $Z_o^e = 100k\Omega$.

use the EAM model to examine the effect that the thickness of a bonding layer (between the piezoelectric crystal and the front surface wear plate) has on the transducer response. Previous studies have suggested that even small changes in the thickness of the bond line can have a profound effect on the transducer response [Silk, Bainton and Hillier, 1988] so that this is an important parameter to study.

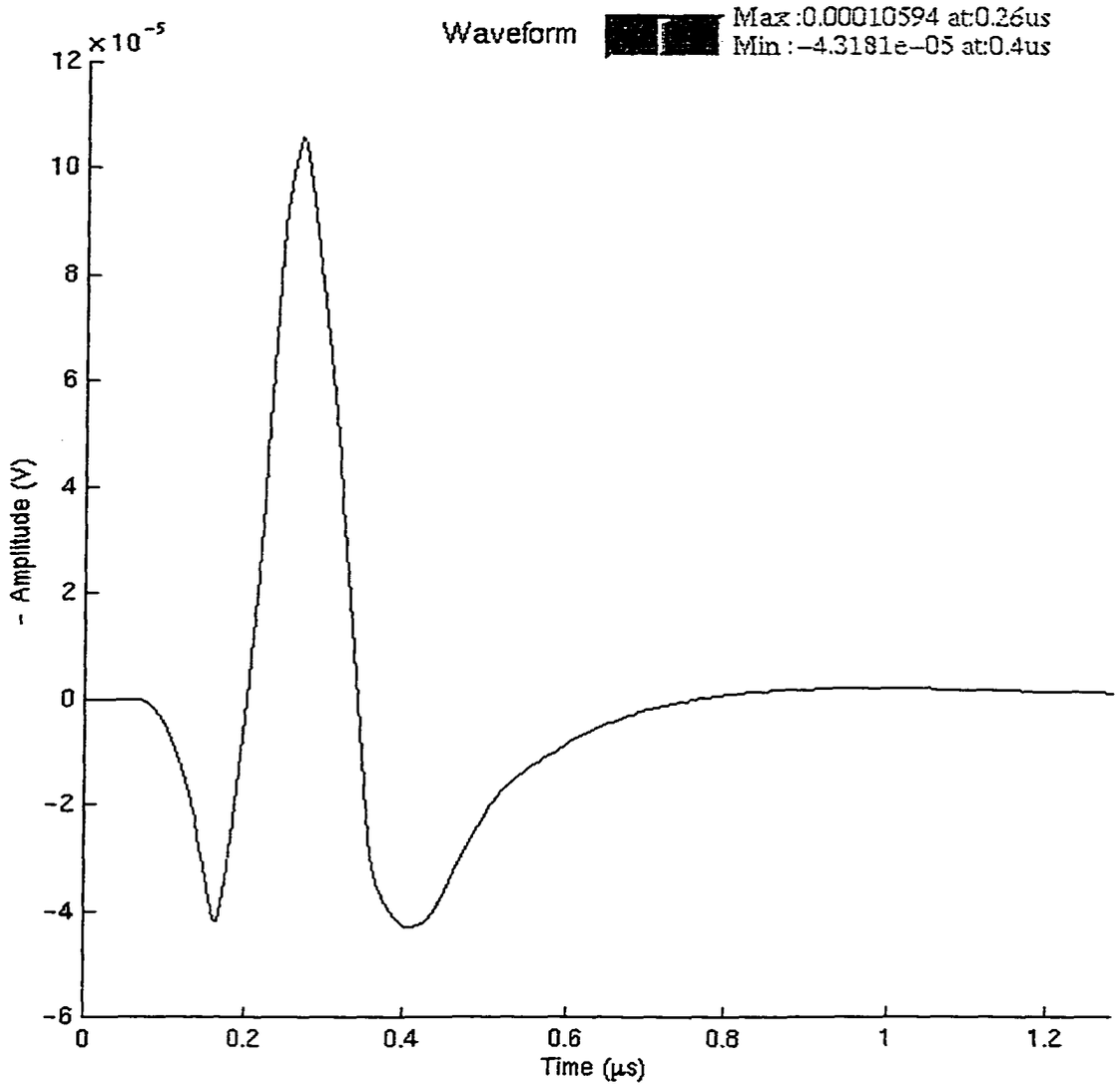

Figure 8.7 The receiving waveform for small D and small Z_o^c with D=0.001m and $Z_o^c = 1\Omega$.

8.2.1 Choice of parameters

The structure of the transducer we will consider in these bond line studies is shown in Figure 8.8. The transducer is modeled as an assembly of four components: backing, piezoelectric plate, bonding ("glue") layer, and wear plate. Although the crystal is normally plated on both of its faces with a conducting material, in this model study the effects of the plating will be ignored. The backing is often made of a mixture of epoxy and tungsten

powder that is cast directly onto the plated crystal so that we do not model a bonding layer at the backing. Also, we model the backing layer itself as a lossless semi-infinite layer so that there are no reflected waves. However, a thin bonding layer of epoxy glue is often present at the front face of crystal as result of attaching the wear plate to the crystal. It is the thickness of this glue layer that we wish to vary.

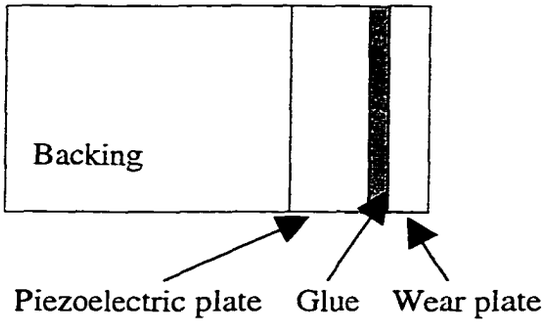

Figure 8.8 Structure of an ultrasonic transducer made of backing, piezoelectric plate, glue and wear plate.

In our EAM model we consider two identical transducers aligned along their axes in a pitch-catch setup. We take the distance between them to be very small so that the configuration factor is approximately 1.0. The material parameters are taken from one of the cases considered by Papadakis, case number 69A2 [Papadakis, 1983]. The nominal frequency of the transducers is 5MHz, and the input electrical impulse was modeled as a rectangular pulse with unit amplitude by adjusting the coefficients in the EAM model of the pulser appropriately, as discussed in the next section. The width of this rectangular pulse was taken to be the half period at the nominal resonant frequency (the free crystal resonant frequency). The internal impedance of the pulser and the impedance at the receiver were made identical and equal to the impedance of the clamped capacitance - a quantity that is defined explicitly in the section 8.3.3. The parameters are listed as follows:

Piezoelectric plate:

Density $\rho = 6750 kg/m^3$
Permittivity $\varepsilon / \varepsilon_0 = 1000$
Thickness $l = 0.2mm$
Stiffness $c^E = 69.12GPa$
Piezoelectric constant $e = 18.55V/m$

Backing:

Density ρ=5000kg/m^3
Sound speed v=4600m/s

Glue (epoxy):

Density ρ=1200kg/m^3
Sound speed v=2600m/s
Thickness l=0 - 0.2mm

Wear plate:

Density ρ=3937kg/m^3
Sound speed v=10160m/s
Thickness l = 0.127mm

Propagation medium:

Density ρ=4000kg/m^3
Sound speed v=4325m/s

Geometry:

Transducer radius r=6.35mm
Transducer distance d=1e-7m

Pulser:

Voltage V=1V
Pulse width t=50ns
Internal impedance Z_i=2.839Ω

Receiver:

Load impedance Z_0=2.839Ω

8.2.2 Simulated results

For the parameters given in the last section the thickness of the epoxy bond line between the crystal and the wear plate was varied from 0 to 0.2mm. In general, as the thickness increased the output voltage, which started as a single cycle waveform at zero thickness (Figure 8.9(a)), developed a higher frequency "ringing" at later times, which eventually dominated the entire response (see Figures 8.10(a), 8.11(a), 8.12(a), and 8.13(a)). In the frequency domain, the magnitude of the received spectrum starts at zero bond thickness as a single peak centered at a frequency near the nominal center frequency, F_m. At a bond thickness of about 0.05mm a second peak in the spectrum appears at a higher frequency, F_c, growing size relative to the first peak until it eventually dominates the entire

response at the largest thickness considered. This behavior is illustrated in the sequence Figures 8.9(b), 8.10(b), 8.11(b), 8.12(b), and 8.13(b). These results are tabulated in Table 8.1 where column one lists the bond thicknesses with starred thicknesses indicating that the corresponding spectra and waveforms are shown in Figures 8.9-8.13. Column 2 lists the

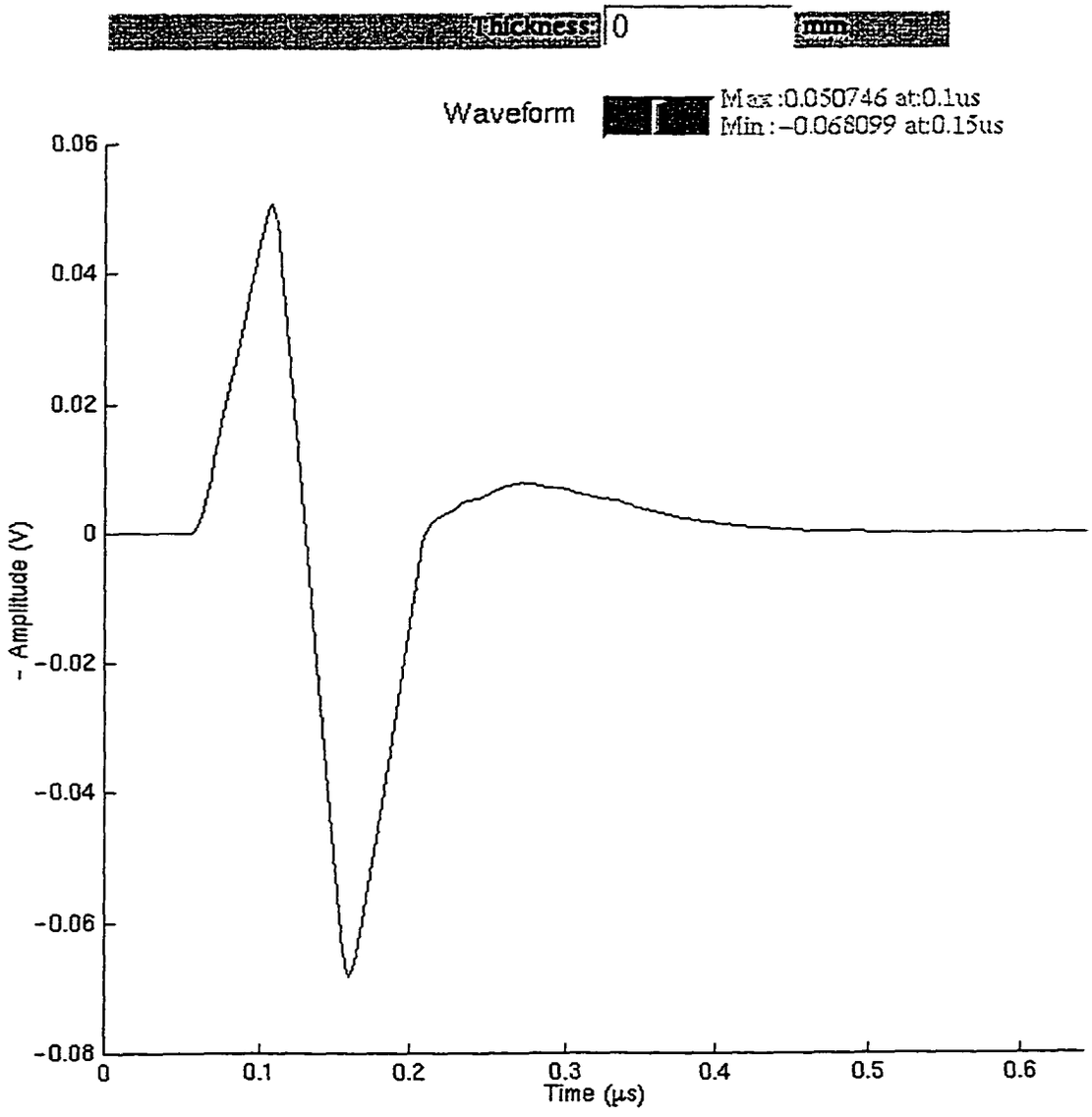

Figure 8.9 (a) Received waveform without glue. The waveform is a single cycle signal.

maximum and minimum values in the time domain waveforms (can be read from the Small window when the waveform is shown in the Result window (see Figure 7.17)). Column 3 lists the location of a peak frequency value, F_m. Column 4 lists a center (mean), F_c. Column 5 (BW) gives the 3-dB bandwidth of the peaks that exist, and Column 6 (V1/V2) lists ratios

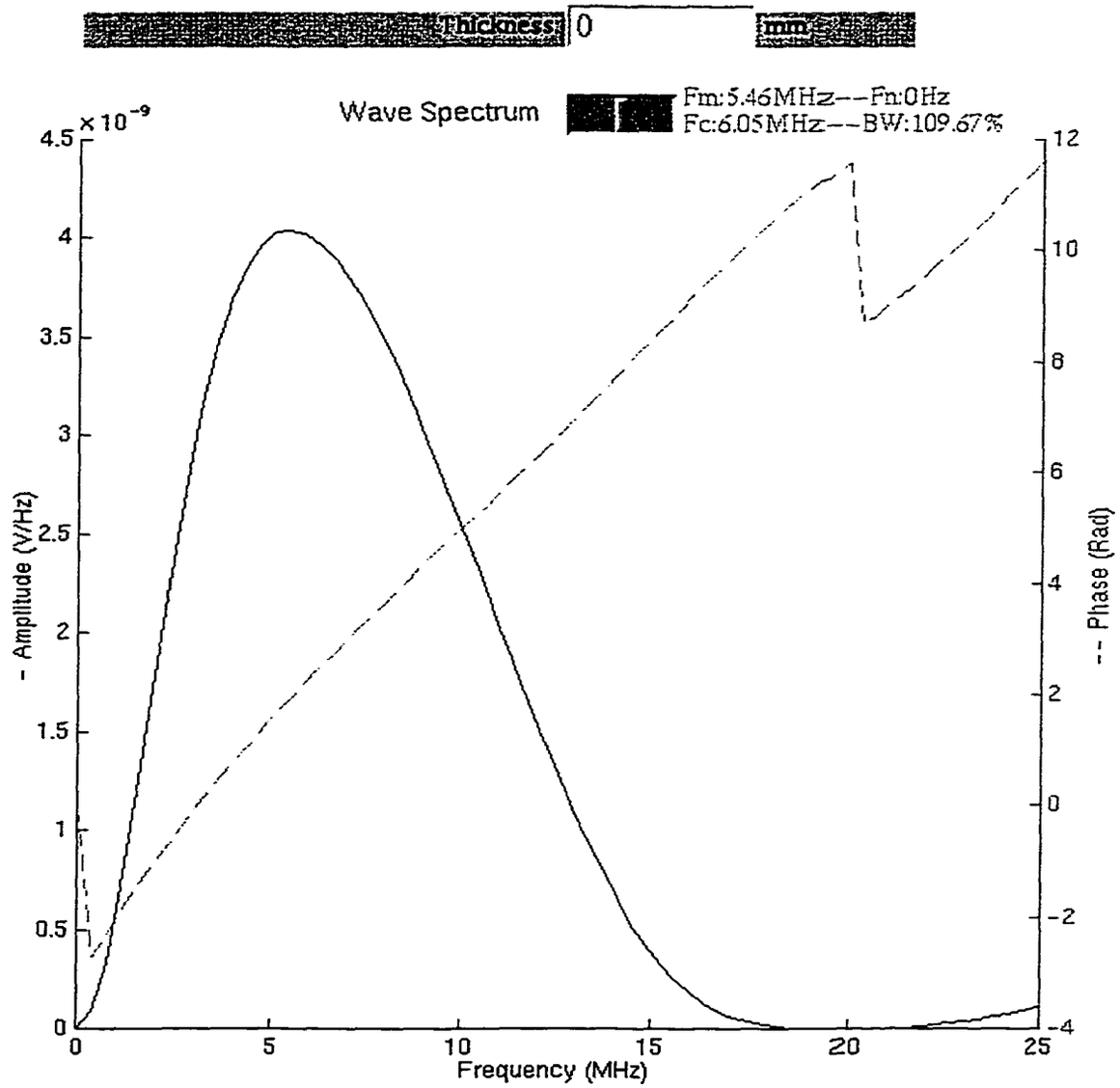

Figure 8.9 (b) Spectrum for the received waveform without glue. The lower frequency component is a single component.

of the spectral amplitudes of the two peaks (low frequency peak/high frequency peak). In columns 3, 4 and 5, every item has two values denoted as "low" and "high" which correspond to measurement based on the lower frequency and higher frequency. These values can be measured using the shift and zoom features provided by the EAM software.

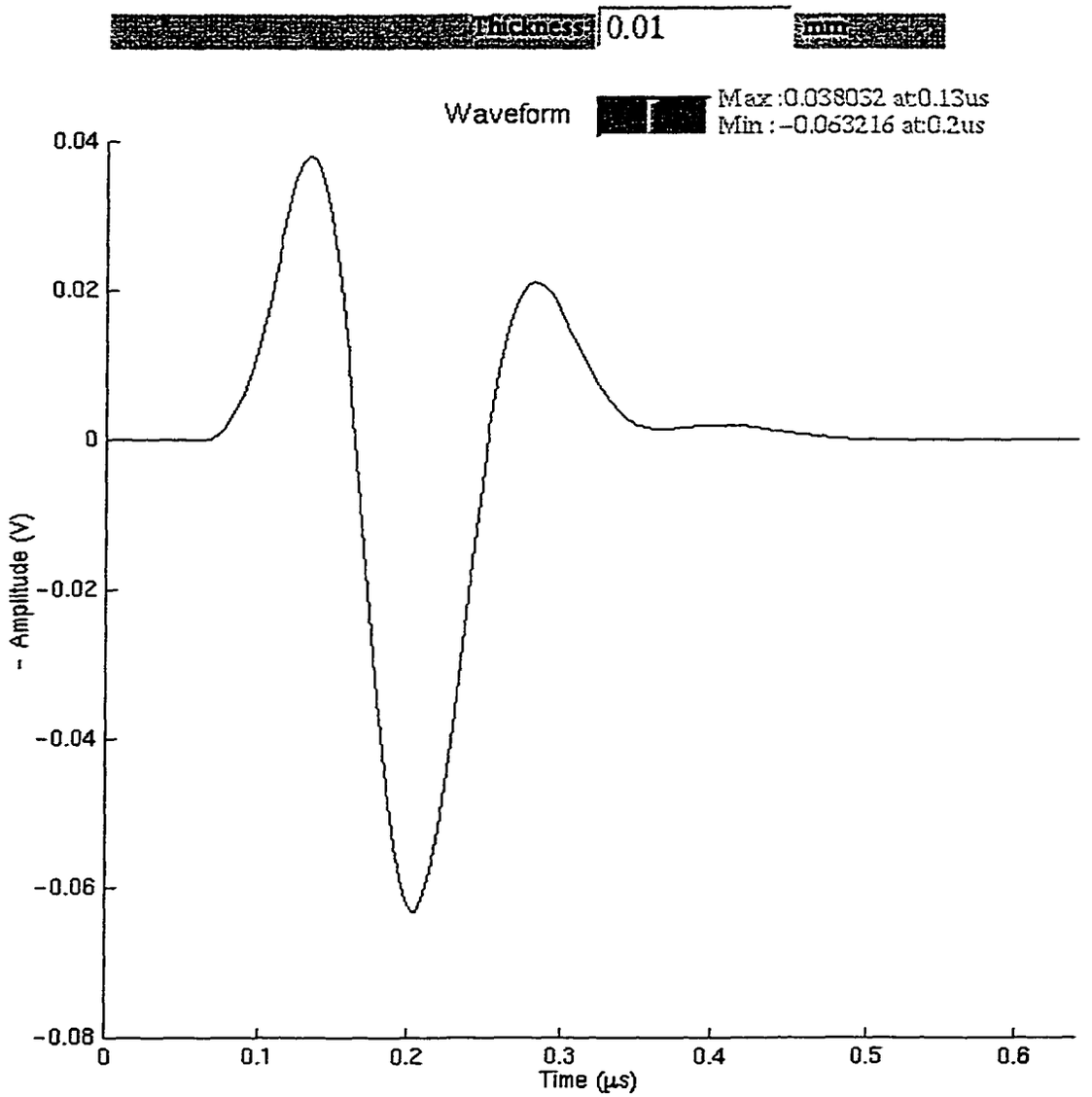

Figure 8.10 (a) Received waveform with the glue thickness of 0.01mm. The waveform is one and a half cycle signal.

When the Result window in Figure 7.17 only shows one peak by shifting and/or zooming the spectrum, the Small window gives us the parameters corresponding to that peak such as Fm, Fc and BW. Of the two spectrum peaks, the lower frequency peak is generated by the nominal frequency of the transducer and the higher one by the glue thickness. By comparing

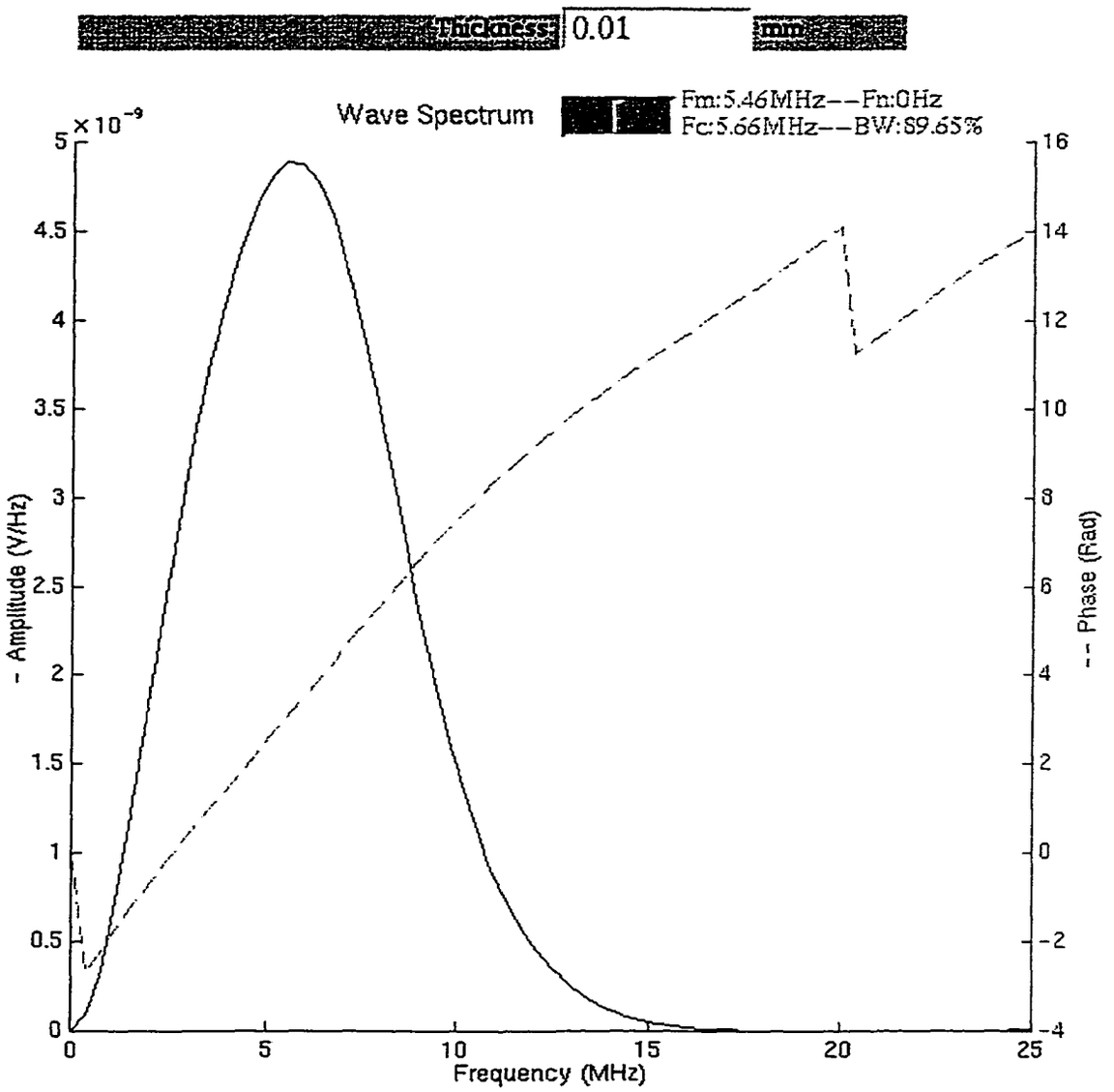

Figure 8.10 (b) Spectrum for the received waveform with the glue thickness of 0.01mm. The lower frequency component is still a single component.

these two peaks, we can see the behavior of the glue thickness variations. If one peak is not measurable, it is given as "-" in Table 8.1.

In summary, from Table 8.1 we observe the following behavior:

a. For a very thin glue layer the peak frequency located near the nominal center

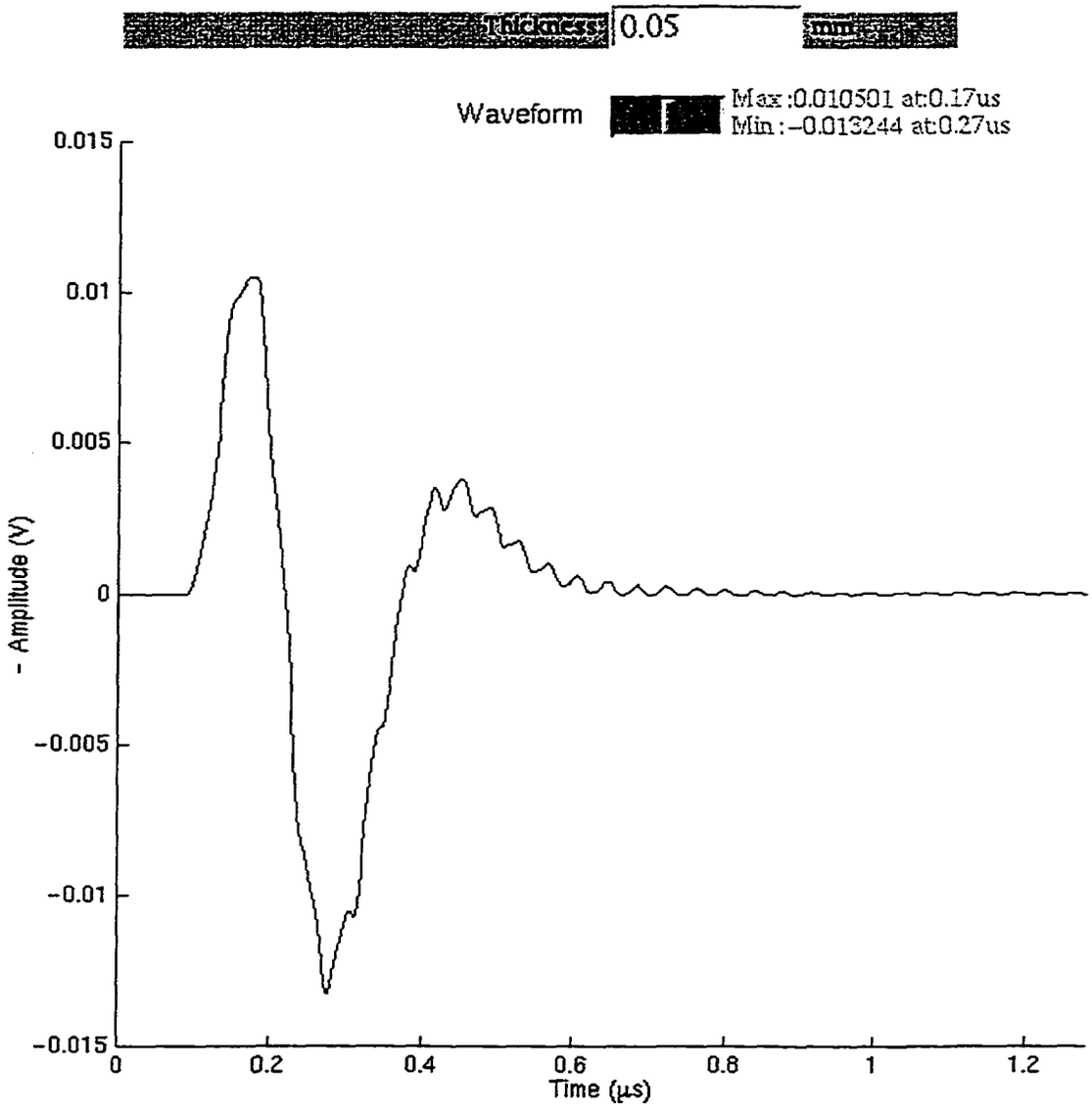

Figure 8.11 (a) Received waveform with the glue thickness of 0.05mm. The higher frequency component appears.

frequency dominates. A high frequency peak is not measurable.

b. As the glue thickness increases, the amplitude of the received waveforms drops rapidly. For example, as the thickness changes from 0 to 0.1mm the amplitude changes from 0.05V to 0.007V, a decrease of almost an order of magnitude.

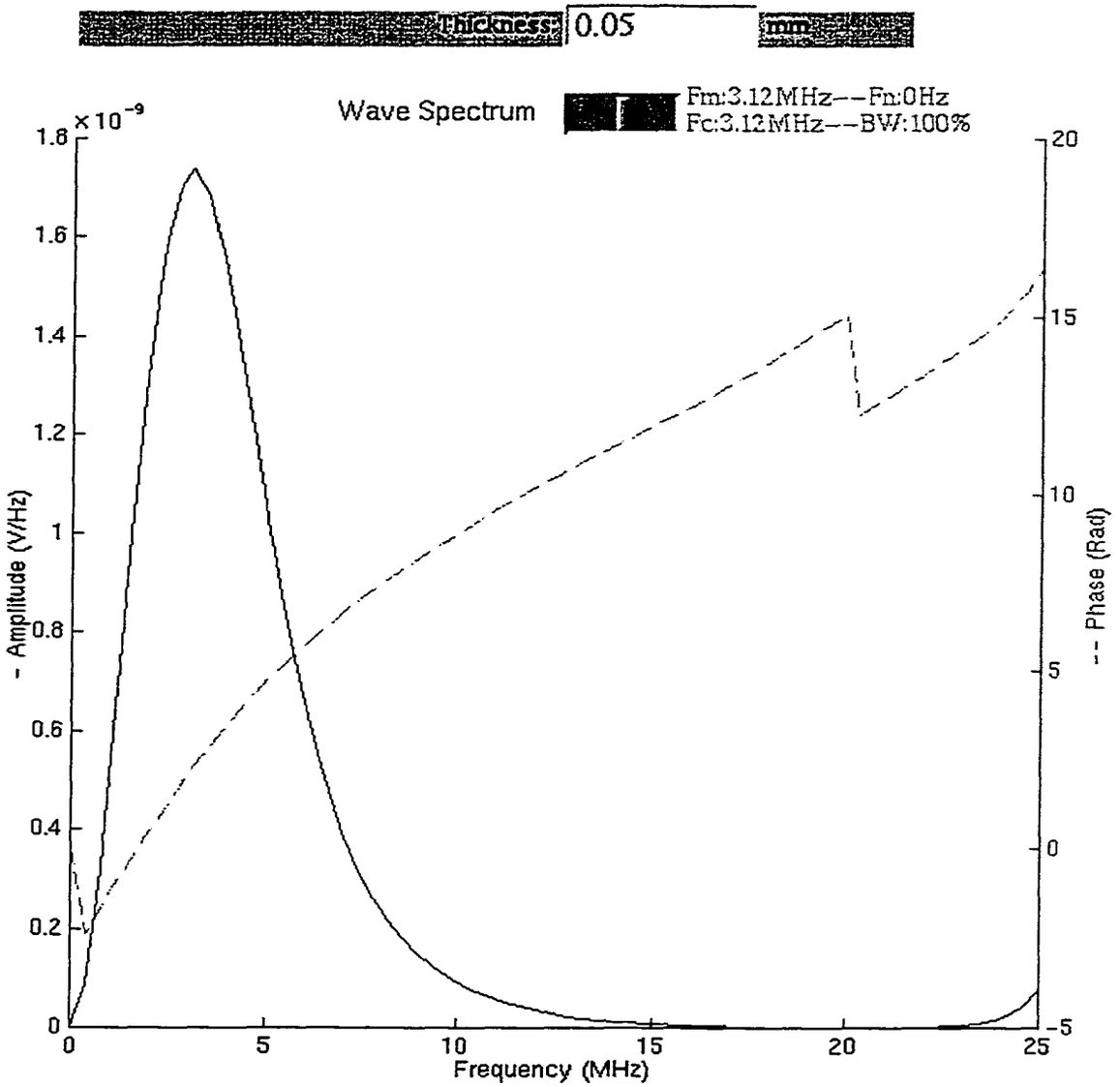

Figure 8.11 (b) Spectrum for the received waveform with the glue thickness of 0.05mm. The higher frequency component is not clear but it appears in the time domain in Figure 8.11(a).

c. As the glue thickness increases, the peak frequency also decreases but the bandwidth does not change much. For example, as the thickness changes from 0 to 0.1mm the peak frequency near the nominal center frequency changes from 5.46MHz to 2.34MHz but the bandwidth changes by less than 5%.

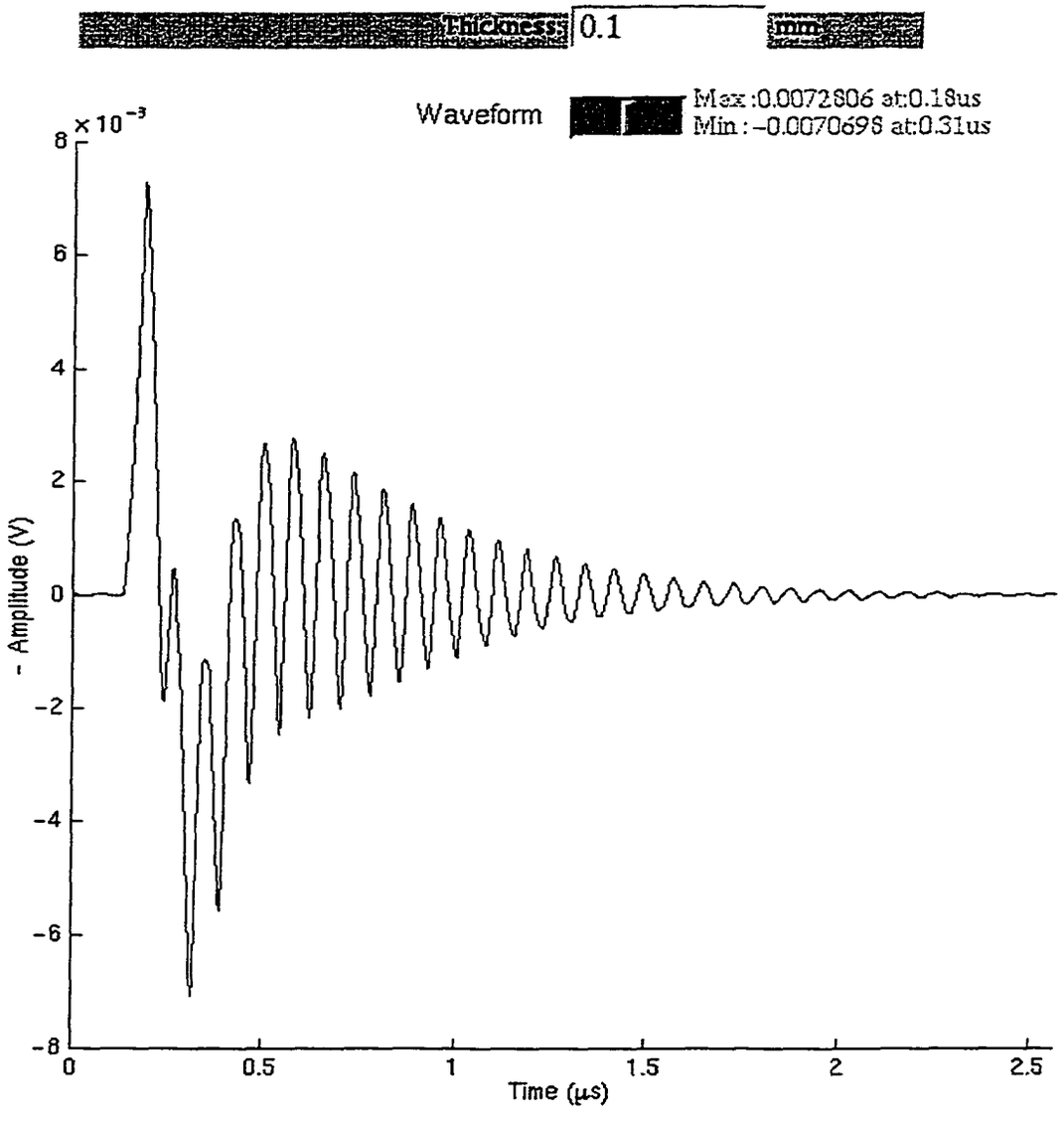

Figure 8.12 (a) Received waveform with the glue thickness of 0.1mm. The higher frequency component is mixed with the lower frequency component.

d. When the glue thickness is larger than 0.05mm a higher frequency peak begins to appear. At larger thickness, a "bi-modal" frequency spectrum with two peaks exists for a range of thickness, but the higher frequency peak eventually dominates the measured response as the thickness continues to increase.

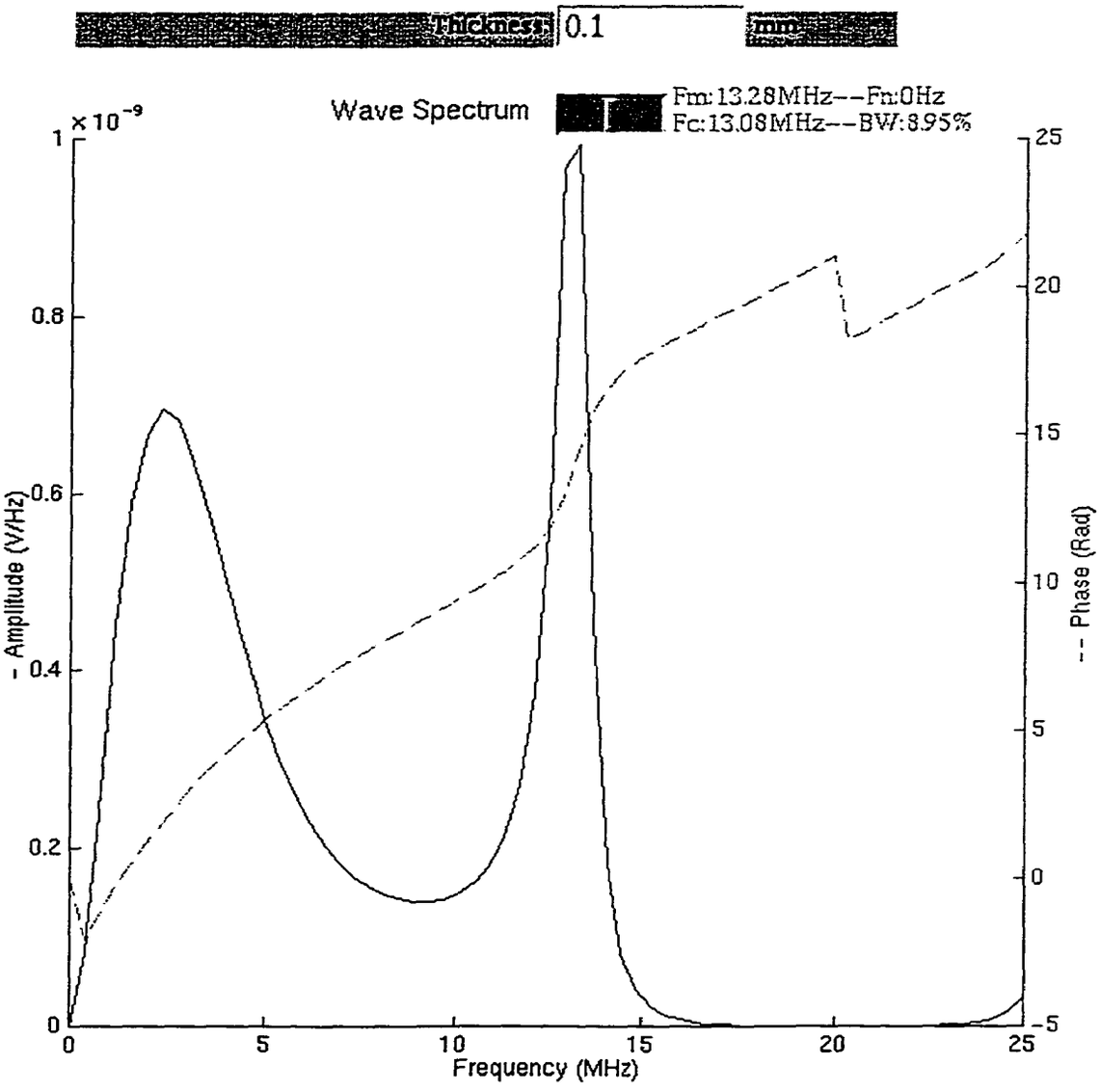

Figure 8.12 (b) Spectrum for the received waveform with the glue thickness of 0.1mm. The higher frequency component is comparable to the lower frequency component.

In conclusion, the transducer behavior is indeed very sensitive to the thickness of the glue between the piezoelectric crystal and the wear plate. The existence of the glue layer reduces not only the waveform amplitude but also the frequency of the crystal, similar to the way the backing material "shifts down" the resonant frequency of the crystal. In the example

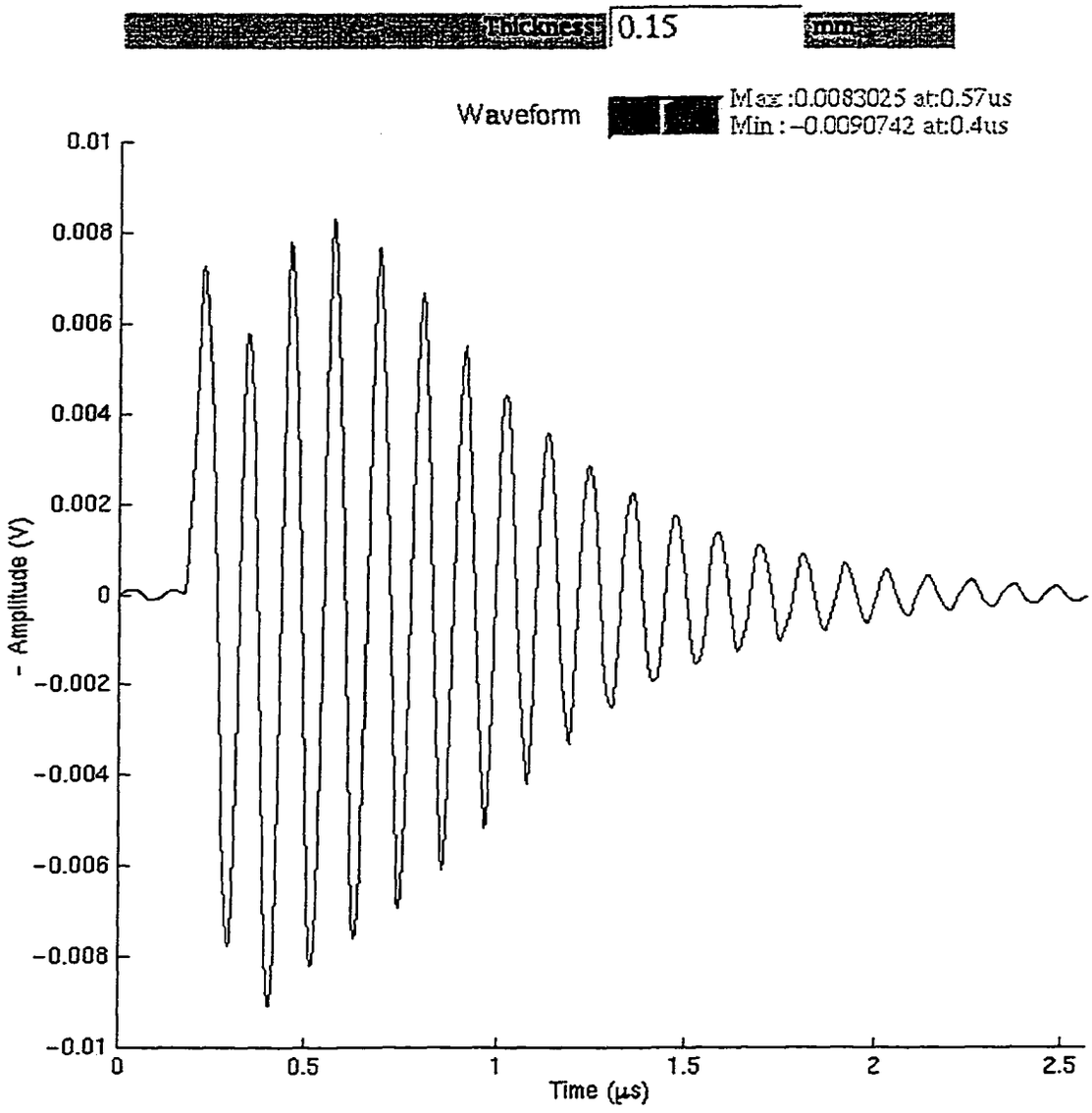

Figure 8.13 (a) Received waveform with the glue thickness of 0.15mm. It is difficult to distinguish the lower frequency component from the received signal.

considered a glue thickness of greater than 0.05 mm begins to have detrimental effects on the received waveform in terms of both amplitude and "ringing". Thus, the bonding of the wear plate to the crystal needs to be controlled with precision to maintain a very small thickness of the glue layer.

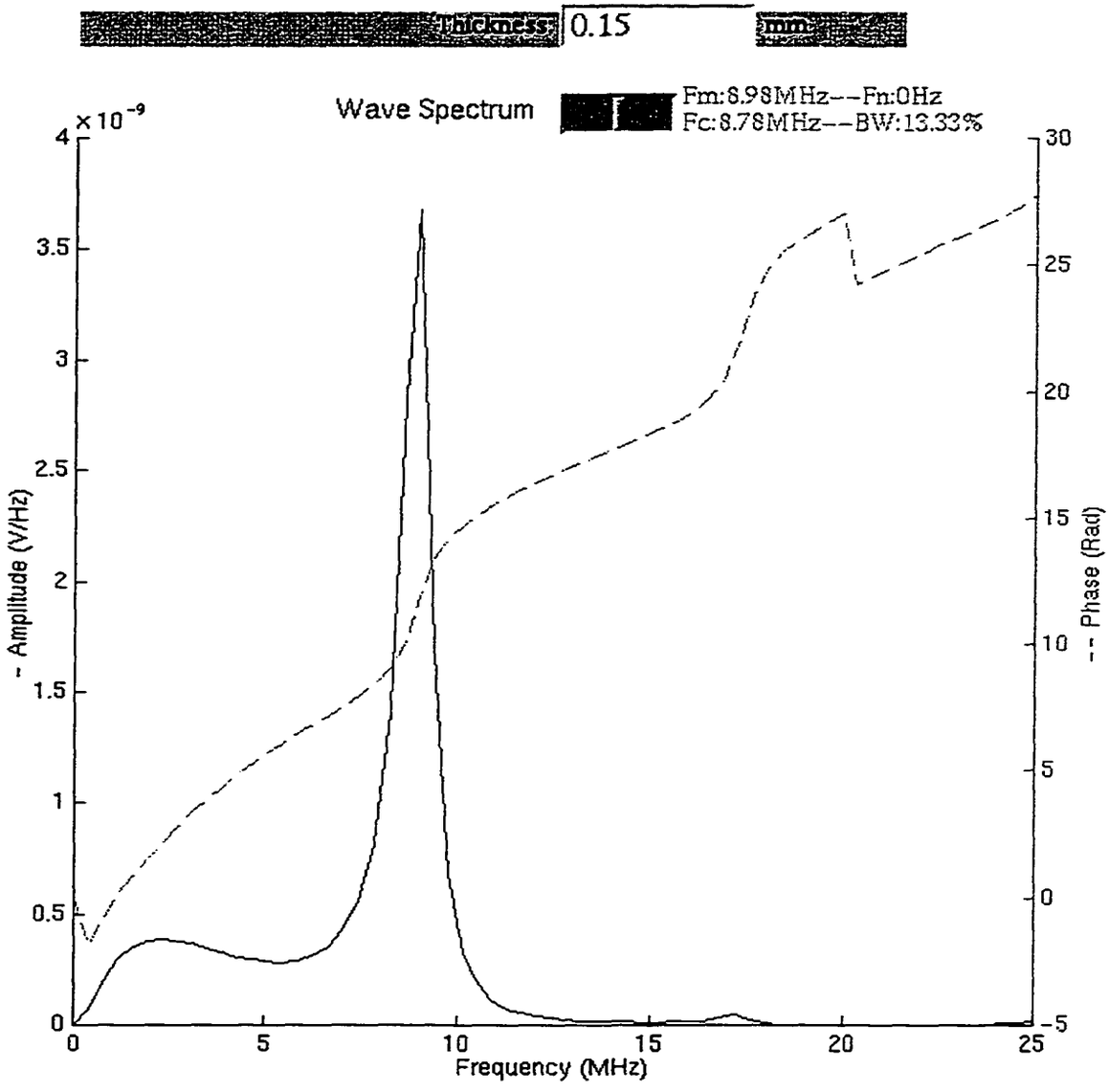

Figure 8.13 (b) Spectrum for the received waveform with the glue thickness of 0.15mm. The higher frequency component is dominant.

Table 8.1 Modeling results with variation of glue thickness

Thickness (mm)	Amplitude (V) (positive/negative)	Fm (MHz) (low/high)	Fc (MHz) (low/high)	BW (%) (low/high)	V1/V2
0(*)	0.050746/-0.068099	5.46/ -	6.05/ -	109.67/ -	-
0.000001	0.050749/-0.068103	5.46/ -	6.05/ -	109.67/ -	-
0.000005	0.050759/-0.068120	5.46/ -	6.05/ -	109.67/ -	-
0.00001	0.050771/-0.068141	5.46/ -	6.25/ -	109.67/ -	-
0.00005	0.051468/-0.071595	5.46/ -	6.25/ -	112.5/ -	-
0.001	0.051389/-0.07233	5.85/ -	6.25/ -	112.5/ -	-
0.005	0.047153/-0.075382	6.25/ -	6.25/ -	100.0/ -	-
0.01(*)	0.038032/-0.063216	5.46/ -	5.66/ -	89.65/ -	-
0.02	0.025341/-0.038578	4.29/ -	4.49/ -	95.65/ -	-
0.03	0.018460/-0.02504	3.90/ -	3.71/ -	94.73/ -	-
0.04	0.014488/-0.01772	3.51/ -	3.51/ -	88.88/ -	-
0.05(*)	0.010501/-0.01324	3.12/25.78	3.12/ -	100.0/ -	-
0.06	0.008742/-0.009398	2.73/22.65	3.12/ -	100.0/ -	-
0.07	0.007395/-0.007225	2.73/ -	2.73/ -	114.3/ -	-
0.08	0.007283/-0.006228	2.73/16.01	2.73/16.01	114.3/9.75	6.25
0.09	0.007290/-0.006711	2.34/14.45	2.73/14.25	114.3/8.21	1.45
0.1(*)	0.007281/-0.007070	2.34/13.28	2.73/13.08	114.3/8.95	0.7
0.11	0.007279/-0.007565	2.34/12.1	2.73/11.91	114.3/9.83	0.37
0.12	0.007308/-0.008119	2.35/10.93	2.53/11.13	138.5/10.5	0.2
0.13	0.007333/-0.008666	2.34/10.15	2.53/10.15	138.5/7.69	0.18
0.14	0.007574/-0.008901	2.34/9.37	2.73/9.57	142.8/12.2	0.12
0.15(*)	0.0083025/-0.00907	2.34/8.98	- /8.78	- /13.3	0.09
0.16	0.0089484/-0.00916	2.34/8.20	- /8.39	- /13.9	0.09
0.17	0.0095817/-0.00925	2.34/7.81	- /7.81	- /10	0.07
0.18	0.0100670/-0.00934	2.73/7.42	- /7.42	- /10.5	0.06
0.19	0.0104260/-0.00938	- /7.03	- /7.03	- /11.1	-
0.2	0.0104580/-0.00954	- /6.64	- /6.64	- /11.8	-

* Spectrum and waveform are shown.

8.3 Comparisons with the Papadakis Model

Papadakis [1983] conducted numerical parametric studies of transducers using a transfer matrix approach (the Sittig model discussed in subsection 2.4) that is very similar to our EAM model. Because the EAM model is very complex, with many input parameters, it is useful to confirm the predictions of this model through comparisons with other modeling simulations. In this section we will make such comparisons with the modeling results of Papadakis.

8.3.1 The Papadakis model

Papadakis used a modeling setup which was a special case of the configuration shown in Figure 8.1. The pulser was modeled by a Thevenin equivalent circuit with a source strength, $V_i(\omega)$, and impedance, Z_i^e. The receiver was modeled as the receiving impedance, Z_o^e, where for all his results, Papadakis took these impedances to be purely real and equal ($Z_i^e = Z_o^e$). The parameters of the two transducers, T and R, were taken to be identical as would be the case in pulse-echo testing. Diffraction effects were ignored in the Papadakis model, i.e. he took $F = 1$. For the source strength, Papadakis modeled the corresponding pulser voltage input as a rectangular pulse of unit amplitude. The duration of this pulse was taken equal to one half the period value given by the resonant frequency of the free vibration of the piezoelectric crystal plate.

In order to make comparisons with the Papadakis model, the EAM model inputs need to be adjusted appropriately. This was done in the following manner:

(a) Beam diffraction effects. Papadakis took $F = 1$, i.e. beam diffraction effects were ignored. This case can be simulated in the EAM model by simply taking the distances between the transducers to be very small. Thus, we set $D = 10^{-7}$ m.

(b) Electrical input pulse. Papadakis took a rectangular pulse as the input waveform while the EAM model is formed by two exponential functions. To simulate a rectangular pulse, we took the two exponential coefficients to be very large ($\alpha_1 = \alpha_2 = 10^{11}$ 1/s). As Figure 8.14 shows, this choice approximates a rectangular pulse very closely [Cheney, 1973].

(c) Material and geometrical input parameters. The set of material and geometry input parameters quoted by Papadakis are different from those of the EAM model. For some parameters, the EAM parameters are identical with those used in the Papadakis model while for other parameters we need to make certain assumptions in order to derive the necessary EAM parameters. Thus, an exact one-to-one correspondence of the two models is not possible to achieve. However, in the following three subsections we will make some reasonable assumptions to derive the necessary EAM parameters from the Papadakis parameters and compare the resulting simulated waveforms.

8.3.2 Input parameters in the Papadakis model

Papadakis provided 17 sets of input parameters used for various simulations (see Table 8.1 in [Papadakis, 1983]). We only studied five of them, which Papadakis lists as cases 70F5, 70F6, 69B1, 69A2 and 69A1. The corresponding simulated receiving waveforms are

shown in Figures 1a, 1b, 1c, 1d and 1e in [Papadakis, 1983]. The parameters quoted by Papadakis for these five cases are listed in Table 8.2. The meanings of these parameters are:

f_0, half-wavelength frequency of piezoelectric plate

z_b, the specific acoustic impedance for the backing

k, the electromechanical coupling factor

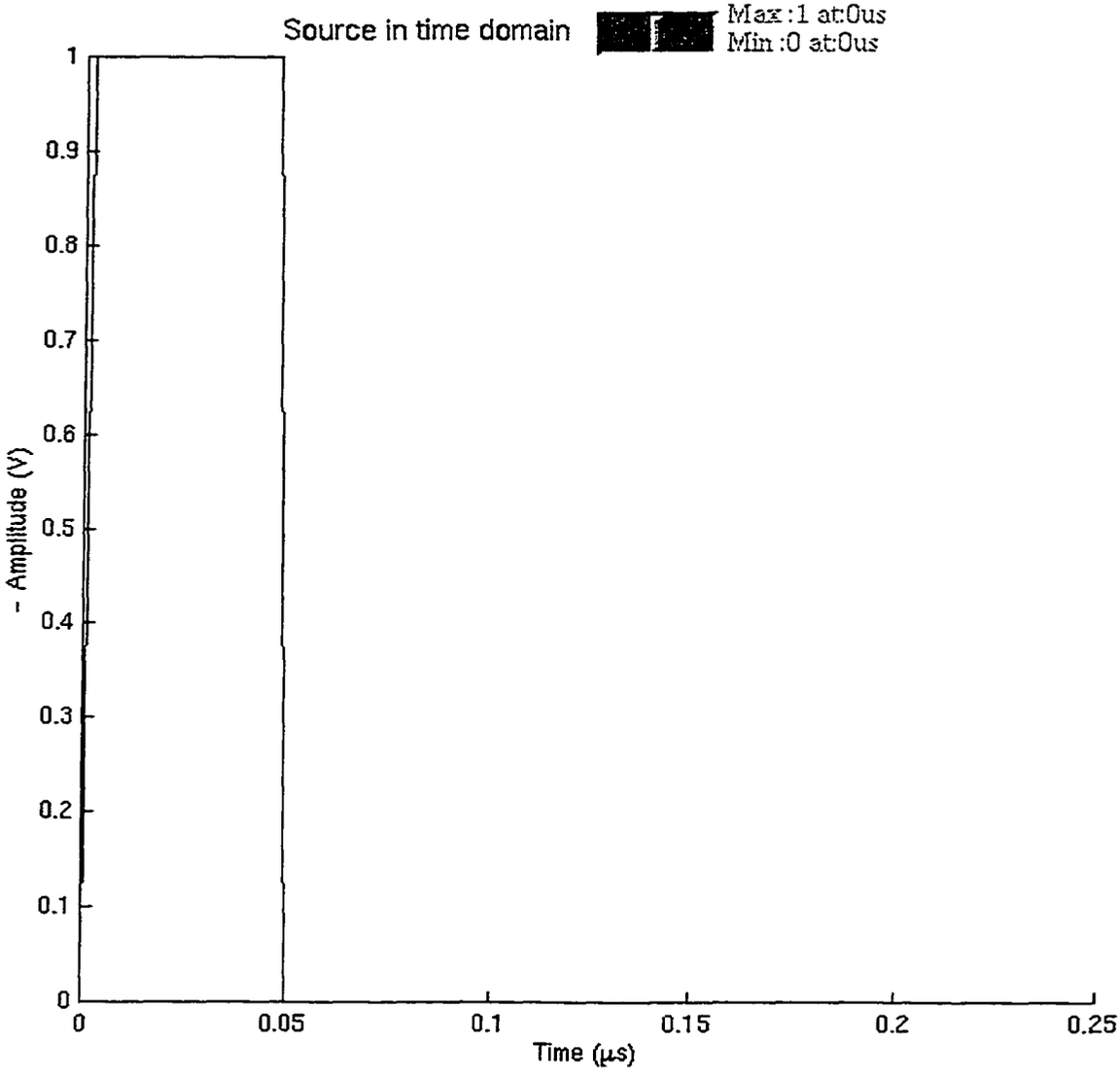

Figure 8.14 Unit amplitude rectangular electrical pulse simulated by choosing attenuation factors $\alpha_1 = \alpha_2 = 10^{11}/s$, amplitude $V_0 = 1V$ and duration time $t_0 = 0.05\,s$ (see Figure 3.3).

z_t, the specific acoustic impedance for the piezoelectric material

z_{wp}, the specific acoustic impedance for the wear plate

z_m, the specific acoustic impedance for the propagation medium

R, the ratio of $Z_i^e = Z_o^e$ to the electrical impedance of the clamped capacitance of the piezoelectric plate at its resonant frequency f_0.

Table 8.2 Input data for Papadakis' paper

Computation number	70F5	70F6	69B1	69A2	69A1
Piezoelectric material	LMN	LMN	Y-Quartz	PZT-5	PZT-5
k	0.35	0.35	0.137	0.6	0.6
f_0 (MHz)	12	12	30	10	10
z_b (x10^6kg/s-m^2)	18.6	18.6	--	23.0	23.0
z_t (x10^6kg/s-m^2)	18.6	18.6	10.2	27.0	27.0
z_{wp} (x10^6kg/s-m^2)	--	--	--	40.0	40.0
z_m (x10^6kg/s-m^2)	18.6	18.6	8.3	17.3	17.3
R	20.00	1.25	1.00	1.00	28.10

In Table 8.2, the dashed lines "--" mean that the corresponding components are not present in transducers. For example, the transducer modeled by case 69B1 does not have backing and wear plate layers. To have the EAM model and the Papadakis model describe the same measurement system, we need to derive the input parameters used for the EAM model from the parameters in Table 8.2.

8.3.3 Input parameters in the EAM model

It is straightforward to derive the input parameters for the Papadakis model from the input parameters for the EAM model. However, if we want to get the input parameters for the EAM model from those given for the Papadakis model, we need to make some assumptions. For example, the acoustic specific impedance of a material is taken as an input parameter in the Papadakis model. On the other hand, the acoustic wave velocity and the density of a material are separate input parameters in the EAM model. To break the acoustic specific impedance into the corresponding velocity and density, we need to make a reasonable assumption on either the velocity or density. The rule of thumb we followed is to make as few assumed quantities as possible. Following this rule, we found that, to determine the complete set of input parameters for the EAM model, it is necessary to make assumptions

on the following quantities: densities of the crystal and other materials, permittivity of the crystal and the radius of the transducer.

Using the parameters given by Papadakis and the set of assumed parameters, the following eight steps were used to determine all the EAM parameters:

(a) For all the materials involved, using the specific acoustic impedances given by Papadakis and a reasonable assumption for the density, the velocities were found for the backing, crystal, and propagating media through the expression for the specific acostic impedance given by:

$$z = \rho v. \tag{8.3.1}$$

(b) The stiffness at constant electric flux, c^D, for the piezoelectric crystal was found from the assumed density and velocity determined from (a) from the relationship:

$$c^D = \rho_T v_T^2. \tag{8.3.2}$$

(c) The piezoelectric constant, e, was determined from the electromechanical coupling coefficient, k, given by Papadakis, an assumed value for the permittivity, ε, and the stiffness, c^D, obtained from (b), using the expression:

$$e = k\sqrt{\varepsilon c^D}. \tag{8.3.3}$$

(d) The stiffness constant at constant electric field, c^E, was computed from the stiffness, c^D, obtained in (b), the assumed permittivity, ε, and the piezoelectric constant, e, obtained in (c), since we have:

$$c^D = c^E + e^2 / \varepsilon. \tag{8.3.4}$$

(e) The thickness, l, of the crystal was obtained from the half-wavelength frequency, f_0, given by Papadakis and the velocity determined in (a), using the relationship:

$$l = v / 2f_0. \tag{8.3.5}$$

The thickness of the wear plate (if any) was given directly by Papadakis (see Table 3.1). The backing in all cases was modeled (if it exists) as a semi-infinite medium so that a thickness parameter is not needed for that "layer".

(f) The clamped capacitance, C_0, of the transducer crystal was found from the assumed permittivity, ε, the thickness, l, determined from (e), and an assumed value for the transducer radius, r, which gives the area $A = \pi r^2$ appearing in the expression for C_0:

$$C_0 = \frac{\varepsilon A}{l}. \tag{8.3.6}$$

(g) The impedance of the clamped capacitance, Z_c^*, is computed from the resonant frequency, f_0, given by Papadakis and the clamped capacitance found in (f) via:

$$Z_c^e = \frac{1}{2\pi f_0 C_0}. \tag{8.3.7}$$

(h) The internal impedance of the pulser and the receiving impedance (which are equal) were found from the ratio factor, R, given by Papadakis and the impedance calculated in (g):

$$Z_i^e = Z_o^e = RZ_c^e. \tag{8.3.8}$$

Table 8.3 lists all the input parameters for the model derived in this manner for the five cases we will consider. The bold quantities are assumed quantities and the italicized quantities are derived parameters that can be obtained from combinations of the others listed. The symbol "n.a." in Table 8.3 indicates that the corresponding quantity is not applicable for the case under consideration. Thus, cases 70F5, 70F6, and 69B1 do not have wear plates and there is no backing layer in case 69B1. Because Papadakis took the same properties for the transmitting and receiving transducers, the parameters of Table 8.3 were used for both transducers in our EAM model.

Table 8.3 Input parameters for the electroacoustic measurement model

Computation number		70F5	70F6	69B1	69A2	69A1
Crystal	**Density** ρ_T (kg/m^3)	4000	4000	2650	6750	6750
	Permitivity $\varepsilon/\varepsilon_0$	1000	1000	200	1000	1000
	Radius r (mm)	6.35	6.35	6.35	6.35	6.35
	Pulse width (ns)	41.67	41.67	16.67	50	50
	Velocity v (m/s)	4650	4650	3849	4000	4000
	Thickness (mm)	0.1938	0.1938	0.0642	0.2	0.2
	Stiffness (c^D)(10^9 N/m^2)	86.49	86.49	39.260	108	108
	Stiffness (c^E) (10^9 N/m^2)	75.895	75.895	38.523	69.12	69.12
	Piezo constant e(N/m)	9.6832	9.6832	1.142	18.55	18.55
	Clamped capacitance(pF)	5.787	5.787	3.4958	5.605	5.605
	Clamped impedance(Ω)	2.292	2.292	1.5176	2.839	2.839
Pulser/ receiver	Z_i^e or Z_o^e (Ω)	45.84	2.865	1.5175	2.839	79.77
Backing	**Density** ρ (kg/m^3)	4000	4000	n.a.	5000	5000
	Velocity v (m/s)	4650	4650	n.a.	4600	4600
Wear plate	Thickness (mm)	n.a.	n.a.	n.a.	0.025	0.025
	Density ρ (kg/m^3)	n.a.	n.a.	n.a.	3937	3937
	Velocity v (m/s)	n.a.	n.a.	n.a.	10160	10160
Acoustic medium	**Density** ρ (kg/m^3)	4000	4000	2000	4000	4000
	Velocity v (m/s)	4650	4650	4150	4325	4325

8.3.4 Simulation results

The parameters listed in Table 8.3 were used as inputs to the EAM model. A number of quantities given by Papadakis to characterize the transducer response were calculated:

A_{max} (V), the amplitude of the largest half-cycle in the calculated wave response.

dB_{loop} (dB), the loop response of the transducer, i.e., $20 \log_{10}(1 / A_{max})$.

f_M (MHz), the frequency of maximum spectrum response.

f_c (MHz), the center frequency midway between the 3dB points in the spectrum.

f_c/f_0, the ratio indicating frequency pulling toward lower frequencies.

BW (%), the percentage bandwidth between the 3dB points in the spectrum.

The simulation results are given in Table 8.4. For every item, the first value listed was copied from Papadakis' paper for comparison purpose and the second value (in italics) gives the results obtained from the EAM model.

From Table 8.4 we see that our assumptions led to transducer characteristics relatively close to those of Papadakis in some cases and far off in others. In the first three cases listed in Table 8.4 (70F5, 70F6 and 69B1) the two models predict very similar values for the frequency at the maximum spectral amplitude, f_M, and the bandwidth, BW, while the other two cases (69A2 and 69A1) show poor agreement in these variables. The waveforms

Table 8.4 Comparison of results

Computation number	70F5	70F6	69B1	69A2	69A1
A_{max} (V)	0.012 *0.00597*	0.057 *0.0290*	0.025 *0.0133*	0.037 *0.0681*	0.308 *0.012*
dB_{loop} (dB)	38.4 *44.48*	25 *30.76*	32.0 *37.53*	28.6 *23.3*	10.3 *38.1*
f_M (MHz)	2.6 *2.34*	8.6 *7.42*	27.5 *26.36*	7.3 *5.46*	6.6 *1.17*
f_c (MHz)	4.7 *3.9*	9.1 *7.91*	28.5 *26.36*	7.3 *6.05*	6.7 *3.51*
f_c/f_0	0.39 *0.325*	0.76 *0.659*	0.95 *0.879*	0.73 *0.605*	0.67 *0.351*
BW (%)	167 *170*	95 *91.4*	41 *51.8*	39 *200*	25 *109.7*

calculated by the EAM model for the first three cases (70F5, 70F6 and 69B1) are shown in Figures 8.15, 8.16, and 8.17, respectively. They are very similar in form to the corresponding waveforms given by Papadakis but the EAM model amplitudes differ by about a factor of two (Papadakis' amplitudes are larger). For the other two cases (69A2 and 69A1) there is very poor agreement between the EAM model and the Papadakis model for both the

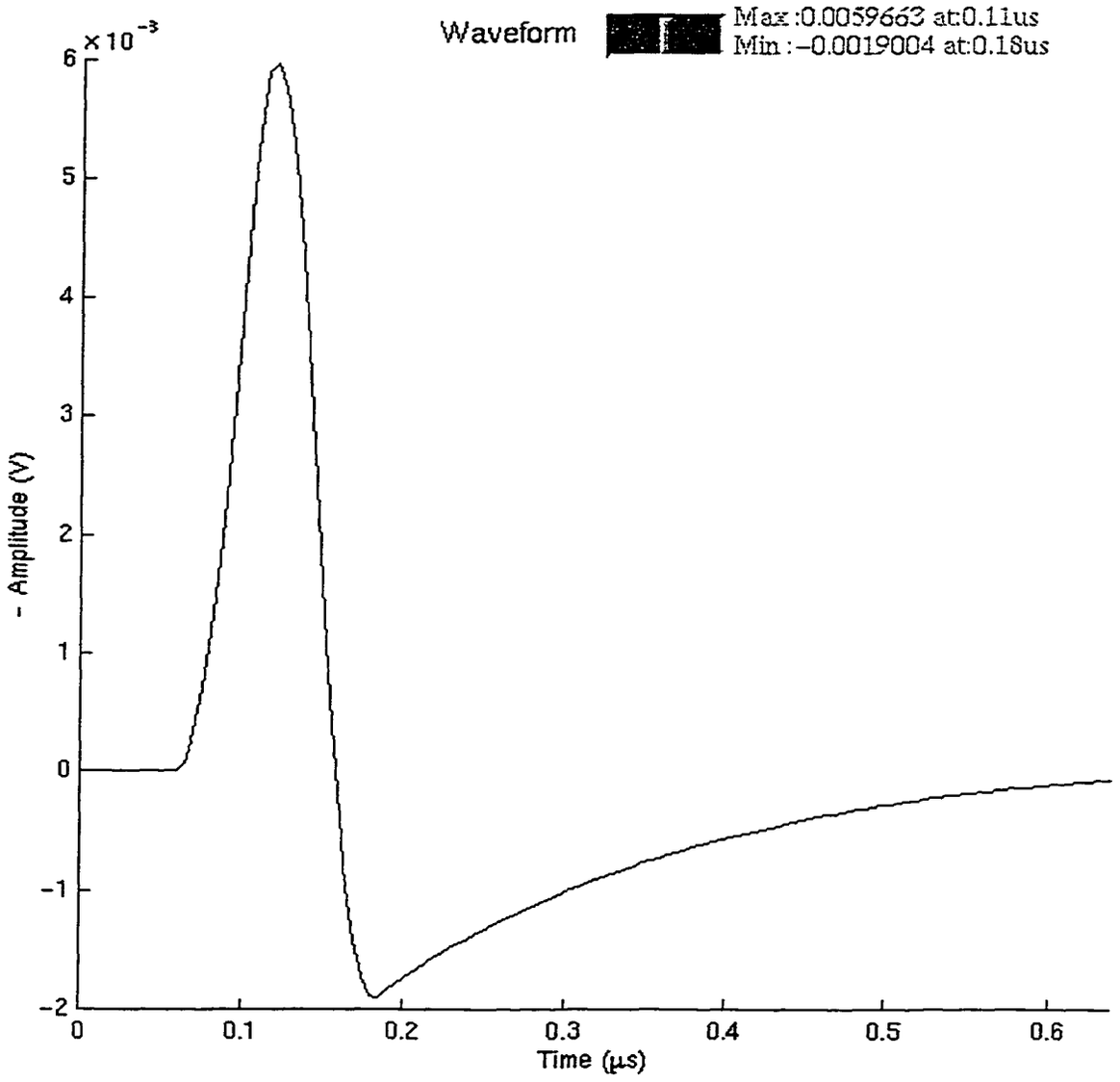

Figure 8.15 Waveform for case 70F5 which is similar to Figure 5a in [Papadakis, 1983].

amplitude and the waveform shape (see Figures 8.18 and 8.19). Many of the differences are due to the uncertainty in guessing the appropriate EAM model parameters, but with the information available these results were the best we were able to obtain.

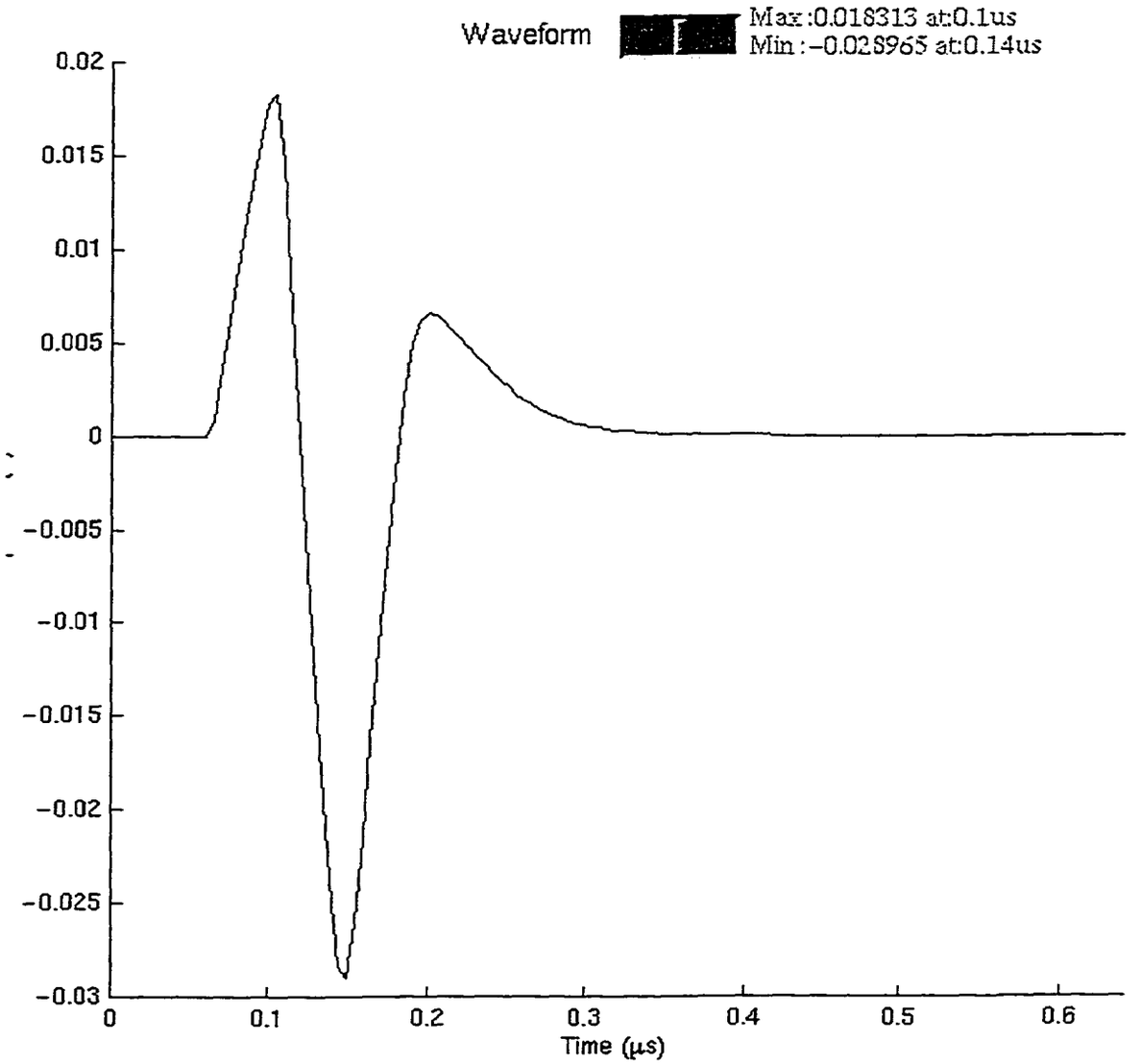

Figure 8.16 Waveform for case 70F6 which is similar to Figure 5b in [Papadakis, 1983].

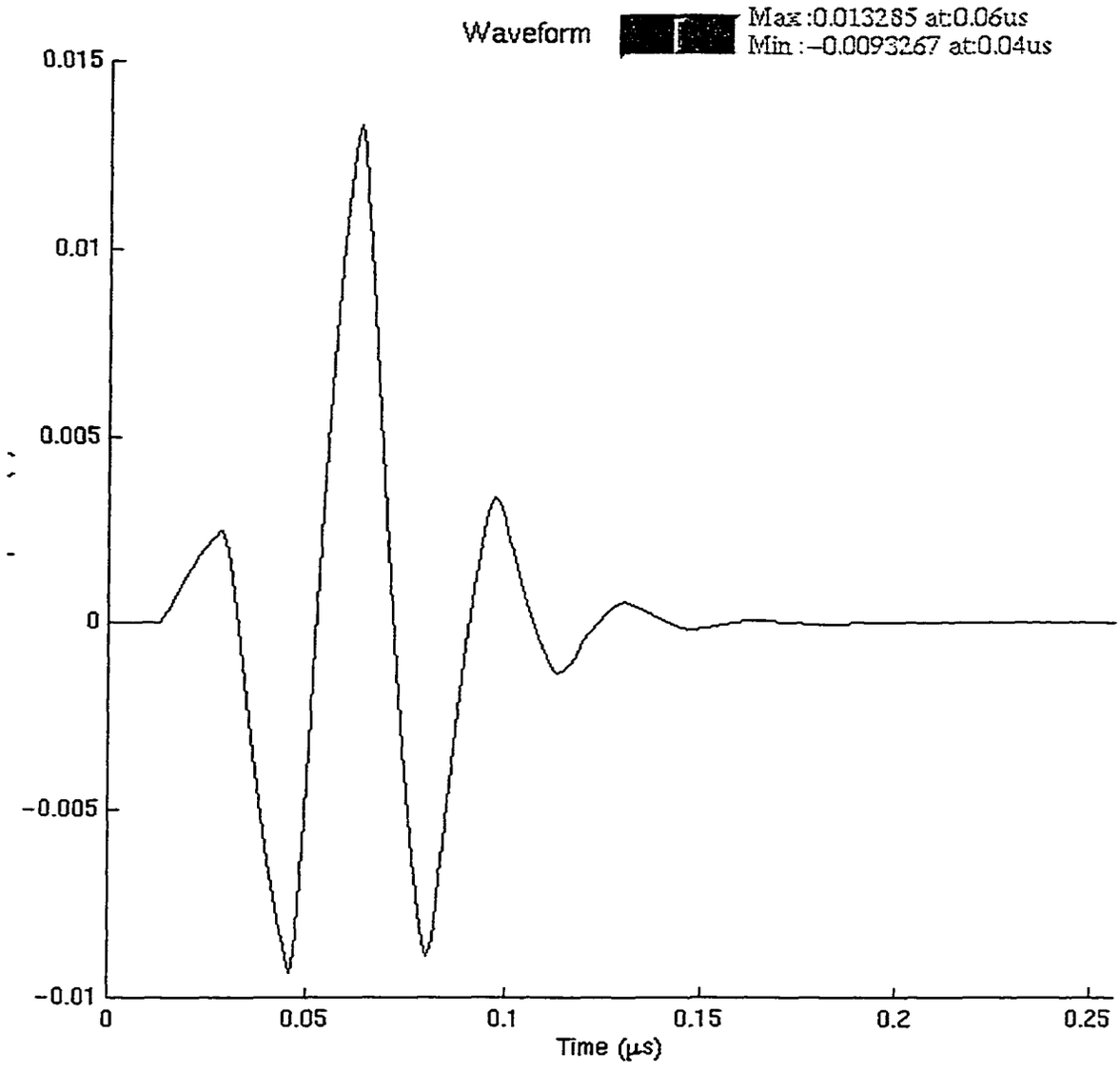

Figure 8.17 Waveform for case 69B1 which is similar to Figure 5c in [Papadakis, 1983].

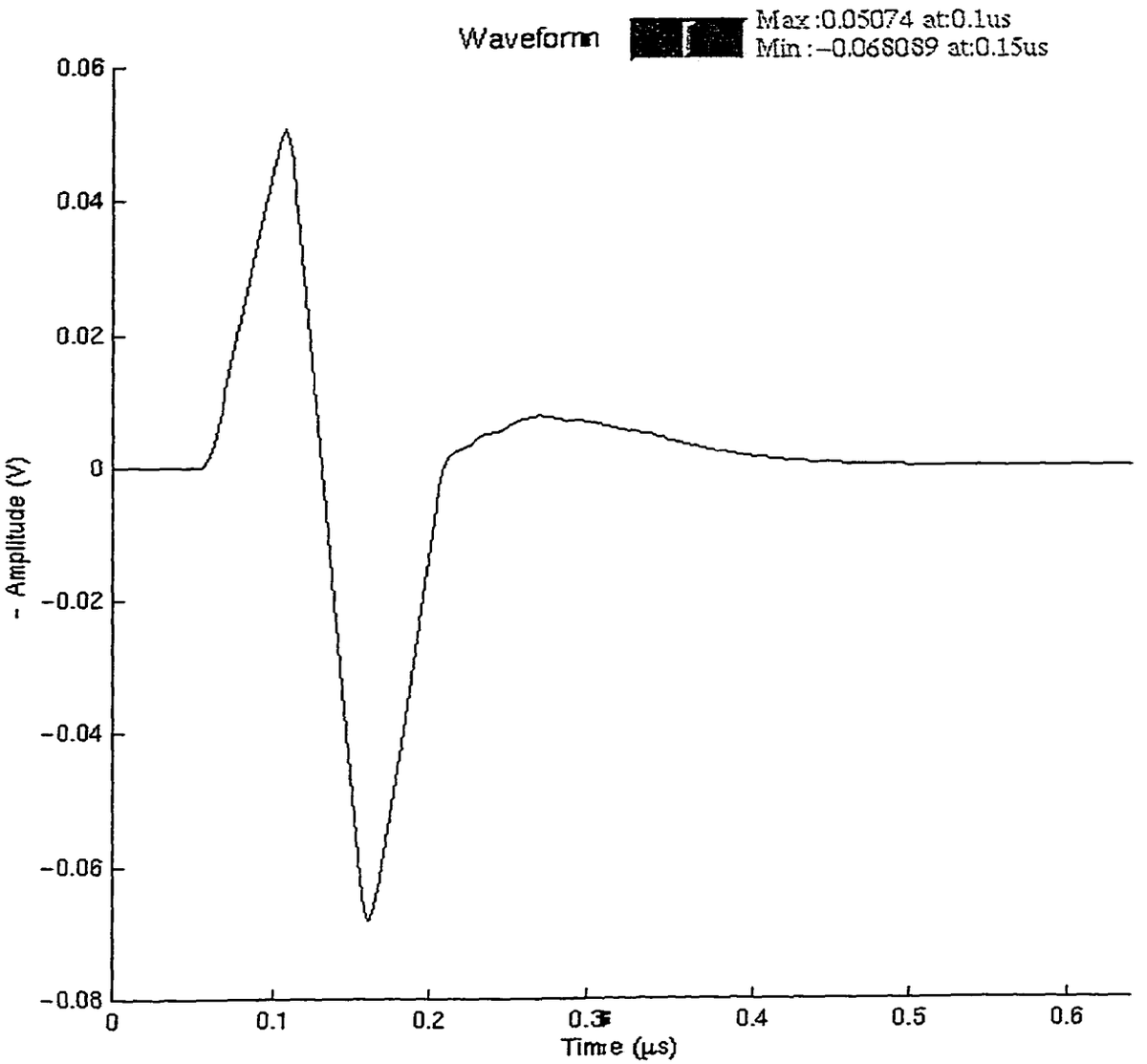

Figure 8.18 Waveform for case G9A2 which is much different from Figure 5d in [Papadakis, 1983].

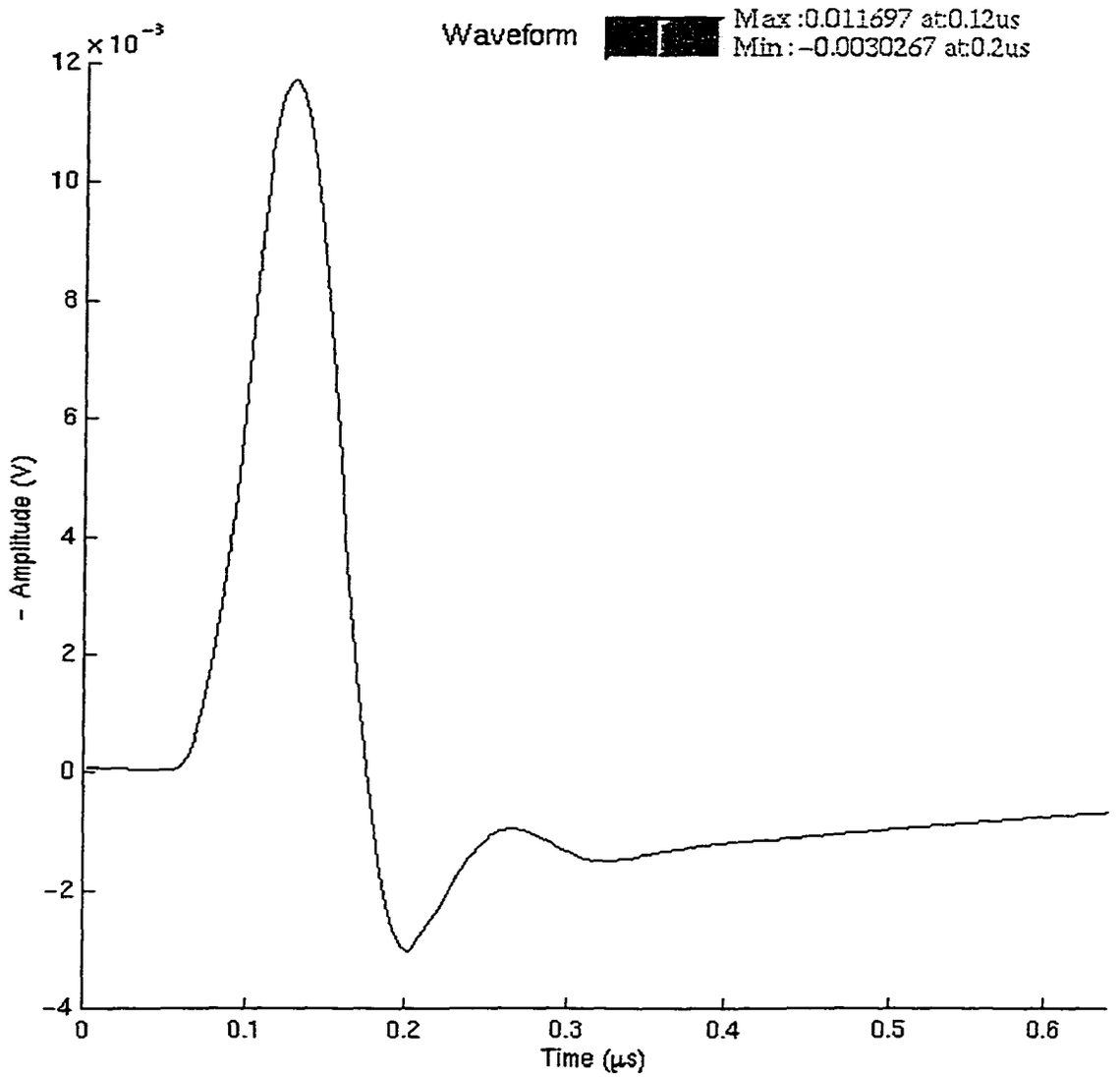

Figure 8.19 Waveform for case 69A1 which is much different from Figure 5e in [Papadakis, 1983].

CHAPTER 9. CHARACTERIZATION OF ULTRASONIC SYSTEM COMPONENTS

In Chapter 7 we discussed all the elements of the EAM model in detail. For modeling studies of the kind conducted in Chapter 8, we needed to have all the system parameters contained in the EAM model. For the transducer, for example, we needed to know the crystal properties, backing and wear plate properties, signal conditioning circuits (if any), etc. However, if we are going to experimentally characterize an ultrasonic immersion measurement system assembled from commercial components it is unlikely that we can obtain all of these underlying parameters. Thus, we need to model the system in terms of a smaller set of quantities that are practical to measure.

In this chapter we will describe measurement procedures that will allow us to completely characterize an ultrasonic measurement system using purely electrical measurements. Figures 6.1 and 6.2 in Chapter 6 illustrate the system model on which we will base our experimental characterization procedures. The pulser will be modeled as a Thevenin equivalent source and internal impedance as shown in Figure 6.1. The cabling will be modeled as a transmission line, which can be characterized by the four elements of a 2x2 transfer matrix. The transducer also can be characterized by a 2x2 transfer matrix, as given in Figures 6.1 and 6.2. However, in modeling the generation and reception processes in Chapter 6 we also showed that these transfer matrix elements appear only in combinations that can be represented by three quantities. Those three quantities were: the input electrical impedance of the transducer acting as a transmitter, the open-circuit, blocked force receiving sensitivity, and the transducer radiation acoustic impedance. Since the radiation acoustic impedance here will be taken as its high frequency value for a piston transducer, which is assumed known, only the transducer input electrical impedance and sensitivity parameters need to be determined experimentally in order to characterize the transducer(s) part of the system response. Finally, the receiver will be modeled as both an impedance and a gain factor (Figure 6.2). We will assume the acoustic transfer function, $t_A = F_B / F_t$, which relates the blocked force input, $F_B(\omega)$, at the receiver (Figure 6.2) to the force output, $F_t(\omega)$, of the transmitter (Figure 6.1), can be modeled explicitly so that we do not need to discuss experimental characterization procedures for that function.

9.1 Pulser Characterization

A pulser generates the electrical impulses that drive the transmitting ultrasonic transducer. The internal structure of the pulser is very complex but in general we do not need to model in detail that complexity. Instead, we can replace the pulser circuits by the Thevenin equivalent circuit shown in Figure 9.1 whose properties can be determined experimentally using the following method.

9.1.1 Measurement principle

Let the source strength of a pulser be $V_i(\omega)$ and let its internal electrical impedance be $Z_i^e(\omega)$. We will obtain these two quantities through the following measurements.

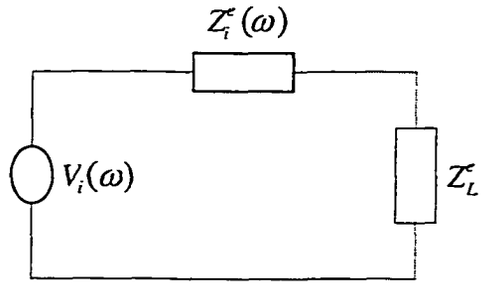

Figure 9.1 An electrical pulser is modeled by the Thevenin equivalent circuit with the source strength of $V_i(\omega)$ and the internal impedance of $Z_i^e(\omega)$.

First, the source strength, $V_i(\omega)$, can be obtained by measuring the open-circuit voltage at the outlet of the pulser. According to the definition of the Thevenin equivalent circuit, the open-circuit voltage is the source strength. To obtain this strength we sample the output electrical impulse of the pulser in the time domain and perform a fast Fourier transform (FFT) on it to obtain $V_i(\omega)$.

After the source strength $V_i(\omega)$ has been measured, it is taken as a known quantity and used to compute the internal electrical impedance, $Z_i^e(\omega)$. We connect a known load, Z_L^e, at the output end of the pulser, and measure the voltage drop, $V_L(t)$, across Z_L^e in the time domain. Again, we take the FFT on $V_L(t)$ to get the voltage $V_L(\omega)$ in the frequency domain. From Figure 9.1, it follows that

$$V_L(\omega)=\frac{Z_L^e}{Z_L^e+Z_i^e(\omega)}V_i(\omega). \qquad (9.1.1)$$

Then the internal electrical impedance is obtained as

$$Z_i^e(\omega)=\left(\frac{V_i(\omega)}{V_L(\omega)}-1\right)Z_L^e. \qquad (9.1.2)$$

9.1.2 Procedure and results

The pulser strength and internal electrical impedance are controlled by the energy level setting and the damping setting. Different energy level settings and damping settings will produce the Thevenin equivalent circuit of the pulser with different strengths and internal electrical impedances.

On the front panel of the 5052PR, there are four energy levels, from energy 1 to energy 4 and there are 11 damping settings from 0 to 10. We chose to model the pulser at all four energy levels and three damping settings, damping 0, damping 5 and damping 10. The combination of these two settings gives 12 different Thevenin equivalent sources and impedances.

At each setting, we first measured the open-circuit voltage, which is taken as the source strength of the pulser. We then used three different external impedances to measure the internal electrical impedance according to Eq. (9.1.2). The external impedances used were a 50Ω terminator, an 82Ω resistor, and a 220Ω resistor. For each of these impedances, we measured the internal impedance of a given setting. The reason for choosing these different external impedances was to study whether the internal impedance of the Thevenin equivalent circuit is dependent on the external impedance. Theoretically, the Thevenin equivalent circuit of a pulser should not depend on these external conditions, but our results below do show some dependency is present.

Figures 9.2-9.5 show the measured Thevenin equivalent sources and impedances for the different energy and damping settings. The left column in each figure shows the magnitude of source strength and right column shows the corresponding magnitude of the internal electrical impedances measured by using the three external impedances.

Figure 9.2 illustrates the measurements for energy 1 and dampings of 0, 5 and 10. Figure 9.3 illustrates the measurements for energy 2 and dampings of 0, 5 and 10. Figure 9.4 illustrates the measurements for energy 3 and dampings of 0, 5 and 10. Figure 9.5 illustrates the measurements for energy 4 and dampings of 0, 5 and 10.

From these figures, the following conclusions can be drawn.

a. The internal electrical impedance is a function of frequency. This behavior is not considered in many modeling studies which treat this impedance as a pure resistance.

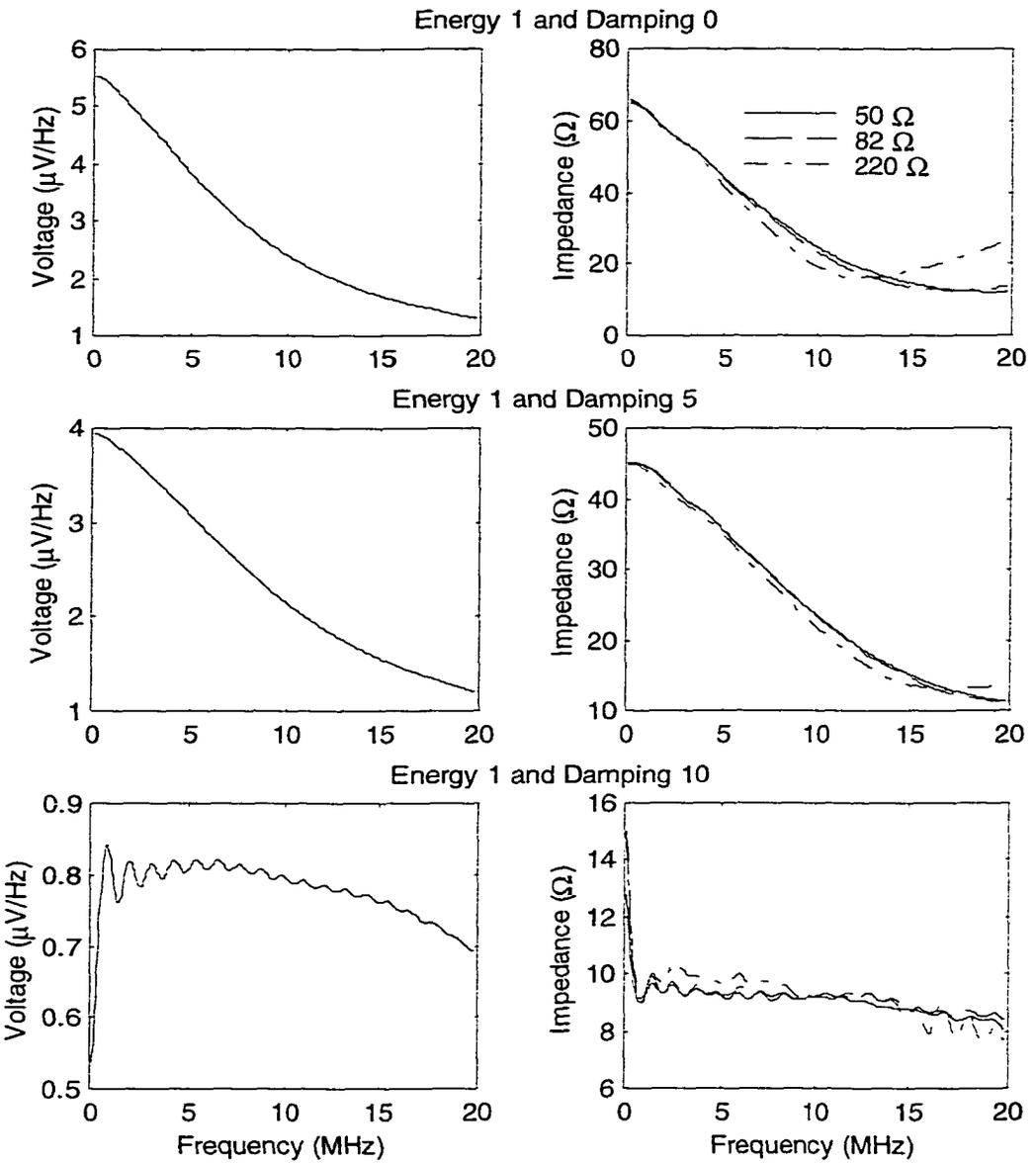

Figure 9.2 Equivalent source measurements for energy 1 and dampings of 0, 5 and 10. The left column shows the source strengths and the right column shows the internal electrical impedances for different external impedances of 50Ω (solid lines), 82Ω (dashed lines) and 220Ω (dotted dashed lines).

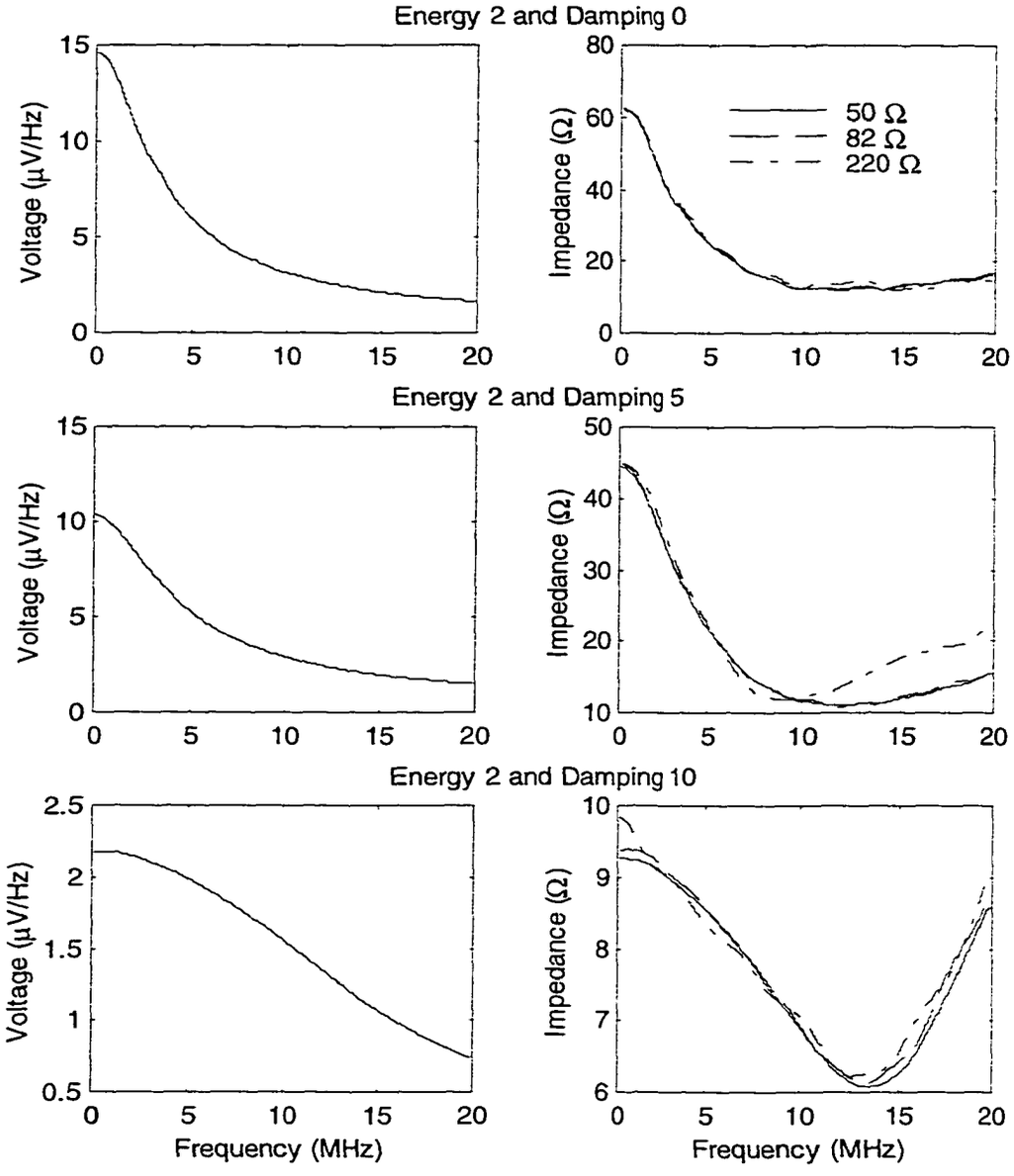

Figure 9.3 Equivalent source measurements for energy 2 and dampings of 0, 5 and 10. The left column shows the source strengths and the right column shows the internal electrical impedances for different external impedances of 50Ω (solid lines), 82Ω (dashed lines) and 220Ω (dotted dashed lines).

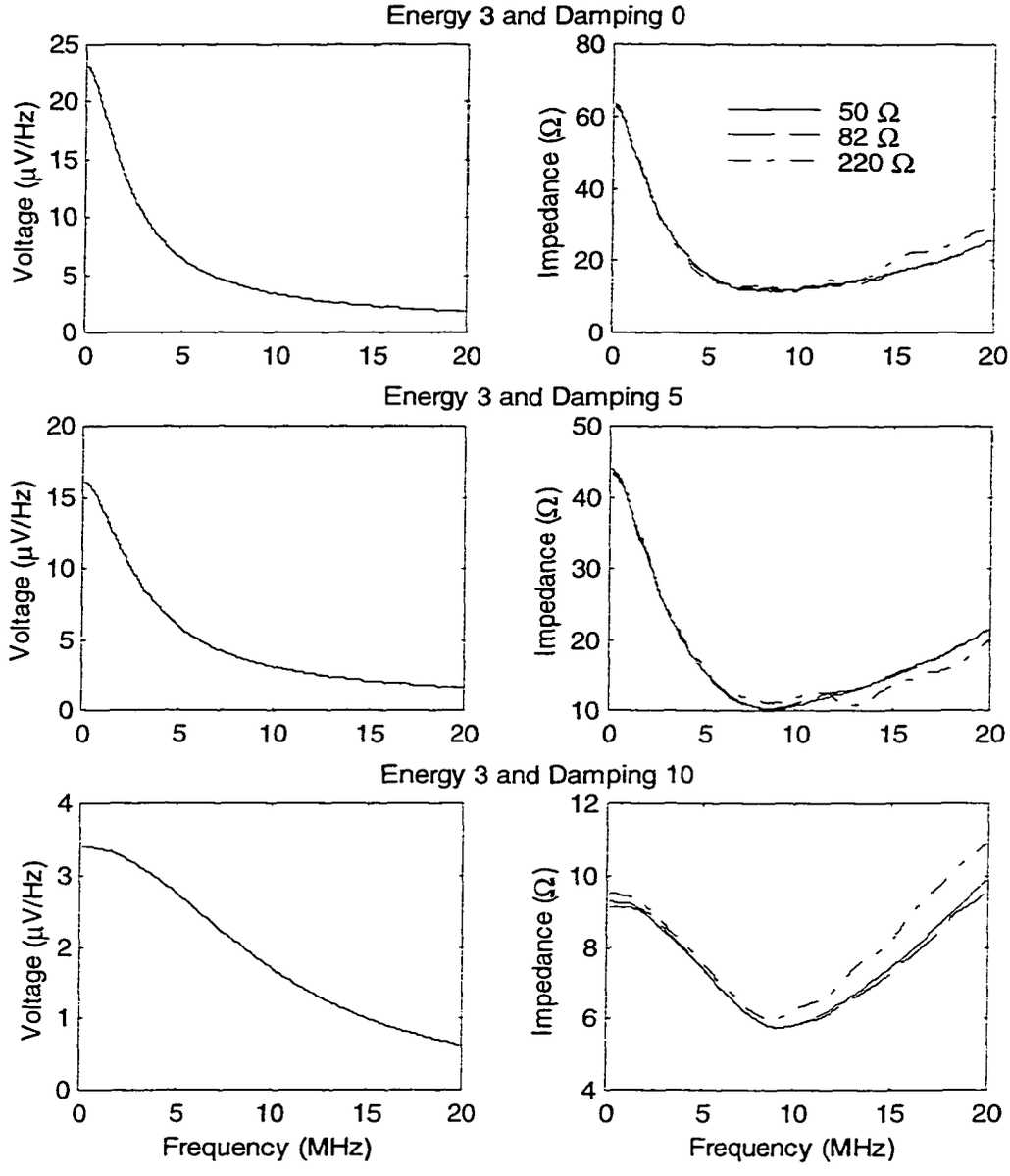

Figure 9.4 Equivalent source measurements for energy 3 and dampings of 0, 5 and 10. The left column shows the source strengths and the right column shows the internal electrical impedances for different external impedances of 50Ω (solid lines), 82Ω (dashed lines) and 220Ω (dotted dashed lines).

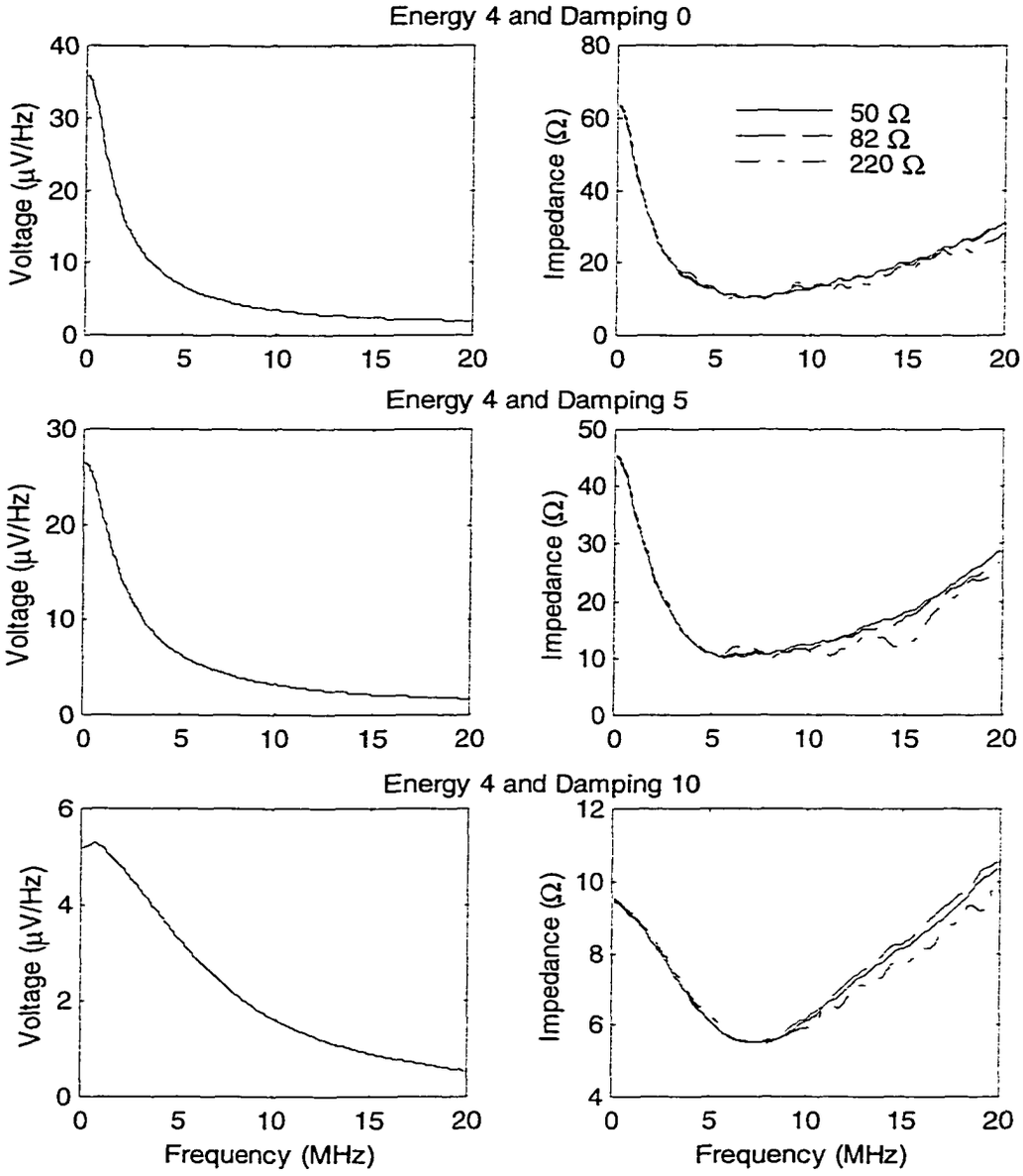

Figure 9.5 Equivalent source measurements for energy 4 and dampings of 0, 5 and 10. The left column shows the source strengths and the right column shows the internal electrical impedances for different external impedances of 50Ω (solid lines), 82Ω (dashed lines) and 220Ω (dotted dashed lines).

b. For a specific energy and damping setting, the internal impedance is dependent somewhat on the external impedance.

c. At a given energy level, increasing the damping lowers the internal impedance and the equivalent source strength.

d. A higher damping gives a wider bandwidth for the source strength.

e. At a given damping setting, a higher energy level gives a higher source strength. The internal impedance also changes with energy level.

9.2 Receiver Characterization

The receiver port of the pulser/receiver is used to receive, amplify and modify the electrical signals from the receiving transducers (see Figure 4.1). On the front panel of the receiver, there are three controls labeled Gain, Attn and Damping. The Gain control is a coarse amplification factor control. It has two positions: 20dB and 40dB. The Attn control is a finer control which changes the attenuation of the received signals from 0-60dB with a step of 2dB. The combination of these two controls gives many possible amplification factor setting of the receiver. Note that the amplification factor could be negative in dB. The third control is the Damping which has 11 positions from 0 to 10. In a pulse-echo mode, it controls the receiving load. In a pitch-catch mode, it should not affect the receiving load. There is also a frequency filter control on the receiver, but this was left "off" in all of the following studies.

9.2.1 Measurement principle

As discussed in section 4.3 in Chapter 4, the receiver is modeled by two factors: the input electrical impedance, or the receiving load, $Z_o^e(\omega)$, and the amplification factor $K(\omega)$. The model of the receiver is depicted in Figure 4.12. Suppose that the input voltage and current, (V_o, I_o), are both measured, together with the output voltage, V_R. Then the amplification factor can be found as (Eq. (4.3.1))

$$K(\omega) = \frac{V_R(\omega)}{V_o(\omega)} \tag{9.2.1}$$

and the receiving load is obtained as

$$Z_o^e(\omega) = \frac{V_o(\omega)}{I_o(\omega)} \tag{9.2.2}$$

where $K(\omega)$ and $Z_o^e(\omega)$ are generally functions of frequency.

9.2.2 Procedure and results

The measurement setup is shown in Figure 9.6. The receiving transducer sends signals to the receiver via a cable. The quantities to be measured are the input voltage V_o and input current I_o in front of the receiver and the output voltage V_R after the receiver. The two voltages, V_o and V_R, were measured using a sampling oscilloscope (Waverunner, LT 342 series). The current I_o was measured by a current probe. It was a CT-2 current probe from Tektronix and is shown in Figure 9.7. The CT-2 current probe is a high frequency current transformer for dynamic current measurement. It has the bandwidth of 1.2kHz to 200MHz. Its sensitivity is 1mV/mA when it is terminated in 50Ω. Figure 9.7(a) illustrates the schematic diagram of a current probe and Figure 9.7(b) illustrates its photo. To measure the current through a conductor, the current probe has a small hole through which the current carrying conductor is passed during circuit assembly.

The amplitude of the current I_o is usually small, so an amplifier, outside of the current probe, is used to amplify the signal. The amplified current is sampled at a sampling frequency of 500MHz using the sampling oscilloscope. To guarantee that V_o and I_o are the voltage and current directly imposed on the receiver, the measuring points need to be as close as possible to the receiver.

After the signals V_o, I_o and V_R were sampled and stored, the FFT was taken to obtain their spectra. Eqs. (9.2.1) and (9.2.2) then were used to compute the electrical load $Z_o^e(\omega)$ and the amplification factor $K(\omega)$ for the receiver.

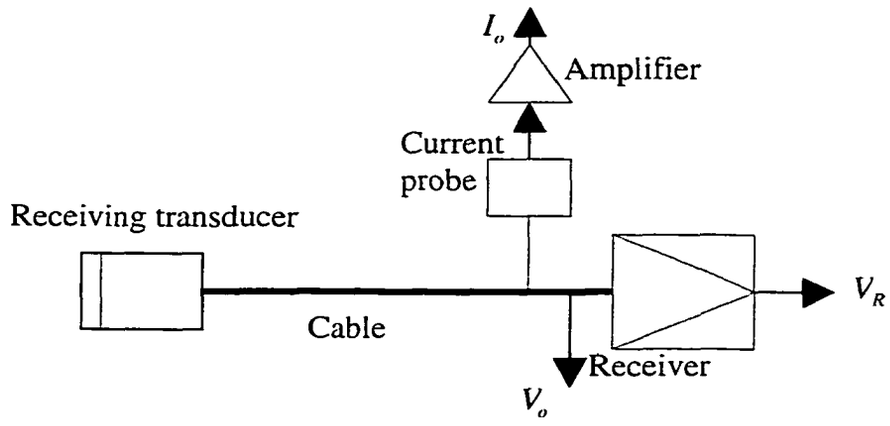

Figure 9.6 Measurement setup of an electrical receiver. The three quantities to be measured are the input voltage V_o, input current I_o and the output voltage V_R.

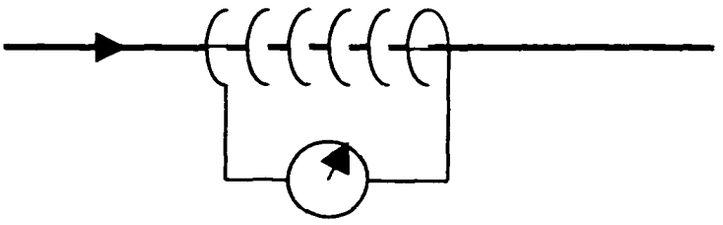

(a)

(b)

Figure 9.7 Current probe (CT-2 Tektronix) measuring input current I_o. (a) Schematic diagram, and (b) photo of the current probe.

We performed these measurements using three ultrasonic transducers with the nominal frequencies of 2.25MHz, 5MHz and 10MHz. This choice allowed us to examine $Z_o^c(\omega)$ and $K(\omega)$ over a wide frequency range. During the experiment, we operated in a pitch-catch mode and set Damping 0, Gain 20dB and Attn 0dB. The energy level was set to be 1 for the 2.25MHz transducer and 4 for the 5MHz and 10MHz transducers.

Figures 9.8-9.10 show the results obtained for the amplitude factor and receiving load as a function of frequency using the three transducers.

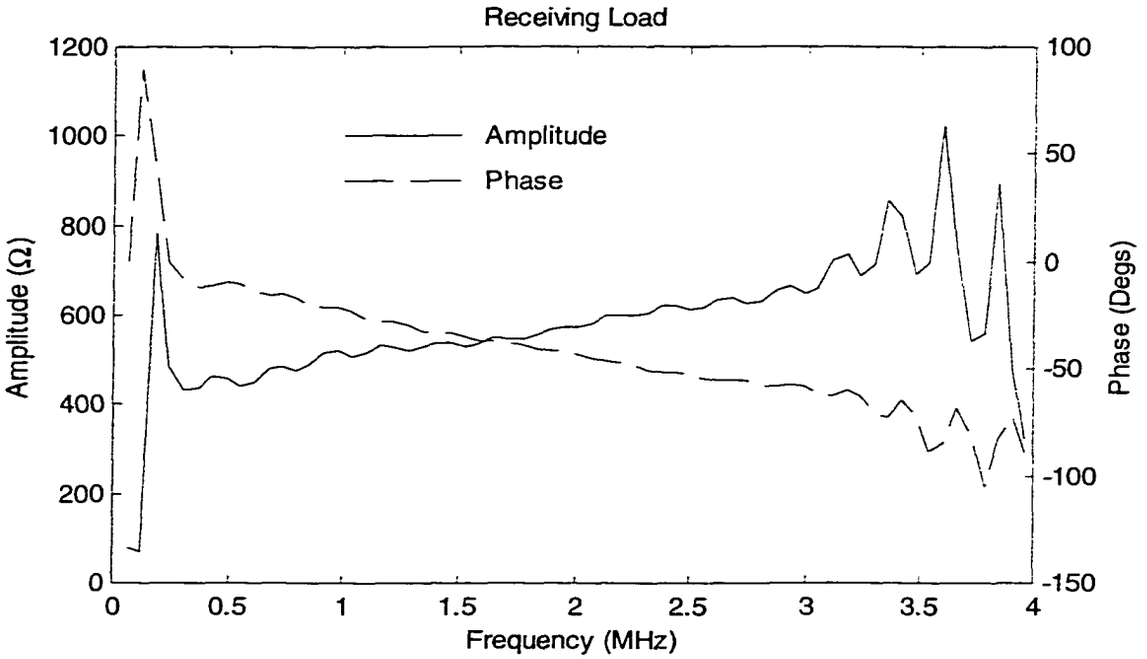

(a)

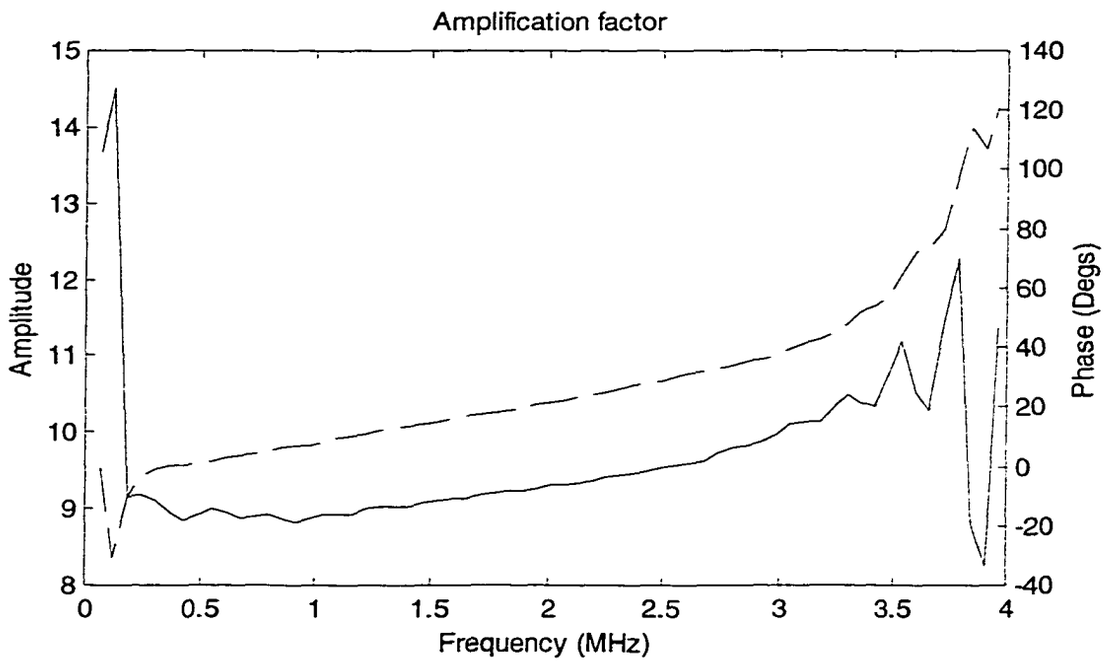

(b)

Figure 9.8 Measurements of receiver using 2.25MHz transducer with solid lines for amplitude and dashed lines for phase (energy 1, damping 0, Gain 20dB and Attn 0dB). (a) Receiving load and (b) Amplification factor.

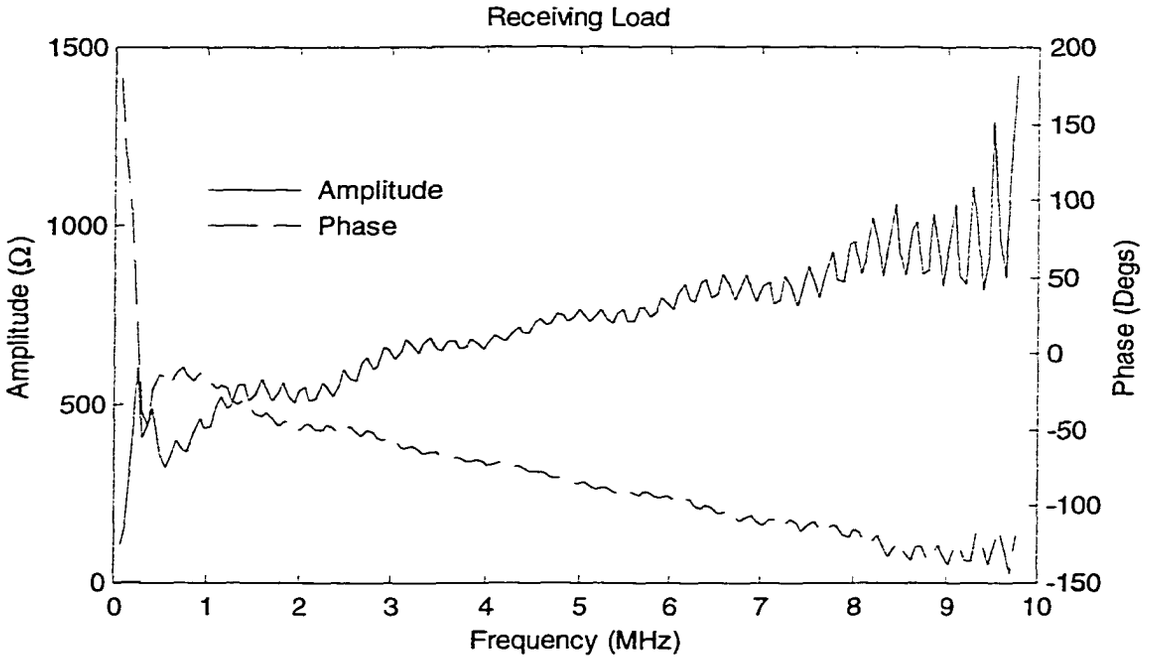

(a)

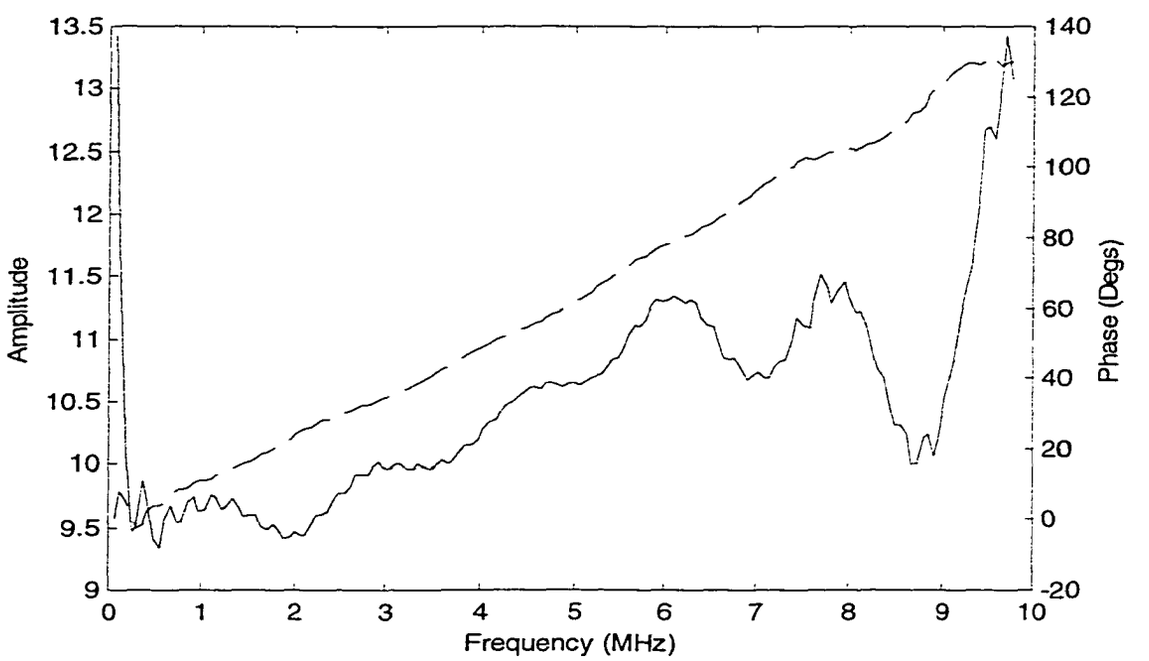

(b)

Figure 9.9 Measurements of receiver using 5MHz transducer with solid lines for amplitude and dashed lines for phase (energy 4, damping 0, Gain 20dB and Attn 0dB). (a) Receiving load and (b) Amplification factor.

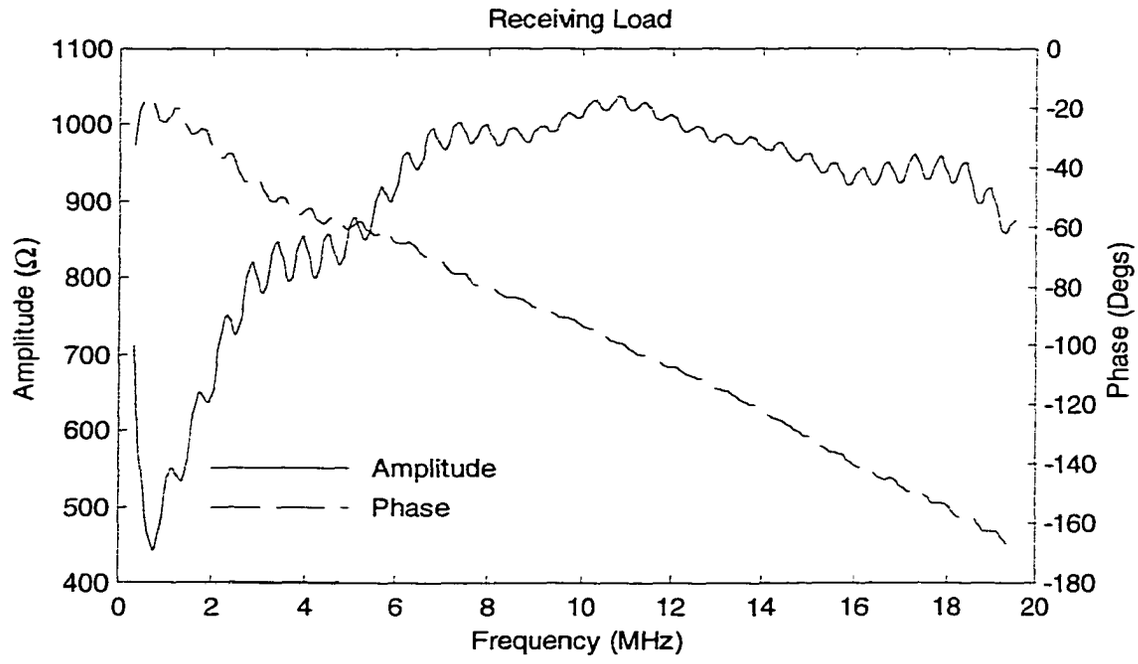

(a)

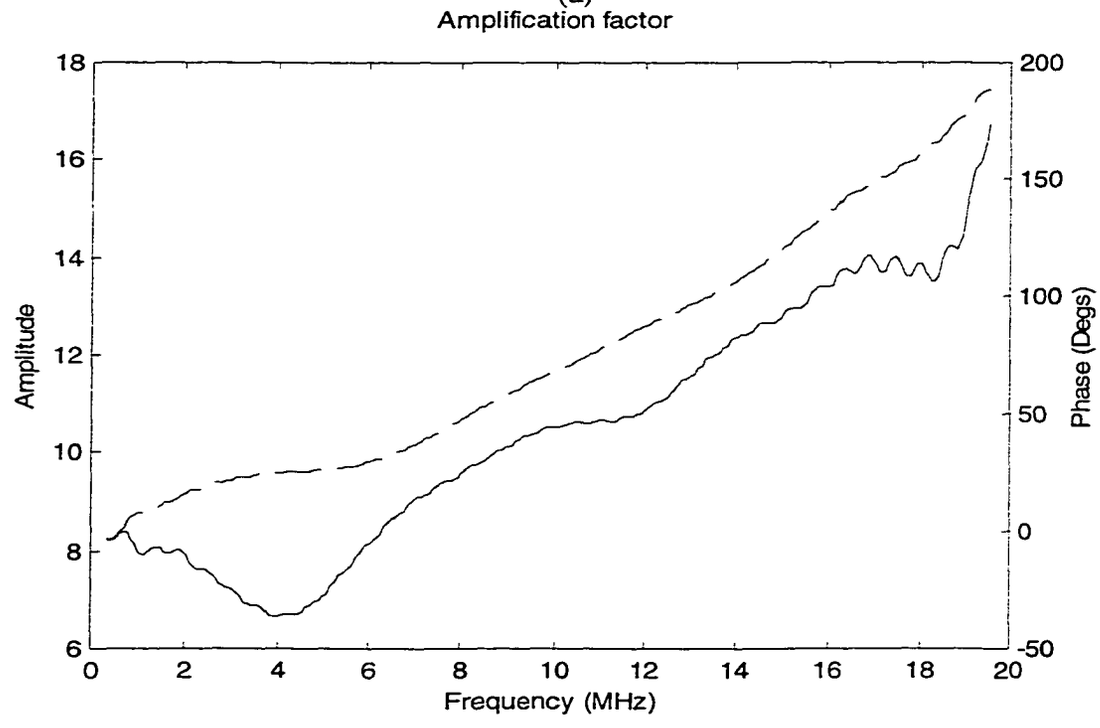

(b)

Figure 9.10 Measurements of receiver using 10MHz transducer with solid lines for amplitude and dashed lines for phase (energy 4, damping 0, Gain 20dB and Attn 0dB). (a) Receiving load and (b) Amplification factor.

From those curves, we can make the following observations.

a. The receiving load is a complex impedance rather than a pure resistance.

b. As the frequency increases, the receiving load increases from 500Ω at 1MHz to 1000Ω at 12MHz.

c. The amplification factor of the receiver is not just a constant value of 10, as would be expected from the 20dB setting. However, these changes are not large, with the effective gain changing from 19dB to 23dB in going from 0-20MHz.

9.3 Cabling Characterization

Cabling is a necessary part of any ultrasonic measurement system. To operate an ultrasonic transducer easily, a flexible cable is used to transit signals between the transducer and a pulser or a receiver. In an immersion test, cabling is run through the fixture rod, which holds the transducer. If a cable is considered as an ideal transmission line, its transfer matrix is described by Eq. (3.2.1) which contains sine and cosine functions. However, we also can describe the cabling more generally as a two port system as shown in Figure 9.11. The two-port system is characterized by the transfer equation:

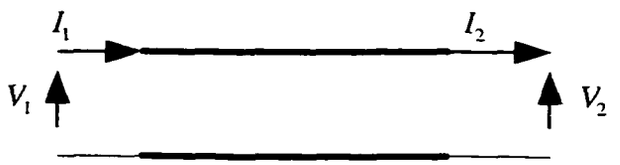

Figure 9.11 Cabling considered as a transmission line with the transfer matrix shown in Eq. (9.3.1).

$$\begin{Bmatrix} V_1 \\ I_1 \end{Bmatrix} = \begin{bmatrix} T_{11}^C & T_{12}^C \\ T_{21}^C & T_{22}^C \end{bmatrix} \begin{Bmatrix} V_2 \\ I_2 \end{Bmatrix} \tag{9.3.1}$$

where (V_1, I_1) are input voltage and current and (V_2, I_2) are output voltage and current. The transfer matrix of the cabling is written as

$$[T^C] = \begin{bmatrix} T_{11}^C & T_{12}^C \\ T_{21}^C & T_{22}^C \end{bmatrix}. \tag{9.3.2}$$

In practice, since the cabling could contain different cable components and connectors, we can not expect its transfer matrix to take the theoretical form shown in Eq. (3.2.1). This is not a problem since it is not difficult to measure directly the four components of the 2x2 transfer matrix.

9.3.1 Measurement principle

To measure all four elements of the cabling transfer matrix in Eq. (9.3.2), we let an electrical signal be imposed on port 1 and consider two termination conditions at port 2: open-circuit and short-circuit.

a. Open-circuit condition at port 2

If port 2 is opened, then

$$I_2 = 0. \tag{9.3.3}$$

Suppose that the voltage measurement at port 2 is V_∞. Then Eq. (9.3.1) is simplified as

$$\begin{cases} V_1 = T_{11}^C V_\infty \\ I_1 = T_{21}^C V_\infty \end{cases}. \tag{9.3.4}$$

By measuring the voltage V_1 and current I_1 at port 1 and the open-circuit voltage V_∞ at port 2, the two components T_{11}^C and T_{21}^C of the transfer matrix $\left[T^C\right]$ can be obtained from Eq. (9.3.4) as

$$T_{11}^C = \frac{V_1}{V_\infty} \tag{9.3.5}$$

$$T_{21}^C = \frac{I_1}{V_\infty}. \tag{9.3.6}$$

b. Short-circuit condition at port 2

If port 2 is shorted, this corresponds to

$$V_2 = 0. \tag{9.3.7}$$

Suppose that the current measurement at port 2 is I_S. Eq. (9.3.1) is simplified as

$$\begin{cases} V_1 = T_{12}^C I_S \\ I_1 = T_{22}^C I_S \end{cases}. \tag{9.3.8}$$

By measuring the voltage V_1 and current I_1 at port 1 and the short-circuit current I_S at port 2, the rest two components T_{12}^C and T_{22}^C of the transfer matrix $\left[T^C\right]$ can be obtained from Eq. (9.3.8) as

$$T_{12}^C = \frac{V_1}{I_S} \tag{9.3.9}$$

$$T_{22}^C = \frac{I_1}{I_S}. \tag{9.3.10}$$

From the above two extreme cases, the transfer matrix of a cabling is obtained. From Eq. (9.3.1), if an arbitrary load Z_L^c is connected at port 2, the input impedance at port 1 is expressed as

$$Z_{in}^c = \frac{V_1}{I_1} = \frac{T_{11}^C Z_L^c + T_{12}^C}{T_{21}^C Z_L^c + T_{22}^C}. \tag{9.3.11}$$

For an open-circuit condition, we have

$$Z_L^c \to \infty \tag{9.3.12}$$

then Eq. (9.3.11) gives

$$Z_\infty^c = \frac{T_{11}^C}{T_{21}^C} \tag{9.3.13}$$

which can also be obtained from Eq. (9.3.4). Theoretically, for an ideal transmission line, Z_∞^c is proportional to a cotangent function with 90 degrees phase shift (see Eq. (3.2.9)).

For a short-circuit condition, we have

$$Z_L^c \to 0 \tag{9.3.14}$$

then Eq. (9.3.11) gives

$$Z_S^c = \frac{T_{12}^C}{T_{22}^C} \tag{9.3.15}$$

which can also be obtained from Eq. (9.3.8). Theoretically, for an ideal transmission line, Z_S^c is proportional to a tangent function with -90 degrees phase shift (see Eq. (3.2.10)).

9.3.2 Procedure and results

The measurement setup is shown in Figure 9.12. The pulser used here was the 5052PR from Panametrics. The cabling to be calibrated was connected to that pulser. The end of the cable close to the pulser is called port 1 and the other end port 2. Our current probe (see Figure 9.7) was used to measure I_1 at port 1. The voltage V_1 at port 1 was measured using a sampling oscilloscope. The open-circuit voltage was also measured by the oscilloscope. Finally, the short-circuit current, I_s, also measured by the current probe. The cabling used in this study was a 1.5m long flexible 50Ω with BNC connectors at its ends.

The measuring procedure was as follows. Under the open-circuit condition, the voltage $V_1(t)$ and current $I_1(t)$ were measured in the time domain at port 1 and the open-circuit voltage $V_\infty(t)$ measured in the time domain at port 2. Then the FFT was taken on these measurements to obtain the corresponding spectra $V_1(\omega)$, $I_1(\omega)$ and $V_\infty(\omega)$. Eqs. (9.3.5) and (9.3.6) were used to compute T_{11}^C and T_{21}^C. Similarly, under the short-circuit condition, the

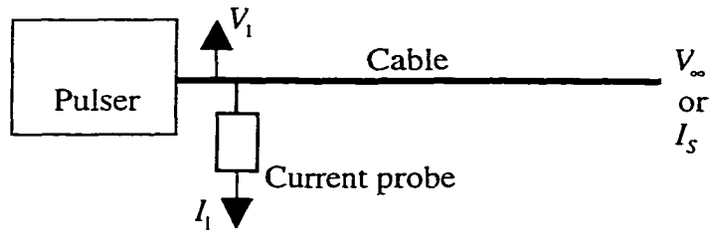

Figure 9.12 Measurement setup of cabling calibration. (V_1, I_1) are input voltage and current, V_∞ open-circuit voltage and I_S short-circuit current.

voltage $V_1(t)$ and current $I_1(t)$ were measured in the time domain at port 1 and the short-circuit voltage $I_S(t)$ measured in the time domain at port 2. The FFT of these measurements gave $V_1(\omega)$, $I_1(\omega)$ and $V_\infty(\omega)$. Eqs. (9.3.9) and (9.3.10) were used to compute T_{12}^C and T_{22}^C. In this manner, four components of the cabling transfer matrix $[T^C]$ could be obtained.

a. Cabling transfer matrix

Figure 9.13 shows the amplitude and phase curves for every component of the cabling transfer matrix $[T^C]$ in the frequency range of 0-20MHz. The amplitudes of the components are shown in the left column and their phases in the right column. As can be seen from Figure 9.13, the amplitudes of T_{11}^C and T_{22}^C do behave like a cosine function with a phase angle of about 0 degrees. The amplitudes of T_{12}^C and T_{21}^C, on the other hand, behave like sine functions with a phase angle of about -90 degrees. These results are consistent with an ideal transmission line made of the cable (see Eq. (3.2.1)).

b. Reciprocity check of the cabling transfer matrix

If the cabling is reciprocal, its transfer matrix satisfies

$$|T^C| = T_{11}^C T_{22}^C - T_{12}^C T_{21}^C \tag{9.3.16}$$

i.e., the determinant of the transfer matrix is unity.

Using the measured results for $[T^C]$ shown in Figure 9.13, the determinant of $[T^C]$ is shown in Figure 9.14. The magnitude of $|T^C|$ is shown by the solid line and its phase by the dashed line. The magnitude is indeed approximately 1 with an error no greater than 10%. The phase of |T| decreases as the frequency increases but always differs from zero by less than 5 degrees. These results show that the transfer matrix of the cabling does approximately satisfy the reciprocity theorem.

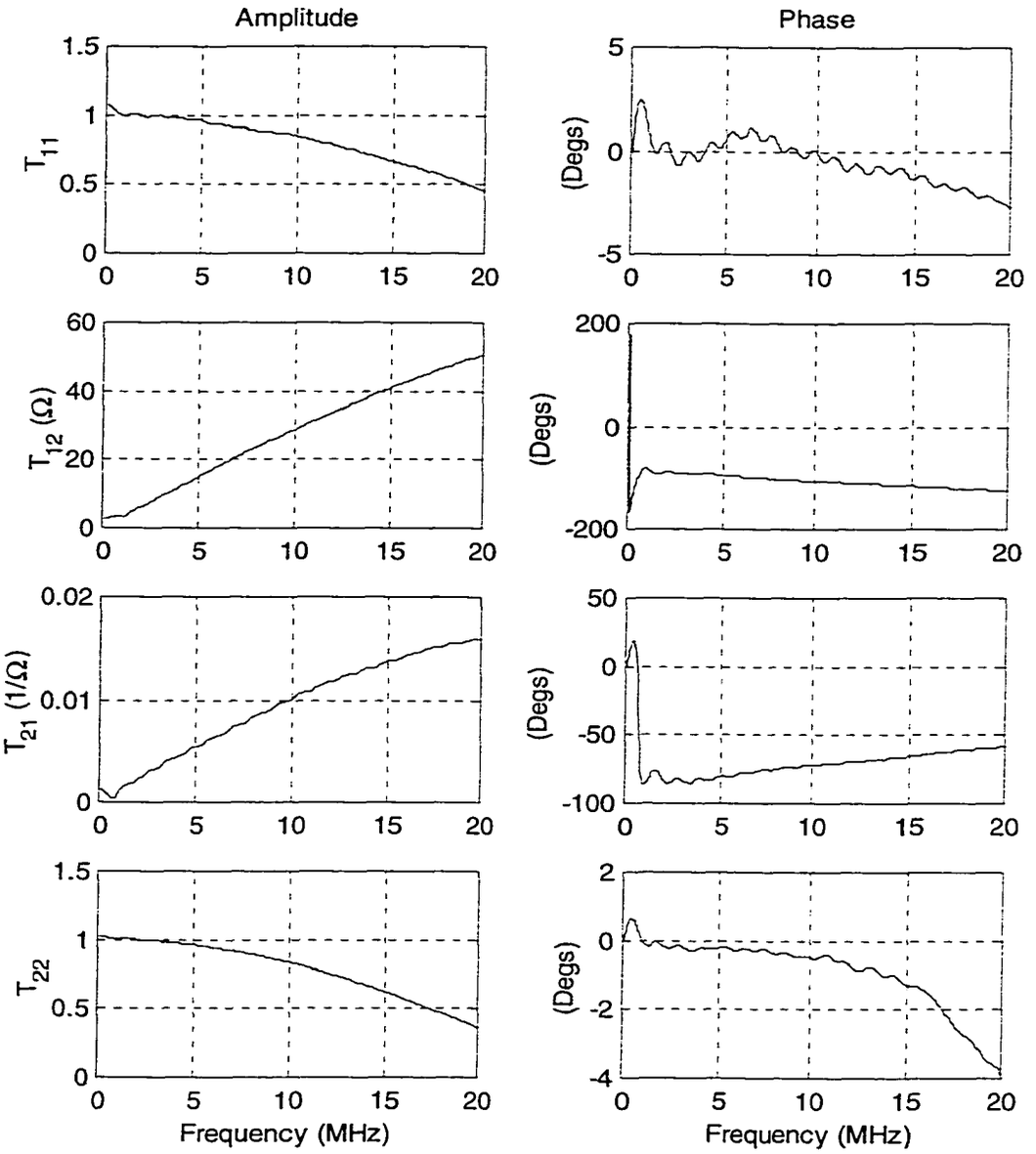

Figure 9.13 Measurements of the transfer matrix of a cable. The left column shows the amplitudes of the matrix components and the right one shows their phases. T_{11}^{C} and T_{22}^{C} present feature of a cosine function and T_{12}^{C} and T_{21}^{C} exhibit feature of a sine function.

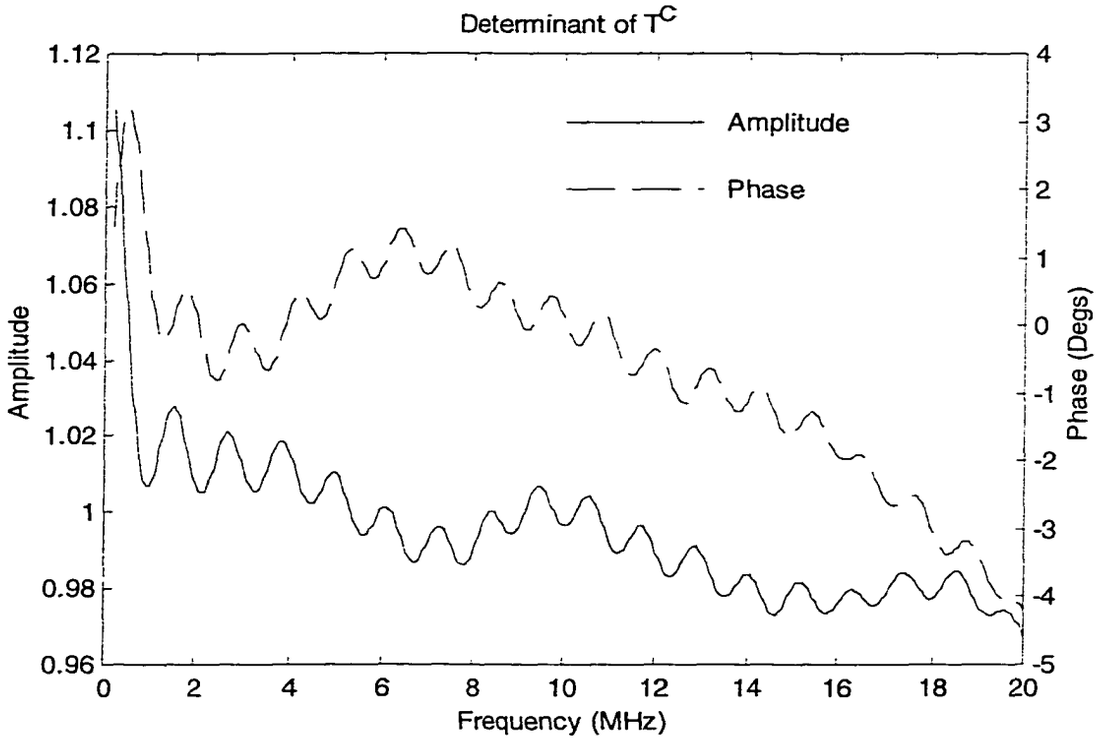

Figure 9.14 Reciprocity check of the cabling transfer matrix with the amplitude about 1 and the phase about 0.

c. Input impedance of the cabling

After we have obtained the transfer matrix of the cabling, we can use it to predict the input impedance of the cable when an arbitrary electrical load is connected to port 2 of the cabling. Eq. (9.3.11) shows the relation of the input impedance, Z_{in}^{e}, of the cabling and the electrical load, Z_{L}^{e}.

We plotted the input electrical impedances of the cabling under these conditions: 1) with port 2 opened, 2) with port 2 shorted and 3) with port 2 terminated with a 50Ω terminator. Figure 9.15 shows the three impedance curves. The upper graph gives their amplitudes and the lower one gives the phase changes.

The dashed lines in Figure 9.15 show the input electrical impedance of the cabling when port 2 is opened. Its magnitude of the impedance decreases with the increasing frequency. Its phase remains almost constant at a value of 90 degrees. Thus, the impedance does behave like the cotangent function predicted theoretically, i.e., $Z_{in}^{e} = iZ_{c}^{e} \cot kl$ (see Eq. (3.2.9)).

The dotted dashed lines in Figure 9.15 show the input electrical impedance of the cabling when port 2 is shorted. Its magnitude increases with the increasing frequency and its phase is now approximately -90 degrees. In these cases, the impedance behaves like the tangent function predicted theoretically, i.e., $Z_{in}^{e} = -iZ_{c}^{e}\tan kl$ (see Eq. (3.2.10)).

The solid lines in Figure 9.15 show the input electrical impedance of the cabling when port 2 is connected to a 50Ω terminator. The magnitude of the impedance always remains near 50Ω with a phase close to 0 degrees. From theory this behavior is expected since, if the impedance of the terminator at port 2 is equal to the intrinsic impedance of the cabling, the input electrical impedance at port 1 should also be equal to the intrinsic impedance.

There are some differences between these measured results and the ideal theoretical model from the lower graph in Figure 9.15. We see the phases for the three cases are not strictly constants but decrease slightly when the frequency increases. Also, we see from the plots of the magnitudes that the three curves in Figure 9.15 do not intersect at a single point as shown in Figure 3.8. One reason for these differences might be due to losses or other non-ideal behavior that is not accounted for in the simple theoretical model.

9.4 Transducer Characterization

An ultrasonic transducer, acting as either a transmitter or a receiver, can be characterized by its transfer matrix. Its transfer matrix is only dependent on the transducer itself and is not related to other conditions such as pulser, receiver and water path. To perform a "complete" characterization of a transducer, we would need to know explicitly all four components of the transducer transfer matrix $(T_{11}, T_{12}, T_{21}, T_{22})$. A possible calibration procedure to obtain those components was described in [Dang and Schmerr, 1999]. However, as shown in Chapter 6, the transducer(s) enter the generation and reception transfer functions only through three transducer quantities: the transducer input impedance, $Z_{in}^{e}(\omega)$, the transducer open-circuit, blocked force receiving sensitivity, $M_{VF_B}^{\infty}(\omega)$, and the transducer radiation acoustic impedance, $Z_{r}^{a}(\omega)$, where in terms of the transfer matrix components

$$Z_{in}^{e}(\omega) = \frac{Z_{r}^{a}T_{11} + T_{12}}{Z_{r}^{a}T_{21} + T_{22}} \tag{9.4.1}$$

and

$$M_{VF_B}^{\infty} = \frac{1}{Z_{r}^{a}T_{21} + T_{22}}. \tag{9.4.2}$$

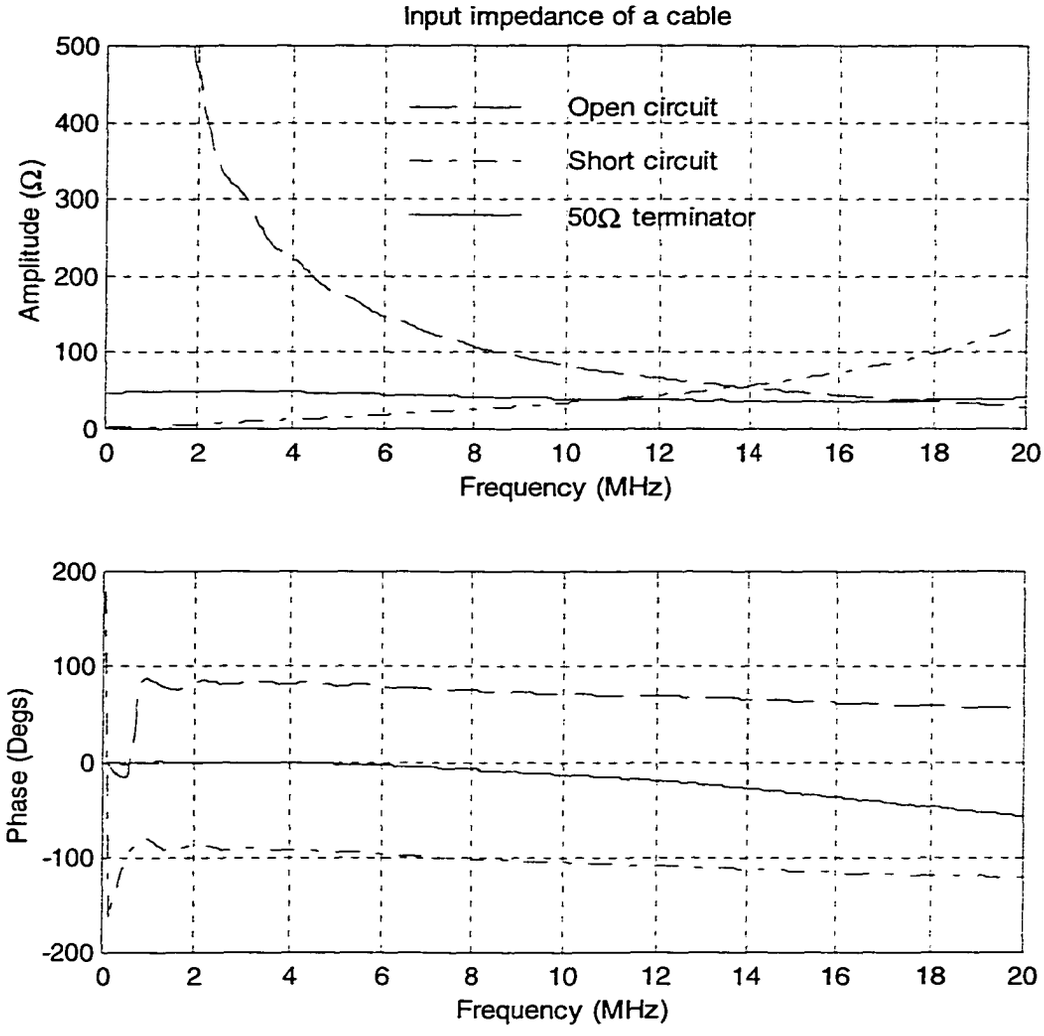

Figure 9.15 Input impedances of the cabling when its port 2 is opened (dashed lines), shorted (dotted dashed lines) and terminated with 50Ω terminator (solid lines). The upper graph shows their amplitudes and the lower one shows their phases.

As shown in Chapter 3, for a piston immersion transducer at high frequencies the acoustic radiation impedance is just a known constant equal to the specific acoustic impedance of the surrounding fluid multiplied by the area of the transducer. Thus, the effects of a transducer on the measurement process can be completely characterized by finding the transducer input impedance and sensitivity. Fortunately, both of these quantities can be

obtained through a series of purely electrical measurements, as will be demonstrated in the following sections.

9.4.1 Input electrical impedance measurement

To measure the transducer input impedance that is appropriate for an immersion inspection, the property of the transducer needs to be obtained with the transducer immersed in water. In this section, we discuss three methods to measure the input electrical impedance.

a. Direct measurement method

The direct measurement method is straightforward. It uses the definition of impedance (voltage/current) to measure the input electrical impedance of a transducer. The measurement setup is shown in Figure 9.16. A pulser directly drives an ultrasonic transducer immersed in a small water bath. The pulser and the transducer are kept as close as possible to avoid cabling effects.

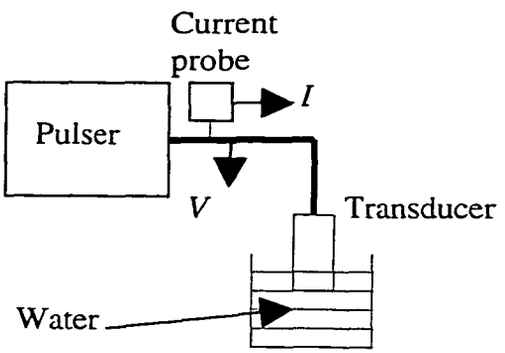

Figure 9.16 Measurement setup for direct measurement method of measuring the input electrical impedance of an immersion ultrasonic transducer.

The input voltage in the time domain is measured by using the sampling oscilloscope and the input current in the time domain is measured by using CT-2 current probe. Taking the FFT of these two quantities gives the input voltage, $V(\omega)$, and current, $I(\omega)$, in the frequency domain. The ratio of these two quantities then gives the input impedance of the transducer, i.e.,

$$Z_{in}^{e}(\omega) = \frac{V(\omega)}{I(\omega)}. \qquad (9.4.3)$$

b. Voltage measurement method

In the direct measurement method, both the voltage and current flowing into the

transducer need to be measured. To avoid having to make a current measurement with a special probe, we can use measurements of voltage only. Thus, we have called this method the voltage measurement method. It is a technique suggested to us by Panametrics.

Recall, the pulser in Figure 9.16 can be modeled by the Thevenin equivalent circuit as shown in Figure 9.1. Its source strength, $V_i(\omega)$, is the output open-circuit voltage which is measurable. Suppose that we also obtain the voltage drop $V_L(\omega)$ across a known resistance R_L^e which is driven by the pulser. From Eq. (9.1.2), the internal impedance of the pulser is written as

$$Z_i^e(\omega) = \left(\frac{V_i(\omega)}{V_L(\omega)} - 1 \right) R_L^e . \tag{9.4.4}$$

Finally, we replace R_L^e with the immersed transducer and measure the voltage across the transducer, $V_{in}(\omega)$. In terms of the input electrical impedance $Z_{in}^e(\omega)$ of the transducer, similar to Eq. (9.4.4), the internal impedance of the pulser is

$$Z_i^e(\omega) = \left(\frac{V_i(\omega)}{V_{in}(\omega)} - 1 \right) Z_{in}^e . \tag{9.4.5}$$

Equating Eqs. (9.4.4) and (9.4.5) gives

$$Z_{in}^e = \frac{V_i(\omega) - V_L(\omega)}{V_i(\omega) - V_{in}(\omega)} \frac{V_{in}(\omega)}{V_L(\omega)} R_L^e . \tag{9.4.6}$$

According to Eq. (9.4.6), to compute the input electrical impedance of an immersed transducer, we need to measure the open-circuit voltage $V_i(\omega)$ of the pulser, the voltage $V_L(\omega)$ across the known load R_L^e and the voltage $V_{in}(\omega)$ across the transducer. Note that this method assumes the effective internal impedance of the pulser is unaffected by the external load. As seen in Section 9.1 this does not appear to be completely true but any loading effects are ignored.

c. Impedance analyzer measurement

An impedance analyzer was also used to measure the input electrical impedance of an ultrasonic transducer. The transducer (immersed in water) is directly connected to the impedance analyzer. The impedance analyzer generates swept frequency signals and imposes them on the electrical port of the transducer. At one frequency, the corresponding voltage and current are measured internally. The ratio of voltage to current gives the input impedance of the transducer at one frequency. After the frequency is swept over the user-specified range, the input impedance of the transducer over this frequency range is obtained.

The measurement setup is shown in Figure 9.17. The impedance analyzer is an HP 4194A. The transducer is connected to the analyzer via a 16047D test fixture. The transducer is immersed into water. The analyzer is controlled by a PC through which a user can choose the swept frequency range. Also the impedance measurements of the transducer are stored in the PC in the form of text data files which can be used directly for further data processing.

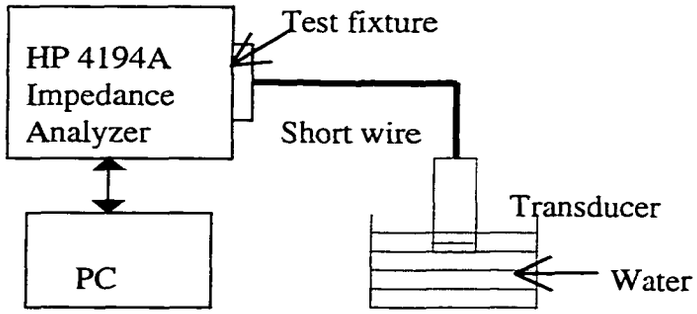

Figure 9.17 Measurement setup for impedance analyzer measurement. The input impedance of the transducer is stored in PC in form of data files.

All three methods discussed above were used to measure the input electrical impedances of three transducers having nominal center frequencies of 2.25MHz, 5MHz and 10MHz, respectively. Figures 9.18 through 9.20 show the impedance measurements of these three transducers. In each figure, the upper graph depicts the amplitude of the impedance and lower one does its phase. Curves denoted by solid lines were obtained by using direct measurement method. Curves denoted by dashed lines were obtained by using voltage measurement method. Curves denoted by dotted dashed lines were obtained by using impedance analyzer method.

Generally the curves decrease with increasing frequency, a behavior which is characteristic of the impedance of a capacitor. As the matter of a fact, in the first order approximation, the piezoelectric plate could be taken as a capacitor. However, if the transducer contains internal "tuning" circuits, as same commercial transducers do, we do not necessarily expect to see this capacitor-like behavior. The curves obtained by the different methods for the same transducer do show some differences but generally all the measurements were within 10% of each other.

The input impedance measurements of the 2.25MHz transducer are shown in Figure 9.18. In this case, the amplitude curves measured using the three methods are all very close to each other. There are some differences in the phase measurements but only on the expanded scale shown. In general, phase variations were less than 10° over the entire frequency range.

The input impedance measurements of the 5MHz transducer are shown in Figure 9.19. The amplitude curves measured by direct measurement and impedance analyzer method are very close, but the curve measured by voltage measurement is somewhat higher than the other two curves. This was also true for the phase plot of Figure 9.19.

The input impedance measurements of the 10MHz transducer are shown in Figure 9.20. The amplitude and phase curves measured by all three measurement methods are close up to a frequency of about 10MHz. The phase curve measured by the impedance analyzer method, however, shows a rapid increase at around 14MHz. We have seen this same type of behavior in other measurements due to cabling effects so that we suspect that the impedance analyzer results are affected by the wire and test fixture connections employed in that method. Figure 9.21 shows two measurements of Z_{in} for a 10MHz transducer with and without a cable. In this figure we see that phase transition occurs at the frequency 10.7MHz.

9.4.2 Receiving sensitivity measurement

We measured the receiving sensitivity of an ultrasonic transducer using the three-transducer calibration procedure described in section 6.3 in Chapter 6 (see Figure 6.5). That procedure was originally developed for characterizing transducers operating at the much lower frequencies present in acoustics applications, using the three setups described in Figure 6.5. However, at the frequencies used in NDE measurement setups, it is not possible to use Figure 6.5 directly. This is because in an immersion test, for example, the transducer is located in water so that it is not practical to make the voltage measurements under open-circuit conditions directly at the transducer output port as required in Figure 6.5. Instead, measurements must be made at a remote location from the transducer after the signals have traveled through a length of cabling. In acoustics, that is not a problem since at low acoustic frequencies open-circuit conditions at the end of the cable are the same as open-circuit conditions at the transducer itself. At NDE frequencies, however, the cabling acts as a receiving load that must be compensated for in making a sensitivity measurement. Cabling effects also enter into the measurement of current that is required at the transmitting

transducer in the calibration procedure (Figure 6.5). Thus, the three-transducer calibration setup that is more appropriate to an NDE setting is shown in Figure 9.22. The cabling effects on the generation and reception sides are represented in Figure 9.22 by the transfer matrices $T^{(1)}$ and $T^{(2)}$, respectively, and a known resistance, R_L^e, is included at the receiving side to make the measurement general. The acoustic transfer functions are taken to be the same in all three setups, i.e. in Figure 9.22 $t_A^I = t_A^{II} = t_A^{II} = t_A$. The actual voltage and current measurements that are made are labeled $V_{CA}^m, V_{CB}^m, V_{BA}^m$ and I_P in Figure 9.22 and the voltages

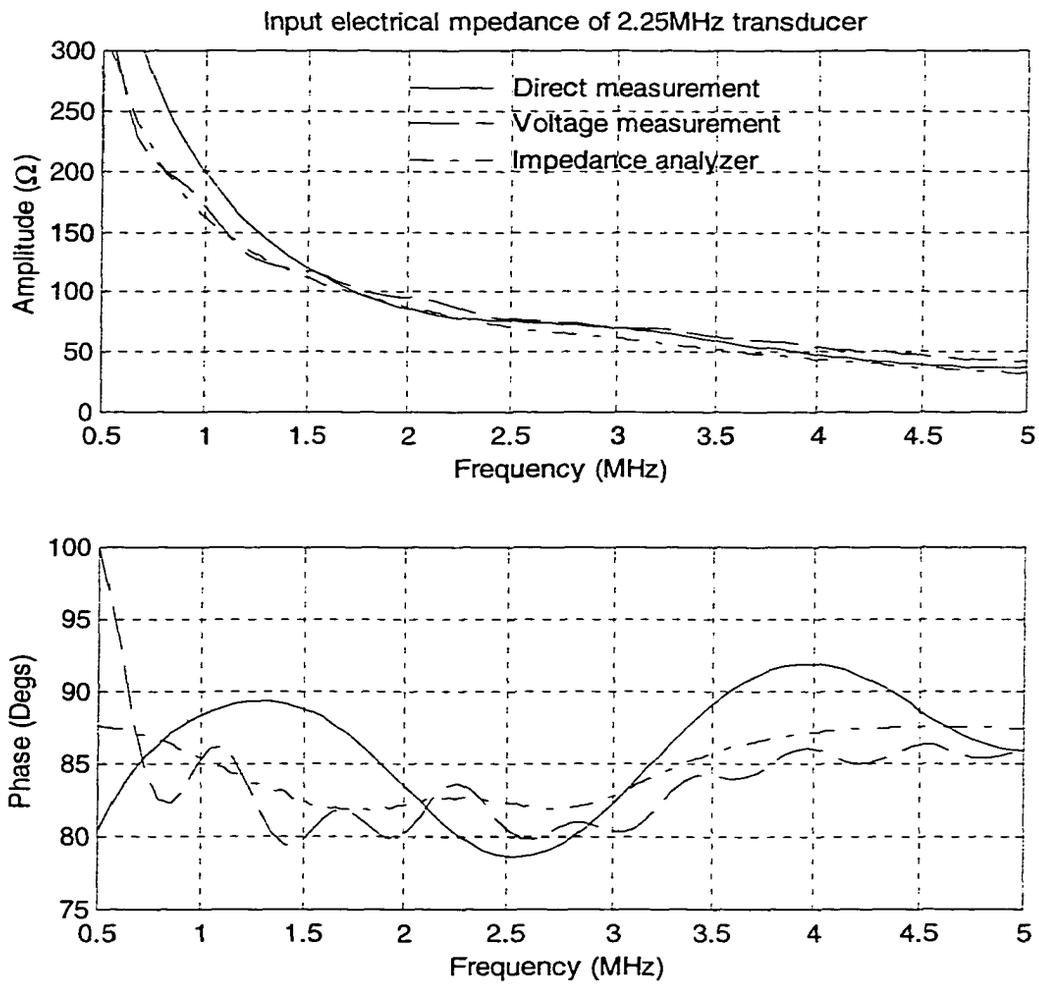

Figure 9.18 The input electrical impedance for 2.25MHz transducer. The upper graph shows its amplitude and the lower one shows its phase.

and currents directly at the transducer electrical port are labeled V_{CA}, V_{CB}, V_{BA} and I_B, respectively. It is these latter quantities that appear in the generalized receiving sensitivity expression obtained in Chapter 6 (Eq. (6.4.19)), which for transducer A is rewritten here as

$$M_{VF_B}^{A} = \sqrt{\frac{V_{CA}V_{BA}}{I_B V_{CB}\left(1 + Z_{in}^{B:e} / Z_o^e\right)} \frac{1}{Z_r^{B:a} t_A}} \qquad (9.4.7)$$

where Z_o^e is the effective receiving impedance under which the voltages V_{CA}, V_{CB}, V_{BA} in Eq. (9.4.7) are obtained. For all three setups shown in Fig 9.22 we have at the receiving end the

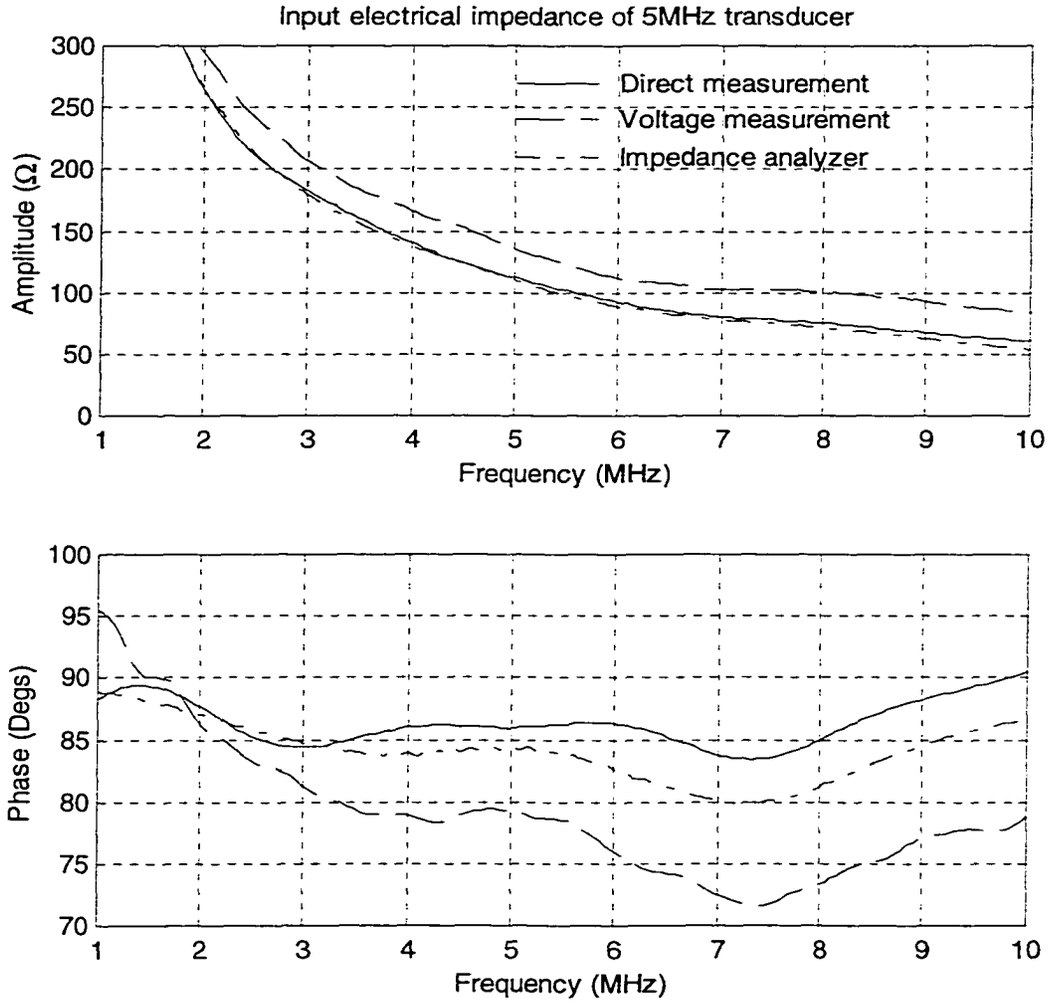

Figure 9.19 The input electrical impedance for 5MHz transducer. The upper graph shows its amplitude and the lower one shows its phase.

configuration shown in Figure 9.23 where V^m is a measured voltage and V is a voltage at the transducer output port that is to go into Eq. (9.4.7). From the transfer matrix of the cabling (Eq. (9.3.1)), V and V^m are related through

$$V = \left(T_{11}^{(2)} + \frac{T_{12}^{(2)}}{R_L^e} \right) V^m \tag{9.4.8}$$

Thus, if V^m is measured, R_L^e is known and the transfer matrix of the cabling has been measured, Eq. (9.4.8) can be used to find V. If this process is followed for setups I, II, and III, the corresponding voltages V_{CA}, V_{CB}, V_{BA} are obtained. Furthermore, the receiving impedance Z_o^e (which is the same for all three setups) can also be obtained (see Figure 9.24)

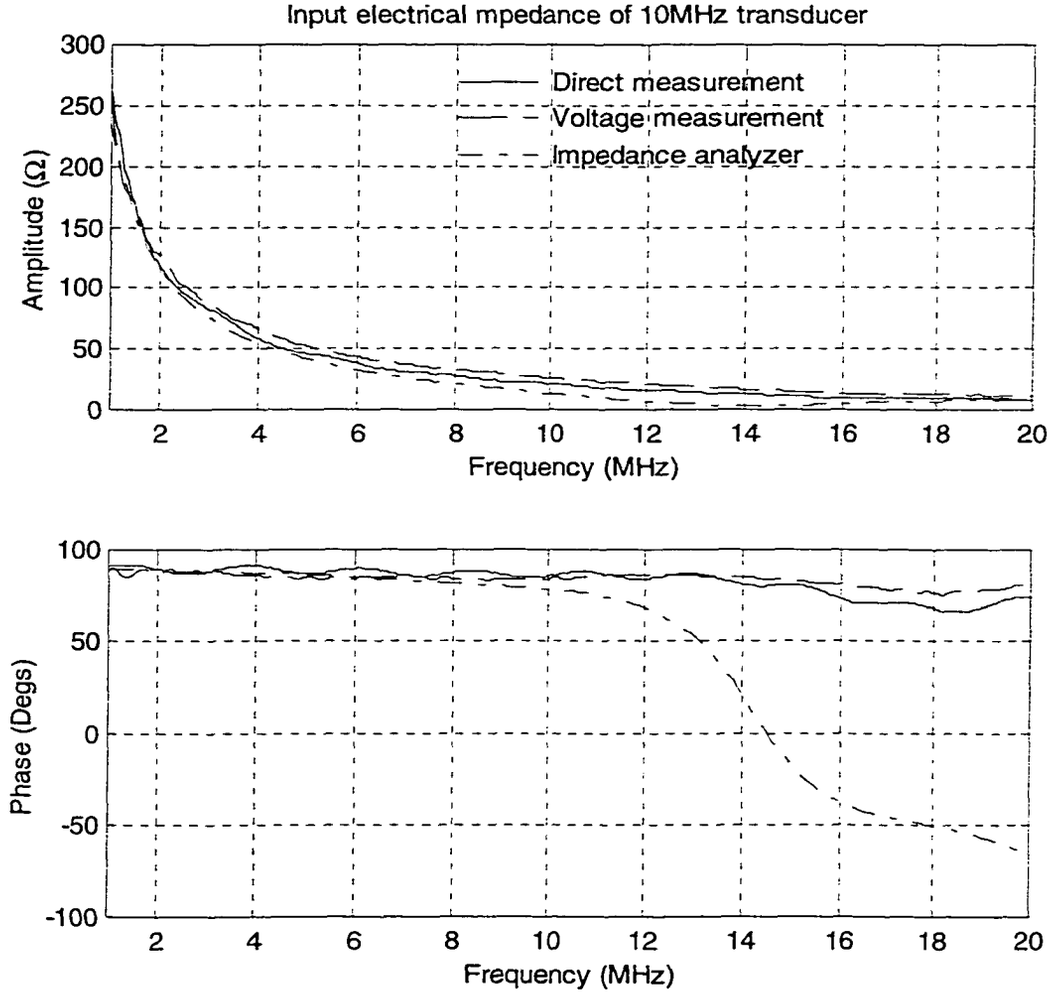

Figure 9.20 The input electrical impedance for 10MHz transducer. The upper graph shows its amplitude and the lower one shows its phase.

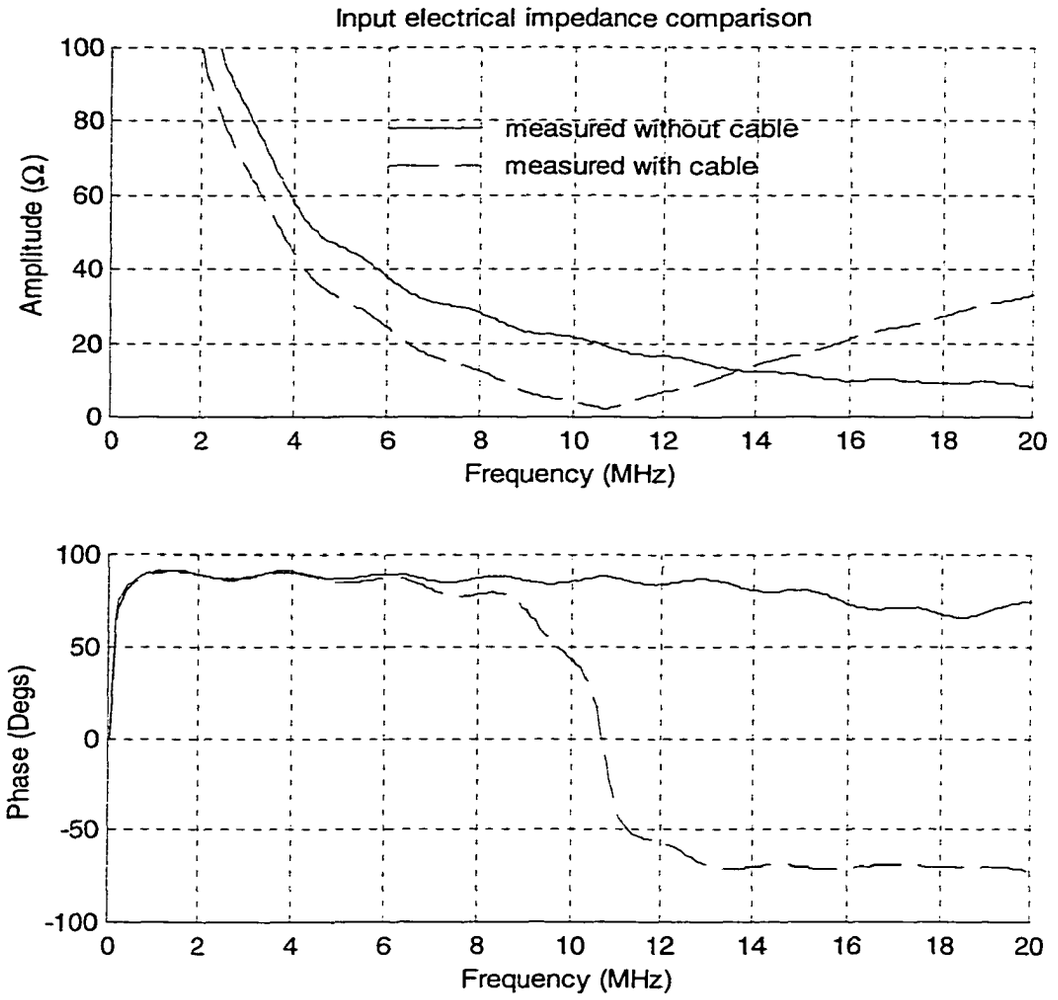

Figure 9.21 The input electrical impedance for 10MHz transducer (a) with and (b) without a cable.

since

$$Z_o^e = \frac{T_{11}^{(2)} R_L^e + T_{12}^{(2)}}{T_{21}^{(2)} R_L^e + T_{22}^{(2)}}. \tag{9.4.9}$$

The current I_B appearing in Eq. (9.4.7) is the current flowing directly into the transducer as shown in Figure 9.22. However, the current that actually can be measured is I_P and again cabling effects make these two currents different. From the second equation represented in Eq. (9.3.1) we find

$$I_P = \left(T_{21}^{(1)} Z_{in}^{B:e} + T_{22}^{(1)}\right) I_B \tag{9.4.10}$$

Setup I

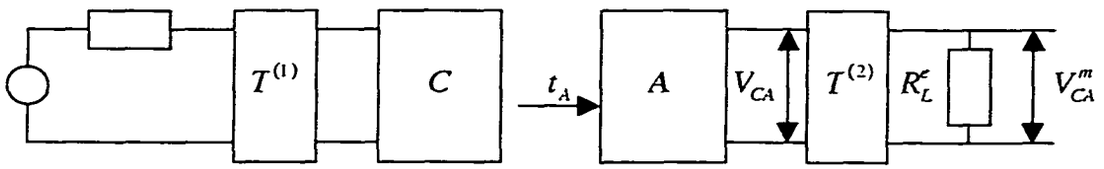

Setup II

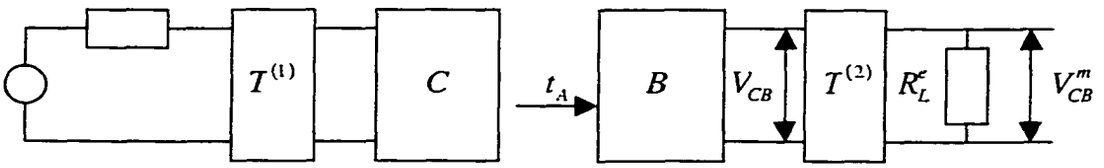

Setup III

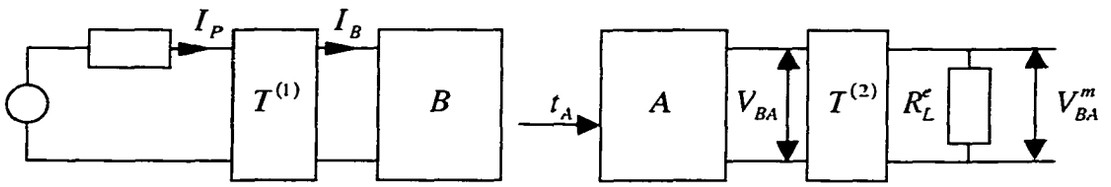

Figure 9.22 Three-transducer calibration setup for an ultrasonic NDE immersion measurement system.

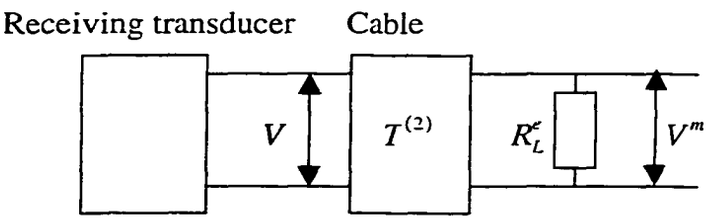

Figure 9.23 General receiving configuration relating a measured voltage, V^m, to a voltage, V, at the receiving transducer output port.

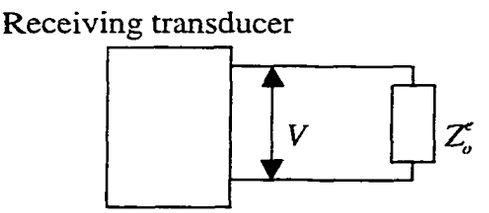

Figure 9.24 Effective receiving impedance, Z_o^e, at which voltage V is evaluated.

which can be solved for I_B, assuming that the cable has been characterized and the input impedance, $Z_{in}^{B:e}$, of transducer B has been measured, to give

$$I_B = \frac{I_P}{T_{21}^{(1)} Z_{in}^{B:e} + T_{22}^{(1)}}. \qquad (9.4.11)$$

Using these results, we now can describe the steps needed to obtain the open-circuit, blocked force receiving sensitivity as follows.

a. In setup I, measure the receiving voltage across the resistor R_L^e. Use Eq. (9.4.8) to compute the voltage V_{CA}.

b. In setup II, replace transducer A with transducer B. Measure the receiving voltage across the resistor R_L^e. Use Eq. (9.4.8) to compute the voltage V_{CB}.

c. In setup III, replace transducer B with transducer A and replace transducer C with transducer B. Measure the receiving voltage across the resistor R_L^e. Use Eq. (9.4.8) to compute the voltage V_{BA}. Measure the current flowing out of the pulser using current probe and use Eq. (9.4.11) to compute the current flowing into transducer B.

d. Use Eq. (9.4.9) to compute the receiving impedance Z_o^e of the cabling terminated with the resistor R_L^e.

e. Use Eq. (9.4.7) to compute the generalized receiving sensitivity of transducer A.

f. Relate the generalized sensitivity of a transducer to its open-circuit value through the relation (see Eq. (6.4.17)):

$$M_{VF_B}^{A:\infty} = M_{VF_B}^{A} \left(1 + \frac{Z_{in}^{A:e}}{Z_o^e} \right). \qquad (9.4.12)$$

Three transducers with frequencies of 2.25MHz, 5MHz and 10MHz were measured using this procedure. Their sensitivities are depicted in Figures 9.25 through 9.27 where three types of sensitivity curves are shown. In each figure, the solid line in each figure shows the open-circuit, blocked force receiving sensitivity. The dashed line shows the generalized receiving sensitivity used to derive the corresponding open-circuit receiving sensitivity by Eq. (9.4.12). The dotted dashed line shows the generalized receiving sensitivity measurement obtained without considering the existence of the cabling.

Comparing these figures, we draw the following conclusions:

a. For the 2.25MHz and 5MHz transducers the sensitivities are largest around the nominal center frequencies of the transducers.

b. The open-circuit receiving sensitivity is larger than the generalized receiving sensitivity.

c. There are some significant variations in the sensitivity at very low frequencies. These may come from the division (deconvolution) processes inherent in Eq. (9.4.7).

d. There is very little phase structure in the sensitivities. In general the phases go up approximately linearly.

e. For the 10MHz transducer, the sensitivity around 18MHz is higher than the sensitivity at 10MHz. This could be a second harmonic frequency phenomenon.

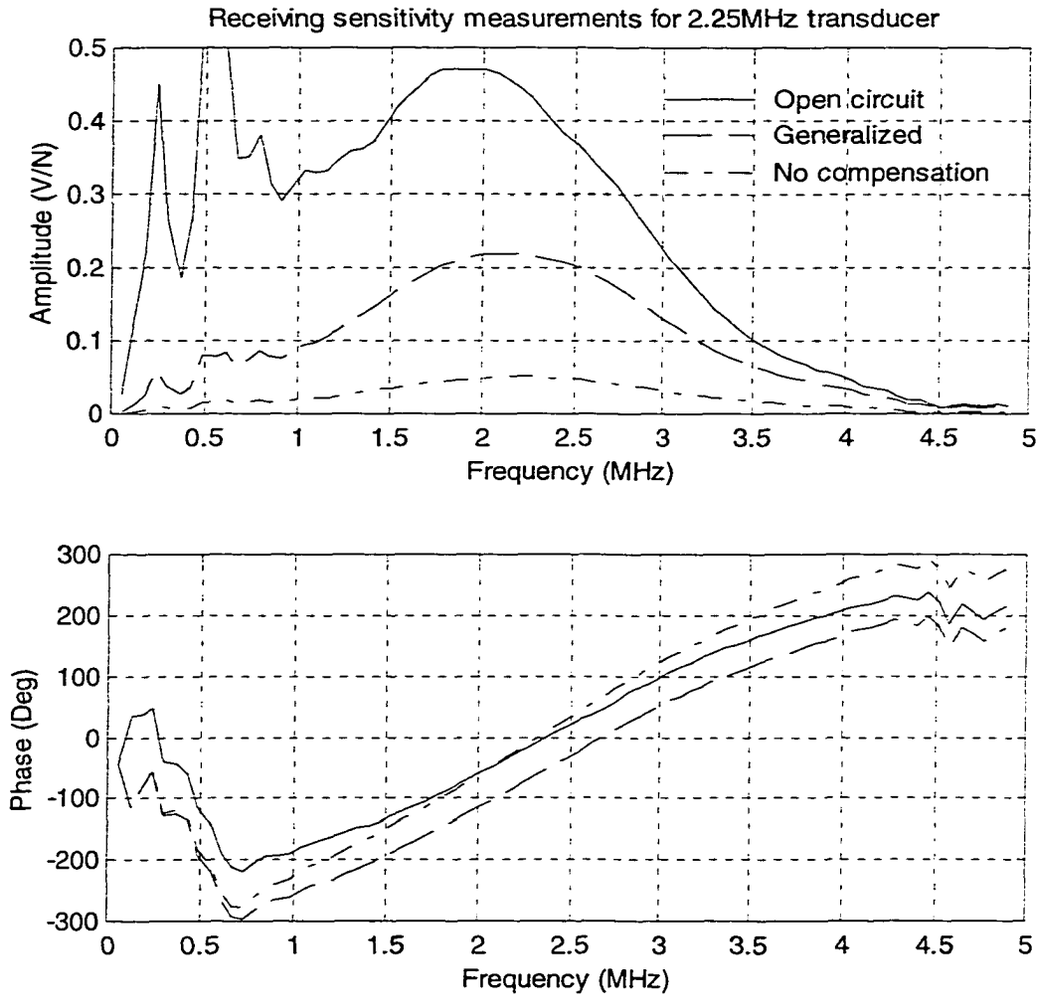

Figure 9.25 Receiving sensitivity measurements for a 2.25MHz transducer: (a) open-circuit, blocked force (solid lines), (b) generalized (dashed lines) and (c) without cabling compensation (dotted dashed lines).

f. Generally, the overall sensitivity decreases with increasing nominal center frequency, i.e., the sensitivity of the 2.25MHz transducer is higher than that of 5MHz transducer and the sensitivity of the 5MHz transducer is higher than that of the 10MHz transducer.

g. The generalized receiving sensitivity measurements with and without considering cabling effects (shown as dashed and dotted, dashed lines respectively) are different. This indicates that the existence of the cabling does affect the measurement results. In ultrasonic measurement, the cabling effect should not be ignored.

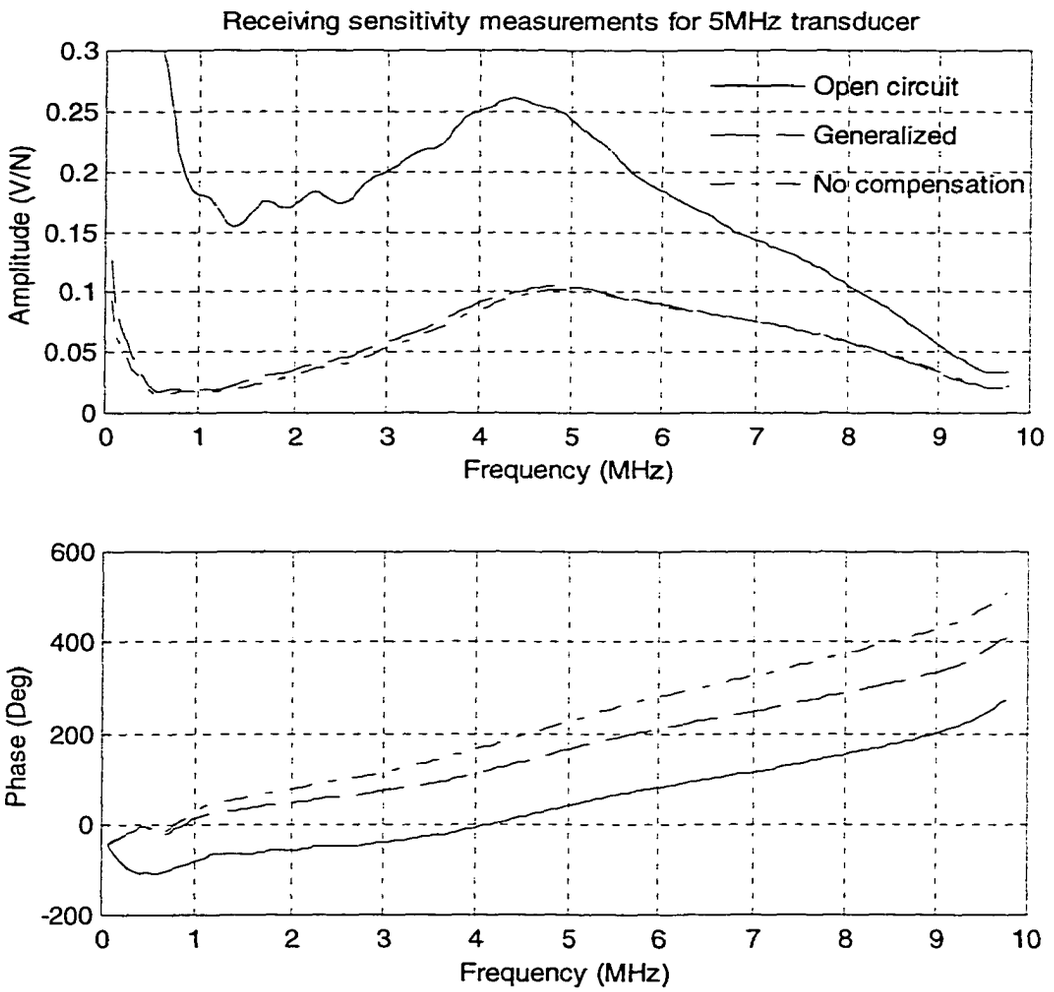

Figure 9.26 Receiving sensitivity measurements for a 5MHz transducer: (a) open-circuit, blocked force (solid lines), (b) generalized (dashed lines) and (c) without cabling compensation (dotted dashed lines).

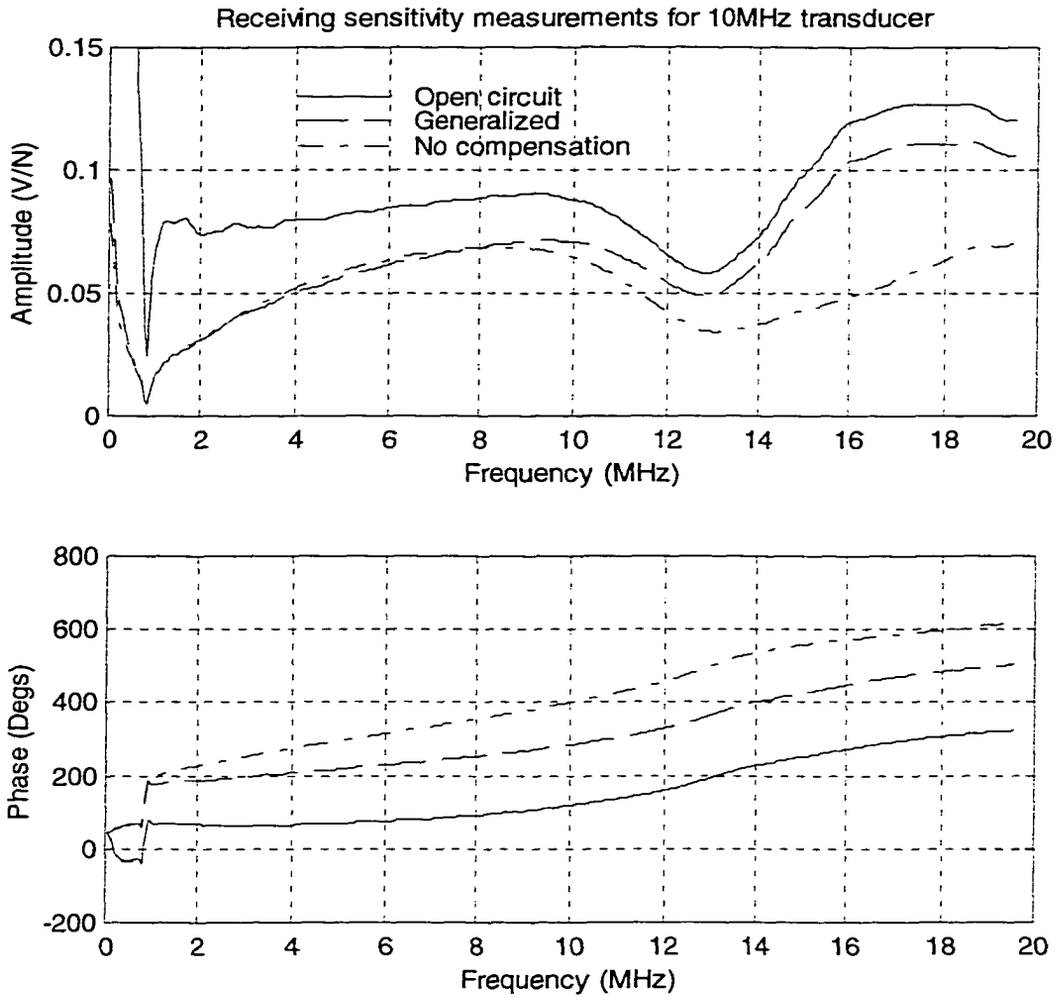

Figure 9.27 Receiving sensitivity measurements for a 10MHz transducer: (a) open-circuit, blocked force (solid lines), (b) generalized (dashed lines) and (c) without cabling compensation (dotted dashed lines).

CHAPTER 10. ULTRASONIC MEASUREMENT SYSTEM CHARACTERIZATION

Methods to experimentally determine all the electrical and electromechanical components of an ultrasonic measurement system were described in Chapter 9. By combining those measured components with a model of the acoustic transfer function, we can completely characterize the entire ultrasonic measurement process. To our knowledge, this is the first time that such a complete system characterization has been obtained. In this chapter, we will measure/model all the elements of a particular ultrasonic measurement setup and demonstrate that this completely characterized system predicts the directly measured received waveform. We will also show that combining our measurements of the electrical and electromechanical components into a single system factor also gives good agreement with direct measurements of that factor.

10.1 Component Measurements

The ultrasonic immersion measurement system we will completely characterize is shown in Figure 10.1. The system has seven components: a commercial pulser, cabling from the pulser to the transducer, a commercial transmitting transducer (transducer A), an acoustic transmission/reception configuration, a commercial receiving transducer (transducer B), cabling from the receiving transducer to the receiver, and the receiver. The acoustic configuration will be taken to be simply the two transducers aligned along their axes and separated by a distance, D, in a water bath (see Figure 10.1). For the receiver, we will replace the commercial receiver section of the pulser/receiver in these comparisons with two known terminations (50Ω resistor and open-circuit) to demonstrate the validity of our approach under very different receiving conditions. As shown in Chapter 9, the commercial receiver measured there acted to first order like a constant (in frequency) receiving impedance and gain factor, so that it can only provide a single receiving termination condition.

The following seven subsections describe in detail the characterization of the measurement system.

10.1.1 Pulser

The commercial pulser used here was a Panametrics 5052PR. All measurements were done at the Energy level of the pulser set to 2 and the Damping set to 5. The open-circuit output voltage of the pulser at this setting was sampled using a LeCroy digital oscilloscope. This voltage is shown in Figure 10.2. From that figure it can be seen that at this setting the 5052PR generates a negative spike-like pulse with an amplitude of about 190V and a duration of about 0.2μsec. As shown in Chapter 9, taking the FFT of this open-circuit voltage gives the source strength, $V_i(\omega)$, of the Thevenin equivalent circuit of the pulser (Figures 9.2-9.5). The Thevenin equivalent impedance of the pulser, $Z_i^e(\omega)$, was measured (at Energy level 2, Damping 5) using the method described in Chapter 9. Since as shown in that chapter the impedance obtained does depend somewhat on the electrical load connected to the pulser, the measurements of $Z_i^e(\omega)$ were made here with the transmitting cable connected to the pulser with the other end of the cable connected to the transducer. Figure 10.3 shows the measured source strength $V_i(\omega)$ and its internal electrical impedance $Z_i^e(\omega)$ in the frequency domain. Figure 10.3(a) illustrates the amplitude of the source strength $V_i(\omega)$ (solid line) and its phase change (dashed line) respectively. Figure 10.3(b) illustrates the amplitude of the internal impedance $Z_i^e(\omega)$ (solid line) and its phase change (dashed line) respectively. As expected, the internal electrical load is not a constant.

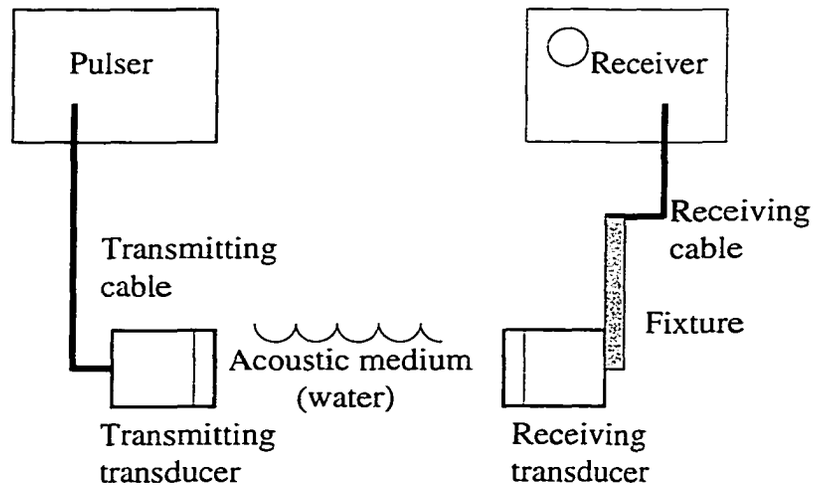

Figure 10.1 An ultrasonic measurement system which contains seven components: pulser, transmitting cabling, transmitting transducer, acoustic medium, receiving transducer, receiving cabling (flexible cable and fixture), and receiver.

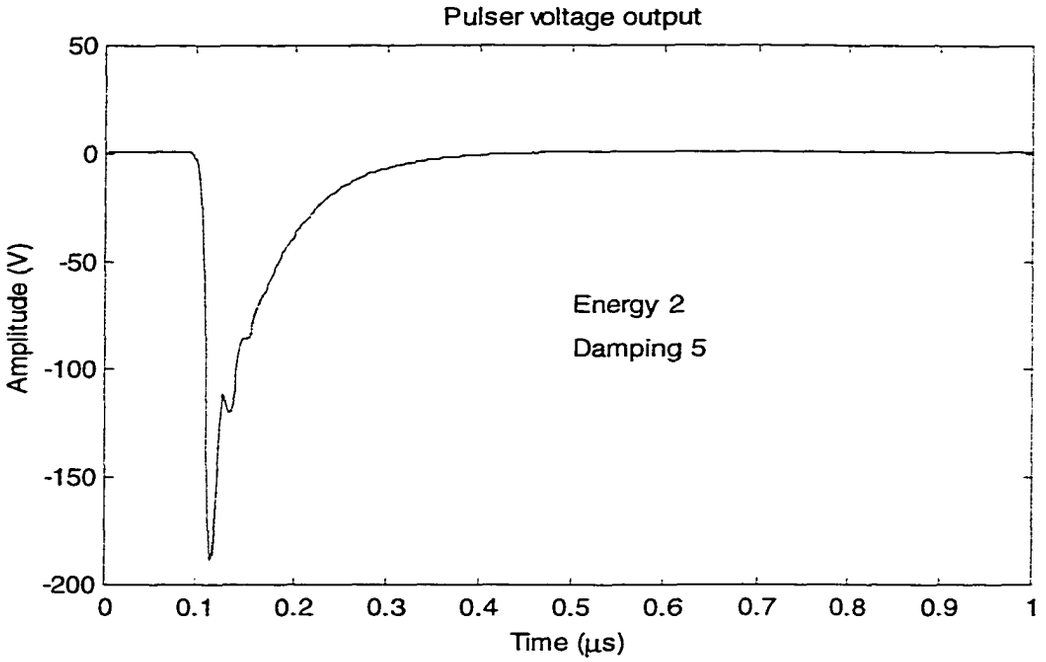

Figure 10.2 A spike-like pulse emitted from Panametrics 5052PR with energy 2, damping 5 and its outlet opened.

10.1.2 Transmitting cabling

The transmitting cabling was a single flexible cable with the length of 5.5ft (1.68m) connected between the pulser and the transmitting transducer. As shown previously, the cable can be described by a 2x2 transfer matrix T:

$$T = \begin{bmatrix} T_{11} & T_{12} \\ T_{21} & T_{22} \end{bmatrix} \tag{10.1.1}$$

where four elements, T_{11}, T_{12}, T_{21} and T_{22}, which are functions of frequency.

Using the cabling measurement method described in section 9.3 of Chapter 9, these four elements of the transmitting cabling matrix were obtained. They are shown in Figure 10.4 where the left column gives the amplitudes of the elements and the right column their phases.

10.1.3 Transmitting transducer

The transmitting transducer, transducer A in Figure 10.1, was a commercial transducer (Panametrics V310, serial no. 257916), having a nominal frequency of 5MHz and a diameter of 0.25in. (6.35mm). As we have discussed previously, an ultrasonic planar piston

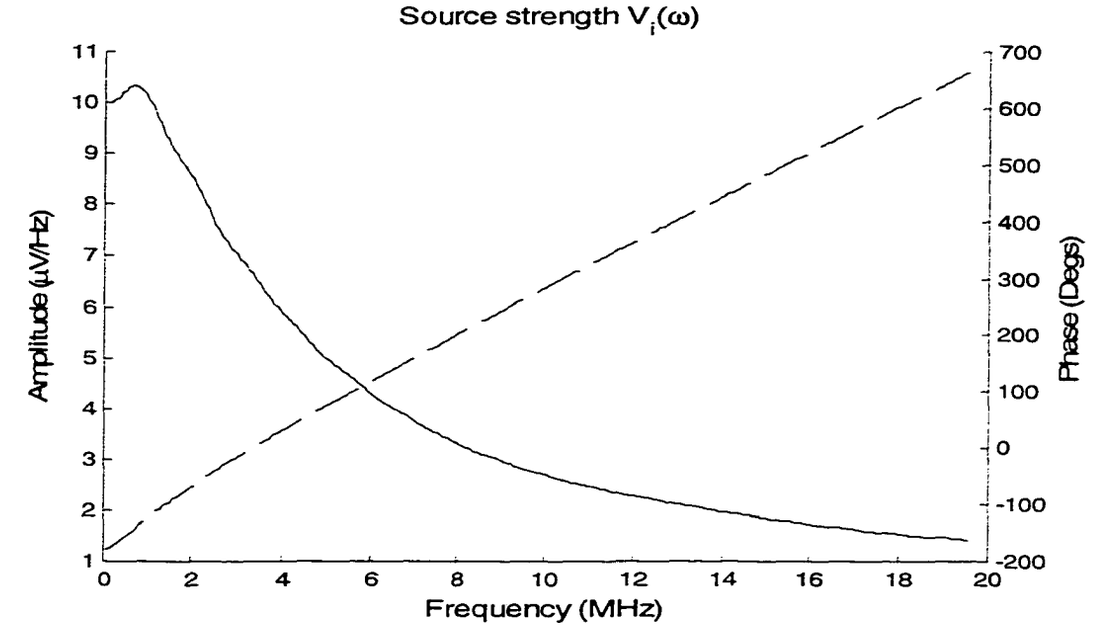

(a)

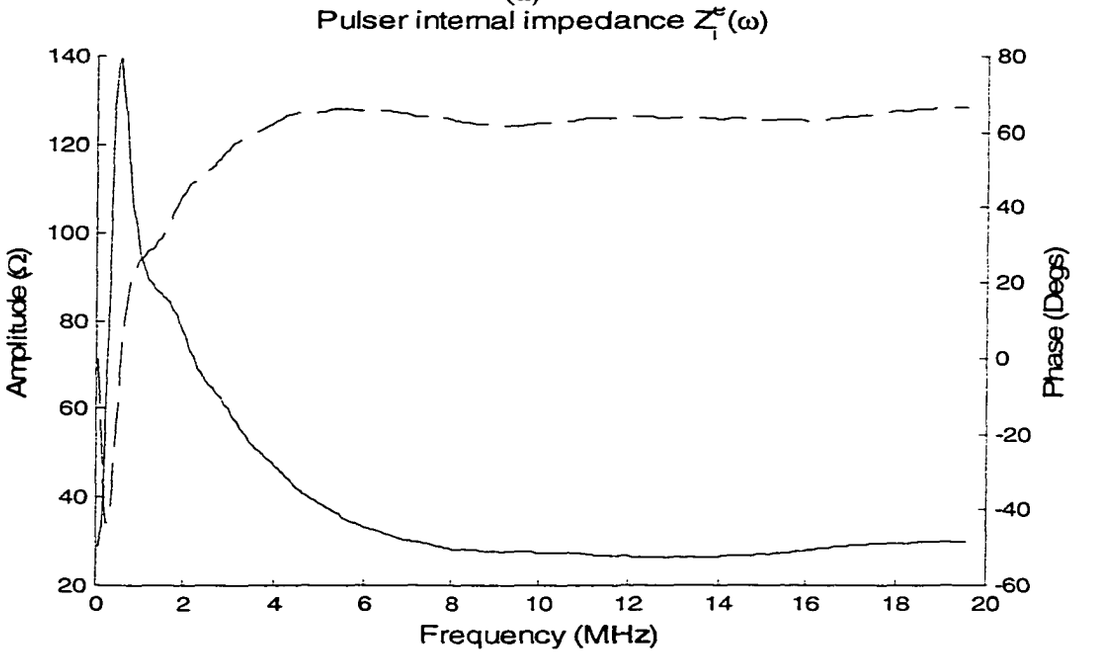

(b)

Figure 10.3 Characteristics of Panametrics 5052PR. (a) Source strength $V_i(\omega)$ with its amplitude (solid line) and its phase (dashed line). (b) The internal electrical impedance $Z_i^e(\omega)$ with its amplitude (solid line) and its phase (dashed line). Transmitting cabling is connected at the pulser.

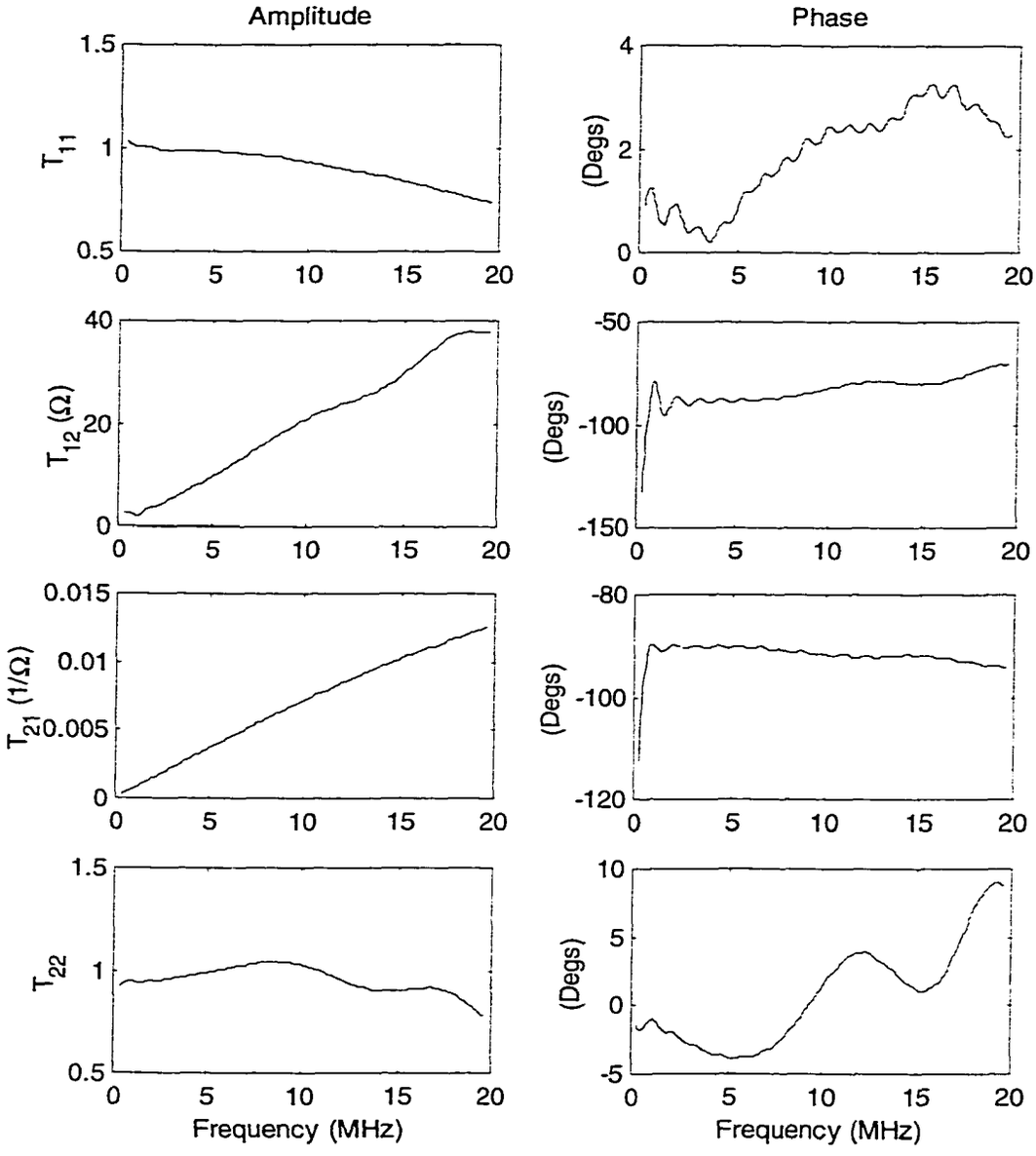

Figure 10.4 The elements of the transfer matrix T of the transmitting cabling. The left shows their amplitudes and the right column their corresponding phases.

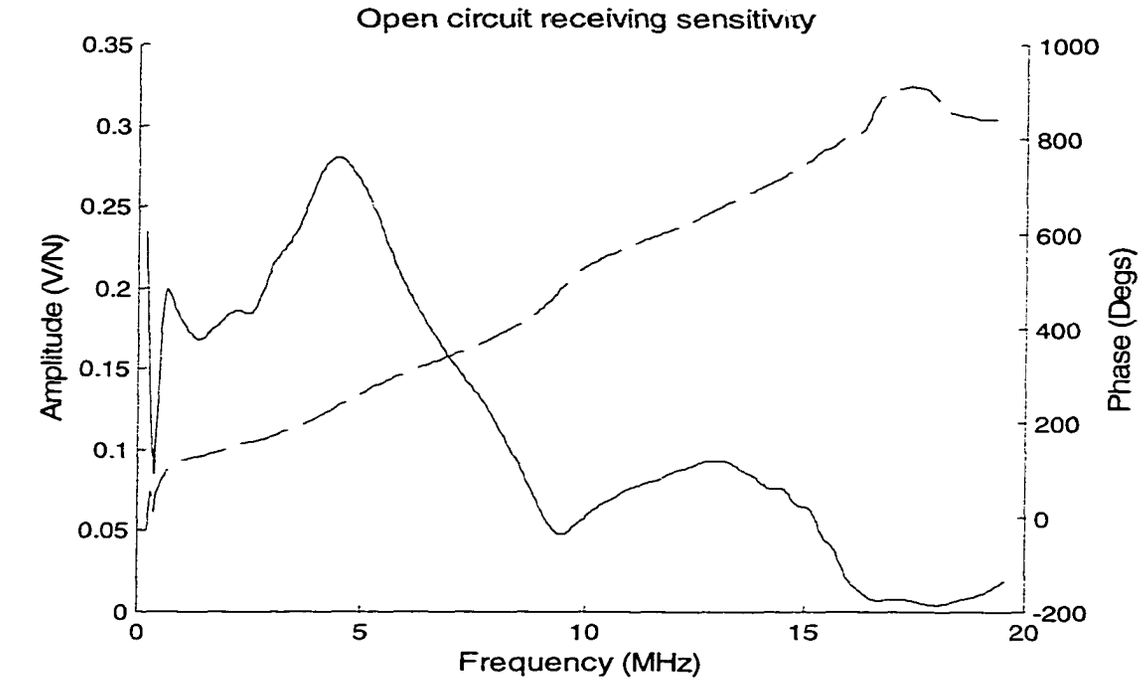

(a)

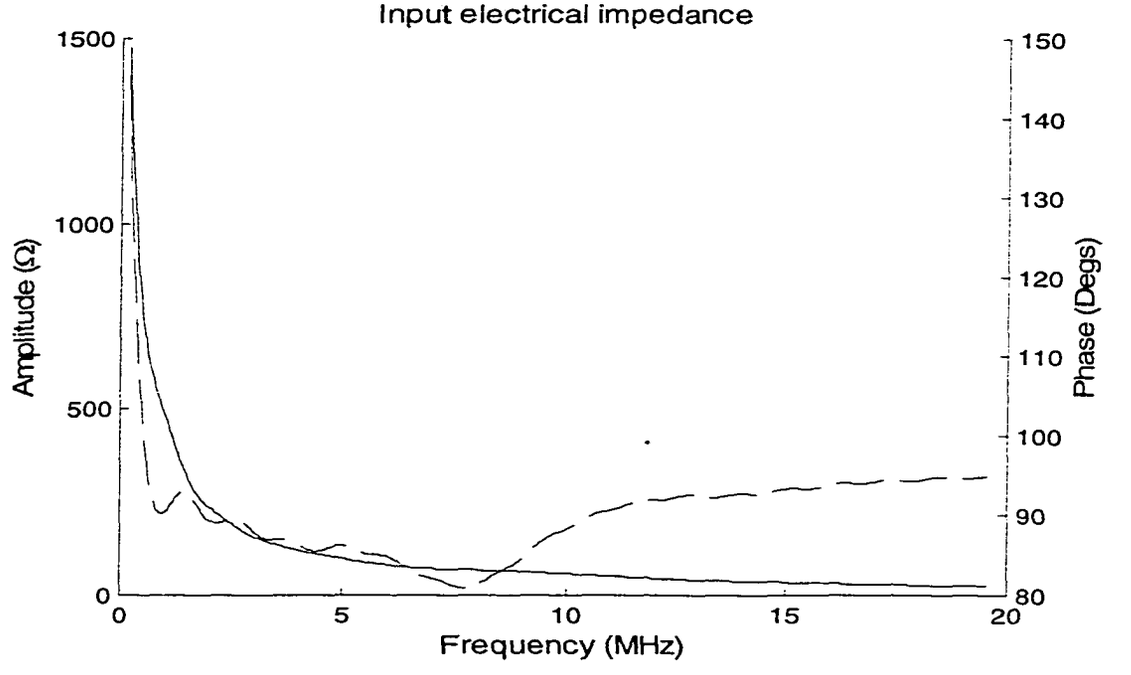

(b)

Figure 10.5 The characteristics of transducer A. (a) Its open-circuit receiving sensitivity $M_{VF_B}^{A:\infty}(\omega)$. (b) Its input electrical impedance $Z_{in}^{A:e}(\omega)$. Solid lines show their amplitudes and dashed lines show their phases.

transducer can be completely described by its input electrical impedance, $Z_{in}^{e}(\omega)$, and its open-circuit receiving sensitivity, $M_{VF_B}^{\infty}(\omega)$. The methods to measure these two quantities were described in section 9.4 in Chapter 9. The direct impedance measurement method was used to measure the input electrical impedance of transducer A. The measurement results of the open-circuit sensitivity $M_{VF_B}^{A:\infty}(\omega)$ of transducer A and its input electrical impedance $Z_{in}^{A:e}(\omega)$ are shown in Figure 10.5. Figure 10.5(a) shows the amplitude (solid line) and phase (dashed line) of the open-circuit sensitivity $M_{VF_B}^{A:\infty}(\omega)$ of transducer A. Figure 10.5(b) shows the amplitude (solid line) and phase (dashed line) of the input electrical impedance.

10.1.4 Acoustic configuration

The acoustic medium between the two aligned transducers A and B was water (wave speed c=1480m/s and density ρ=1000kg/m^3). The attenuation factor for the water was taken as $\alpha(f) = 25.3\times10^{-15} f^2$ Np/m with f the frequency (in Hz) of acoustic waves [Schmerr,

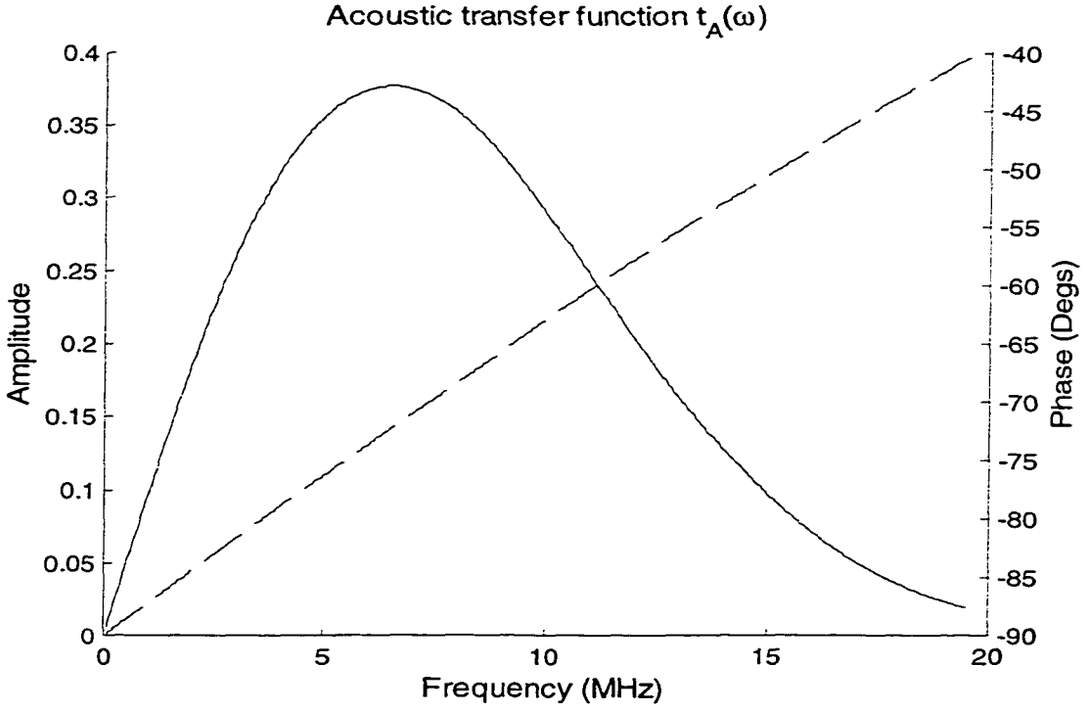

Figure 10.6 The acoustic transfer function $t_A(\omega)$ with distance between two transducers D=0.444m, wave speed of water c=1480m/s, density of water ρ=1000kg/m^3 and transducer radii r=3.175mm. It behaves like a band limited filter.

1998]. The distance between the two transducers was D=0.444m (producing a 300μs time delay). The radii, r, of the transducers were both given by r=3.175mm. The radiation acoustic impedance of the transducers was taken as

$$Z_r^a = A\rho c. \tag{10.1.2}$$

The acoustic configuration considered here can be described by its acoustic transfer function, $t_A(\omega)$, as obtained in Chapter 6 (see Eq. (6.3.19)). By including the water attenuation effects in those results, we find

$$t_A(\omega) = 2\exp\left[(ik - \alpha(f))D\right] \cdot \left[1 - \exp\left(ika^2 / D\right)\left\{J_0\left(ka^2 / D\right) - iJ_1\left(ka^2 / D\right)\right\}\right] \tag{10.1.3}$$

The acoustic transfer function for the measurement system show in Figure 10.1 is depicted in Figure 10.6, where the solid line shows the amplitude and the dashed line the phase of the acoustic transfer function. This function behaves like a band limited filter because of the frequency dependent attenuation of the water and the beam spreading effects contained in Eq. (10.1.3). As can be seen in Figure 10.6, this "filter" has a peak at a frequency of about 6.8MHz.

10.1.5 Receiving transducer

The receiving transducer, transducer B (Panametrics V310, serial no. 184577), had the same nominal frequency and size as those of transducer A, i.e., 5MHz nominal frequency and 0.25in (6.35mm) diameter. The input electrical impedance, $Z_{in}^{B:e}(\omega)$, and the open-circuit receiving sensitivity, $M_{VF_B}^{B:\infty}(\omega)$, of this transducer were measured and are shown in Figure 10.7. Figure 10.7(a) depicts the amplitude (solid line) and phase (dashed line) of the open-circuit sensitivity, $M_{VF_B}^{B:\infty}(\omega)$, of transducer B while Figure 10.7(b) depicts the amplitude (solid line) and phase (dashed line) of the input electrical impedance, $Z_{in}^{B:e}(\omega)$, of transducer B.

Comparing Figure 10.7 with Figure 10.5, we see that the two transducers have very similar input impedances. Their open-circuit sensitivities also are similar but do show some differences in their detailed behavior. Note that the two transducers should be similar since they came from the same family (Panametrics V301 series) of probes.

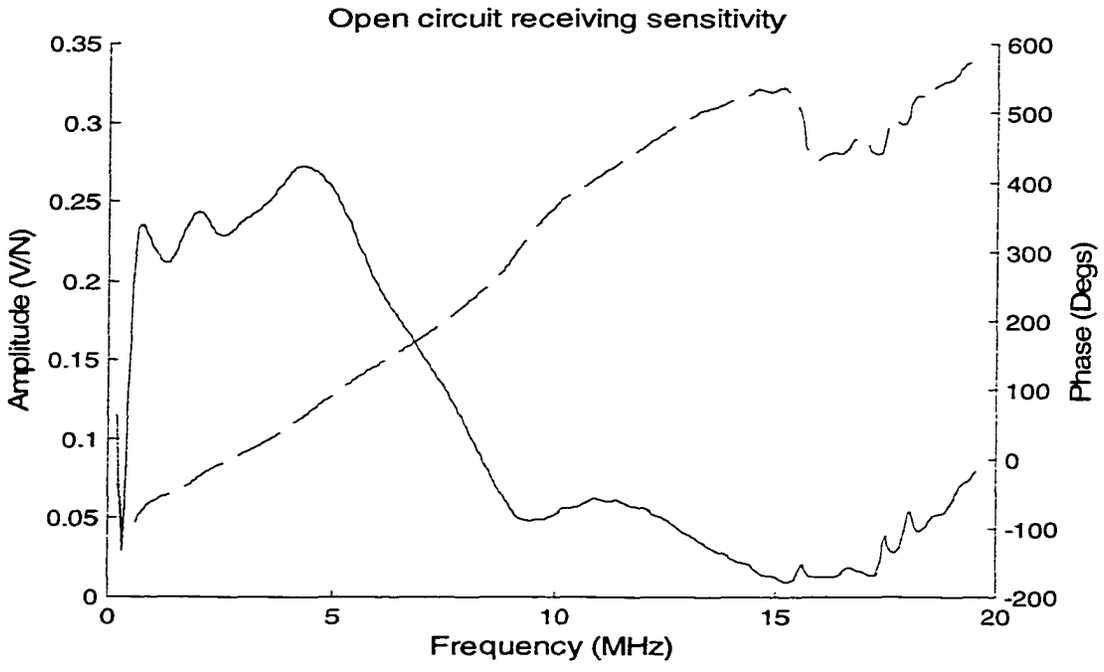

(a)

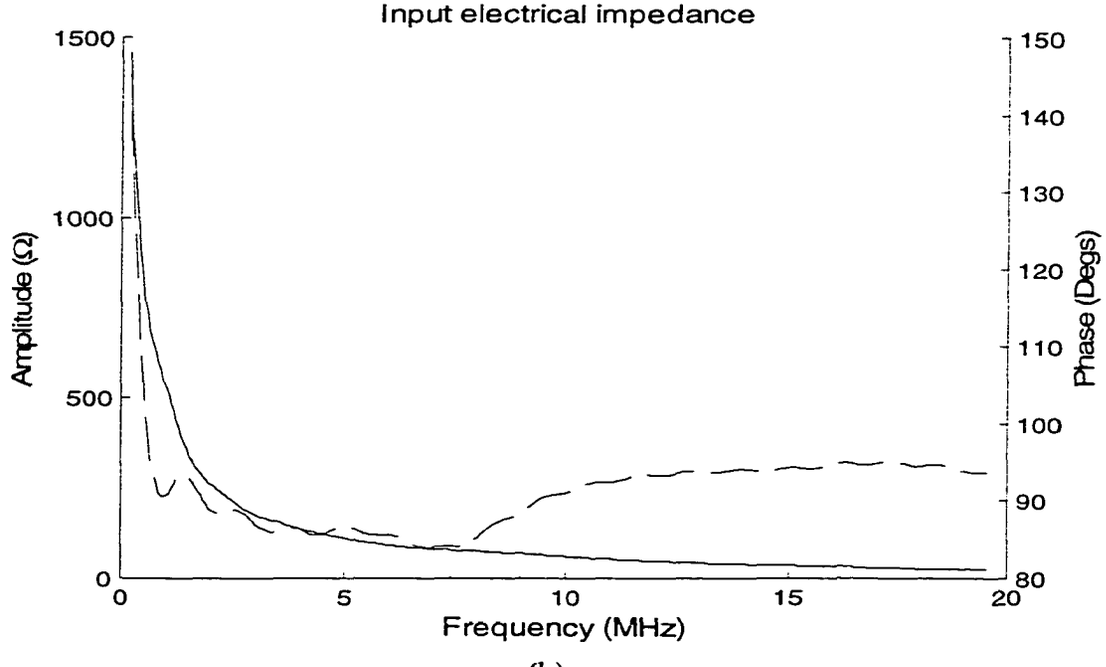

(b)

Figure 10.7 The characteristics of transducer B. (a) Its open-circuit receiving sensitivity $M_{VF_B}^{B:\infty}(\omega)$. (b) Its input electrical impedance $Z_{in}^{B:e}(\omega)$. Solid lines show their amplitudes and dashed lines show their phases.

10.1.6 Receiving cabling

The receiving cabling transmits receiving signals from the receiving transducer to the receiver. In our measurement system, it consisted of two components: a flexible cable and a fixture rod. The fixture rod has a length of 2.5ft (0.77m) and was used to hold the receiving transducer. The flexible cable had a length of 5ft (1.52m) and connected the fixture rod to the receiver (see Figure 10.1). Similar to the transmitting cabling, the receiving cabling can be considered as a transmission line whose transfer matrix is

$$R = \begin{bmatrix} R_{11} & R_{12} \\ R_{21} & R_{22} \end{bmatrix}. \qquad (10.1.4)$$

The four elements of the transfer matrix R are R_{11}, R_{12}, R_{21} and R_{22} which were measured and are shown in Figure 10.8. The left column in Figure 10.8 gives their amplitudes and the right column their phases. Note that there is a phase transition point after 15MHz for both R_{11} and R_{22}. Such a transition point does not exist in the transmitting cabling (see Figure 10.4). This is because the receiving cabling is much longer than the transmitting cabling.

10.1.7 Receiver

During our immersion test, the receiver consisted of only a known termination impedance, $Z_o^e(\omega)$, at the end of the necessary cable, as discussed earlier. We chose their termination to be either $Z_o^e(\omega)$=50Ω resistor or $Z_o^e(\omega)$=∞ (open-circuit). The receiving load is denoted as $Z_o^e(\omega)$.

10.2 Transfer Functions

In Chapters 5 and 6 we expressed the voltage output (in the frequency domain), $V_R(\omega)$, of the entire ultrasonic measurement system in terms of three transfer functions $(t_G(\omega), t_R(\omega), t_A(\omega))$ and the Thevenin equivalent input pulser voltage, $V_i(\omega)$, as (see Eq. (6.6.1)):

$$V_R(\omega) = t_G(\omega)t_R(\omega)t_A(\omega)V_i(\omega) \qquad (10.2.1)$$

where $t_G(\omega)$ is the generation transfer function (defined in Chapter 3), $t_R(\omega)$ is the reception transfer function (defined in Chapter 4), and $t_A(\omega)$ is the acoustic transfer function (defined in Chapter 5). For the system shown in Figure 10.1, we have shown that it is possible to experimentally determine $V_i(\omega)$ and explicitly model $t_A(\omega)$ (Eq. (10.1.3)). The generation

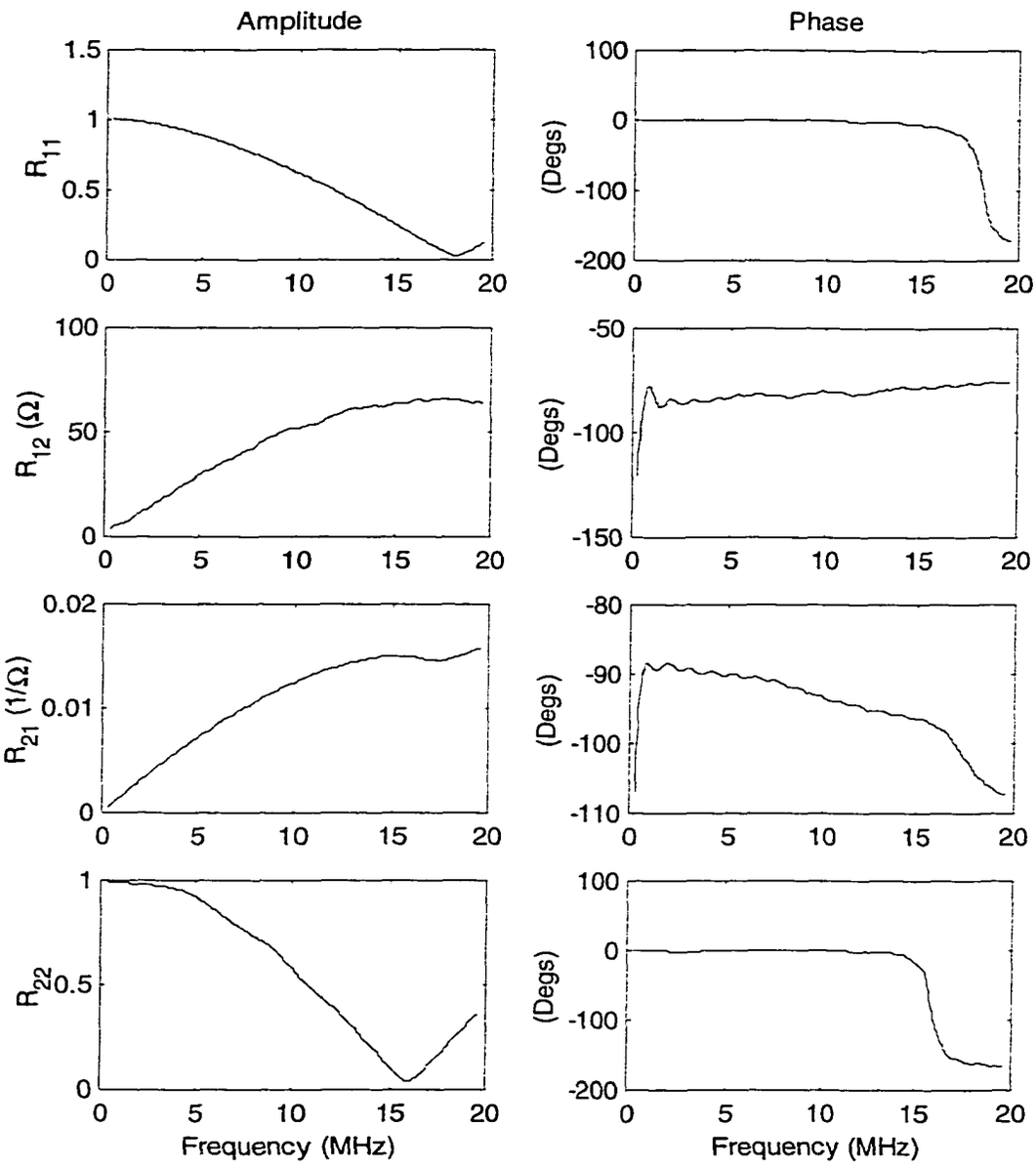

Figure 10.8 The elements of the transfer matrix R of the receiving cabling. The left column shows their amplitudes and right column shows their phases.

and reception transfer functions can also be explicitly written in terms of the components measured in section 10.1 since we have (see Eqs. (6.2.14) and (6.2.15)):

$$t_G(\omega)=\frac{Z_r^a M_{VF_B}^{A:\infty}(\omega)}{\left[Z_{in}^{A:e}(\omega)T_{11}(\omega)+T_{12}(\omega)\right]+\left[Z_{in}^{A:e}(\omega)T_{21}(\omega)+T_{22}(\omega)\right]Z_i^e(\omega)} \qquad (10.2.2)$$

and

$$t_R(\omega)=\frac{Z_o^e(\omega)K(\omega)M_{VF_B}^{B:\infty}}{\left[Z_{in}^{B:e}(\omega)R_{11}(\omega)+R_{12}(\omega)\right]+\left[Z_{in}^{B:e}(\omega)R_{21}(\omega)+R_{22}(\omega)\right]Z_o^e(\omega)}. \qquad (10.2.3)$$

Both of these transfer functions are rather complicated looking, but they can be easily justified from an equivalent circuit standpoint, as we will show in the following subsections. In those subsections we will also place the measured component values obtained in section 10.1 into these transfer function expressions to obtain these functions explicitly for the system shown in Figure 10.1.

10.2.1 Generation transfer function

The complete generation process is shown in Figure 10.9 where both the cabling and transducer are represented as 2x2 transfer matrices T and T^A, respectively. As shown in Chapter 6, the transducer transfer matrix terminated by the acoustic radiation impedance, Z_r^a, can be replaced by transducer A's electrical input impedance, $Z_{in}^{A:e}(\omega)$, where

$$Z_{in}^{A:e}=\frac{Z_r^a T_{11}^A+T_{12}^A}{Z_r^a T_{21}^A+T_{22}^A} \qquad (10.2.4)$$

to arrive at the equivalent circuit shown in Figure 10.10. From Figure 10.10 we can easily obtain the ratio of the voltage across transducer A's input port, V_{in}^A, to the source strength, V_i, as

$$\frac{V_{in}^A}{V_i}=\frac{Z_{in}^{A:e}}{\left(Z_{in}^{A:e}T_{11}+T_{12}\right)+\left(Z_{in}^{A:e}T_{21}+T_{22}\right)Z_i^e}. \qquad (10.2.5)$$

From the definition of the transmitting transducer sensitivity in terms of output force and

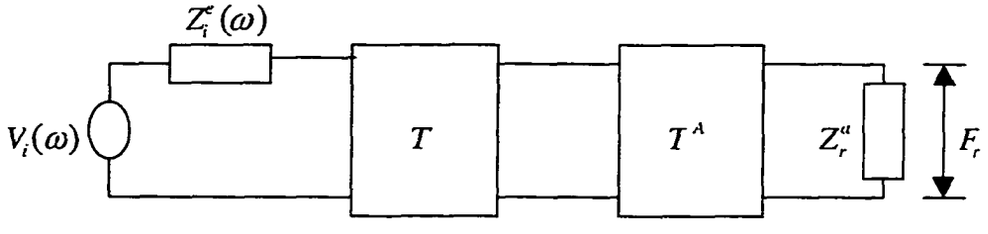

Figure 10.9 The generation process simulated in terms of transfer matrices.

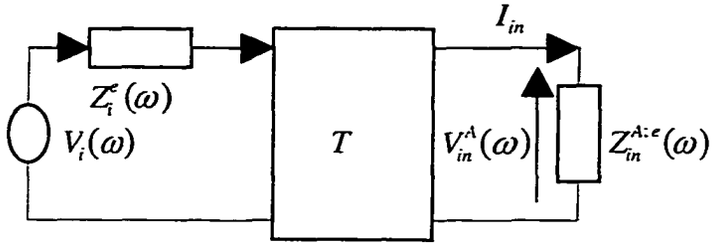

Figure 10.10 The generation process where transducer A is represented by its input electrical impedance.

input current, we have (using, from Figure 10.10, $V_{in}^A = Z_{in}^{A:e} I_{in}$)

$$S_{FI}^A = \frac{F_r}{I_{in}} = \frac{F_r Z_{in}^{A:e}}{V_{in}^A}. \tag{10.2.6}$$

But, from Chapter 6 we know that we can express this transmitting sensitivity in terms of the open-circuit, blocked force receiving sensitivity of A as (see Eq. (6.5.6)):

$$S_{FI}^A = Z_r^a M_{VF_B}^{A:\infty} \tag{10.2.7}$$

so that we have from Eqs. (10.2.6) and (10.2.7)

$$F_r = \frac{Z_r^a M_{VF_B}^{A:\infty}}{Z_{in}^{A:e}} V_{in}^A. \tag{10.2.8}$$

Eq. (10.2.8) can be viewed from an equivalent circuit standpoint as representing an ideal "amplifier" which takes the voltage input, V_{in}^A, and applies a "gain" factor, K', to obtain the output "voltage", F_r, i.e. $F_r = K' V_{in}^A$ where

$$K' = \frac{Z_r^a M_{VF_B}^{A:\infty}}{Z_{in}^{A:e}}. \tag{10.2.9}$$

Thus, the complete generation process can be modeled as the equivalent circuit shown in Figure 10.11. From that figure the generation transfer function, $t_G(\omega)$, can be found since

$$t_G = \frac{F_r}{V_i} = \frac{F_r}{V_{in}^A}\frac{V_{in}^A}{V_i} \tag{10.2.10}$$

so placing Eq. (10.2.5) and Eq.(10.2.8) into Eq.(10.2.10) we find

$$t_G = \frac{Z_r^a M_{VF_B}^{A:\infty}}{\left(Z_{in}^{A:e} T_{11} + T_{12}\right) + \left(Z_{in}^{A:e} T_{21} + T_{22}\right) Z_i^e} \tag{10.2.11}$$

which is identical to Eq. (10.2.2).

Collecting the measured results, $V_i(\omega)$ and $Z_i^e(\omega)$ shown in Figure 10.3 (for the pulser), T_{11}, T_{12}, T_{21} and T_{22} shown in Figure 10.4 (for the transmitting cabling), $M_{VF_B}^{A:\infty}(\omega)$ and $Z_{in}^{A:e}(\omega)$ shown Figure in 10.5 (for the transmitting transducer) and placing these results into Eq. (10.2.11), we can obtain the generation process transfer function $t_G(\omega)$ shown in

Figure 10.12. The solid line gives the amplitude of $t_G(\omega)$ and the dashed line gives its phase. It is interesting that there are two peaks on the amplitude curve. One is at about 5MHz which is the nominal frequency of the transducer and the other is at about 13.5MHz. The amplitude of the higher frequency peak is even greater than that of the lower frequency peak. However,

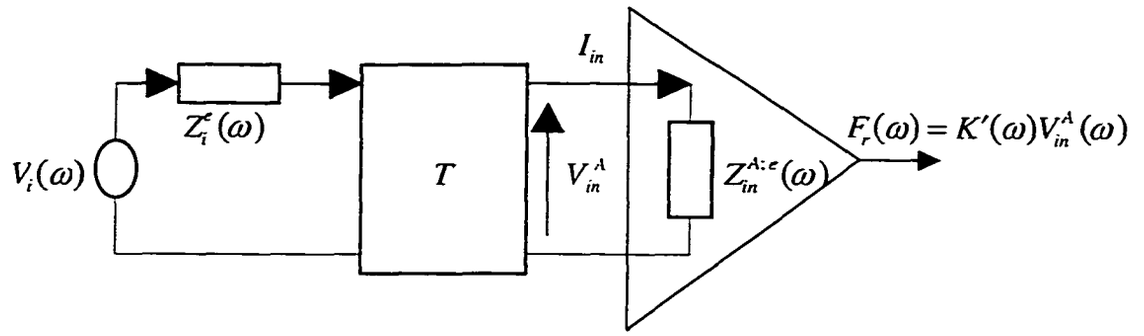

Figure 10.11 Equivalent circuit for the generation process in terms of the directly measurable terms $V_i(\omega)$, $Z_i^e(\omega)$, $(T_{11}, T_{12}, T_{21}, T_{22})$, $Z_{in}^{A:e}(\omega)$, and $M_{VF_8}^{A:\infty}(\omega)$.

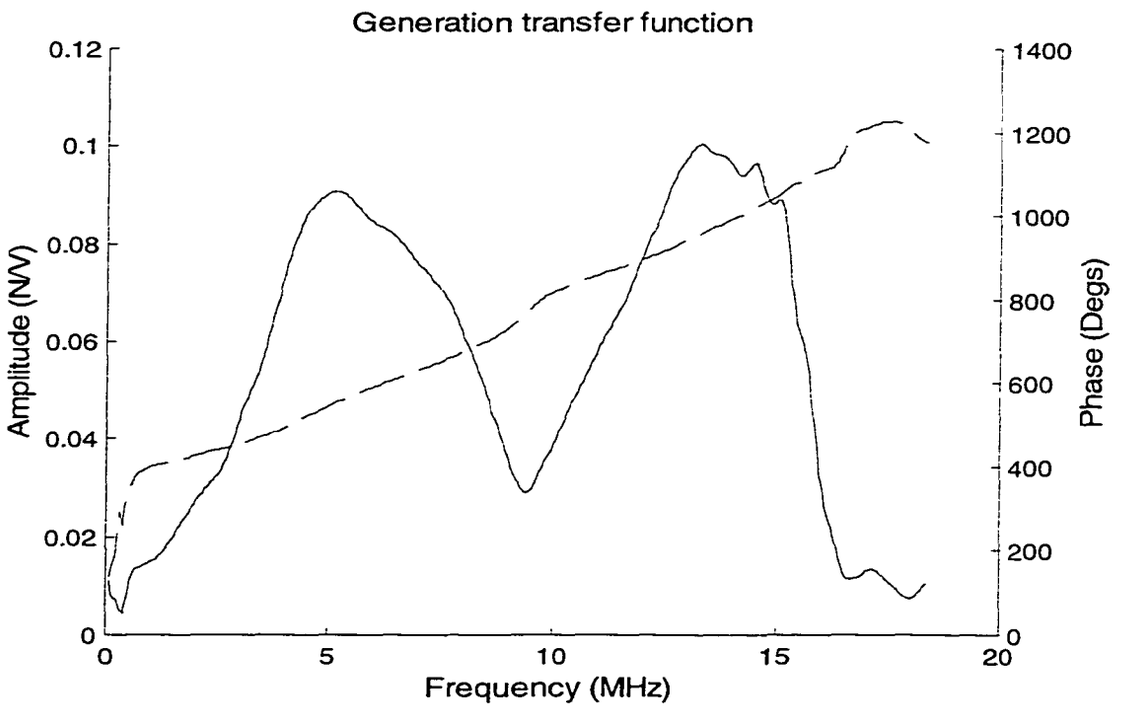

Figure 10.12 Generation transfer function $t_G(\omega)$. The solid line shows its amplitude and the dashed line shows its phase.

in the convolution of this function with the other transfer functions, the higher frequency peak will be depressed, as will be shown later on.

10.2.2 Reception transfer function

The reception process is shown in Figure 10.13 with both the cabling and transducer modeled as 2x2 transfer matrices. As with the generation process, we can obtain a simpler equivalent circuit model that leads directly to the transfer function given by Eq. (10.2.3). First, we consider the elements contained in the dotted box shown in Figure 10.13. We can reduce those elements to a Thevenin equivalent circuit consisting of a voltage source and an equivalent impedance to arrive at the equivalent circuit shown in Figure 10.14. The values for the Thevenin equivalent source and impedance shown in Figure 10.14 can be obtained as

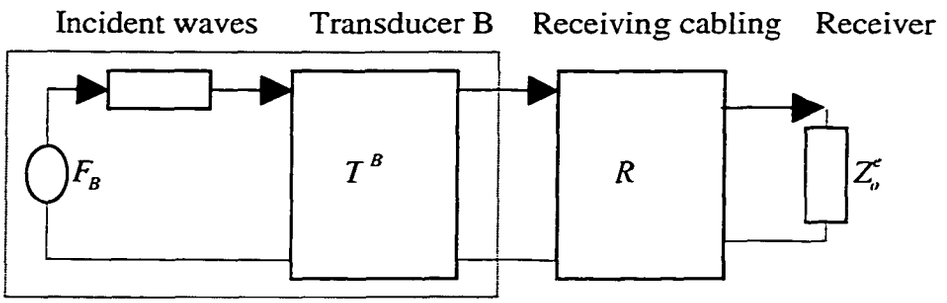

Figure 10.13 The reception process which includes four components: incident acoustic waves, receiving transducer B, receiving cabling R and electrical receiving resistance Z_o^e.

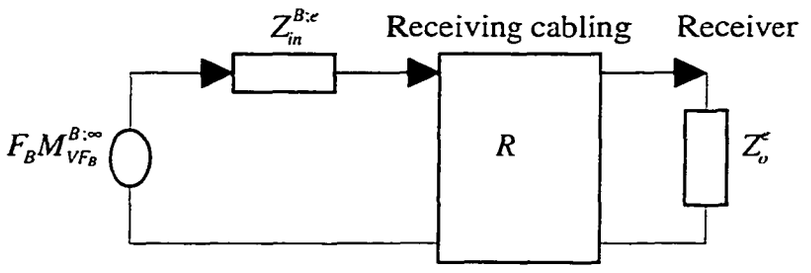

Figure 10.14 Simplified reception process which assimilates the two-port network representation of transducer B and contains measurable quantities in reception process.

follows. First, we note that if we short out the source, F_B, of Figure 10.13 and look from the electrical port of the transducer, the impedance seen is just the internal impedance of the Thevenin equivalent circuit. But the circuit that results from shorting the source is shown in Figure 10.15, which is identical to the circuit shown in Figure 6.3 for a transmitting transducer, which was used to obtain the input impedance of the transmitter (see Eq. (6.2.8)), so that the Thevenin equivalent impedance of the circuit of Figure 10.15 is clearly just the internal input impedance of the receiving transducer, $Z_{in}^{B:e}$. To obtain the Thevenin equivalent source strength shown in Figure 10.14, we simply note that the open-circuit, blocked force receiving sensitivity of the receiving transducer B, $M_{VF_B}^{B:\infty}$, is by definition the open-circuit receiving voltage at the electrical port of transducer B, $V^{B:\infty}$, divided by the blocked force, F_B. Thus the open-circuit voltage can be expressed as

$$V^{B:\infty} = M_{VF_B}^{B:\infty} F_B . \tag{10.2.12}$$

But, this open-circuit voltage is equal to the source strength of the Thevenin equivalent circuit, so that we obtain the source strength expression shown in Figure 10.14.

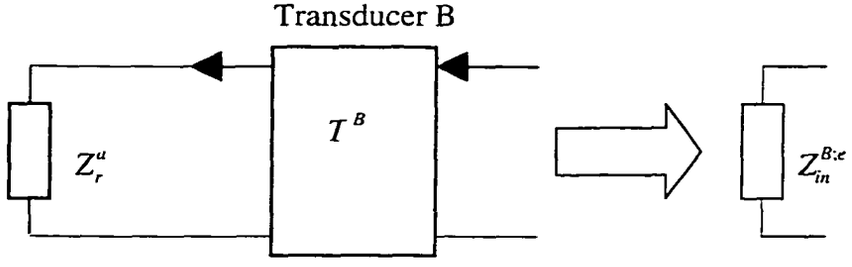

Figure 10.15 Evaluation of internal impedance of the Thevenin equivalent circuit. The impedance is $Z_{in}^{B:e}$ which is measurable.

From Figure 10.14 we can obtain the ratio of the receiving voltage, $V_R(\omega)$, across the electrical load, Z_o^e, to the equivalent source strength, $M_{VF_B}^{B:\infty} F_B$, by following the same steps outlined in Chapter 4 (see Eqs. (4.4.7) – (4.4.18)),

$$\frac{V_R}{M_{VF_B}^{B:\infty} F_B} = \frac{Z_o^e}{\left(Z_{in}^{B:e} R_{11} + R_{12}\right) + \left(Z_{in}^{B:e} R_{21} + R_{22}\right) Z_o^e} . \tag{10.2.13}$$

Multiplying both sides of Eq. (10.2.13) by $M_{VF_B}^{B:\infty}$ then gives the reception process transfer function directly as

$$t_R = \frac{V_R}{F_B} = \frac{Z_o^e M_{VF_B}^{B:\infty}}{\left(Z_{in}^{B:e} R_{11} + R_{12}\right) + \left(Z_{in}^{B:e} R_{21} + R_{22}\right) Z_o^e} \qquad (10.2.14)$$

which is identical to Eq. (10.2.3) if we take $K(\omega)=1$.

All the components of Eq. (10.2.14) were measured experimentally in section 10.1. Collecting the measured results, $M_{VF_B}^{B:\infty}(\omega)$ and $Z_{in}^{B:e}(\omega)$ shown in Figure 10.7 (for transducer B), R_{11}, R_{12}, R_{21} and R_{22} shown in Figure 10.8 (for the receiving cabling) and placing them into Eq. (10.2.14) we obtain the reception transfer function $t_R(\omega)$ shown in Figure 10.16 for a receiving load Z_o^e=50Ω. The solid line shows the amplitude of $t_R(\omega)$ and the dashed line shows its phase. Again there are two peaks on the amplitude curve. One is at about 5MHz which is the nominal frequency of the transducer and the other is smaller and is at about 11MHz.

10.3 Characterizing the Measurement System

In section 10.1.1 we obtained the Thevenin equivalent voltage of the pulser, $V_i(\omega)$, for the setup of Figure 10.1. In subsection 10.1.4 we modeled the acoustic transfer function,

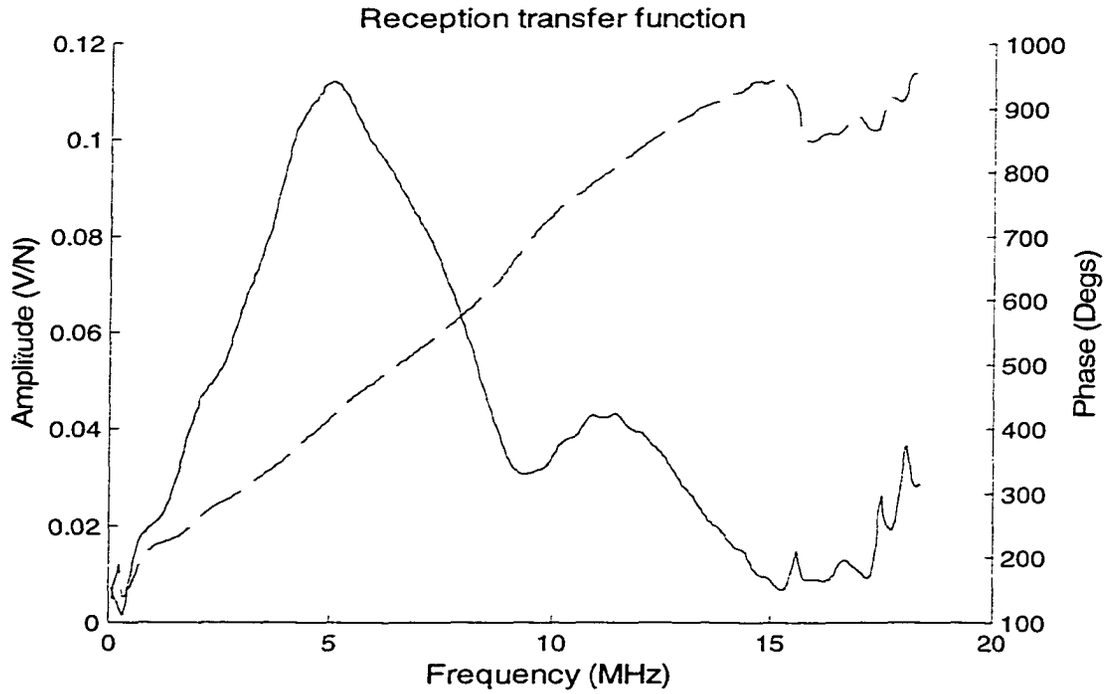

Figure 10.16 Reception transfer function $t_R(\omega)$ when the receiving load Z_o^e=50Ω. The solid line shows its amplitude and the dashed line shows its phase.

$t_A(\omega)$. In section 10.2 we found both the generation and reception transfer functions $t_G(\omega)$ and $t_R(\omega)$, respectively. Thus, from Eq. (10.2.1) we now have a complete characterization of the entire measurement system and can predict the output voltage as a function of frequency, $V_R(\omega)$, as a simple product of all the above components. By taking an inverse FFT of $V_R(\omega)$, we can also directly obtain the measured output voltage, $V_R(t)$.

We can also combine the generation and reception transfer functions, which together contain all the electrical and electromechanical components of the measurement system, into an explicit expression for the system function, $s(\omega)$, (see section 6.6 in Chapter 6) where

$$V_R(\omega) = s(\omega) t_A(\omega) \tag{10.3.1}$$

and

$$s(\omega) = t_G(\omega) t_R(\omega) V_i(\omega). \tag{10.3.2}$$

Our results for $s(\omega)$ and the output voltage, $V_R(t)$, are given in the following subsections.

10.3.1 System factor

On one hand we can obtain the system factor, $s(\omega)$, by simply multiplying the generation and reception transfer functions we have already obtained, as shown in Eq. (10.3.2). On the other hand, we could directly measure the received output voltage, $V_R^m(t)$, of the system shown in Figure 10.1 and, with our known model of the acoustic transfer function, $t_A(\omega)$ (Eq. (10.1.3)), obtain a measured value of the system factor, $s^m(\omega)$, through the process of deconvolution, i.e.

$$s^m(\omega) = \frac{V_R^m(\omega) t_A^*(\omega)}{|t_A(\omega)|^2 + \gamma^2} \tag{10.3.3}$$

where $(\,)^*$ denotes the complex conjugate and $V_R^m(\omega)$ are the frequency components of the measured output voltage. Equation (10.3.3) represents a Wiener filter deconvolution expression where the Wiener filter constant, γ, is a parameter that is used to desensitize the deconvolution process to noise [Schmerr, 1998].

Figures 10.17 and 10.18 show the system factors when $Z_o^e = 50\Omega$ and $Z_o^e = \infty$, respectively. The solid lines show the synthesized results, $s(\omega)$, and the dashed lines show the measured results, $s^m(\omega)$. For both cases, the Wiener filter constant γ was taken as 2% of the maximum amplitude of $|t_A(\omega)|$. We see that the amplitudes of the synthesized and measured system factors show very similar behavior, with the synthesized results usually somewhat higher than the measured results and the phases matching very well.

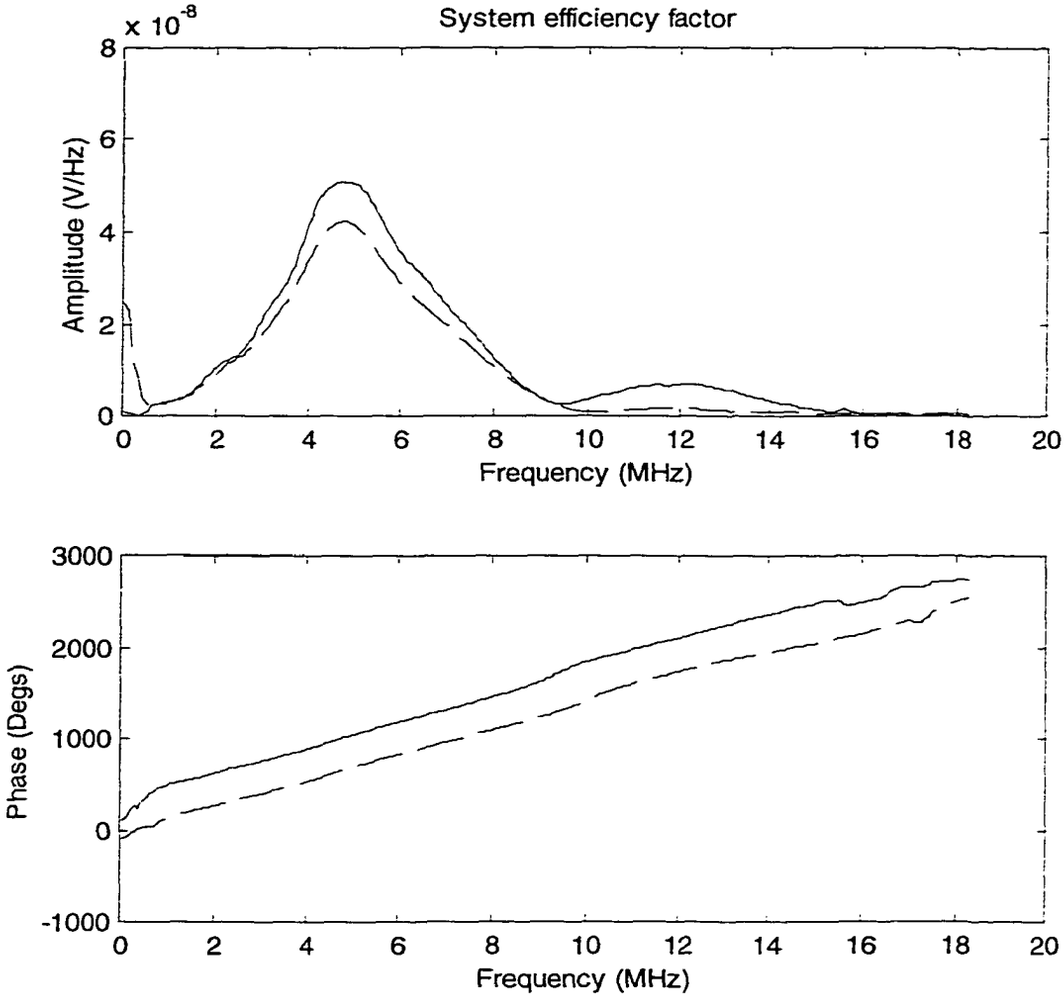

Figure 10.17 The system efficiency factor of the ultrasonic measurement system in Figure 10.1 when the receiving load Z_o^r=50Ω. The solid lines show the synthesized result and the dash lines show the measured result. The upper figure depicts their amplitudes and the lower one depicts their phases.

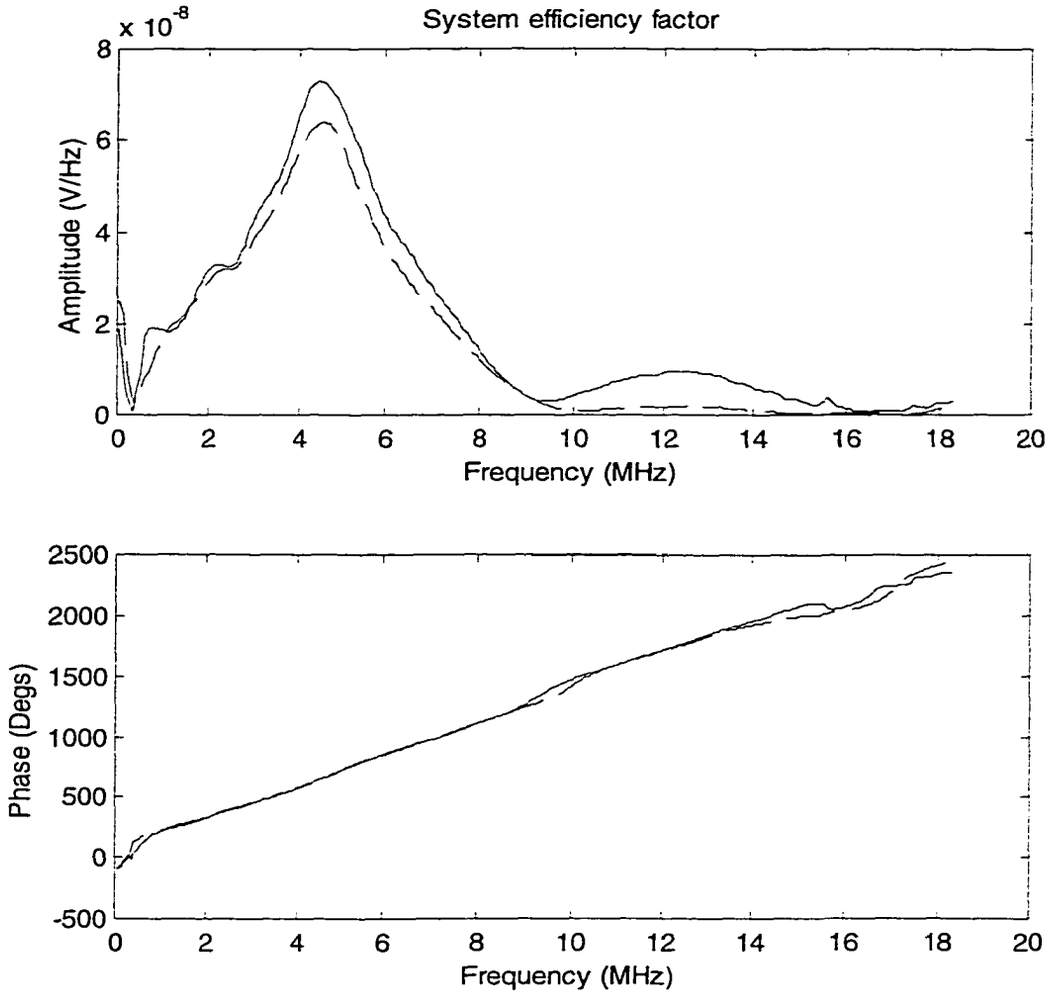

Figure 10.18 The system efficiency factor of the ultrasonic measurement system in Figure 10.1 when the receiving load $Z_o^r = \infty$. The solid lines show synthesized result and the dash lines show the measured result. The upper figure depicts their amplitudes and the lower one depicts their phases.

10.3.2 Receiving waveforms

From Eq. (10.3.1), we can obtain the synthesized receiving time-domain waveforms by taking the FFT on this equation. The synthesized waveforms are shown as solid lines in Figures 10.19 and 10.20 when $Z_o^r = 50\Omega$ and $Z_o^r = \infty$, respectively. On the other hand, we can directly measure the receiving waveforms for these two termination conditions. These measured results are shown as dashed lines in Figures 10.19 and 10.20. We can observe that the synthesized receiving waveforms and the measured receiving waveforms have very similar shapes for both cases. However, the amplitudes of the synthesized receiving waveforms are somewhat larger than that of the measured ones. This is consistent with our results for the synthesized and measured system factors in subsection 10.3.1.

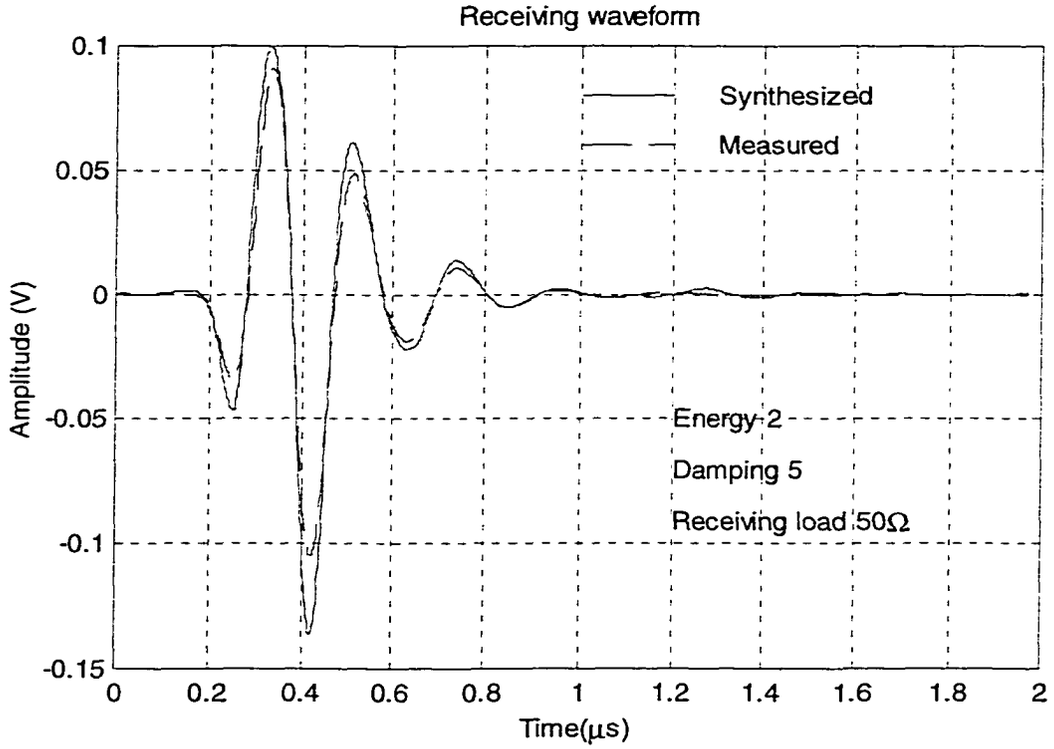

Figure 10.19 The receiving waveform from the ultrasonic measurement system in Figure 10.1 when the receiving load $Z_o^r = 50\Omega$. Solid line and dashed line show the synthesized and measured waveforms respectively.

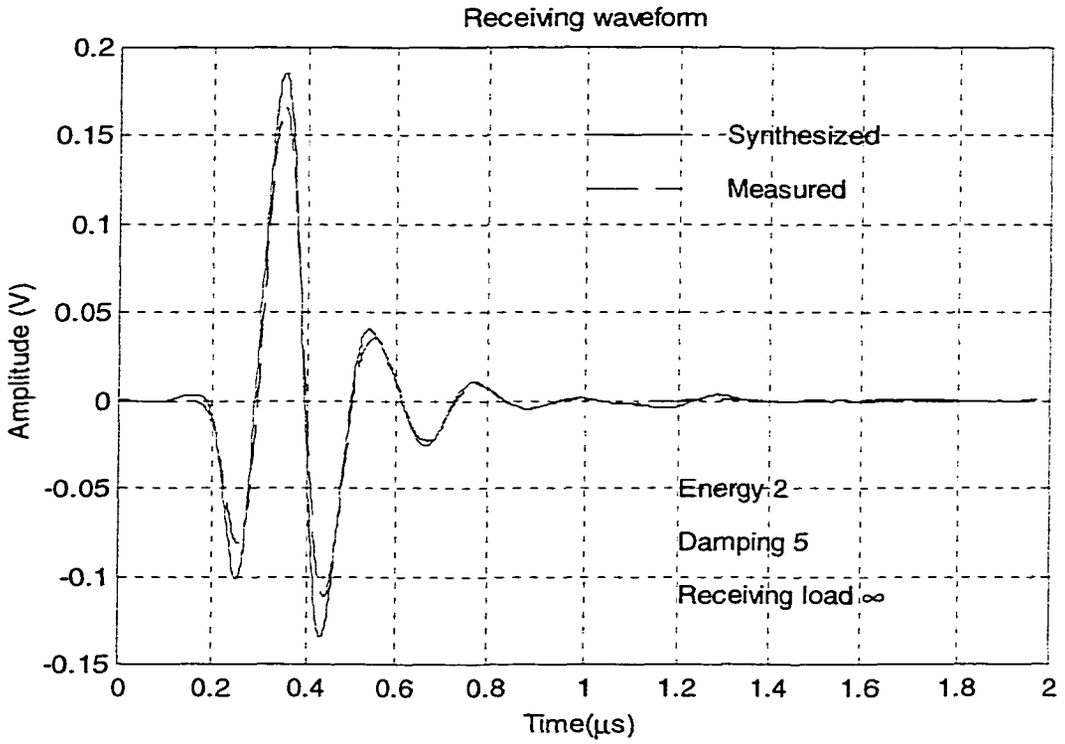

Figure 10.20 The receiving waveforms from the ultrasonic measurement system in Figure 10.1 when the receiving load $Z_o^c = \infty$. Solid line and dashed line show the synthesized and measured waveforms respectively.

CHAPTER 11. SUMMARY AND CONCLUSIONS

This thesis has developed a comprehensive model of an ultrasonic NDE system that can serve as the basis for performing quantitative studies of system performance at many different levels ranging from an individual component, such as a transducer crystal, for example, to the entire system itself. In developing this comprehensive model, there have been a number of significant accomplishments made in the thesis. These are:

1. New, explicit models of the generation and reception transfer functions have been given in a form (see Eqs. (6.2.14) and (6.2.15)) that now makes it possible to experimentally characterize these important parts of the measurement process using purely electrical measurements. These forms are

$$t_G(\omega)=\frac{Z_r^a M_{VF_B}^{A:\infty}(\omega)}{\left[Z_{in}^{A:e}(\omega)T_{11}(\omega)+T_{12}(\omega)\right]+\left[Z_{in}^{A:e}(\omega)T_{21}(\omega)+T_{22}(\omega)\right]Z_i^e(\omega)} \qquad (11.1.1)$$

$$t_G(\omega)=\frac{K(\omega)Z_0^e(\omega)M_{VF_B}^{B:\infty}(\omega)}{\left[Z_{in}^{B:e}(\omega)R_{11}(\omega)+R_{12}(\omega)\right]+\left[Z_{in}^{B:e}(\omega)R_{21}(\omega)+R_{22}(\omega)\right]Z_0^e(\omega)}. \qquad (11.1.2)$$

   The importance of these forms is that they show clearly what properties of the pulser, receiver, cabling, and transducer(s) need to be measured in order to characterize the electrical and electromechanical components. In the case of the transducer(s), this is especially important since these equations demonstrate that it is the transducer open-circuit, blocked force sensitivity and the transducer input electrical impedance that are the fundamental transducer quantities needed to model the generation and reception processes.

2. We have modified a three transducer reciprocity-based calibration procedure borrowed from acoustics and shown that a generalized transducer sensitivity can be found in a form similar to the open-circuit sensitivity expression given in the acoustics literature, namely (see Eq. 6.4.19)

$$M_{VF_B}^{A}=\sqrt{\frac{V_{CA}V_{BA}}{I_B V_{CB}\left(1+Z_{in}^{B:e}/Z_0^e\right)}\frac{t_A^{II}}{Z_r^{B:e}t_A^{I}t_A^{III}}}. \qquad (11.1.3)$$

   This generalization is important since in ultrasonic systems cabling effects often do not allow us to obtain open-circuit sensitivities directly, in contrast to the case for acoustics, where frequencies are low enough that cabling effects are non existent. However, in

ultrasonics we can experimentally measure this generalized sensitivity, as shown in Chapter 9. This generalized sensitivity can then be used to obtain the open-circuit sensitivities that appear in the generation and reception process models.

3. We have combined all the system elements together to form the *electroacoustic measurement model.* This EAM model is a new, consistent formulation of an ultrasonic system that explains and removes many of the overly restrictive assumptions present in the literature when dealing with the 3-D acoustic generation and reception processes, in particular. Another important accomplishment has been the implementation of this EAM model in the form of an interactive software package built with MATLAB.

4. For the first time it has been shown that it is possible to measure all the components of an ultrasonic measurement system and then combine those component measurements to predict the overall system response. Also, for the first time it has been shown that a system factor (which combines all the electrical and electromechanical elements together into a single term) can be obtained from these same component measurements instead of from a "black box" deconvolution process. This capability opens up new possibilities for characterizing and optimizing these important elements of the ultrasonic system.

All of these accomplishments can serve as a foundation for some significant extensions and future work. For example, the present modeling has dealt exclusively with immersion systems. But, contact ultrasound systems are widely used and this modeling approach should be applicable to them as well. We have already identified some key issues (such as the behavior of the radiation impedance, for example) that need to be carefully examined for contact problems. One potential use of a contact model that could have far reaching implications is its use in compensating for variations in measured response due to changes in the coupling layer between the transducer and the part being inspected [Canella, 1974]. It appears possible that a couplant compensation system could be developed which relies on a monitoring of the input impedance of the transducer (a quantity that is demonstrably quite sensitive to couplant changes) and corrects for the couplant variations. To make this possible, however, a model such as the EAM model is needed so that the effects of the other system elements (cabling, etc.) can be accounted for explicitly.

Another extension that could be made in the future is to replace the three transducer calibration procedure for obtaining the transducer sensitivity with a simpler, single transducer pulse-echo setup [Carstensen, 1947, White, 1957, Reid, 1974, Widener, 1980]. Again, reciprocity principles could be used to define a calibration procedure for a case where the pulse-echo acoustic transfer function is able to be explicitly modeled, as in the reflection from a plane surface, for example. Obtaining sensitivity factors via the three transducer calibration setup is a rather delicate measurement process and going to a single transducer calibration procedure could help to make those measurements much easier.

Although the EAM model is a very comprehensive model, there are some effects that are not modeled at present. These include loss terms in the various system components and models of electrical noise sources during both the generation and reception processes. Both of these types of effects could be added to the current model.

Finally, another area where significant extensions of this modeling approach could be made in the future is in the detailed characterization of the radiated velocity of the transmitting transducer through mechanical measurements. Assuming that the transducers act as piston sources (which is what we have typically done in these studies) is a reasonable assumption in many cases but for transducers that do not act like pistons, this assumption could lead to significant modeling errors. Developing a practical capability for measuring the output velocity experimentally would allow us to obtain a consistent value for the radiation acoustic impedance of the transducer and serve as a more accurate basis for modeling the 3-D radiated acoustic wave field.

REFERENCES

Auld, B. A., "General electromechanical reciprocity relations applied to the calculation of elastic wave scattering coefficients," Wave Motion, North-Holland Publishing Company, Vol. 1, 1979, pp. 3-10.

Auld, B. A, Acoustic Fields and Waves in Solids, 2nd Ed. Vols. I and II, Krieger Publishing Co., Maldras, Florida, 1998.

Balanis, C. A., Advanced Engineering Electromagnetics, John Wiley and Sons, Inc., 1989.

Barnard, D. J., Dace, G. E., Rehbein, D. K. and Buck, O., "Acoustic harmonic generation at diffusion bonds," Journal of Nondestructive Evaluation, Vol. 16(2), 1997, pp. 77-89.

Beatty, L. G., "Reciprocity calibration in a tube with active-impedance termination," J. Acoust. Soc. Am., Vol. 39, 1966, pp. 40-47.

Beatty, L. G., Bobber R. J. and Phillips, D. L., "Sonar transducer calibration in a high-pressure tube," J. Acoust. Soc. Am., Vol. 39, 1966, pp. 48-54.

Beissner, K., "Exact integral expression for the diffraction loss of a circular piston source," Acustica, Vol.19, 1981, pp.212-217.

Bladel, J. V., Electromagnetic Fields, Hemisphere Publishing Corporation, 1985.

Bobber, R. J. and Sabin, G. A., "Cylindrical wave reciprocity parameter," J. Acoust. Soc. Am., Vol. 33(4), 1961, pp. 446-451.

Bobber, R. J., "General reciprocity parameter," J. Acoust. Soc. Am., Vol. 39(4), 1966, pp. 680-687.

Bobber, R. J., Underwater Electroacoustic Measurements, Naval Research Laboratory Washington, D.C., July 1970.

Brendel, K. and Ludwig, G.,"Calibration of ultrasonic standard probe transducers," Acustica, Vol. 36, 1976, p.203.

Brown, L.F., "Design considerations for piezoelectric polymer ultrasound transducers," IEEE Transactions on Ultrasonics, Ferroelectrics, and Frequency Control, Vol. 47(6), November 2000, pp. 1377-1396.

Canella, G., "The effect of couplant thickness in ultrasonic contact testing," British Journal of NDT, November 1974, pp. 179-182.

Carstensen, E. L., "Self-reciprocity calibration of electroacoustic transducers," J. Acoust. Soc. Am., Vol. 19(6), 1947, pp. 961-965.

Cheney, S. P., Lees, S., Gerhard Jr., F. B. and Kranz, P. R., "Step excitation source for ultrasonic pulse transducers," Ultrasonics, May 1973, pp. 111-113.

Chertock, G., "General reciprocity relation," J. Acoust. Soc. Am., Vol. 34(7), 1962, p. 989.

Dang, C. and Schmerr, L. W., "Use of an electroacoustic measurement model for ultrasonic transducer characterization," Review of Progress in Quantitative Nondestructive Evaluation, Vol.18A, D. O. Thompson and D. E. Chimenti, Eds., Plenum Press, New York, 1999, pp.1115-1122.

Diestel, H. G., "Reciprocity calibration of microphones in a diffuse sound field," J. Acoust. Soc. Am., Vol. 33(4), 1961, pp. 514-518.

Fay, B., Ludwig, G. and Reimann, H. P., "Determination of the sensitivity of ultrasonic contact transducers," Acustica, Vol. 69, 1989, pp. 73-80.

Fay, B. and Reimann, H. P., "Reciprocity calibration of ultrasonic contact transducers," IEEE Transactions on Ultrasonics, Ferroelectrics, and Freqency Control, Vol. 41(1), January 1994, pp. 123-129.

Foldy, L. L. and Primakoff, H., "A general theory of passive linear electroacoustic transducers and the electroacoustic reciprocity theorem. I," J. Acoust. Soc. Am., Vol. 17(2), 1945, pp. 109-120.

Garrett, S., "Reciprocity calibration of transducers in a plane wave resonator," J. Acoust. Soc. Am., Suppl. 1, 66, S39, 1979.

Ge, L., "Impedance characteristics of transducers and reciprocity calibration," J. Acoust. Soc. Am., Vol. 86(1), 1989, pp. 210-214.

Goldstein, A., Gandhi, D. R., and O'Brien, W. D., "Diffraction effects in hydrophone measurements," IEEE Transactions on Ultrasonics, Ferroelectrics, and Frequency Control, Vol. 45(4), July 1998, pp. 972-979.

Gradshteyn, I. S. and Ryzhik, I. M., Table of Integrals, Series, and Products, Corrected and Enlarged Edition, Academic Press, 1980.

Greenspan, M., "Piston radiator: some extensions of the theory," J. Acoust. Soc. Am. Vol. 65(3), 1979, pp. 608-621.

Hambly, A. R., Electrical Engineering: Principles and Applications, Prentice Hall Inc., Englewood Cliffs, New Jersey, 1997.

Hanselman, D. and Littlefield, B., Mastering MATLAB 5, Prentice-Hall, Inc., Upper Saddle River, New Jersey, 1998.

Harris, G.R., "Review of transient field theory for a baffled planar piston," J. Acoust. Soc. Am., Vol.70, 1981, pp.10-20.

Hayward, G., "The influence of pulser parameters on the transmission response of piezoelectric transducers," Ultrasonics, Vol.23, 1985, pp. 103-112.

Hayward, G., "Using a block diagram approach for the evaluation of electrical loading effects on piezoelectric reception," Ultrasonics, Vol.24, 1986, pp. 156-163.

Hayward, G., Macleod, C. J. and Durrani, T. S., "A systems model of the thickness mode piezoelectric transducer," J. Acoust. Soc. Am., Vol.76, no.2, 1984, p.369.

Hill E. K. and Egle, D. M., "A reciprocity technique for estimation the diffuse-field sensitivity of piezoelectric transducers," J. Acoust. Soc. Am., Vol. 67(2), 1980, pp. 666-672.

Jiang, P. and Apfel, R. E., "Plane wave approximation in a pulse transmission system and its application to attenuation measurements," Proc. 1991 Ultrasonics Symposium, IEEE Press, 1991, pp. 671-674.

Karmel, P. R., Colef,G. D. and and Camisa, R. L., Introduction to Electromagnetic and Micorwave Engineering, John, Wiley and Sons, New York, NY, 1998.

Khimunin, A. S., "Numerical calculation of the diffraction corrections for the precise measurement of ultrasound absorption," Acustica, Vol. 27, 1972, pp. 173-181.

King, L. V., "On the acoustic radiation field of the piezoelectric oscillator and the effect of viscosity on the transmission," Can. J. Res., Vol. 11,1934, pp. 135-155.

Kino, G. S., Acoustic Waves: Devices, Imaging, and Analog Signal Processing, Prentice Hall, Englewood Cliffs, New Jersey, 1987.

Kinsler, L.E., Frey, A.R., Coppens, A.B. and Sanders, J.V., Fundamentals of Acoustics, 3rd Ed., John Wiley and Sons, New York, NY, 1982.

Krimholtz, R., Leedom, D. A. and Matthaei, G. L., "New equivalent circuits for elementary piezoelectric transducers," Electronics Letters, Vol. 6(13), 1970, pp. 398-399.

Leedom, D. A., Krimholtz, R. and Matthaei, G. L., "Equivalent circuits for transducers having arbitrary even- or odd-symmetry piezoelectric excitation," IEEE Transactions on Sonics and Ultrasonics, Vol. SU-18(3), July 1971, pp. 128-141.

Lewis, G. K., "A matrix technique for analyzing the performance of multilayered front matched and backed piezoelectric ceramic transducers," Acoustic Imaging, Vol. 8, A. F. Mecherell, Ed., Plenum Press, New York and London, 1978, pp. 395-416.

Luan, G., Zhang, J. and Wang, R., Piezoelectric Transducers and Transducer Arrays, Peking University Press, 1st Ed., 1990.

Ludwig, G. and Brendel, K., "Calibration of hydrophones based on reciprocity and time delay spectrometry," IEEE Transactions on Ultrasonics, Ferroelectrics, Frequency Control, Vol. 35(2), 1988, pp. 168-174.

MacLean, W. R., "Absolute measurement of sound without a primary standard," J. Acoust. Soc. Am., Vol. 12, 1940, pp. 141-146.

Magnusson, P. C., Alexander, G. C. and Tripathi, V. K., Transmission Lines and Wave Propagation, 3rd Ed., CRC Press, Boca Raton, Florida, 1992.

Marchand, P., Graphics and GUIs with MATLAB, CRC Press, Inc., Boca Raton, Florida, 1996.

Martin, R. W. and Sigelmann, R. A., "Force and electrical thevenin equivalent circuits and simulations for thickness mode piezoelectric transducers," J. Acoust. Soc. Am., Vol. 58(2), 1975, pp. 475-489.

Mason, W. P., (ed), Physical Acoustics, Vol.1-Part A, Academic Press, New York and London, 1964.

MathWorks, The, Inc., http://www.mathworks.com.

Oakley, C. G., "Calculation of ultrasonic transducer signal-to-noise ratios using the KLM model," IEEE Transactions on Ultrasonics, Ferroelectrics, and Frequency Control, Vol. 44(5), 1997, pp. 1018-1026.

Oppenheimer, S. L., Fundamentals of Electric Circuits, Prentice-Hall, Inc., Englewood Cliffs, New Jersey, 1984.

Panametrics, Inc., Model 5058, Instruction Manual -- High Voltage Pulser-Receiver, 1989.

Papadakis, E. P. and Fowler, K. A., "Broad-band transducers: radiation field and selected applications," J. Acoust. Soc. Am., Vol. 50(3), 1971, pp.729-745.

Papadakis, E. P., "Use of computer model and experimental methods to design, analyze, and evaluate ultrasonic NDE transducers," Materials Evaluation, Vol. 41(12), 1983, pp. 1378-1388.

Pozar, D.M., Microwave Engineering, 2nd Ed., John Wiley and sons, New York, NY, 1998.

Primakoff, H. and Foldy, L. L., "A general theory of passive linear electroacoustic transducers and the electroacoustic reciprocity theorem. II," J. Acoust. Soc. Am., Vol. 19(1), 1947, pp. 50-58.

Ramos, A., San Emeterio, J. L. and Sanz, P. T., "Dependence of pulser driving responses on electrical and motional characteristics of NDE ultrasonic probes," Ultrasonics, Vol. 38, 2000, pp. 553-558.

Redwood, M., "Transient performance of a piezoelectric transducer," J. Acoust. Soc. Am., Vol. 33(4), 1961, pp. 527-536.

Reid, J. M., "Self-reciprocity calibration of echo-ranging transducers," J. Acoust. Soc. Am., Vol. 55(4), 1974, pp. 862-868.

Ristic, V. M., Principles of Acoustic Devices, John Wiley and Sons, New York, N.Y., 1983.

Rogers, P. A. and Van Buren, A. L., "An exact expression for the Lommel diffraction correction integral," J. Acoust. Soc. Am., Vol. 55(4), April 1974, pp. 724-728.

Rudnick, I., "Unconventional reciprocity calibration of transducers," J. Acoust. Soc. Am., Vol. 63(6), 1978, pp. 1923-1925.

Sachse, W. and Hsu, N. N., "Ultrasonic transducers for materials testing and their characterization," Physical Acoustics -- Principles and Methods, W. P. Mason and R. N. Thurston, Eds, Academic Press, Vol. XIV, 1979, pp. 277-406.

Schmerr Jr., L. W., Fundamentals of Ultrasonic Nondestructive Evaluation -- A Modeling Approach, Plenum Presss, New York, 1998.

Schmerr Jr., L. W., Dang, C. and Sedov, A., "Electromechanical modeling of ultrasonic transducers," Review of Progress in Quantitative Nondestructive Evaluation, Vol. 17, D. O. Thompson and D. E. Chimenti, Eds., Plenum Press, New York, 1998, pp. 891-898.

Schmerr Jr., L. W., Song, S. J. and Zhang, H. "Model-based calibration of ultrasonic system responses for quantitative measurements," in Nondestructive Characterization of Materials, VI, R.E. Green, Jr., K. J. Kozaczet, and C. O. Ruud, Eds., Plenum Press, New York, 1984, pp. 111-118.

Selfridge, A. R. and Gehlbach, S., "KLM transducer model implementation using transfer matrices," Proc. IEEE Ultrason. Symp., 1985, pp. 875-877.

Seshadre, S. R., Fundamentals of Transmission Lines and Electromagnetic Fields, Addison-Wesley Publishing Company, 1971.

Sigelmann, R. A., "Design method for ultrasound transducers using experimental data and computers," J. Acoust. Soc. Am., Vol. 62(6), 1977, pp. 1491-1501.

Silk, M. G., Ultrasonic Transducers for Nondestructive Testing, Adam Hilger Ltd., Techno House, Redclife Way, Bristol, 1984.

Silk, M. G., Bainton, K. F. and Hillier, M. J., "A mathematical model of the operation of an ultrasonic probe," Mathematical Modelling in Non-Destructive Testing, M. Blakemore and G. A. Georgiou, Eds., Clearendon Press, Oxford England, 1988, pp. 175-189.

Simmons, B. D. and Urick, R. J., "The plane wave reciprocity parameter and its application to the calibration of electroacoustic transducers at close distances," J. Acoust. Soc. Am., Vol. 21(6), November 1949, pp. 633-635.

Sittig, E. K., "Transmission parameters of thickness-driven piezoelectric transducers arranged in multilayer configurations," IEEE Transactions on Sonics and Ultrasonics, Vol. SU-14(4), October 1967, pp. 167-174.

Sittig, E. K., "Effects of bonding and electrode layers on the transmission parameters of piezoelectric transducers used in ultrasonic digital delay lines," IEEE Transactions on Sonics and Ultrasonics, Vol. SU-16(1), January 1969, pp. 2-10.

Sittig, E. K., "Design and technology of piezoelectric transducers for frequencies above 100MHz," Physical Acoustics IX -- Principles and Methods, W.P. Mason and R.N. Thurston, Eds, Academic Press, New York and London, 1972, pp. 221-275.

Staelin, D. H., Morgenthaler, A. W. and Kong, J. A., Electromagnetic Waves, Prentice Hall, Inc., New Jersey, 1994.

Thompson, R. B. and Gray, T. A., "A model relating ultrasonic scattering measurements through liquid-solid interfaces to unbounded medium scattering amplitudes," J. Acoust. Soc. Am., Vol. 74, 1983, pp. 140-146.

Trott, W. J., "Reciprocity parameter derived from radiated power," J. Acoust. Soc. Am., Vol. 34(7), 1962, pp. 989-990.

Wathen-Dunn, W., "On the reciprocity free-field calibration of microphone," J. Acoust. Soc. Am., Vol. 21(5), 1949, pp. 542-546.

White, R. M., "Self-reciprocity transducer calibration in a solid medium," J. Acoust. Soc. Am., Vol. 29(7), 1957, pp. 834-836.

Widener, M. W., "The measurement of transducer efficiency using self-reciprocity techniques," J. Acoust. Soc. Am., Vol. 67(3), 1980, pp. 1058-1060.

Williams, A.O., "The piston source at high frequencies," J. Acoust. Soc. Am., Vol. 23, 1951, pp. 1-6.

Yamada, K. and Y. Fujii, Acoustic response of a circular receiver to a circular source of different radius, J. Acoust. Soc. Am., Vol. 40, 1966, p.1193.

Zhang, H. L., Li, M. X. and Ying, C. F., "Complete solutions of the transient behavior of a transmitting thickness-mode piezoelectric transducer and their physical interpretation," J. Acous. Soc. Am., Vol. 74, 1983, pp. 1105-1114.

ACKNOWLEDGEMENTS

I would like to thank Dr. Lester Schmerr, my advisor, without whose patience, support and guidance this research would never have been possible.

Special thanks are given to Dr. Alex Sedov from Lakehead University in Canada for several derivations which contributed to this thesis.

Many thanks are given to Dr. Daniel Barnard, Mr. John Peters, Mr. Sam Wormly, Mr. Dave Orman and Dr. Norio in Iowa State University and Ms. Pat Iverson at Panametrics, Inc., who were kind enough to share with me their NDE knowledge and experimental equipment during my research. I would also like to thank the rest of the staff at the Center for NDE for their friendship and support.

A special note of thanks goes out to Professors Bruce Thompson, Dave Hsu, Satish Udpa, and Gurpur Prabhu for serving as my committee members and supporting and advising me on my research. Special mention should be made of the faculty and staff of the Department of Aerospace Engineering and Engineering Mechanics.

BIOGRAPHICAL SKETCH

Changjiu Dang was born on June 14, 1965. He graduated from the Department of Radio Electronics in Peking University in 1987 with a Bachelor of Science degree. Then he was recommended into the Institute of Acoustics, Chinese Academy of Sciences as a Master's degree candidate. In 1990, he concluded his MS in Acoustics and then joined the Institute of Acoustics as a research engineer. He was involved in ultrasonic testing, ultrasonic signal processing, transducer design and development, piezocomposite investigation and software development. In 1996, he was with the Center for nondestructive evaluation as a PhD candidate in the Department of Aerospace Engineering and Engineering Mechanics with a Minor in the Department of Computer Science. He also has worked on a concurrent degree in the Department of Computer Engineering as a Master's degree candidate. His research work in the Center for NDE was funded by the National Science Foundation Industry/ University (NSF I/U) Cooperative Research Program.

The awards he has obtained are: "5.4" science prize in Peking University in 1986, Excellent Research Work Award in the Institute of Acoustics in 1990, Lien Yueh Tu Acoustics Award in Beijing Acoustics Society in 1995, and Best Paper Award at Chinese Youth Conference of Acoustics.